# The role of primary cilia in Townes-Brocks Syndrome

Scientific memory of the research carried out inside the PhD Programme in Molecular Biology and Biomedicine at the University of Basque Country (UPV-EHU). This work was done by Laura Bozal Basterra at the CIC bioGUNE.

## Laura Bozal Basterra

### 2019

**Supervisor:  Dr. María Rosa Barrio Olano.**

Tutor: Dr. Ana Zubiaga.

Supported by:

*"Genius is two percent inspiration, ninety-eight percent perspiration".*

— Thomas Edison

**A mis padres y abuelos, que me mostraron el poder de trabajar duro para alcanzar tus sueños…**
*(To my parents, who show me the power of working hard to reach your dreams…)*

**A mis hermanos, modelos a seguir…**
*(To my brothers, true models to follow…)*

**A Wandert, por soñar juntos…**
*(To Wandert, to our dreams together…*

## Acknowledgements

Thanks to an endless search for the best lab to work on, I was lucky to send my CV number 1.000.000 to Rosa Barrio´s lab. I will never forget our unexpected Skype interview at 10 pm where I was wearing my pijama underneath my "official clothes". Since that moment, I realized two things. The first one that I was going to have two of the most hard-working persons I know as my supervisors. Second, that Science does not understand about timetables. Indeed it has been a long and not always easy way to reach this point, but… totally worth it!!! One successful experiment accounted for a lot of failed ones. This experience has allowed me to grow not only as a scientist, but also at the personal level. Of course, I would have not make it that far without all the support I received all along the way. And for that reason, I would like to thank you all:

First, more than gratitude, I would like to express my admiration to you Rosa. You have been a wonderful mentor ALWAYS available to solve problems and share good discussions (even on holidays, nights and weekends). I am sorry to test your heart condition in several occasions when it comes to deadlines. Thanks for believing in me and giving me the opportunity to work in a wonderful scientific and personal atmosphere. You have provided me with the knowledge and skills to face any challenge on my scientific career. Not only inside the lab but outside I got to know a great person during our "tertulias post-pandriales", Valverde´s retreats and escape rooms among others (by the way… we won last one haha). Seriously, THANKS for everything.

If there is a catalizer of the Big Bang of ideas in this project, that is Jim or how I like to call him: Jimmypedia. Your endless curiosity, knowledge, guidance, crazy ideas and support have been fundamental for the successful completion of this project. I have really enjoyed our scientific and not so scientific talks (including weird but always shocking movie recommendations i.e. Anomalisa) that are always an inspiration to me. I got to know a brillant mind (always available to clone), a friend that taught me soooo much I could never say enough times THANK YOU.

I would also like to thank my labmates, past and present that made the lab a fun place to be. Cori, my mother from Bilbao, la que me amuebla y equipa la bodega y me malcría con sus chupitangas. Millones de gracias por siempre velar por mí, por estar siempre dispuesta a compartir las penas, una tostada de jamón o un frigorífico. Me llevo a una confidente y a una de las más leales amistades que una pueda tener. Monika, my every-day positive energy shot. Working with you implied deep conversations (about science or clothes haha) and lots of laughs. Imma, thanks for your different vision of the world that sometimes made me change my mind and thanks for our fun coffee breaks. Ana, thank you for your wise advice and always being ready to listen to me. Also, big thanks to our new acquisitions Leiore, Marco Orhi and Aitor and the ones who left: Majo, Esti, Angela, Iria, Aida, Karolina, Aiora, Lucia, Leire, Wendy and Ugo Mayor´s lab (Aitor and Juanma). I also learnt a lot from you all. And, to you María, a special thank for being such a great and fast learner, a very nice flatmate (that forgets where we live) and such a naïve and sincere person that always makes me laugh (with you, not of you haha). LUZP1 forever!

Thanks also to all the labs on the 0 floor. @AC lab, @Genome analysis platform, @JA lab, @AW lab, @Biología Celular and @EB. Thank you all for sharing with me this experience. Many thanks to all our collaborators that, with their labs, contributed to this project: Dr. Josean Rodríguez, Dr. Ugo Mayor, Dr. Arkaitz Carracedo, Dr. Ana Aransay, Dr. Jurgën Kohlhase, Dr. Andreu O.M Wilkie, Dr. Kathryn Anderson and Dr. Michael Rauchman.

A big clap to the Facebook page "Parents of children with Townes-Brocks Syndrome". Thank you for all the support that has been crucial to the development of this project. We learned a lot from you, even that Facebook can also be used for the good of humanity.

And because not everything is about work, big and special thanks to my favourite partners in crime: Iskander, Esti, Vir, Teresa and Encarni and the great last discovery, Marta Palomo. Our frontenis matches, beers, Bidegorri, nights out in

Bilbao and holidays together will be never forgotten. You contributed to make my time in Bilbao awesome!! Also, thanks Nati and Amaia for our amazing time in NYC and Alba, Willy, Marta, Myriam, Silvia, Bea, Jone, Tami y Lauri for our wonderful times at the University.

Outside Biogune, I was really lucky to find my "Extranjeros en Bilbao", always ready to gather together and share our deeper feelings: Sandrita, María+Tommaso=Inés and..., Aritz+Naroa=Alex, Jon, Carmen y Eva. Also my third brother Juan, it is a pleasure to share our daily life with you.

And how to forget the friends that know you better than you do and that are and will always be there, a mi cuadrilla de siempre, mi Carrillo querido. Os llevo en el corazón. Espero qué sepáis lo importantes que sois en mi vida. Viva Valverde!!

Also thanks to those who initially were the friends and family of your partner that soon became yours and it looks like you know them for your whole life. Anne and Haydee, thanks for raising an amazing good kid and for you unconditional love to us. You are the best parents in law ever! Thanks to my foreign brothers and sisters: Paul, Amber, Dedmer, Jocelyne and my nieces and nephews that are the light of my life. Also to Beppe, Lydia+Chun Ket, Elle+Herman, Sjaak+Nele. It is always a pleasure to be with you all. You make me always want to go back home to the Nederlands! Gezellig!

Last but not least, the most important pieces of my life´s puzzle: my family. ¡En especial a vosotros papis! Si estoy aquí es por todo el amor, sacrificio, trabajo duro, la humildad y constancia que habéis demostrado. Sois mis modelos en la vida y mi orgullo más grande. GRACIAS por hacerme una persona feliz. A vosotros también tatos, a esos a los que siempre encuentras cuando necesitas y a los que admiro profundamente y a ti Raquel por ser la cuñada molona que me va a hacer la tía más feliz del mundo. GRACIAS por educarme y protegerme con mucho amor. Una gratitud plena también a los que ya no están y que me siguen cuidando, mis

abuelillos. Un beso enorme para el cielo. Os quiero.

A special thank to the love of my life, Wandert. You make my life even more beautiful every day. All your support and your positive mind are priceless to me. Together we are LAUWA, one of our millions of dreams that already became true. Many of them still to come…Ik hou van je!!

## Chapter 4: Results

**Abbreviations**

| | |
|---|---|
| **AcGTub** | Acetylated alpha and gamma tubulin |
| **ADF** | Actin Depolymerising Factor |
| **ADPKD** | Autosomal-dominant polycystic kidney diseases |
| **ANOVA** | Analysis of Variance |
| **Arg** | Arginin |
| **ARL13B** | ADP-ribosylation factor-like protein 13B |
| **Arp2/3** | Actin-Related Proteins 2 and 3 |
| **BB** | Basal body |
| **BCA** | Bicinchoninic acid assay |
| **BSA** | Bovine serum albumin |
| **C** | Cytosin |
| **CCP110** | Centriolar coiled-coil protein of 110 kDa |
| **cDNA** | Complementary DNA |
| **CEP164** | Centrosomal protein of 164 kDa |
| **CEP97** | Centrosomal protein of 97 kDa |
| **CHD3** | Chromodomain Helicase DNA Binding Protein 3 |
| **CHD4** | Chromodomain Helicase DNA Binding Protein 4 |
| **cm** | Centimetre |
| **CNT2** | Centrin 2 |
| **CO2** | Carbon dioxide |
| **CRISPR** | Clustered regularly interspaced short palindromic repeats |
| **CTCF** | Corrected total cell fluorescence |
| **CytB** | Cytochalasin B |
| **DAPI** | 4 ',6-diamino-2-fenilindol |
| **DMEM** | Dulbecco's modified Eagle medium |
| **DMSO** | Dimethyl sulfoxide |
| **DRAQ7** | Deep Red Anthraquinone 7 |
| **DTT** | Dithiothreitol |
| **Dup** | Duplication |

| | |
|---|---|
| **E13** | Embryonic stage 13 |
| **EDTA** | Ethylenediaminetetraacetic acid |
| **F-actin** | Filamentous actin |
| **FACS** | Fluorescence-activated cell sorter |
| **FBS** | Fetal bovine serum |
| **FL** | Full length |
| **FLNA** | Filamin A |
| **fs** | Frameshift |
| **g-actin** | Globular actin |
| **GAPDH** | Glyceraldehyde-3-Phosphate Dehydrogenase |
| **GFP** | Green fluorescent protein |
| **GFS** | Green fluorescent Streptavidin |
| **Gli1/GLI1** | Glioma-associated oncogene 1 |
| **Gli3/GLI3** | Glioma-associated oncogene 3 |
| **GO** | Gene Ontology |
| **h** | Hours |
| **HA** | Human influenza hemagglutinin |
| **HCl** | Hydrochloric Acid |
| **HDAC1** | Histone deacetylase 1 |
| **HDAC2** | Histone deacetylase 2 |
| **HEK 239FT** | Human embryonic fibroblasts |
| **HFF** | Human neonatal foreskin fibroblasts |
| **Hh** | Hedgehog |
| **His** | Histidine |
| **HRP** | Horseradish Peroxidase |
| **i.e** | Id est |
| **IBAQ** | Intensity-based absolute quantification |
| **IMCD3** | Mouse Inner Medullary Collecting Duct-3 |
| **IP** | Immunoprecipitation |
| **kDa** | Kilodaltons |
| **KO** | Knocked-out |

| LC | Liquid chromatography |
|---|---|
| LFQ | Label-free quantitation |
| log | Logarithm |
| LUZP1 | Leucine zipper motif containing protein 1 |
| Lys | Lysine |
| M | Molar |
| MARK4 | MAP/microtubule affinity-regulating kinase 4 |
| MBD3 | Methyl-CpG-binding domain protein 3 |
| MC | Mother centriole |
| MEF | Mouse embryonic fibroblasts |
| MgCl$_2$ | Magnesium Chloride |
| ml | Millilitres |
| MLCII | Myosin light chain 2 |
| mM | Millimolar |
| MS | Mass spectrometry |
| MT | Microtubules |
| MTA1 | Metastasis Associated 1 |
| MTA2 | Metastasis Associated 2 |
| NaCl | Sodium Chloride |
| NCBI | National Center for Biotechnology Information |
| Neo | Neomycine |
| NLS | Nuclear localization signal |
| nm | Nanometres |
| Nups | Nucleoporins |
| NuRD | Nucleosome Remodeling and Deacetylase |
| °C | Celsius degrees |
| ODF2 | Outer dense fiber protein 2 |
| ORPK | Oak Ridge Polycystic Kidney mouse |
| P | Proline |
| PBS | Phosphate Buffered Saline |
| PCR | Polymerase Chain Reaction |

| | |
|---|---|
| **PD** | Pulldowns |
| **Per** | Pericentrin |
| **PKA** | Protein kinase A |
| **PKD** | Polycystic kidney disease |
| **Ptch1/PTCH1/Ptc1** | Protein patched homolog 1 |
| **PVDF** | Polyvinylidene difluoride |
| **qPCR** | Quantitative Polymerase Chain Reaction |
| **qRT-PCR** | Quantitative Retrotranscriptase Polymerase Chain Reaction |
| **Rac1** | Ras-related C3 botulinum toxin substrate 1 |
| **RbAp46** | Retinoblastoma-Binding Protein 46 |
| **RhoA** | Ras homolog gene family, member A |
| **RIPA** | Radioimmunoprecipitation assay buffer |
| **ROCK1/2** | Rho-associated protein kinases 1/2 |
| **RPE1** | Telomerase reverse transcriptase-retinal pigment epithelial 1 |
| **RPLP0** | Ribosomal Protein Lateral Stalk Subunit P0 |
| **RT** | Room temperature |
| **SALL1** | Spalt Like Transcription Factor 1 |
| **SDS** | Sodium dodecyl sulfate |
| **SDS-PAGE** | Sodium dodecyl sulfate polyacrylamide gel electrophoresis |
| **SEM** | Standard error of the mean |
| **Ser** | Serine |
| **Shh/SHH** | Sonic Hedgehog |
| **SMO** | Smoothened |
| **SSH1** | Slingshot homologue 1 phosphatase |
| **SuFu** | Suppressor of Fused |
| **T** | Thymine |
| **TBS** | Townes-Brocks syndrome |
| **TGFbeta** | Transforming growth factor beta |
| **TTBK2** | Tau Tubulin Kinase 2 |

**Figure and table index**

**Abstract**

Townes-Brocks Syndrome (TBS) is characterized by a spectrum of malformations in digits, ears and kidneys. These anomalies overlap with those seen in a growing number of genetic syndromes linked to defects in the formation or function of the primary cilia, collectively known as ciliopathies. TBS is caused by mutations in the gene encoding the transcriptional repressor SALL1 and is associated with the presence of a truncated protein, which localizes to the cytoplasm. In this Thesis, we studied the hypothesis that *SALL1* mutations might cause TBS by means beyond its transcriptional capacity. We hypothesized that TBS might be caused by defects in cilia formation and/or function through its dominant interaction with cilia-related proteins. In fact, TBS patient-derived fibroblasts, a CRISPR/Cas9-generated model cell line and TBS-modeled mouse embryonic fibroblasts, display cilia at a higher frequency compared to wild-type controls. Furthermore, TBS-like cells show changes in cilia length and disassembly rates, accompanied by aberrant Sonic hedgehog (Shh) signalling transduction. By using proximity proteomics, we identified two main ciliogenesis suppressors, CCP110 (Centriolar coiled-coil protein, 110 KD) and CEP97 (Centrosomal protein, 97 KD), and a novel cilia and actin-related protein named LUZP1 (Leucine zipper protein 1) as interactors of TBS-causing truncated SALL1 protein. The higher rate of ciliogenesis detected in TBS-derived fibroblasts is consistent with an observed reduction in CCP110, CEP97 and LUZP1 protein levels at the mother centriole (MC) compared to controls. In addition, we demonstrated that LUZP1 localizes to the centrosome, actin cytoskeleton, and midbody. CRISPR/Cas9-mediated loss of LUZP1 in mouse fibroblasts changed actin dynamics and cell migration, while facilitating ciliogenesis and altering Sonic Hedgehog signaling. Given its localization to both actin stress fibers and the centrosome, LUZP1 might be a key factor for integrating cytoskeletal changes to cilia formation and function.

These results indicate that truncated proteins arising from certain SALL1 mutations can disrupt cilia formation and function. Therefore, TBS might be considered as a ciliopathy-like disease opening a possibility for pharmacological intervention by cilia/cytoskeletal modulators.

**Resumen**

El síndrome de Townes-Brocks (TBS) se caracteriza por un espectro de malformaciones en los dedos, orejas y riñones. Estos síntomas coinciden con los observados en los síndromes genéticos relacionados con defectos en la formación y/o función de los cilios primarios, conocidos colectivamente como ciliopatías. TBS está causado por mutaciones en el gen que codifica el represor transcripcional SALL1 que mayoritariamente dan lugar a una proteína truncada que se localiza en el citoplasma. Los estudios sobre TBS se han centrado tradicionalmente en los defectos que la proteína SALL1 truncada podría ocasionar en el núcleo a nivel transcripcional. Sin embargo, en este trabajo estudiamos la hipótesis de que dicha proteína truncada podría interferir con la formación o señalización de los cilios debido a su interacción dominante negativa con proteínas ciliares o del centrosoma. De hecho, tanto fibroblastos derivados de pacientes de TBS, como una línea celular modelo generada mediante tecnología CRISPR / Cas9 y fibroblastos embrionarios del modelo de TBS en ratón, muestran mayor frecuencia de ciliación en comparación con los controles. Además, las células modelo de TBS muestran una mayor longitud de cilios y retrasos en el desemblaje de los mismos, acompañados por una transducción aberrante de la señalización por la vía Sonic Hedgehog (Shh). Mediante el uso de proteómica de proximidad, identificamos interactores de la proteína SALL1 truncada en los pacientes de TBS. Entre ellos, encontramos a dos de los principales supresores de la ciliogénesis, CCP110 (*Centriolar coiled-coil protein, 110 KD*) y CEP97 (*Centrosomal protein, 97 KD*), y a LUZP1 (*Leucine zipper protein 1*), una proteína no muy estudiada que interacciona con el citoesqueleto de actina y el centrosoma . La mayor tasa de ciliogénesis detectada en los fibroblastos derivados de TBS es consistente con una reducción en los niveles de las proteínas CCP110, CEP97 y LUZP1 en el centriolo madre (MC) en comparación con los controles. Además, demostramos que LUZP1 se localiza en el centrosoma, en el citoesqueleto de actina y en el cuerpo medio (o *midbody*). Las células *knocked-out* de LUZP1 que generamos mediante la tecnología CRISPR-Cas9 mostraron una ciliogénesis prematura y alteraciones en la señalización por Shh, la dinámica de actina, y la división y migración celular. Estos hallazgos apoyan la hipótesis de que LUZP1 podría ser un factor clave en la integración de los

cambios del citoesqueleto de actina y la función/formación de los cilios, procesos que se encuentran alterados en TBS. Estos resultados indican que las truncaciones en SALL1 pueden afectar la formación y función de los cilios. Por lo tanto, TBS podría considerarse como una ciliopatías, abriendo las posibilidades de intervención farmacologica mediante moduladores del cilio primario y/o del citoesqueleto de actina.

# Chapter 1: Introduction

## 1.1 Townes-Brocks Syndrome (TBS)

Townes-Brocks Syndrome (TBS, MIM: 107480) is a rare genetic disease with a stimated prevalence of 1 per 350,000 live births. TBS is characterized by these major features: imperforate anus, dysplastic ears, and thumb malformations such as triphalangeal thumbs, duplication of the thumb (preaxial polydactyly) and thumb hypoplasia (**Figure I 1**) (Powell and Michaelis, 1999).
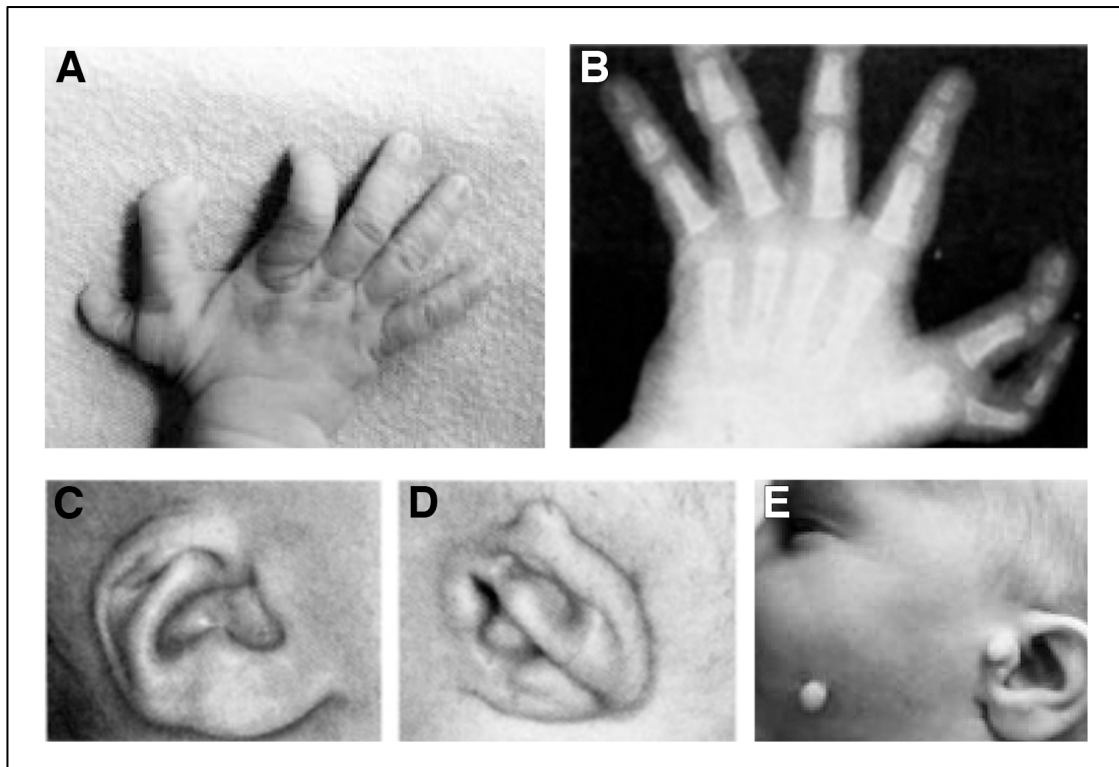


**Figure I 1. Classical symptoms of Townes-Brocks Syndrome.** TBS individuals exhibit polydactyly in hands (**A,B**) and dysplastic ears (**D**, compare to normal ear in **C**). TBS individuals might also exhibit preauricular and cheek tags (**E**). Pictures after (Kohlhase et al., 1998; Powell and Michaelis, 1999).

TBS is also frequently associated with other minor features such as sensorineural and/or conductive hearing impairment, foot malformations, renal impairment including end-stage renal disease or polycystic kidneys, together with genitourinary malformations and congenital heart disease (**Table I 1**). Although less common, radius hypoplasia and cleft/lip palate are also observed (Kohlhase, 1993).

The diagnosis of TBS is established by the presence of three major features. If only two major features are present, the presence of minor features and the absence of atypical features further support the diagnosis.

**Major features**

- Imperforate anus or anal stenosis in 84%

- Dysplastic ears in 87% (overfolded superior helices, microtia)

- Typical thumb malformations in 89% (preaxial polydactyly, triphalangeal thumbs, hypoplastic thumbs) without hypoplasia of the radius

**Minor features**

- Sensorineural and/or conductive hearing impairment

- Foot malformations

- Renal impairment with or without renal malformations

- Genitourinary malformations

- Congenital heart disease

**Atypical (not suggestive of TBS)**

- Radius hypoplasia on clinical examination or radiographs

- Cleft lip/palate

**Table I 1. Major, minor and atypical features in Townes-Brocks Syndrome.** The diagnosis of TBS is established by the presence of three major features. If only two major features are present, the presence of minor features and the absence of atypical features further support the diagnosis.

## 1.1.1 TBS is caused by mutations in *SALL1*

TBS is an autosomal dominant genetic disease caused by mutations in *SALL1* (Spalt-like 1, MIM: 602218) (Botzenhart et al., 2007; Kohlhase et al., 1998), one of the four members of the *SALL* gene family in vertebrates. In *Drosophila*, SALL factors are implicated in the formation of the wing via control of cell differentiation in imaginal discs, trachea, sensory organs and the nervous system (Cantera et al., 2002; de Celis and Barrio, 2000; de Celis and Barrio, 2009). In the wing, SALLs control growth and patterning by transcriptionally regulating downstream genes (Barrio and de Celis, 2004; de Celis and Barrio, 2000). *SALL1* encodes a zinc-finger transcription factor linked to chromatin-mediated repression (de Celis and Barrio, 2009). SALL proteins are characterized by the presence of stereotypical pairs of zinc finger domains along

the protein (**Figure I 2**), which are thought to mediate interactions with DNA via an AT-rich sequence (Netzer et al., 2006). In vertebrates, the N-terminal region of SALL1 mediates transcriptional repression via the interaction with the nucleosome remodeling deacetylase (NuRD) complex through a conserved 12 amino acid sequence (Kiefer et al., 2002). Another important N-terminal motif is a conserved polyglutamine domain involved in dimerization with itself or other SALL family members (Sweetman et al., 2003).

Dominant genetic syndromes are often caused by a gain-of-function or dominant-negative effect of the underlying mutant proteins. More than 50 point-mutations were described that cause premature stop codons by frame shifts, short insertions or deletions, mainly in a hot-spot region located between the N-terminal part of the protein and the second zinc-finger pair (Botzenhart et al., 2007; Botzenhart et al., 2005; Kohlhase et al., 1998) (**Figure I 2**). In addition, three different deletions, including most part of the SALL1 coding region, have been reported in TBS patients (Borozdin et al., 2006; Miller et al., 2012).
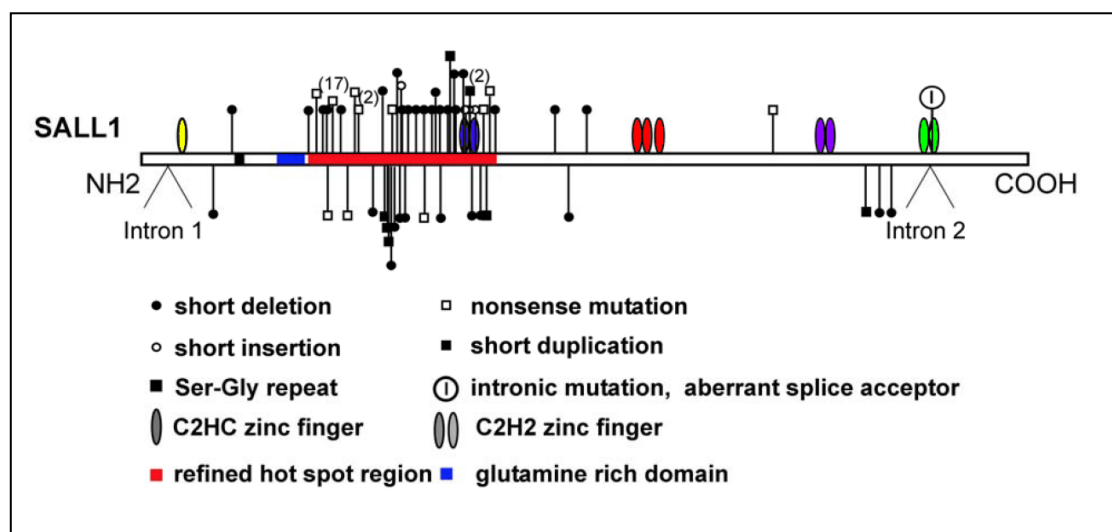


**Figure I 2. Schematic representation of SALL1 protein.** Schematic representation of the SALL1 protein and localization of the mutations identified (upward and downward symbols). Zinc fingers are indicated as colored ovals. (17) indicates that the c.826C>T mutation had been found in 15 sporadic and 2 familial cases, including one individual studied in this work. At position c.1115, two different nonsense mutations had been detected (2), and the mutation c.1403_1404insG was found in two unrelated families (2). All other mutations have been found only once. The red horizontal bar marks the refined "hot spot region" and the blue bar assigns the glutamine rich domain. Positions of the introns are indicated. Scheme adapted from (Botzenhart et al., 2007).

### 1.1.2 TBS is not caused by haploinsufficency

Many TBS-causing *SALL1* mutations could result in truncated proteins that lack some or all the zinc finger pairs that are thought to mediate chromatin/DNA interactions, but retain the N-terminal domain. Previous studies have addressed the expression of mutant *SALL1* gene, showing that mutant mRNA transcripts are stable and resistant to nonsense-mediated decay (Furniss et al., 2007). Truncated proteins causing TBS are able to interact with the NuRD complex and to form multimers with themselves, with full-length (FL) SALL1 (SALL1$^{FL}$) or with other SALL proteins (Lauberth et al., 2007). Inappropriate protein interactions of truncated SALL1 may underlie TBS symptoms (Kiefer et al., 2003). This possibility is supported by animal models of TBS, where *Sall1$^{+/-}$* and *Sall1$^{-/-}$* mice fail to show TBS-like phenotypes (Kiefer et al., 2003; Kiefer et al., 2008; Nishinakamura et al., 2001), discarding haploinsufficiency as the most plausible cause of the disease. Only when murine *Sall1* is altered to mimic human mutations (i.e. to generate a truncated protein in a single copy), mice display TBS symptoms such as hearing loss and anus and limb malformations (Kiefer et al., 2003). The etiology of the disease thus depends on the presence of a truncated SALL1 protein, which localizes to the nucleus and cytoplasm, in contrast to SALL1$^{FL}$, which resides primarily in the nucleus (Sato et al., 2004). Elucidating the role of truncated SALL1 and its possible interference with SALL1$^{FL}$ and other factors would fill a major gap in our understanding of TBS.

## 1.2 The primary cilia

Intriguingly, some of the features shown in TBS individuals match those seen in a growing number of diseases linked to the formation and function of primary cilia, collectively called ciliopathies (**Figure I 3**). Depending on the underlying mutation, ciliopathies present a spectrum of overlapping phenotypes such as polycystic kidneys, hearing loss, limb defects and mental retardation, among others (Hildebrandt et al., 2011). These coincidental features could suggest similar molecular causes between ciliopathies and TBS, but a characterization of primary cilia formation and function has not been reported for cells derived from TBS individuals.
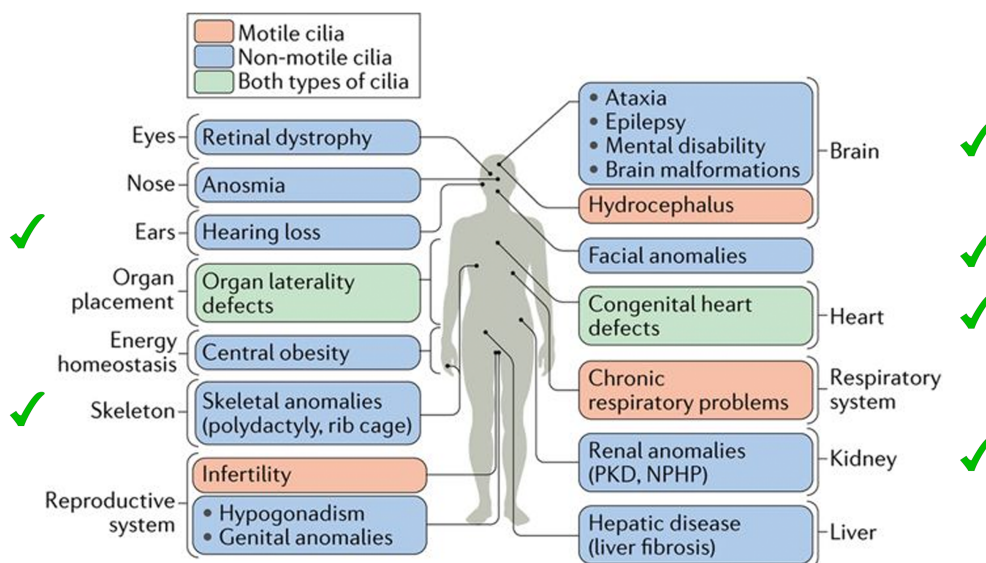
**Figure I 3. Overlapping defects between ciliopathies and TBS.** Different organ systems or tissues are affected in diverse ciliopathies. Phenotypic manifestations of the disease in each organ are shown. Ciliopathies that are caused primarily by defects in motile cilia are shown in orange, those that result from defects in non-motile (primary) cilia are shown in blue and those associated with defects in both types of cilia are shown in green. TBS symptoms overlapping with those of ciliopathies are marked with a green tick according to (Kohlhase, 1993). NPHP, nephronophthisis; PKD, polycystic kidney disease. Figure adapted from (Reiter and Leroux, 2017).

### 1.2.1 Cilia structure and formation

Cilia are microtubule-based organelles that emerge from centriole-containing basal bodies. Centrioles together with their surrounding matrix, the pericentriolar material, form the centrosome (**Figure I 4A**). Once anchored to the plasma membrane, centrioles behave as basal bodies giving rise to two different kinds of cilia: motile cilia (or flagella) (**Figure I 4B**) or immotile cilia (or primary cilia) (**Figure I 4C**). Cilia assembly and disassembly are accurately coordinated during the cell cycle (Gilula and Satir, 1972; Sorokin, 1962). Centrosomal duplication starts during the S-phase of the cell cycle when procentrioles form at the proximal end of both mother and daughter centrioles **(Figure I 5).** In the G2-phase the procentrioles elongate, mature and during mitosis they migrate to polar ends of the cell to nucleate and organise microtubules
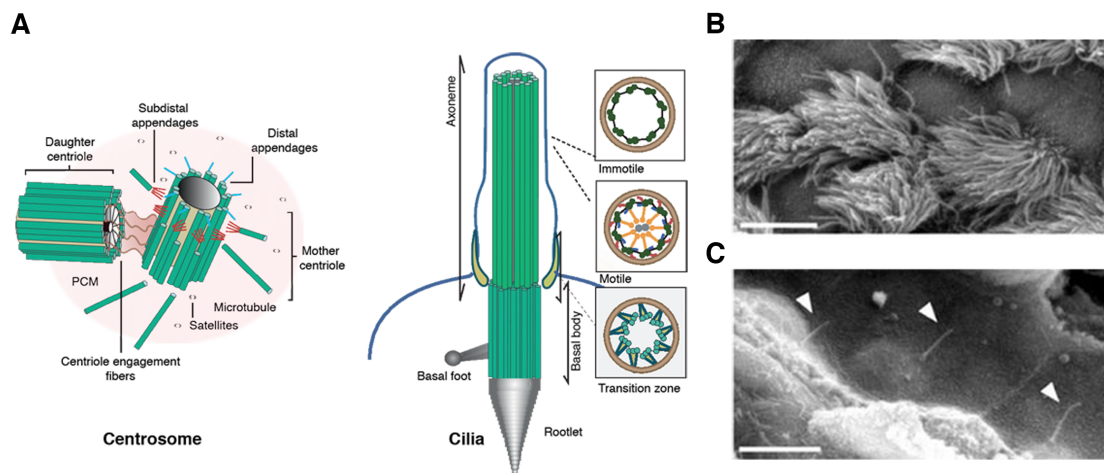
**Figure I 4. Centrosome and cilia structure.** (**A**) Centrosome and cilia are composed of centrioles. Each centrosome comprises a mother and daughter centriole in a barrel-shaped configuration and surrounded by a matrix of proteins called the pericentriolar material (PCM). The older centriole (mother) has subdistal appendages, where microtubules are docked, and distal appendages, which are important for docking to the plasma membrane. Satellites are granular structures surrounding the centrosome that are implicated in the trafficking of material involved in centriole assembly. Once anchored to the plasma membrane, the centriole, called the basal body at this point, starts nucleating cilia. The skeleton of cilia, known as the axoneme, is composed either of nine microtubule doublets with no dynein arms or central pair (as in most immotile cilia) or of nine microtubule doublets with dynein arms and a central microtubule pair (as in most motile cilia). The distal part of the basal body is the transition zone, where the outer tubule stops growing. During centriole to basal body differentiation, the acquisition of specialised structures, such as rootlets, basal feet and transitional fibers, provides mechanical support to the cilia, anchoring the basal body to the apical cytoskeleton and serving as platforms for the docking of ciliary components, respectively. Image adapted from (Bettencourt-Dias et al., 2011). (**B**) Scanning electron micrograph showing numerous motile cilia protruding from epithelial cells of a mouse trachea. (**C**) Scanning electron micrograph showing solitary primary cilia (white arrowheads) projecting from mouse renal epithelial cells lining the nephron. Scale bar = 5μm. Modified after (Green and Mykytyn, 2010).

to form the mitotic spindle. The centrioles attach to chromosomes and have a role in their segregation in the process of mitosis. Each of the newly formed daughter cells retains one of the centrosomes following cytokinesis. Only upon completion of mitosis and cytokinesis, mainly in G0 phase, the centrosomes are free to mature into the basal body and form primary cilia (Rezabkova et al., 2016). However, some reports described the presence of cilia throughout the cell cycle with the exception of
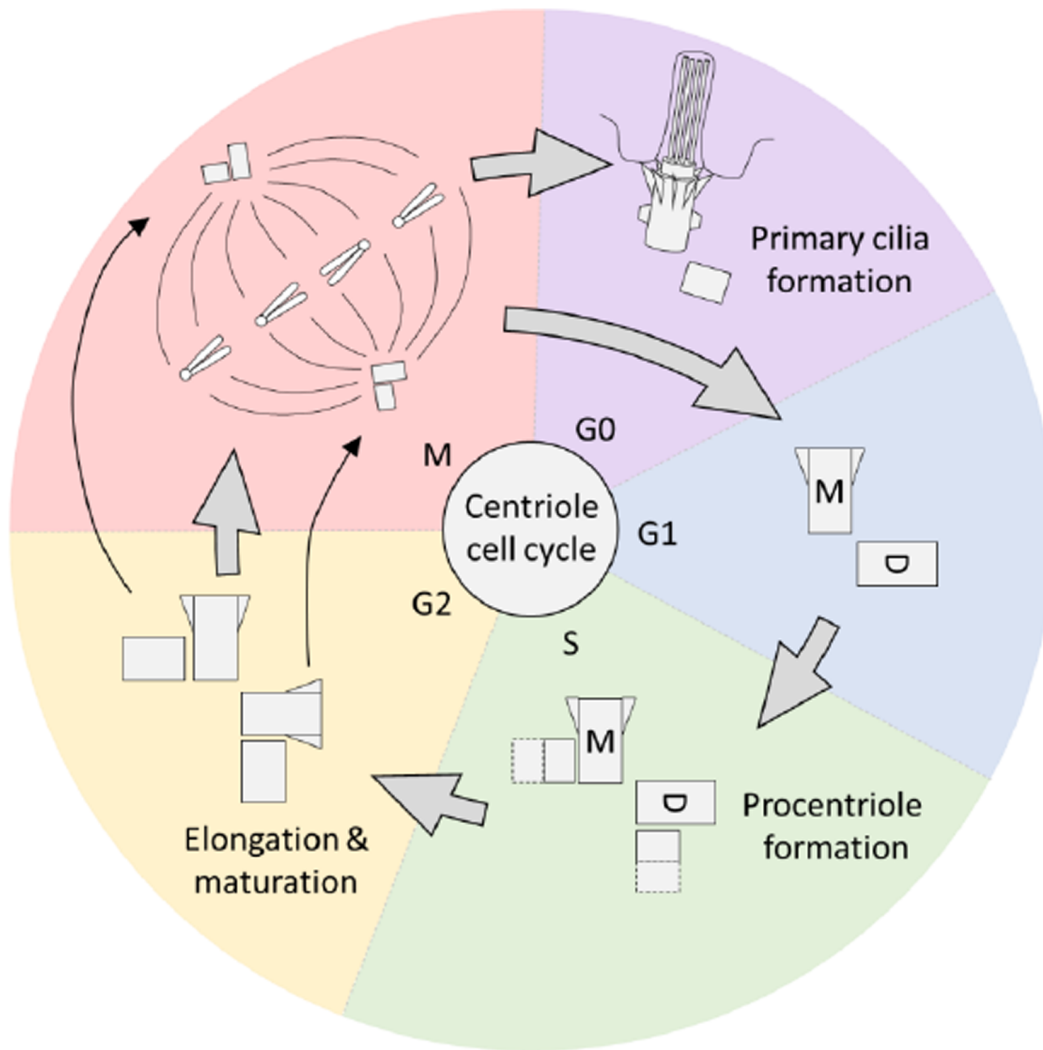
**Figure I 5. The centrosome cell cycle.** During S phase both mother (M) and daughter (D) centrioles form procentrioles. During G2 the procentrioles elongate and mature and upon transition into mitosis (M phase) they separate to form the spindle poles leading to equal division of the genetic material. In G0/G1 the centrioles are able to mature, form the basal body and assemble a primary cilium. Image adapted from (Nigg, 2002).

mitosis (Dingemans, 1969; Fonte et al., 1971; Ford et al., 2018) suggesting they are actively assembled and disassembled in response to mitotic signals.

## A. Key steps in cilia initiation

The initiation of primary cilia formation (or ciliogenesis) is the basal body consisting of a mother (MC) and a daughter centriole (DC). The basal body matures and becomes surrounded by the pericentriolar material composed of specialized

proteins that attach directly to the centrioles or nearby as satellite structures. During maturation, the centrioles also migrate to the plasma membrane where the MC "docks". This membrane-associated MC acquires three characteristic features: rootlets, basal feet and transition fibers, serving the last ones as connection between the centriole and the plasma membrane (Anderson, 1972). During the process of docking, before the centrosome becomes fully associated with the plasma membrane, the distal tip of the MC recruits and docks small vesicles originating from the Golgi apparatus that fuse to form a cap known as the ciliary vesicle (**Figure I 6)**.
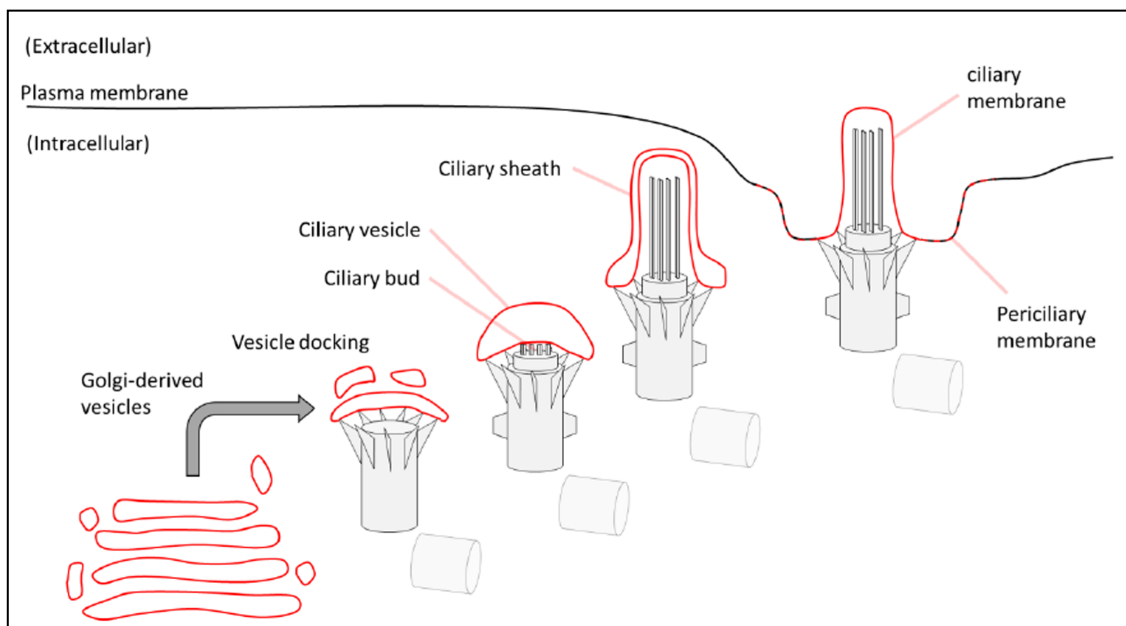


**Figure I 6. Schematic illustration of primary cilia formation.** Golgi-derived vesicles dock with distal appendages to form the ciliary vesicle and begin axonemal elongation. The ciliary sheath surrounding the growing axoneme fuses with the plasma membrane to form the primary cilium.

Microtubules start to elongate from the centriole and invaginate the vesicle into a mushroom shape, known as the ciliary bud. The microtubules continue to elongate forming the ciliary sheath. Eventually the ciliary sheath fuses with the plasma membrane allowing the primary cilium to emerge from the cell covered in the ciliary membrane (Sorokin, 1962). Cilia continue to elongate and become highly specialized with proteins trafficking along the microtubules and transmembrane proteins become embedded in the ciliary membrane. Cilia assembly is tightly

controlled through a balance of essential proteins (e.g. elements contributing to structure and transport to/from/inside the cilia) and negative regulators.

## B. The cilia negative regulators CCP110 and CEP97

Two of the most relevant proteins in the process of cilia formation are CCP110 and CEP97. Removal of these inhibitory capping proteins from the MC has been proposed as a key initiator of ciliogenesis (Bettencourt-Dias and Carvalho-Santos, 2008; Bettencourt-Dias et al., 2011; Kobayashi et al., 2011; Sanchez and Dynlacht, 2016; Tsang and Dynlacht, 2013). Previous studies demonstrated that TTBK2, MARK4, and Centrin2 are required for CCP110 and CEP97 depletion (Goetz et al., 2012; Kuhns et al., 2013; Prosser and Morrison, 2015) and some miRNAs affect ciliogenesis by controlling the expression levels of CCP110 (Cao et al., 2012; Song et al., 2014). It has been recently demonstrated that the ubiquitin-proteasome system controls serum-starvation-induced CEP97 degradation leading to CCP10 removal and ciliogenesis (Nagai et al., 2018). Their results showed that both CCP110 and CEP97 are required for their co-recruitment to the centrioles and that CEP97 appears to play a dominant role in controlling the stability of the CCP10-CEP97 complex on the centrioles. While some studies demonstrated that removal of CCP110 was sufficient to induce ectopic cilia formation (Spektor et al., 2007; Tsang et al., 2008), others reported that its depletion promoted abnormal elongation of non-docked centriolar microtubules (Franz et al., 2013; Schmidt et al., 2009). A recent publication suggested a dual and context-dependent role of CCP110 in cilia formation relying on the proteins interacting with CCP110 in a determined subcellular environment (Yang et al., 2016).

## 1.2.2 Primary cilia function

As previously mentioned, cilia within the mammalian body are generally classified as either motile or primary. Motile cilia are mainly responsible for generating flow or movement and include respiratory cilia, ependymal cilia, oviduct cilia and sperm flagella. On the other hand, non-motile or primary cilia are present in

most vertebrate cells (Wheatley, 1995) and function principally as sensory organelles. However, these functional classifications are not mutually exclusive, as some types of primary cilia on the embryonic node are motile and generate flow across the node establishment of the left right asymmetry axis and motile respiratory cilia also possess sensory functions (Bloodgood, 2010; Nonaka et al., 1998; Shah et al., 2009). Further, primary cilia lack radial spokes and the central axoneme surrounding the central microtubule pair present in motile cilia (Satir and Christensen, 2008).

### A. Primary cilia-mediated signalling: Shh pathway

Significant advances have revealed the crucial role of primary cilia in cell signalling, polarity and protein trafficking. During development, several key pathways (Hedgehog, Wnt, TGFbeta) are dependent or influenced by primary cilia function. Specifically, the vertebrate Sonic Hedgehog (Shh) pathway is crucial for vertebrate digit patterning and fully dependent on primary cilia (Huangfu et al., 2003; Yin et al., 2009).

The generally accepted model of Shh signalling in mammals is summarized in **Figure I 7**. In unstimulated cells, the inhibitory transmembrane receptor, Patched1 (Ptch1), localises at the base of the cilium. Here it exerts a repressive effect on the seven-pass transmembrane protein Smoothened (Smo) that is found in vesicles in the cytoplasm (Rohatgi et al., 2007). In this inactivated state, members of the glioma-associated oncogene (Gli) family are bound to Suppressor of Fused (SuFu), which is thought to inhibit their nuclear translocation (Ding et al., 1999). In addition, some Gli proteins are proteolytically processed into short repressor forms (Gli-R), which then translocate to the nucleus where they directly repress transcription of Shh-target genes (Wang et al., 2000a). This proteolytic processing is initiated by the activity of protein kinase A (PKA) which targets it for proteosomal degradation (Wang et al., 2000b). The Gli-SuFu complex is trafficked through the ciliary axoneme but it has been suggested that PKA activity on Gli occurs at the basal body after its exit from the cilium (Tuson et al., 2011). In the unstimulated state, the kinesin Kif7 has also been shown to localise at the basal body where it is thought to form a complex with Gli proteins and promote the formation of Gli-R and limit their accumulation in the
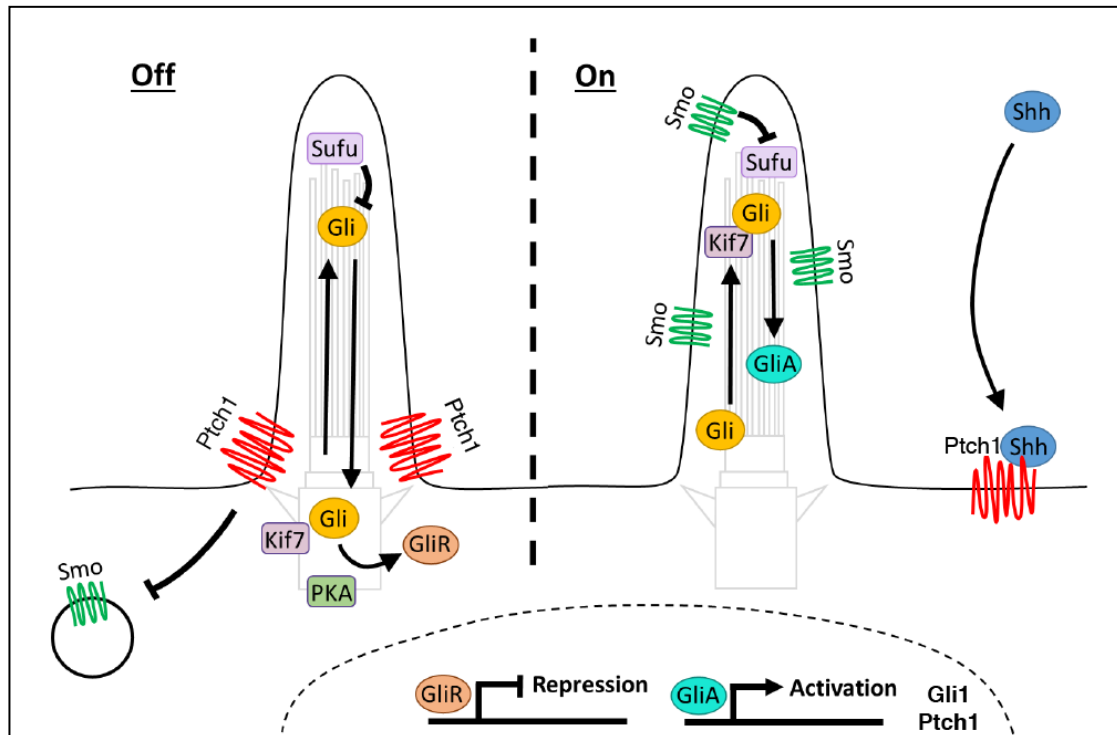
**Figure I 7. The Hedgehog signalling pathway.** In the 'Off' state, Ptch1 is found at the base of primary cilia and has a repressive effect on Smo present in cytoplasmic vesicles. SuFu acts as an inhibitor, preventing the nuclear translocation of Gli. Gli protein is also proteolytically processed into short repressor forms (Gli-R) through protein kinase A (PKA) to repress Shh target gene transcription. Kif7 forms a complex with Gli to prevent its accumulation in the cilia axoneme. In the 'On' state, Shh can bind to Ptch1 to release its repression on Smo. This allows Smo, Kif7, Gli and Sufu to accumulate in the primary cilia. Smo inhibits the action of SuFu and active Gli. Gli-A is able to translocate to the nucleus to activate Shh target gene transcription. Image adapted from (Goetz & Anderson, 2010).

axoneme (Liem et al., 2009). Upon activation, the binding of the Shh ligand to the transmembrane receptor Ptch1 abolishes the inhibitory effect of Ptch1 on Smo. Following the loss of Ptch1 activity, Smo is enriched in the cilia where, through SuFu inhibition, it is able to transduce a signal via *Gli* transcription factors to the nucleus that initiate expression of Shh target genes. Kif7 also translocates into the cilia axoneme and promotes the accumulation of SuFu and Gli in the cilia tip (Goetz and Anderson, 2010). There are three *Gli* transcription factors, Gli1-3, where Gli1 functions as a constitutive activator (Hynes et al., 1997; Liu et al., 2005). In contrast, Gli2 and Gli3 have an N-terminal transcriptional repressor domain and a C-terminal transcription activator domain. The translocation of Smo to the cilia leads to the

proteolytic events that convert Gli3 from a repressor (Gli3-R) into an activator (Gli3-A), promoting the activation of Shh target genes (Huangfu and Anderson, 2006; Pan et al., 2006). Two such genes are *Gli1* and *Ptch1,* encoding the Shh receptor and a transcriptional activator, respectively.

The trafficking of these multiprotein complexes through primary cilia is tightly regulated by several anterograde and retrograde systems called the intraflagellar transport (IFT) machinery (Behal and Cole, 2013; Pigino et al., 2009). Mutations in genes that encode IFT proteins deregulate Shh signalling and result in limb formation and neural tube closure defects, similar phenotypes to those observed in mutations of genes encoding Shh pathway components (Cabrera et al., 2004; Corbit et al., 2005; Haycraft et al., 2005).

## B. Shh function as a morphogen

*Shh* acts both as a mitogen by influencing cell proliferation and as a morphogen, inducing distinct molecular responses at distinct concentrations (McMahon et al., 2003). The best understood functions of *Shh* as a morphogen are in the patterning of the neural tube and limb bud. During mouse development, the expression of *Shh* in the notochord of the developing neural tube results in a gradient of *Shh* (highest at the notochord and the floor plate, FP) determining the different ventral neuron fates in a gradient and time-dependent manner (**Figure I 8A**) (Ribes and Briscoe, 2009; Wong and Reiter, 2008). As a consequence, dorsal neural subtypes are largely expanded into the ventral neural tube in *Shh* deficient mutants (Chiang et al., 1996). The neural tube is formed from an initially flat sheet of neuroepithelial cells whose edges roll up and fuse to form a tube in aprocess termed neural tube closure. (Colas and Schoenwolf, 2001). Together with the planar cell polarity/Wnt pathway, the Shh pathway, which relies on the presence of functional cilia, regulates neural tube closure and patterning (Campbell, 2003; Copp, 2005; Fuccillo et al., 2006). Another well-characterized example of Shh activity is its role in the limb bud patterning, where its expression in the zone of polarizing activity (ZPA) establishes an anterior to posterior concentration and temporal gradient specifying digit type and number (**Figure I 8B**). Cells localized in the close proximity of the ZPA are exposed to

higher concentrations of Shh for a longer period of time and are specified to form digit #5 (little finger). In contrast, cells at the anterior side are exposed to low Shh and are specified to form digit #1 (thumb). $Shh^{-/-}$ mutants form only a single digit (Chiang et al., 2001).
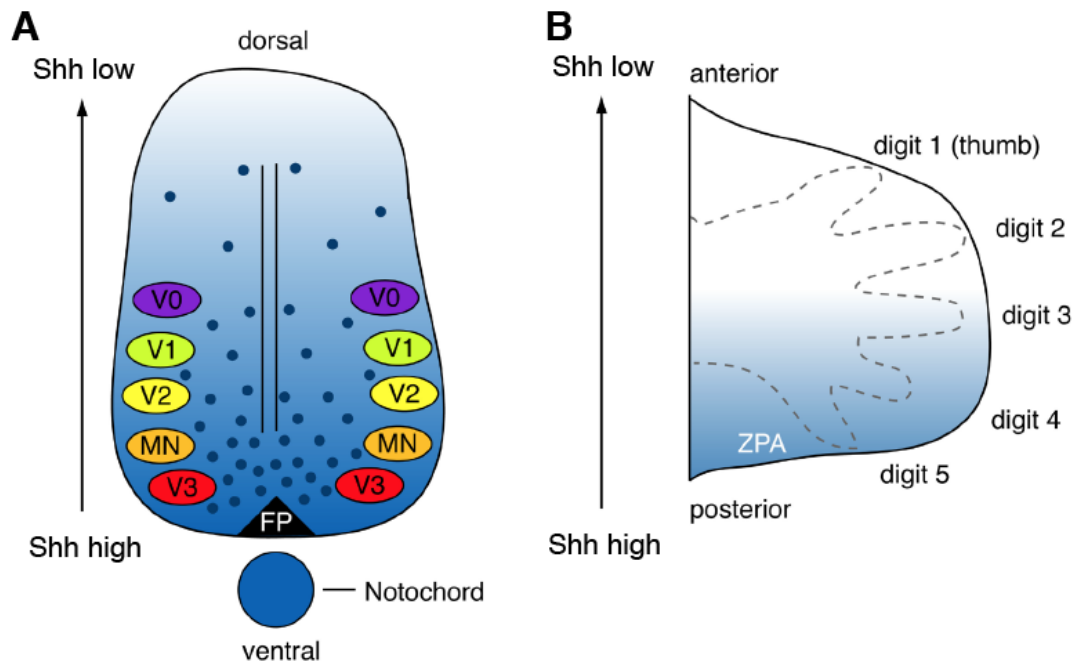


**Figure I 8. Hedgehog gradients during development.** (**A**) During neural tube development, Shh is secreted from the floor plate (FP) and the notochord to stablish a ventral [V] to dorsal concentration gradient leading to a spatially restricted expression profile of various transcription factors. The unique combination of transcription factors leads to the formation of neural progenitor cells along the dorsal/ventral axis, which generates V0-V3 interneurons and motorneurons (MN). (**B**) The production of Shh in the zone of polarizing activity (ZPA) establishes a posterior to anterior concentration gradient specifying digit identity and number in the developing vertebrate limb bud. Not only the spatial, but also temporal establisment of the Shh gradient is important. Figure adapted from (Harfe et al., 2004).

### 1.2.3 Primary Cilia and human disease

Ciliopathies are a group of phenotypically heterogeneous diseases that can affect almost all organs, reflecting the near ubiquity of primary cilia in human cells and highlighting the important functions of this organelle in diverse cell types. It has been predicted that over 100 known conditions fall into this category with only a few studied to date. The characteristic spectrum of overlapping phenotypes in ciliopathies that include polydactyly, cystic-fibrotic kidney, congenital heart diseases, skeletal anomalies, situs inversus, retinal degeneration, brain problems and hepatic fibrosis are caused by mutations that lead to cilia formation or function defects (**Figure I 3**). Due to the overlapping with TBS and their recurrence in the disease, polydactyly and polycystic kidney disease and their association with primary cilia will be further explained.

### A. Polydactyly

Importantly, defective Shh signalling can explain several of the phenotypes that characterize the ciliopathies such as polydactyly. It has been reported that ablation of the IFT kinesin *Kif3a* in the developing limb leads to aberrant Shh signalling and results in polydactyly and altered digit patterning (Haycraft et al., 2007). When *Kif7*, another kinesin required for generating Shh signalling response, is depleted mice display phenotypes such as polydactyly that are associated with compromised Gli3-R function. The role of *Gli* genes in development was first revealed by the discovery of deleterious mutations of *GLI3* in several human congenital malformations, including Pallister-Hall syndrome (Kang et al., 1997), mainly characterized by polydactyly and craniofacial features. Loss-of-function, as well as dominant-negative mutations in *GLI2*, have also been identified in patients with holoprosencephaly-like features and pituitary anomalies but not with limb defects (Roessler et al., 2003; Roessler et al., 2005). However, *GLI1* mutations have not yet been reported in human congenital malformations. Of note, polydactyly and triphalangeal thumb are also present in TBS patients and in the TBS model adult mice *Sall1$^{tg/tg}$* (**Figure I 9**). These genotype-phenotype correlations and molecular analyses demonstrate the crucial role of Shh, and by extension, the primary cilia function and regulation in limb development.
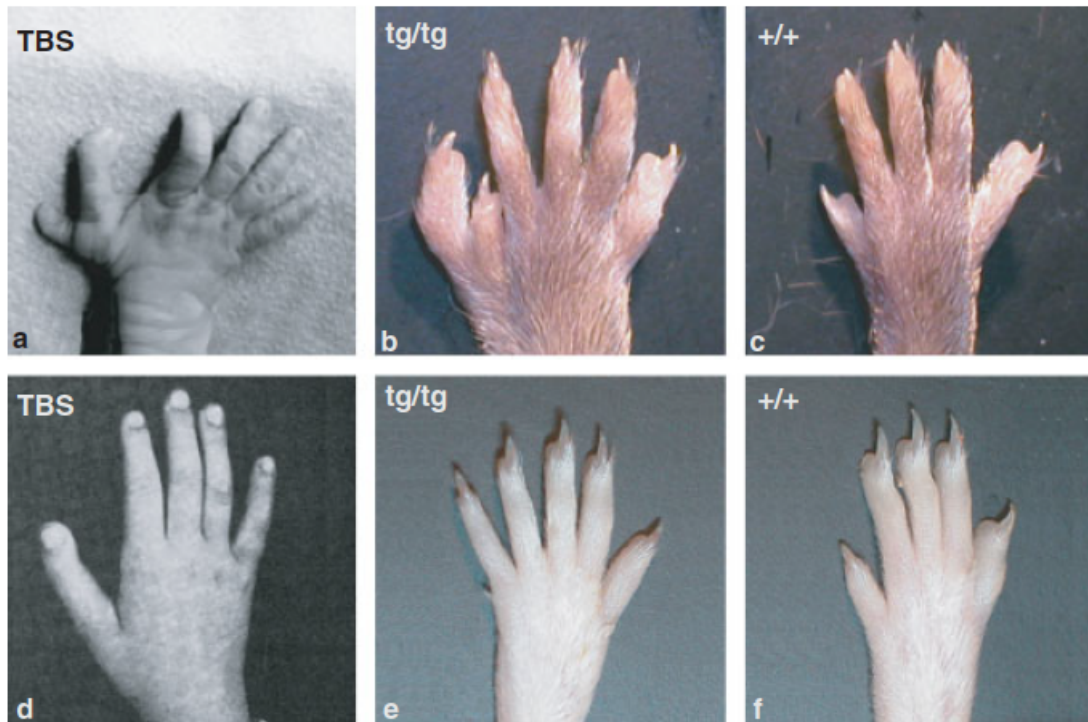
**Figure I 9. Limb defects in TBS individuals and model mice**. (**a**,**d**) Patients exhibit preaxial polydactyly (**a**) and triphalangeal thumb (**d**). (**b,c,e,f**) These defects are also found in mice homozygous for a mutated *Sall1* transgene in the limb, *Sall1*$^{tg/tg}$ (**b**,**e**), but not in littermate controls *Sall1*$^{+/+}$ (**c**,**f**). Taken and reprinted in (Kiefer, Robbins, Barina, Zhang, & Rauchman, 2008) with permission from (Powell & Michaelis, 1999) and (Kurnit, Steele, Pinsky, & Dibbins, 1978).

## B. Polycystic kidney disease

One of the first diseases to be related to dysfunctional primary cilia was the polycystic kidney disease (PKD) when the gene encoding the Ift88/Tg737/Polaris protein in the Oak Ridge Polycystic Kidney mouse (ORPK mouse, or currently named Ift88$^{Tg737Rpw}$) was mutated. Both in Chlamydomonas and in mice, *Ift88* mutants showed defective ciliogenesis (Moyer et al., 1994; Pazour et al., 2002). In the case of the mouse kidney, cilia were also abnormally short or missing, which suggested that PKD was a cilia-related disease (Pazour et al., 2000). The resultant phenotype resembles that of human autosomal recessive polycystic kidney.

Primary cilia project from the apical surface of epithelial cells along the nephron tubule and collecting ducts, in contact with urine flow. In the adult kidney,

cilia act as sensory antennae that respond to modifications of urine flow, composition, and osmolality by modulating important intracellular signalling pathways. For instance, polycystin-1 and −2, the two proteins mutated in autosomal-dominant polycystic kidney diseases (ADPKD), were found to regulate urine-flow dependent signalling pathways, such as Shh (Saigusa and Bell, 2015). Likewise, mutations in ciliary proteins such as inversin or nephrocystin-3, which cause nephronophthisis (NPH), alter the balance between canonical and non-canonical Wnt pathways that is crucial to regulate the correct polarity of epithelial tubular cells, thus explaining the pathogenesis of cyst formation (Lienkamp et al., 2012). In contrast to polycystic kidney disease that typically presents enlarged kidneys and massive cysts, nephronophthisis (NPHP) rather presents shrunken, or normal sized, fibrotic kidneys and small cysts at the cortico-medullary junction. The renal phenotype of NPHP frequently occurs in a syndromic manner and is accompanied by anomalies in other organ systems, specifically retinal degeneration, cerebellar vermis hypoplasia, hepatic fibrosis, skeletal anomalies, ectodermal dysplasia, brain malformations, and neurological impairment. Of note, numerous small and, on occasion, large cysts covered the kidney surface of some TBS model adult mice (**Figure I 10**) (Kiefer et al., 2003). All these data imply that there is a connexion between ciliary dysfunction and cystic kidney disease.
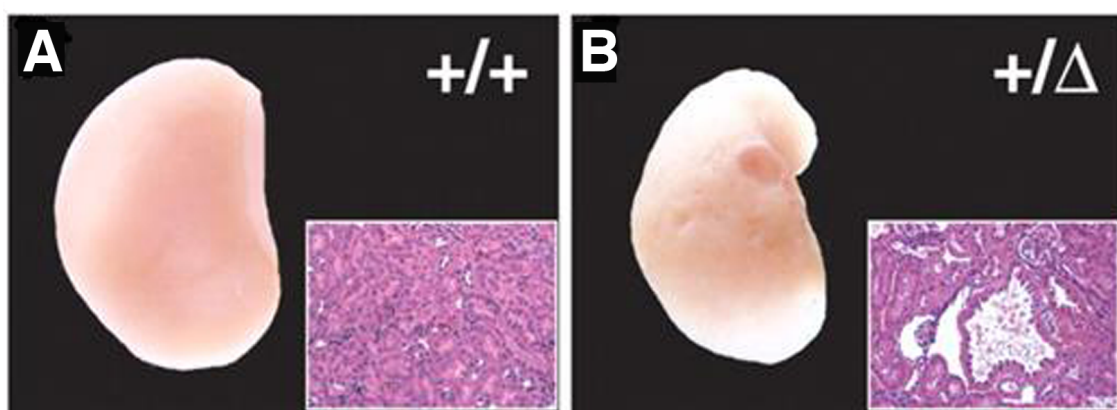


**Figure I 10. Kidney defects in the TBS model mice *Sall1*$^{+/\Delta}$.** Some *Sall1*$^{+/\Delta}$ mice showed cystic and hypoplastic kidneys with dilated renal tubules (**B**) that were never observed in their wild-type littermates *Sall1*$^{+/+}$ (**A**). Figure taken from (Kiefer et al., 2003).

## 1.3 The actin cytoskeleton

Actin is one of the most abundant proteins in cells and plays crucial roles in cytokinesis during cell division, protrusion of the leading edge of motile cells and maintaining the physical integrity of the cell (Pollard and Cooper, 2009). Its implication in primary cilia dynamics is an emerging trend in the field.

### 1.3.1 Actin structure, assembly and dissasembly

Actin monomers (glomerular or g-actin) polymerize into dimmers, trimers and finally double helical polymers with all of the subunits oriented in the same direction to form filamentous actin (F-actin) (**Figure I 11A**).
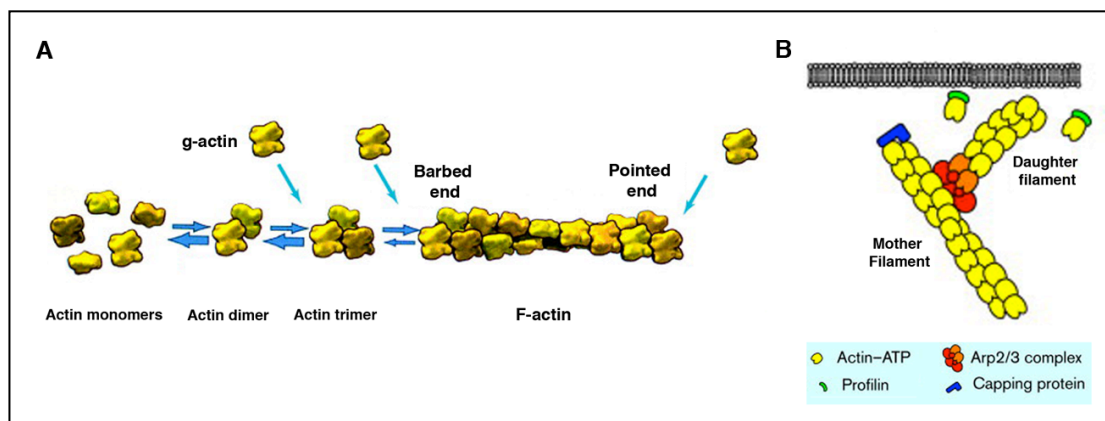


**Figure I 11. Actin polimerization.** (**A**) Actin monomers (g-actin) combine to form dimers and trimers, which can elongate rapidly from both its 'barbed' and 'pointed' ends to give rise to filamentous actin (F-actin).Figure adapted from (Amann & Pollard, 2001). (**B**) Arp2/3 complex nucleates a new actin filament (daughter filament) growing from its barbed end at a 70° angle from the mother filament. Figure adapted from (Amann & Pollard, 2001).

Based on decoration with myosin heads, one end of the filament is called the barbed end and the other, the pointed end. Myosin and many other proteins act synergistically to regulate every aspect of actin dynamics. These proteins (i.e profilin) maintain a pool of unpolymerized actin monomers to grow filaments when needed, nucleate actin filaments, promote elongation, terminate the elongation of actin

filaments by capping, sever actin filaments, and crosslink filaments into tertiary structures.

Two factors that appear to play an essential role in regulating actin polymerization are the Arp2/3 complex and ADF/cofilin, thereafter referred to as cofilin. The spontaneous nucleation of filaments by actin monomers is unfavorable and profilin suppresses nucleation. As a consequence, cells use other proteins to initiate new actin filaments such as the Arp2/3 complex. On the other hand, cofilin promotes the actin severing that leads to actin turnover.

## A. The Arp2/3 complex

The Arp2/3 complex consists of two actin-related proteins, Arp2 and Arp3, together with five other protein subunits (Machesky et al., 1994). The Arps prime the new filament formed as a branch of an existing actin filament called the mother filament (Rouiller et al., 2008) (**Figure I 11B**). The complex assembles networks of branched actin filaments (Mullins et al., 1998) for cellular motility (Pollard and Borisy, 2003) and endocytosis (Weinberg and Drubin, 2012). To be activated, the Arp2/3 complex requires proteins called nucleation-promoting factors to favor the conformational change and the formation of a daughter filament (Machesky et al., 1999). Nucleation-promoting factors (Campellone and Welch, 2010) include the Wiskott-Aldrich syndrome protein (WASP) and related proteins with V motifs that bind actin monomers, and CA motifs that bind Arp2/3 complex (Marchand et al., 2001). Another nucleation-promoting factor, cortactin, stabilizes actin filament branches (Weaver et al., 2001), while tropomyosin bound to the mother filament inhibits branch formation (Blanchoin et al., 2001).

## B. Cofilin

Hydrolysis of the ATP bound to polymerized actin and dissociation of the phosphate prepare the filament for disassembly. The main player to promote actin filament turnover and F-actin severing is cofilin, a small protein that binds ADP-actin monomers and filaments with higher affinity than ATP-actin and that is inactivated when phosphorylated (Blanchoin and Pollard, 1999). Actin filaments saturated with cofilin are very stable (Andrianantoandro and Pollard, 2006). On the other hand, filaments sparsely occupied with cofilin are severed rapidly because of instability

between parts of the filament with different flexibilities (Elam et al., 2013a; Elam et al., 2013b; Ngo et al., 2015). Sparse occupancy occurs constantly during the turnover of actin filaments, given that older parts are converted to ADP-actin and then bind cofilin. Severing by cofilin promotes turnover and filaments can regrow (Bravo-Cordero et al., 2013), but many are likely to be capped at their barbed ends.

The organization of the F-actin (as well as the microtubule) network and the formation of cell–matrix adhesions in response to extracellular stimuli are controlled by small GTPases of the Rho family (Etienne-Manneville and Hall, 2002). In their activated GTP-bound state, Rho GTPases can activate multiple downstream effector pathways. Both Rac1 and RhoA GTPases have been reported to activate a pathway that results in the inhibition of cofilin through phosphorylation at Ser3 (Edwards et al., 1999; Maekawa et al., 1999), but Rac1 is mostly linked to lamellipodia extension and the formation of nascent adhesions, whereas RhoA stimulates stress fiber formation and maturation of cell–matrix adhesions (Rottner et al., 1999). The activation of the Arp2/3 complex downstream of Rac initiates actin polymerization (**Figure R 12**). The increase in polymerized actin stimulates the phosphatase activity of the *slingshot homologue 1* phosphatase*,* SSH1, leading to cofilin dephosphorylation and consequential increase in its severing action. Active actin depolymerization by cofilin can then free up actin monomers for Arp2/3-dependent polymerization and a dynamic actin turnover of actin remodeling is achieved (Chiu et al., 2010).

## 1.3.2 The role of actin cytoskeleton in cilia-related processes

The regulation of actin dynamics is also considered a major ciliogenesis driver in cycling cells (Pitaval et al., 2010). Processes such as cilia initiation, elongation and maintenance or cell proliferation and migration are intrinsically linked to actin dynamics. Furthemore, genes involved in neural tube defects (NTD) such as *Abelson-related gene* (*Arg*) (Koleske et al., 1998), *Vinculin* (*Vcl*) (Xu et al., 1998) and *Shroom* (*Shrm*) (Hildebrand and Soriano, 1999) have a role in the actin cytoskeleton dynamics.
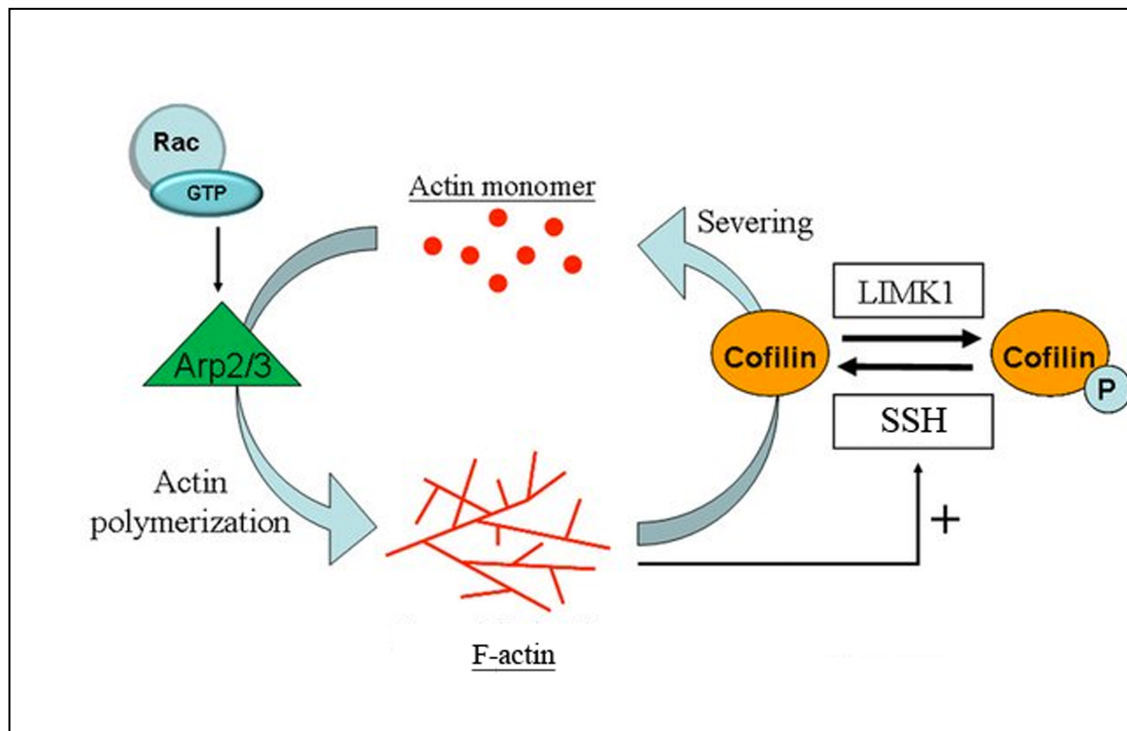
**Figure I 12. F-actin formation dynamics.** The formation of the remodeled actin is achieved by the polymerization activity of Arp2/3 acting downstream of active Rac. The accumulation of polymerized F-actin poses a stimulatory factor in the phosphatase activity of SSH (Slingshot homologue 1 phosphatase), which leads to net dephosphorylation and activation of cofilin. Hereon, the actin-severing function of cofilin maintains the flexibility of remodeled actin and enables regeneration of free monomeric actin for further polymerization. LIMK: LIM domain kinase 1. Scheme by (Chiu, Patel, Shaw, Bamburg, & Klip, 2010).

## A. Cilia initiation

Actin dynamics coordinate several processes that are crucial for ciliogenesis (**Figure I 13**). Placing the MC to the appropriate area at the cell cortex is an actin-dependent process (Euteneuer and Schliwa, 1985). After that, focal adhesion proteins anchor the basal body to the underlying actin cytoskeleton (Antoniades et al., 2014) followed by local removal of the actin (Francis et al., 2011) and the elongation of the axoneme.

After the basal body docking, a reduction in cortical actin might potentially promote ciliogenesis, as there would be no physical restriction to prevent cilium growth. Supporting this hypothesis, several studies have found that changes in the

actin network architecture, induced either chemically or genetically, promote ciliogenesis or affect cilia length (Drummond et al., 2018; Hernandez-Hernandez et al., 2013; Kang et al., 2015; Kim et al., 2015; Kim et al., 2010).
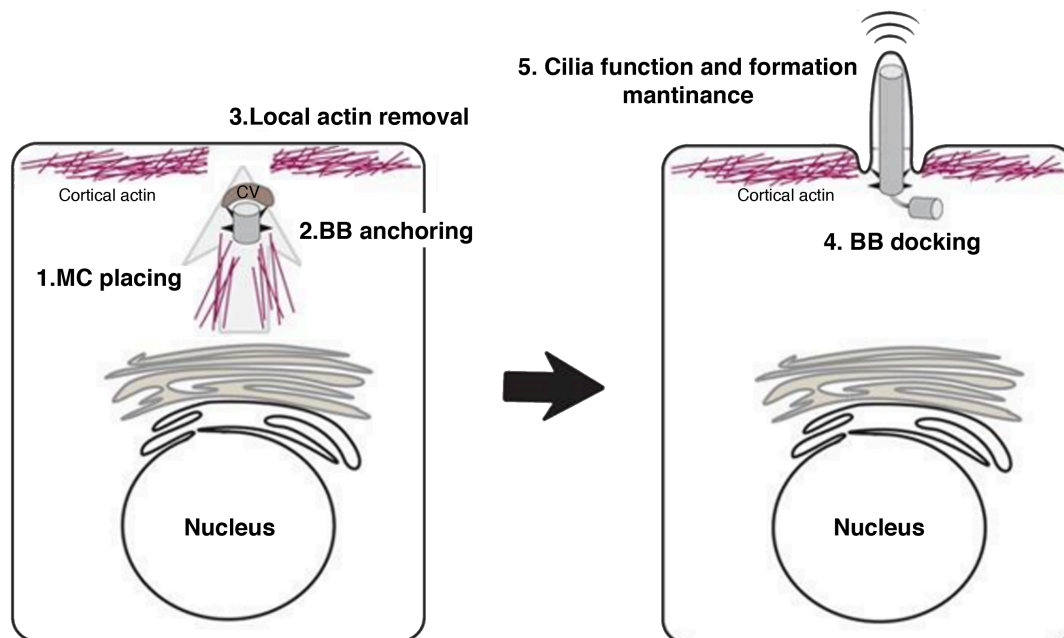


**Figure I 13. Diverse roles of cytoplasmic actin cytoskeleton in ciliogenesis.** Cellular actin and myosins mediate accumulation and fusion of vesicles to form the ciliary vesicle, mother centriole (MC) location to the cell cortex, basal body (BB) anchoring and docking to the apical surface, ciliary function and formation maintenance

## B. Cilia length

Interfering with actin dynamics through CytB has been demonstrated to promote ciliogenesis (Cao et al., 2012). How actin regulates cilium length is less clear. One hypothesis is that cortical actin stretches the ciliary necklace to prevent vesicle trafficking and anterograde transport to grow the ciliary shaft. Alternatively, actin may serve as a constricting force that promotes ectocytosis and cilium tip scission preventing the axoneme from growing too long (Nager et al., 2017; Phua et al., 2017). In the same way, actin surrounding the basal body might provide the relaxation or constriction to either allow or restrict the axoneme growth, respectively.

## C. Cell proliferation

During mitosis, the actin cytoskeleton must rearrange and localize to the cortical plasma membrane in early mitotic phases and to the contractile ring during cytokinesis (Heng and Koh, 2010). This recruitment of actin and actin regulatory proteins to the cell cortex during mitosis is essential for the interaction between astral microtubules and cortical actin, which is believed to be important in regulating mitotic spindle orientation (Rankin and Wordeman, 2010). The role of actin and its regulatory proteins in these processes ranges from regulating centrosome separation (Cao et al., 2010) to proper spindle assembly and orientation (Woolner et al., 2008) and to elongate kinetochore microtubules. Numerical and structural centriole aberrations can also perturb the formation and the function of cilia.

## 1.4 LUZP1

The leucine-zipper motif containing protein LUZP1 has been identified as a nuclear protein mainly expressed in the brain. In addition to three leucine zipper motifs located at the N-terminus, it contains three nuclear localization signals and a large number of putative Ser/Thr phosphorylation sites (Sun et al., 1996). Interestingly, mutations in *Luzp1* resulted in cardiovascular defects and cranial NTD (**Figure I 14**), demonstrating its crucial role in embryonic heart and brain development (Hsu et al., 2008; Lee et al., 2001; Sun et al., 1996). Remarkably, ectopic Shh signalling was observed in the dorsal lateral neuroepithelium of the NTD *Luzp*^{-/-} mice, suggesting that LUZP1 might have a role in Shh signalling (Hsu et al., 2008). In humans, specific mutations in *LUZP1* have not yet been reported. However deletions of chromosome 1p36, including the complete deletion of *LUZP1*, lead to the 1p36 deletion syndrome that affects approximately 1 in 5,000 newborns (Zaveri et al., 2014). The symptoms include developmental delay, intellectual disability, seizures, vision problems, hearing loss, short stature, distinctive facial features, brain defects, orofacial clefting, congenital heart defects, cardiomyopathy, and renal anomalies. Although the exact contribution of *LUZP1* in the pathogenesis of the 1p36 syndrome is unknown, it has been proposed to contribute to the development of the

cardiovascular malformations. In spite of the phenotypic overlaps and the Shh signalling defects observed in *Luzp1*^{-/-} mice, a link between LUZP1 and ciliogenesis, until this work had not been previously investigated.
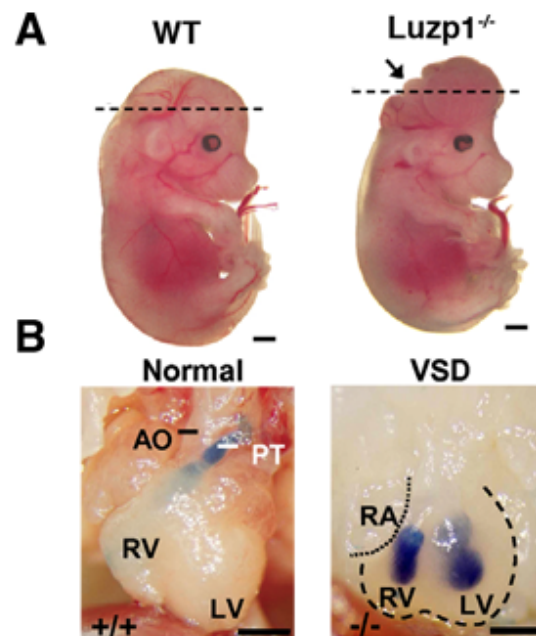


**Figure I 14. Cranial and cardiovascular defects in *Luzp1*^{-/-} mutant embryos.** (**A**) Exencephaly (black arrow) was visible in 42 % of the *Luzp1*^{-/-} but not in WT embryos. Dotted lines indicate the open neural tube from midbrain to hindbrain at E9.5. (**B**) Ventriculoarterial connection is revealed by inserting blue dye into the right ventricle (RV) of neonate pups. In WT, dye flows from RV to only the pulmonary trunk (PT). One of the three types of connection defects that are present in *Luzp1*^{-/-} pups is ventricular septal defect (VSD, right pannel) where dye pours into the left ventricle (LV) before entering the great arteries. AO: aorta. RA: right atrium. Scale bar: 1 mm. Image adapted from {Hsu, 2008 #115}.

# Chapter 2: Hypothesis and Objectives

## 2.1 Hypothesis

TBS is an autosomal dominant genetic disease caused by mutations in *SALL1* (Botzenhart et al., 2007; Kohlhase et al., 1998) that in most of the cases lead to the expression of SALL1 truncated proteins. Although the genetic cause of TBS is well defined, the cellular and molecular mechanisms mediating TBS are still undefined. TBS is characterized by the presence of imperforate anus, dysplastic ears, thumb and heart malformations, and renal impairment, among other symptoms. Intriguingly, these features are commonly reported in a variety of diseases, collectively known as ciliopathies, caused by defects in the primary cilia formation or primary cilia-dependent signalling (Hildebrandt et al., 2011). Depending on the underlying mutation, ciliopathies present a broad spectrum of phenotypes, ranging from cystic kidneys to polydactyly, obesity and heart failure. These coincidental features could suggest similar molecular causes between ciliopathies and TBS, but a characterization of primary cilia formation and function has not been yet reported for TBS. Therefore, **we hypothesized that defects in primary cilia formation and/or function might be contributing factors in TBS.**

---

**Hypothesis**

**SALL1** has a **role in primary cilia formation and function** that might contribute to the etiology of TBS. Specifically, **truncated SALL1** might **interphere** with **cilia formation and/or Shh signalling**, leading to TBS.

---

## 2.2 Objectives

In order to prove this hypothesis, we proposed as a **general objective** to **study the cellular and molecular mechanisms mediating TBS**. In particular, we defined the following specific aims:

**1. To analyse the role of SALL1 in cilia formation and function.**

We obtained TBS patient-derived cells and generated TBS-model cell lines to analyse the effect of SALL1 truncations on cilia formation and cilia function.

**2. To identify the cellular and molecular mechanisms mediating the cilia defects observed in TBS.**

In order to identify candidate proteins that might mediate the cilia-related aberrations detected in TBS, we employed the BioID method to identify potential SALL1 interactors. Some promising centrosome and/or cilia-related candidates were further characterized in the context of TBS.

# Chapter 3: Materials and Methods

## 3.1 Cell culture

Human control and TBS-derived primary fibroblasts, mouse embryonic fibroblasts (MEF), U2OS (ATCC HTB-96), HEK 293FT (Invitrogen) and mouse Shh-LIGHT2 cells (Taipale et al., 2000) were cultured at 37°C and 5% $CO_2$ in Dulbecco's modified Eagle medium (DMEM) supplemented with 10% fetal bovine serum (FBS, Gibco) and 1% penicillin/streptomycin (Gibco). Mouse IMCD3 (Inner Medullary Collecting Duct-3) and human TERT-RPE1 cells (telomerase reverse transcriptase-retinal pigment epithelial 1, TCC CRL-4000) were cultured in DMEM:F12 (Gibco) supplemented with 10% FBS and 1% penicillin and streptomycin. Dermal fibroblasts carrying a *SALL1* c.995delC mutation (*SALL1[c.995delC]*), that produce a truncated protein p.Pro332Hisfs*10 (SALL1[332]), were derived from a male TBS individual OX3335 (TBS[332], herein) (Botzenhart et al., 2007; Furniss et al., 2007). Dermal fibroblasts carrying the *SALL1* pathogenic variant c.826C>T (*SALL1[c.826C>T]*), that produce a truncated protein p.Arg275* (SALL1[275] herein), were derived from a male TBS individual UKTBS#3 (TBS[275]) (Bozal-Basterra et al., 2018). Human neonatal foreskin fibroblasts (HFF; ATCC CRL-2429) and adult female dermal fibroblasts (ESCTRL#2) from healthy donors were used as controls. We derived MEFs from wild-type (WT) and three heterozygous embryos carrying the *Sall1-ΔZn2-10* mutant allele (Kiefer et al., 2003). All the embryos were at stage E13. WT and mutant alleles were detected by PCR genotyping using established methods. Cultured cells were maintained between 10 and 20 passages, tested for senescence by γ-H2AX staining, and grown until confluence (6-well plates for RNA extraction and Western blot assays; 10 cm dishes for pulldowns). Cells were treated with Cytochalasin B (CytB; Sigma, 20 μM) for 30 minutes to stimulate actin polymerization and with the proteasome inhibitor MG132 (Calbiochem, 5 μM) for 24 hours. Cells were transfected using calcium phosphate method, with the exception of primary fibroblasts (Lipofectamine 3000; Invitrogen). To induce primary cilia, cells were starved for 24 hours (DMEM, 0% FBS, 1% penicillin and streptomycin). In the case of HEK 293FT cells, we followed the conditions previously reported (Boldt et al., 2016). The use of human samples in this study was approved by the institutional review board (Ethics Committee at CIC bioGUNE) and appropriate informed consent was obtained from human subjects.

Work with mouse embryos to derive MEFs was approved by the University of Saint Louis. All experiments conform to the relevant regulatory standards.

## 3.2 SALL1 proximity proteomics

Using the BioID method (Roux et al., 2012) proteins in close proximity to SALL1 were biotinylated by fusion to a promiscuous form of the enzyme BirA (BirA*) and isolated by streptavidin-bead pulldowns (**Figure M 1**).
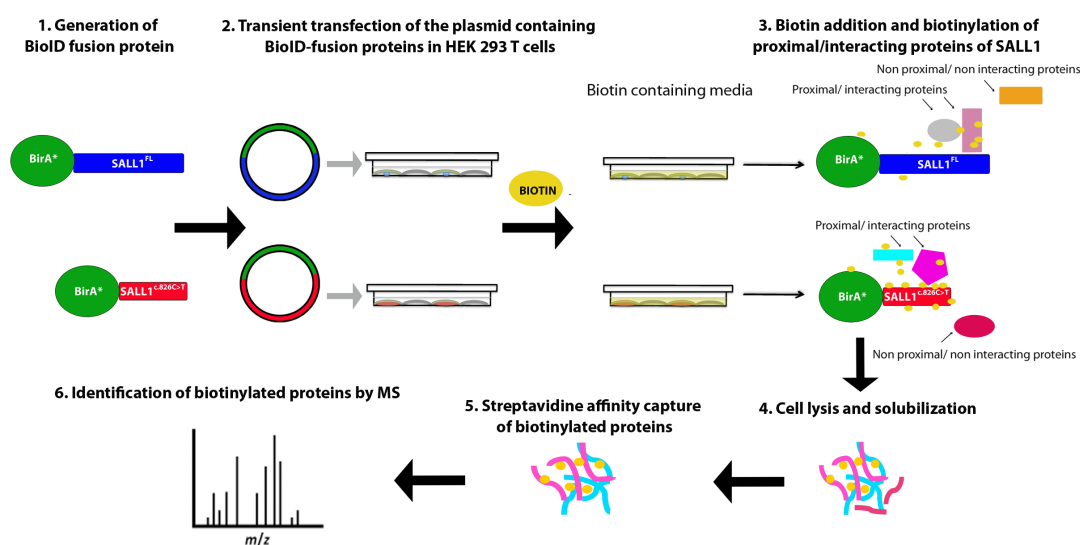


**M 1. Schematic representation of the BioID method.** Figure adapted from (Roux, Kim, Raida, & Burke, 2012). Only those proteins in close proximity to SALL1-BirA fusions will be labelled with biotin and captured by streptavidin"

*Myc-BirA\*-SALL1$^{c.826C>T}$* (BirA\*-SALL1$^{826}$) or *Myc–BirA\*-SALL1$^{FL}$* (BirA\*-SALL1$^{FL}$) were transfected in HEK 293FT cells (5x 10 cm dishes per condition). 24 hours after transfection, medium was supplemented with biotin at 50 µM. Cells were collected after 48 hours, washed 3 times on ice with cold phosphate buffered saline (PBS) and scraped in lysis buffer [8 M urea, 1% SDS, 1x protease inhibitor cocktail (Roche), 1x PBS; 1 ml per 10 cm dish]. At room temperature, samples were sonicated and cleared by centrifugation. Cell lysates were incubated overnight with 40 µl of equilibrated NeutrAvidin-agarose beads (Thermo Scientific). Beads were subjected to stringent washes using the following washing buffers (WB), all prepared in PBS: WB1 (8 M urea, 0.25% SDS); WB2 (6 M Guanidine-HCl); WB3 (6.4 M urea, 1 M NaCl, 0.2% SDS), WB4 (4 M urea, 1 M NaCl, 10% isopropanol, 10% ethanol and 0.2% SDS); WB5

(8 M urea, 1% SDS); and WB6 (2% SDS). For elution of biotinylated proteins, beads were heated at 99°C in 50 μl of Elution Buffer (4x Laemmli buffer, 100 mM DTT). Beads were separated by centrifugation (18000 x g, 5 minutes) or alternatively removed by centrifugation through a 0.8 μm filter (Vivaspin, Sartorius). Samples were used for mass spectrometry analysis as well as for western blotting to validate selected candidates.

## 3.3 Mass spectrometry

Three independent pulldown experiments were analysed by MS. Samples eluted from the NeutrAvidin beads were separated in SDS-PAGE and stained with Brilliant Blue G-Colloidal Concentrate (Sigma) according to manufacturer's instructions. The entire gel lanes were excised, divided into pieces and distained, and proteins were reduced and alkylated before being in-situ digested with trypsin. The resulting peptide mixtures were extracted, concentrated and analysed using and EASY nLC system (Proxeon). Peptide ionization was performed on a Proxeon ion source and sprayed directly into the mass spectrometer (Q-Exactive, Thermo Scientific). MaxQuant software (version 1.4.0.3) was used for the processing and analysis of recorded LC-MS/MS raw-files using default parameters applying a 1% false discovery rate at both peptide and protein levels. Label-free quantitation (LFQ) based on summed extracted peptide ion chromatograms was used for identifying differentially interacting proteins.

The lists of proteins identified by LC-MS/MS were analysed as follows: only proteins identified by more than 1 peptide and present in at least two out of the three experiments were considered for analysis. Protein IDs were ranked according to the number of peptides found and their corresponding intensities. Hits were classified into those that interact with both FL and truncated SALL1[275] or those interacting preferentially with one or the other. A threshold of two-fold change in iBAQ value (intensity-based absolute quantification) was considered significant. Calculation was done taking into account a baseline for each experiment, which corresponds to the minimum value of iBAQ registered for every specific sample.

Gene ontology (GO) term enrichment was analysed using g:Cocoa, a tool

integrated in the g:Profiler web server (Reimand et al., 2016). GO enrichment was obtained by calculating $-\log_{10}$ of the P-value.

## 3.4 GFP pulldowns

All steps were performed at $4^{o}$C. Transfected HEK 293FT cells were collected after 48 hours, washed 3 times with 1x PBS and lysed in 1 ml of lysis buffer [25 mM Tris-HCl pH 7.5, 150 mM NaCl, 1 mM EDTA, 1% NP-40, 0.5% Triton X-100, 5% glycerol, protease inhibitors (Roche)]. Lysates were kept on ice for 30 minutes vortexing every 5 minutes and spun down at 25,000 x g for 20 minutes. After saving 40 μl of supernatant (input), the rest was incubated overnight with 30 μl of pre-washed GFP-Trap resin (Chromotek) in a rotating wheel. Beads were washed 5 times for 5 minutes each with WB (25 mM Tris-HCl pH 7.5, 300 mM NaCl, 1 mM EDTA, 1% NP-40, 0.5% Triton X-100, 5% glycerol). Beads were centrifuged at 2,000 x g for 2 minutes after each wash. For elution, samples were boiled for 5 minutes at $95^{o}$C in 2x Laemmli buffer.

## 3.5 Immunoprecipitation

All steps were performed at $4^{o}$C. Cells were collected after 48 hours, washed 3 times with 1x PBS and lysed in 1 ml of lysis buffer [20 mM Tris-HCl pH 7.5, 137 mM NaCl, 2 mM EDTA, 1% NP-40, 5% glycerol, protease inhibitor mixture (Roche)]. Lysates were processed as described for GFP pulldowns. Lysates were incubated overnight with 1 μg of CCP110 or CEP97 antibody (Proteintech) and for additional 4 hours with 40 μl of pre-washed Protein G Sepharose 4 Fast Flow beads (GE Healthcare) in a rotating wheel. Beads were washed 5 times for 5 minutes each with WB (10 mM Tris-HCl pH 7.5, 137 mM NaCl, 1 mM EDTA, 1% Triton X-100). Beads were centrifuged at 2,000 x g for 2 minutes after each wash. For elution, samples were boiled for 5 minutes at $95^{o}$C in 2x Laemmli buffer.

## 3.6 Western blot analysis

Cells were lysed in cold RIPA buffer or weak buffer (10 mM PIPES pH 6.8, 100 mM NaCl, 1 mM EGTA, 3 mM $MgCl_2$, 300 mM sucrose, 0.5 mM DTT, 1% Triton X-100) supplemented with 1x protease inhibitor cocktail (Roche), and also in some cases with PhosphoStop 1x (Roche). Lysates were kept on ice for 30 minutes vortexing every 5 minutes and then cleared by centrifugation (25,000 x g, 20 minutes, $4^oC$). Supernatants were collected and protein contents were quantified by BCA protein quantification assay (Pierce). After SDS-PAGE and transfer to nitrocellulose or PVDF, membranes were blocked in 5% milk, or in 5% BSA (Bovine Serum Albumin, Fraction V, Sigma) in 1x PBS 0.1% Tween-20. In general, primary antibodies were incubated overnight at 4°C and secondary antibodies for 1 hour at room temperature. Antibodies used: CCP110 (Proteintech, 1:1000), CEP97 (Proteintech, 1:1000), LUZP1 (Sigma, 1:1000), GLI3 (R&D, 1:1000), FLNA (Cell Signalling, 1:1000), vinculin (Sigma, 1:1000) Cofilin (Cell Signalling Technology, 1:1000), phospho-cofilin (Cell Signalling Technology, 1:1000), Rac1 and pRac1 (Cell Signalling Technology, 1:1000), Arp3 (Machesky et al., 1997), 1:1000), Biotin-HRP (Cell Signalling Technology, 1:2000), GFP (Roche, 1:1000), HA (Sigma, 1:1000), GFP (Roche, 1:1000), tubulin-HRP (Proteintech, 1:2000), GAPDH (Proteintech, 1:1000), Actin (Sigma, 1:1000). Anti-SALL1 antibodies were: R&D, 1:1000, detects $SALL1^{FL}$ protein; anti-SALL1 (Kiefer et al., 2002) detects the N-terminal part of both truncted SALL1 and $SALL1^{FL}$ (check antibody specificity in **Figure R 1A and Figure R 1B**). Secondary antibodies were HRP-conjugated anti-mouse or anti-rabbit (Jackson Immunoresearch). Proteins were detected using Clarity ECL (BioRad) or Super Signal West Femto (Pierce). Quantification of bands was performed using ImageJ software and normalized against actin, GAPDH or tubulin levels. At least three independent blots were quantified per experiment.

## 3.7 Immunostaining

hTERT-RPE, U2OS cells, Shh-LIGHT2 cells, HEK 293FT cells and primary fibroblasts from control and TBS individuals were seeded on 11 mm coverslips (15,000-50,000 cells per well on a 24 well-plate). HEK 293FT cells were plated on coverslips coated with 0.01% poly-L-lysine (Sigma) to enhance adhesion. After washing 3 times with cold 1x PBS, cells were fixed with methanol 100% for 10

minutes at -20$^{o}$C or with 4% PFA supplemented with 0.1% Triton X-100 in PBS for 15 minutes at RT or pre-permeabilized for 2 min in PTEM buffer (20 mM PIPES pH 6.8, 0.2 % Triton X-100, 10 mM EGTA and 1 mM MgCL$_2$ (Tanos et al., 2013) and fixed for 10 min with 4% PFA for centrosomal staining. Then, coverslips were washed 3 times with 1x PBS. Blocking was performed for 1 hour at 37$^{o}$C in blocking buffer (BB: 2% fetal calf serum, 1% BSA in 1x PBS). Primary antibodies were incubated overnight at 4$^{o}$C and cells were washed with 1x PBS 3 times. To label the ciliary axoneme and the basal body/pericentriolar region, we used mouse antibodies against acetylated alpha-tubulin (Santa Cruz Biotechnologies, 1:160) and gamma-tubulin (Proteintech, 1:160) and rabbit antibodies against ARL13B (Proteintech) and pericentrin (1:160; Covance). Other antibodies: mouse anti-SALL1 (R&D, 1:100); rabbit anti-CCP110 (Proteintech, 1:100); rabbit anti-CEP97 (Proteintech, 1:100); mouse monoclonal anti-CEP164 (Genetex, 1:100); rabbit anti-ODF2 (Atlas, 1:100) and mouse anti-phospho-Histone H2A.X (Millipore; 1:500), anti-LUZP1 (Sigma, 1:100), anti-vinculin (Sigma, 1:200) and anti-actin (Sigma, 1:500).

Donkey anti-mouse, anti-rabbit or anti-rat secondary antibodies (Jackson Immunoresearch) conjugated to Alexa 488 or Alexa 568 (1:200), GFP booster (Chromotek, 1:500) and Alexa 568-conjugated phalloidin (Invitrogen 1:500), were incubated for 1 hour at 37$^{o}$C, followed by nuclear staining with DAPI (10 minutes, 300 ng/ml in PBS; Sigma). Transfected HEK 293FT cells with *Myc-BirA\*-SALL1$^{c.826C>T}$* or *Myc-BirA\*-SALL1$^{FL}$* were incubated with 50 µM biotin for 24 hours, washed, fixed, and stained with Alexa 594-conjugated Streptavidin (1:100, Jackson Immunoresearch). Fluorescence imaging was performed using an upright fluorescent microscope (Axioimager D1, Zeiss) or a confocal microscope (Leica SP2) with 40x or 63x objectives. Cilia frequency was obtained dividing the number of total cilia by the number of nuclei on each micrograph. Number of cells per micrograph was similar in both control and experimental conditions. For cilia measurements and counting, primary cilia from at least fifteen different fluorescent micrographs from each experimental condition were analysed using the ruler tool from Adobe Photoshop. To obtain the level of fluorescence in a region, mean intensity or corrected total cell fluorescence (CTCF) was calculated as described (McCloy et al., 2014), using parameters obtained by ImageJ.

## 3.8 qPCR analysis

TBS[332], control fibroblasts, and Shh-LIGHT2 cells were starved for 24 hours with or without purmorphamine treatment (5 μM; ChemCruz) to induce Shh signalling pathway. Total RNA was obtained with EZNA Total RNA Kit (Omega) and quantified by Nanodrop spectrophotometer. cDNAs were prepared using the SuperScript III First-Strand Synthesis System (Invitrogen) in 10 μl volume per reaction. Human *LUZP1, GLI1, PTCH1, GAPDH,* and mouse *Gli1*, *Ptch1,* and *Rplp0* primers were tested for efficiency and products checked for correct size before being used in test samples. qPCR was done using PerfeCTa SYBR Green SuperMix Low (Quantabio) or Mi-Hot Taq Mix (Metabion) adding 20x Evagreen (Biotium). Reactions were performed in 10 μl, adding 1 μl of cDNA and 0.5 μl of each primer (10 μM), in a CFX96 thermocycler (BioRad) using the following protocol: 95°C for 10 minutes and 40 cycles of 95°C for 10 seconds and 55-60°C for 30 seconds. Melting curve analysis was performed for each pair of primers between 65°C and 95°C, with 0.5°C temperature increments every 5 seconds. Relative gene expression data were analysed using the ΔΔCt method. Reactions were done in triplicates and results were derived from at least three independent experiments normalized to *GAPDH* and *Rplp0* and presented as relative expression levels. Primer sequences: *GLI1-F*: 5'-AGCCTTCAGCAATGCCAGTGAC-3'; *GLI1-R*: 5'-GTCAGGACCATGCACTGTCTTG-3'; *PTCH1-F*: 5'-CTCATATTTGCCTTCG-3'; *PTCH1-R*: 5'-TCTCCAATCTTCTGGCGAGT-3', *LUZP1-F:* 5´-GGAATCGGGTAGGAGACACCA-3´; *LUZP1-R:* 5´-TTCCCAGGCAGTTCAGACGGA-3; *GAPDH-F*: 5'-AGCCACATCGCTCAGACAC-3'; *GAPDH-R*: 5'-GCCCAATACGACCAAATCC-3'; *Gli1-F*: 5'-AGCCTTCAGCAATGCCAGTGAC-3'; *Gli1-R*: 5'-GTCAGGACCATGCACTGTCTTG-3'; *Ptch1-F*: 5'-AAGCCGACTACATGCCAGAG-3'; *Ptch1-R*: 5'-TGATGCCATCTGCGTCTACCAG-3', *Rplp0-F*: 5'-ACTGGTCTAGGACCCGAGAAG-3'; *Rplp0-R*: 5'-CTCCCACCTTGTCTCCAGTC-3'.

## 3.9 CRISPR-Cas9 genome editing

CRISPR-Cas9 targeting of *SALL1* locus was performed to generate a HEK 293FT

cell line carrying a TBS-like allele. We used online resources (CRISPRdesign and CRISPOR) to search for high-scoring sites in proximity to the site mutated in the TBS[332] fibroblasts. We chose the highest scoring sgRNA target to design our vectors. All constructs were confirmed by sequencing and cloning. Transient transfection and puromycin selection was followed by single-cell cloning and screening. After CRISPR-Cas9 mediated cutting, we selected a clone that gave rise to a single base insertion (*SALL1*[*c.1003dup*]) and the SALL1[p.Ser335Lysfs*20] protein (SALL1[335]), hereinafter referred to as 293[335]. Presence of the truncated protein was confirmed by Western blot. This mutation was heterozygous as confirmed by Sanger sequencing of a pooled mutant/WT amplicon, as well as individual sequencing of TOPO-cloned amplicons, where both mutant and WT clones were detected.

Using the same online resources, we chose 6 of the highest scoring off-target sites for additional analysis (mm2_exon_SALL1P1_chrX_49432372; mm4_exon_NACA_chr12_57110706; mm4_intergenic_CDCA7L|RAPGEF5_chr7_22092853; mm4_intergenic_RNU6-996P|AL162389.1_chr9_110472444; mm4_exon_LEMD2_chr6_33744586; mm4_exon_GPRIN2_chr10_46999700). Using genomic DNA from our targeted clone as template, we performed PCR and Sanger sequencing. In all cases, no mutations were found.

The mouse *Luzp1* locus was targeted in NIH3T3-based Shh-LIGHT2 fibroblasts (Taipale et al., 2000) (kind gift from A. McGee, Imperial College). Cas9 was introduced into Shh-LIGHT2 cells by lentiviral transduction (Lenti-Cas9-blast; Addgene #52962; kind gift from F. Zhang, MIT) and selection with blasticidin (5 μg/ml). Two high-scoring sgRNAs were selected (http://crispr.mit.edu/) to target near the initiation codon (sg2: CTTAAATCGCAGGTGGCGGT_TGG; sg3: CTTCAATCTTCAGTACCCGC_TGG). These sequences were cloned into px459 2.0 (Addgene #62988; kind gift of F. Zhang, MIT), for expressing both sgRNAs and additional Cas9 with puromycin selection. Transfections were performed in Shh-LIGHT2/Cas9 cells with Lipofectamine 3000 (Thermo). 24 hours after transfection, transient puromycin selection (0.5 μg/ml) was applied for 48 hours to enrich for transfected cells. Cells were plated at clonal density, and well-isolated clones were picked and propagated individually. Western blotting was used to identify clones lacking *Luzp1* expression. Further propagation of

a selected clone (#6) was carried out with G418 (0.4 mg/ml) and zeocin (0.15 mg/ml) selection to maintain expression of luciferase reporters. Genotyping was performed using genomic PCR (*MmLuzp1_geno_*F: 5'-GTTGCCAAAGAAGGTTGTGGATGCC-3'; *MmLuzp1_geno_R*: 5'-CGTAAGGTTTTCTTCCTCTTCAAGTTTCTC-3') and revealed a homozygous deletion of bases between the two sgRNA target sites, predicting a frame-shifted truncated protein (MAELTNYKDAASNRY*), and resulting in a null *Luzp1* allele (*Luzp1$^{-/-}$* cells). A rescue cell line was generated by transducing Shh-LIGHT2 *Luzp1* KO clone #6 with a lentiviral expression vector carrying *EFS-LUZP1-YFP-P2A-blastR*, with a positive population selected by fluorescence-activated cell sorting (+LUZP1 cells). A similar approach was used for disrupting *LUZP1* in human HEK 293FT cells, using sgRNAs targeting sequences located in exon 1, namely sg1: CTTAAACCGCAAGTGGCGGC_TGG and sg2: AAGCCGCCGCCTTGATGAGT_TGG. A knockout clone, called 293$^{LUZP1\ KO}$, was selected by absence of LUZP1 signal in western blots.

## 3.10 Plasmid construction

A FL human *SALL1* clone was used for high-fidelity PCR amplification and subcloning into *EYFP-N1* (Clontech) as truncated (*SALL1$^{826}$-YFP*) or FL versions (*SALL1$^{FL}$-YFP*). Clones were validated by Sanger sequencing and correspond to current annotations (NCBI RefSequence: NM_002968.2). *EYFP* was exchanged for two copies of *HA* tag to build *SALL1$^{FL}$-2xHA*. For BioID vectors, Ac5-STABLE2-neo (Gonzalez et al., 2011) was modified to contain a CAG promoter, a *Myc*-tagged version of BirA (R118G, human codon-optimized), and a multiple cloning site into which *SALL1$^{826}$* or *SALL1$^{FL}$* was inserted (Roux et al., 2012). Lentiviral expression vectors were prepared in *Lentilox-GFS-IRESpuro*, a derivative of LL3.7 (*GFS=GFP-FLAG-STREP*) (Rubinson et al., 2003).

The human *LUZP1* ORF was amplified by high-fidelity PCR (Platinum SuperFi; Thermo) from hTERT-RPE1 cDNA and cloned to generate *CB6-GFP-LUZP1*. This was used as a source clone to generate additional variants (*CB6-HA-LUZP1, CMV-LUZP1-YFP, CMV-LUZP1-2xHA*). The *LUZP1-YFP* lentiviral expression vector was generated by replacing Cas9 in Lenti-Cas9-blast (Addgene #52962). All constructs were verified by

Sanger sequencing.

## 3.11 SALL1 silencing

A human *SALL1* target sequence (5'-CTGCTATTTGTATTGTGCTTT-3'; based on validated Mission shRNA TRCN0000003958; Sigma/Merck) was cloned into the inducible shRNA vector Tet-pLKO-puro (Addgene #21915) (Wiederschain et al., 2009). Lentivirus was produced in HEK 293FT cells and used to transduce and stably select HEK 293FT cells using puromycin (1 µg/ml). *SALL1* silencing was induced for 72 hours using doxycycline (1 µg/ml).

## 3.12 Lentiviral transduction

Lentiviral expression constructs were packaged using psPAX2 and pVSVG (Addgene) in HEK 293FT cells, and lentiviral supernatants were used to transduce TBS-derived human cells, Shh-LIGHT2 and hTERT-RPE1 cells. Stable-expressing populations were selected using puromycin (1 µg/ml). For primary fibroblasts, lentiviral supernatants were concentrated 100-fold before use (Lenti-X concentrator, Clontech).

## 3.13 Luciferase assays

Firefly luciferase expression was measured using the Dual-Luciferase Reporter Assay System (Promega) according to the manufacturer's instructions. For each construct, luciferase activity upon purmorphamine treatment was divided by the activity of cells before treatment induction to obtain the fold change value. Luminescence was measured and data were normalized to the Renilla luciferase readout. Experiments were performed with both biological and technical replicates.

## 3.14 Fluorescence-activated cell sorting

To evaluate apoptosis, Shh-LIGHT2 cells were washed with 1x PBS and then stained with Annexin V (BD Biosciences) and DRAQ7 (Biostatus Ltd). For cell cycle

analysis, Shh-LIGHT2 cells were washed with cold PBS and fixed with 70% ethanol overnight. Cells were then washed twice with PBS and resuspended in PBS containing 5 µg/ml propidium iodide (PI) and 100 µg/ml RNase A (Sigma-Aldrich, St. Louis, MO, USA). A total of 20,000 events were counted for each sample. Data were collected on a Fluorescence-activated Cell Sorting (FACS) Canto (BD Biosciences) and were analysed using FlowJo software (www.flowjo.com).

## 3.15 Proliferation assay

$5 \times 10^3$ cells were plated in triplicate in 12-well dishes. 24 hours later, the cells were considered day 0 ($t_0$) and were fixed in formalin 10% for 15 minutes. The same procedure was performed after 3 and 6 days. Cell proliferation was measured by staining with crystal violet (0.1% in 20% methanol) for 45 minutes at RT. After washing 3 times with water, all samples were air dried. The precipitate was solubilized in 10% acetic acid for 20 minutes at RT and the absorbance was measured at 595 nm. For each timepoint, 4 biological replicates were measured.

## 3.16 Wound-healing assay

Shh-LIGHT2 control, Luzp1$^{-/-}$ mutant cells and Luzp1$^{-/-}$ cells transduced with LUZP1 (+LUZP1 cells) were grown in 24-well plates and a scratch (wound) was done using a 20 µm pipette tip. Subsequently, medium was changed to remove detached and dead cells. Pictures were taken at three different positions per sample and three biological replicates were analysed of each. The scratch width was measured using ImageJ Fiji.

## 3.17 Filopodia quantification

Filopodia were quantified by staining cells with Alexa 594-conjugated wheat germ agglutinin (WGA) and using FiloQuant, a plugin for the ImageJ software (Jacquemet et al., 2017).

## 3.18 Statistical analysis

Statistical analysis was performed using GraphPad 6.0 software. Data were analysed by Shapiro-Wilk normality test and Levene´s test of variance. We used two tailed unpaired Student´s t-test or Mann Whitney-U tests for comparing two groups, One-way ANOVA or Kruskall-Wallis and the corresponding post-hoc tests for more than two groups and two-way ANOVA for comparing more than one variable in more than two groups. P values were represented by asterisks as follows: (*) P-value < 0.05; (**) P-value < 0.01; (***) P-value < 0.001; (****) P-value < 0.0001. Differences were considered significant when P < 0.05.

# Chapter 4: Results

## 4.1 Objective 1: the role of SALL1 in cilia formation and function

### 4.1.1 Truncated SALL1 abnormally recruits SALL1$^{FL}$ to the cytoplasm in TBS fibroblasts

It has been reported that the presence of truncated SALL1 protein is sufficient to cause TBS-like phenotype in a mouse model (Kiefer et al., 2008). In humans, a truncated SALL1 protein was observed in B-cells derived from a TBS individual (Kiefer et al., 2008), but its presence in fibroblasts has not been reported. We obtained dermal fibroblasts derived from a male TBS$^{332}$ individual (see Materials and Methods) (Botzenhart et al., 2007; Furniss et al., 2007). It was previously shown that mRNA from the truncated allele was expressed in TBS$^{332}$ fibroblasts (Furniss et al., 2007), therefore we checked for the presence of truncated SALL1 protein by Western blot. For that, we took advantage of distinct antibodies recognizing different epitopes of SALL1 (see Materials and Methods; **Figure R 1A and Figure R 1B**), which allowed us to distinguish SALL1$^{FL}$ from the truncated forms. Using an antibody directed against the N-terminal portion of SALL1, a truncated protein of about 62 kDa was identified in TBS$^{332}$ cells but not in control fibroblasts (HFF) (**Figure R 1C**). Furthermore, SALL1$^{FL}$ protein was less abundant in the TBS$^{332}$ compared to control HFF fibroblasts. As previously reported, the observed size of SALL1 by Western blot is higher than expected (Kiefer et al., 2008).

FL SALL1 proteins (SALL1$^{FL}$) are normally enriched in the nucleus, while truncated forms have been observed in both nucleus and cytoplasm (Sato et al., 2004; Sweetman et al., 2003). These studies used overexpression of truncated murine or chicken forms of *Sall1*, which induced a mislocalization of the SALL1$^{FL}$ into the cytoplasm, likely due to the interaction of the different SALL1 proteins through their glutamine-rich domains (Sato et al., 2004; Sweetman et al., 2003). We therefore analysed whether the reported change in localization of endogenous SALL1 was also occurring in human TBS$^{332}$-derived cells. By immunofluorescence, TBS$^{332}$-derived fibroblasts presented abnormal cytoplasmic staining of SALL1$^{FL}$ (**Figure R 1D**). We quantified the fluorescence intensity of SALL1$^{FL}$ in the nuclei and cytoplasm in both control and TBS$^{332}$ human fibroblasts. SALL1$^{FL}$ intensity was
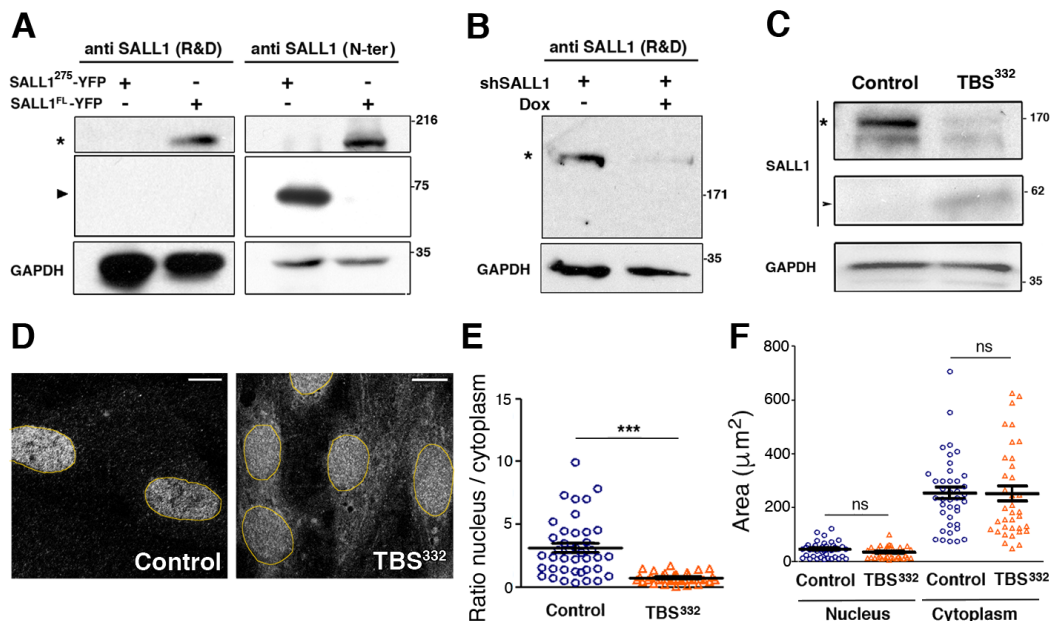
**Figure R 1. Truncated SALL1 expressed in TBS individualss disrupts the localization of SALL1$^{WT}$ protein. (A**) Western blot analysis of total lysates of HEK 293FT cells transfected with *SALL1$^{c.826C>T}$-YFP* (SALL1$^{275}$-YFP) or *SALL1$^{FL}$-YFP* (SALL1$^{FL}$–YFP). Samples were run in duplicate on the same gel and probed against SALL1 using two different antibodies. Anti-SALL1 antibody from R&D specifically recognizes SALL1$^{FL}$ (asterisk), but not the truncated form (black arrowhead), while anti-SALL1 N-terminal specific detects both. (**B**) Western blot analysis of HEK 293FT lysates expressing SALL1 specific shRNA under the control of a doxycycline inducible promoter. Cells were subjected to doxycycline (+) or DMSO treatment (-) for 72h. SALL1$^{FL}$ protein was detected using anti-SALL1 antibody from R&D (asterisk) and GAPDH was used as a loading control. TBS$^{332}$ dermal fibroblasts express truncated SALL1 protein (SALL1$^{\Delta995C}$). (**C**) Western analysis of control HFF or TBS$^{332}$ human fibroblast lysates shows loss of the wild-type protein (asterisk) and expression of a truncated protein of 62 kDa (arrowhead) recognized by SALL1 specific antibodies in TBS-derived fibroblasts. Molecular weight markers (kDa) are shown to the right in A, B and C. (**D**) Confocal micrographs showing SALL1$^{FL}$ detected by FL specific antibodies (R&D) in control HFF or TBS$^{332}$ fibroblasts, shown as black and white images. Nuclei were counterstained with DAPI (represented by yellow circles). (**E**) Graphical representation of three independent experiments showing the ratio between the fluorescence quantification of the levels of SALL1$^{FL}$ in the nucleus or cytoplasm of control HFF (n=40 cells; blue circles) or TBS$^{332}$-derived fibroblasts (n=36 cells; orange triangles) and the area in µm$^2$ of control (n=33 cells, blue circles) or TBS$^{332}$ (n=33 cells, orange triangles) (**F**). P-values were calculated with the Mann-Whitney two-tailed test. Median and interquartile range of the median are represented. Scale bars, 10 µm.

significantly lower in the nuclei, while significantly higher in the cytoplasm of TBS[332] fibroblasts leading to a decrease in the nuclear/cytoplasmic ratio (**Figure R 1E**). No significant differences in nuclei or cytoplasm size were found between control and TBS fibroblasts, indicating that the changes in intensity are not due to differences in size (**Figure R 1F**).

To check whether the presence of the truncated protein in human cells is sufficient to produce the localization change of SALL1$^{FL}$, we chose a mutation (*SALL1$^{c.826C>T}$*) that encodes for SALL1$^{p.Arg275*}$ (SALL1$^{275}$, herein) and that it has been reported in several independent TBS individuals (Botzenhart et al., 2007), making it the most common allele in this rare syndrome. Therefore, U2OS cells were transiently transfected with *SALL1$^{FL}$-2xHA* (SALL1$^{FL}$-2xHA), with *SALL1$^{c.826C>T}$-YFP* (SALL1$^{275}$-YFP) or with a combination of both. As expected, SALL1$^{275}$-YFP localization was diffuse in the nucleus and cytoplasm (**Figure R 2A**), while SALL1$^{FL}$ localization was limited to the nuclei in a typical pattern of subnuclear spots (**Figure R 2B**). However, in the presence of SALL1$^{275}$, SALL1$^{FL}$ changed its localization and colocalized with SALL1$^{275}$ (**Figure R 2C**). All together, these findings imply that SALL1$^{275}$ compromises SALL1$^{FL}$ localization by recruiting it to the cytoplasm in TBS-derived fibroblasts. In addition, these results further support the conclusion that the expression of the truncated form is crucial in the pathogenesis of TBS in humans

### 4.1.2 SALL1 localizes to the primary cilia

Intrigued by the overlapping phenotypic characteristics between TBS individuals and ciliopathies (polydactyly, imperforate anus, hearing loss and polycystic kidneys), we further explored the subcellular localization of SALL1 in cells that are able to develop cilia and checked whether it localizes at the centrosome or ciliary shaft. For this purpose, we chose human fibroblast HEK 293FT and the murine cell lines IMCD3 and NIH 3T3. Immunofluorescence staining was performed on cells that had been starved for 48h. In addition to the reported localization of SALL1$^{FL}$ in the nuclei, we detected the remarkable presence of SALL1$^{FL}$ in the ciliary axoneme of HEK 293FT cells, determined by co-staining with a monoclonal antibody against ARL13B (ciliary
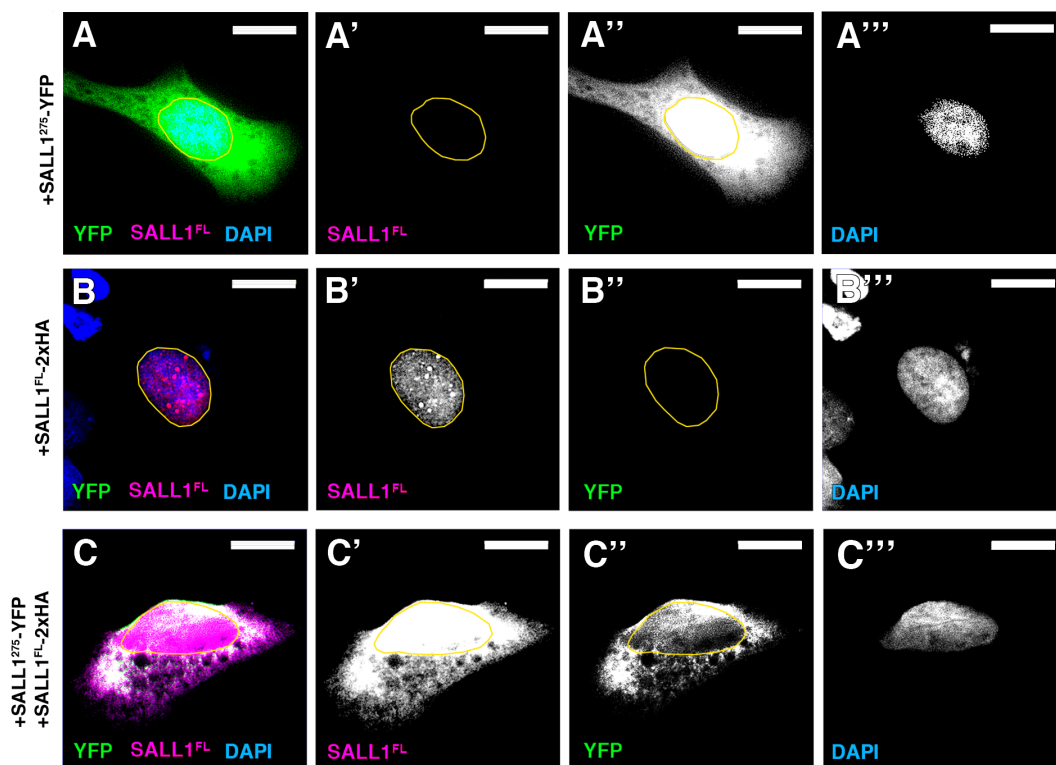
**Figure R 2. Truncated SALL1 interacts with SALL1$^{FL}$ in the cytoplasm.** (**A-C**) Confocal micrographs of U2OS cells transfected with *SALL1$^{c.826C>T}$-YFP* (SALL1$^{275}$-YFP) (**A**), *SALL1$^{FL}$-2xHA* (SALL1$^{FL}$–2xHA) (**B**) or both (**C**). SALL1$^{FL}$-2xHA is in purple, SALL1$^{275}$-YFP in green and nuclei in blue (DAPI). SALL1$^{FL}$ is recognized with FL specific antibodies (R&D) that do not recognize SALL1$^{275}$, which localizes diffusely thorough nucleus and cytoplasm (**A**). SALL1$^{FL}$ exhibits a nuclear pattern (**B**) that is impaired when SALL1$^{275}$ is present (**C**). Black and white images show the single purple (**A'-C'**), green (**A''-C''**) and blue channels (**A'''-C'''**). Images were taken with a Zeiss Axioimager D1, 63x objective. Scale bar, 10 μm.

shaft) (**Figure R 3A**). SALL1 was also present in the nuclei and the ciliary shaft of the inner medullar conducting duct cell line IMCD3, in a pattern that was surprisingly reminiscent of intrafragellar transport proteins (**Figure R 3B**), and of the mouse-derived NIH 3T3 cells (**Figure R 3C**).

Whereas SALL1$^{FL}$ was localized to the nuclei and ciliary shaft in human control fibroblasts (**Figure R 4A**), it was diffusely observed in the nucleus, cytoplasm and ciliary shaft in TBS$^{332}$ patient-derived fibroblasts (**Figure R 4B**). When SALL1 signal was quantified exclusively along the cilia, SALL1$^{FL}$ was less present in the ciliary shaft of TBS$^{332}$ fibroblasts compared to control-derived fibroblasts (**Figure R 4C**). Together,
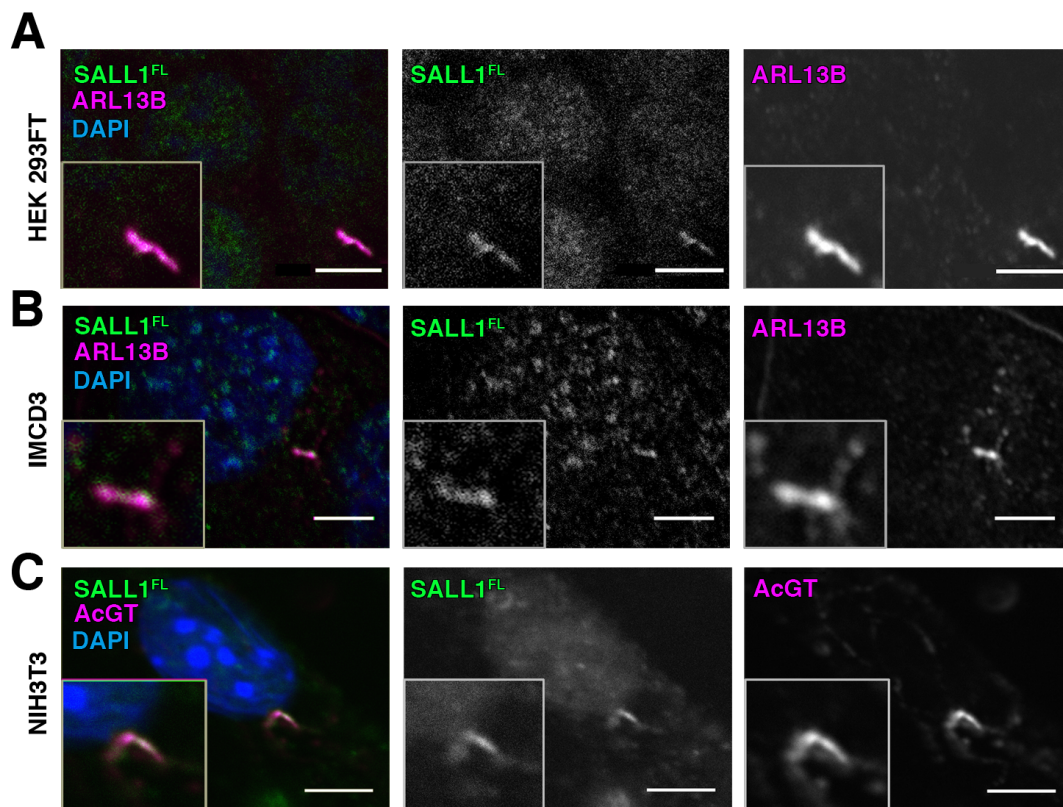
**Figure R 3. SALL1$^{FL}$ localizes to cilia shaft in human and mouse cell lines.** Confocal micrographs show SALL1$^{FL}$ localizing to the nucleus and primary cilia of HEK 293FT (**A**), IMCD3 (**B**) and NIH 3T3 (**C**) cells. SALL1 stained in green (middle panels) and microtubule axoneme and basal body using acetylated alpha tubulin and gamma tubulin (AcGT), respectively, or primary cilia using ARL13B in purple. Black and white images show the single green and purple channels. Confocal images were taken with a Leica SP2 confocal microscope. Scale bar, 5μm.

these results imply that endogenous SALL1$^{FL}$ might be a ciliary protein and that truncated SALL1 might disrupt its localization in a dominant-negative manner.

## 4.1.3 TBS-derived cells show increased cilia frequency and length

Based on the localization of SALL1$^{FL}$ to the ciliary shaft and the overlapping symptoms between TBS and ciliopathies, we hypothesized that primary cilia formation might be altered in TBS cells. To test this hypothesis, we checked cilia assembly and disassembly in fibroblasts derived from both control (HFF) and TBS[332]. Primary cilia assembly was promoted by starving cells at high confluency for 48
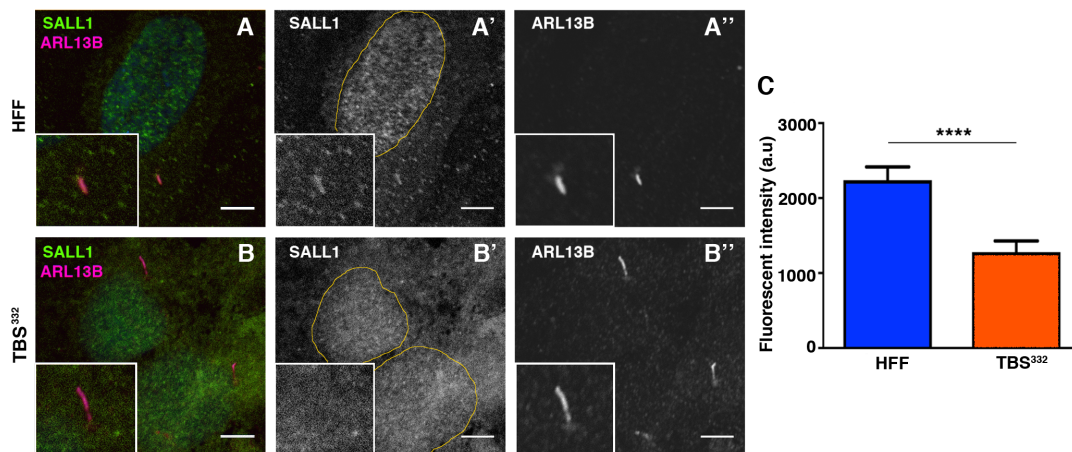
**Figure R 4. SALL1$^{FL}$ localizes to cilia shaft and its levels are reduced in TBS$^{332}$cells.** Confocal micrographs show SALL1$^{FL}$ localizing to the nucleus and primary cilia of human control dermal fibroblasts (**A**) and diffusely thorough nucleus and cytoplasm of TBS$^{332}$ dermal fibroblasts (**B**). SALL1 is stained in green (middle panels) and primary cilia using ARL13B in purple (right panels). Black and white images show the single green and purple channels. (**C**) Bar graph representing SALL1$^{FL}$ fluorescent signal at the ciliary shaft of control (blue bar) and TBS$^{332}$ fibroblasts (orange bar). SALL1$^{FL}$ levels were significantly reduced at the ciliary shaft of TBS$^{332}$ fibroblasts (1278 ± 151.3; n=129; three independent experiments) compared to control (2240 ± 177.3; n=108; three independent experiments). Black and white images show the single green and purple channels. P-values were calculated with the two-tailed unpaired Student´s t-test. Mean and standard error of the mean (SEM) are represented. Confocal images were taken with a Leica SP2 confocal microscope. Scale bar, 5µm.

hours, whereas cilia disassembly was induced by adding complete media to ciliated cells previously subjected to serum starvation. We quantified frequency of ciliation and primary cilia length at all mentioned timepoints. TBS fibroblasts showed a significantly higher frequency of primary cilia formation when the cells were not subjected to starvation (**Figure R 5A-C**). 7.9% of the control cells *vs* 24.7% of the TBS cells exhibited a primary cilium in cycling conditions (**Figure R 5C**). TBS cells were also significantly more ciliated than control fibroblasts upon 48 hours of starvation. In those conditions, 36.1% of the control cells *vs* 78.8% of the TBS fibroblasts displayed a primary cilium. In addition, TBS cells were significantly more ciliated 30 minutes and 2h after serum induction (**Figure R 5C**). Whereas 100% of the control cells had completely dismantled their cilia 24h after inducing cilia disassembly, 12% of the TBS fibroblasts were still ciliated (data not shown). Furthermore, primary cilia in TBS
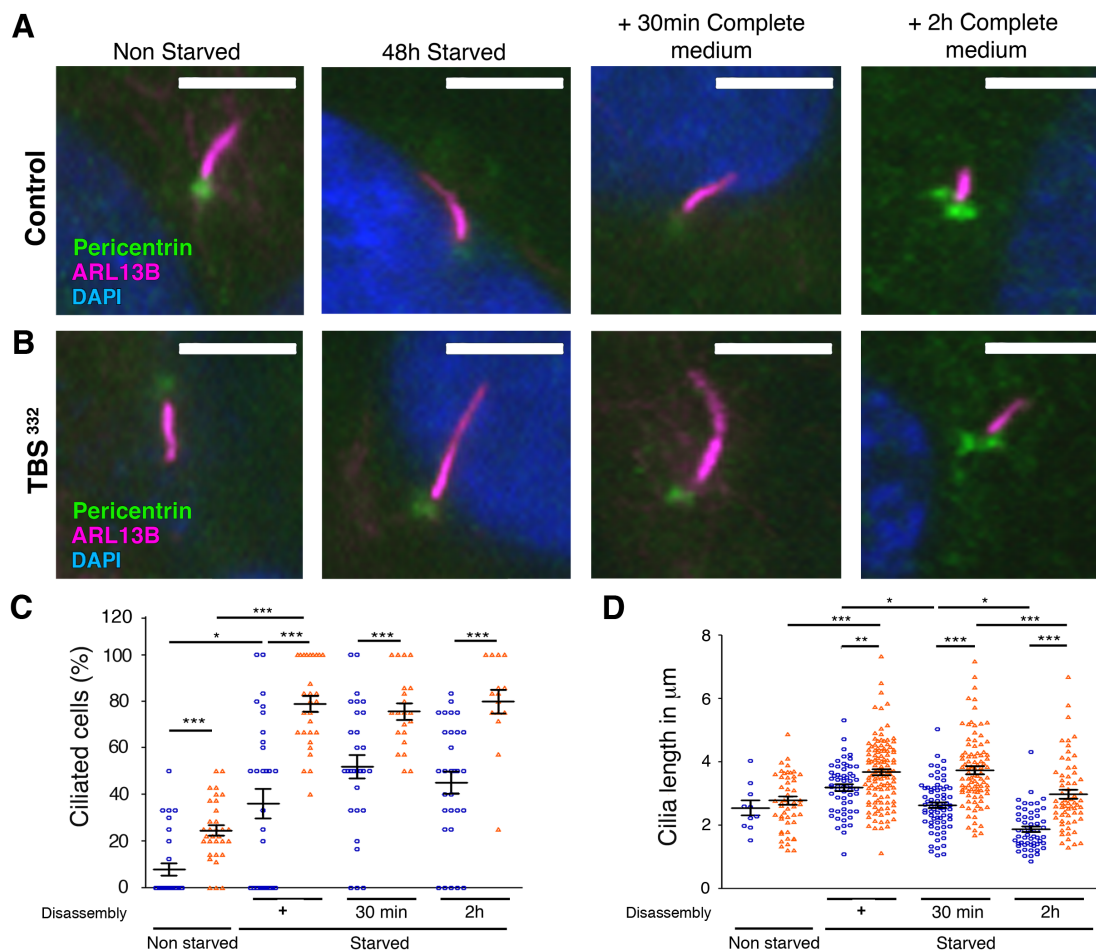
**Figure R 5. TBS[332] cells show aberrant cilia frequency and length. (A,B)** Micrographs of control HFF (**A**) or TBS[332]cells. (**B**) analysed during cilia assembly and disassembly. Cilia were visualized by ARL13B (purple), basal body by pericentrin (green) and nuclei by DAPI (blue). (**C,D**) Graphical representation of cilia frequency (**C**) and cilia length (**D**) measured in control HFF (blue dots, n=58 cilia) or TBS[332] cells (orange triangles, n=116 cilia) from three independent experiments. Cells that underwent 48 hours of starvation were compared to non-starved cells. After starvation, cells were supplied with serum for 30 minutes or 2 hours (n=21-30 micrographs for all the cases).

were significantly longer upon 48 hours of starvation compared to control (average 3.2 μm in control *vs* 3.7 μm in TBS) (**Figure R 5A-B and Figure R 5D**). Cilia were significantly longer in TBS than in control cells at all the studied timepoints during cilia disassembly (30 minutes with complete medium: average 2.6 μm in control *vs* 3.7 μm in TBS; 2 hours with complete medium: 1.9 μm in control *vs* 3 μm in TBS). The observed increase in cilia frequency after the addition of complete medium in

control cells is consistent with a reported reciliation wave during the first hours of cilia disassembly (Spalluto et al., 2013). These results show that TBS cells have longer and more abundant primary cilia compared to control cells in all tested conditions.

As mentioned previously, it has been reported that the presence of truncated SALL1 protein is sufficient to cause TBS-like phenotype in a mouse model (Kiefer et al., 2008). Confluent HFF control cells (**Figure R 6A**) or hTERT-RPE1 cells (**Figure R 6C**) stably transduced with lentiviral *GFS-SALL1*$^{c.826C>T}$ (GFS-SALL1$^{275}$) displayed longer cilia than those stable for *GFS alone* (GFS) (**Figure R 6B and Figure R 6D**), further confirming that the presence of a truncated form of SALL1 is sufficient to promote longer cilia. Taken together, these results suggest that truncated SALL1 can affect cilia frequency, as well as the dynamics of cilia assembly and disassembly.
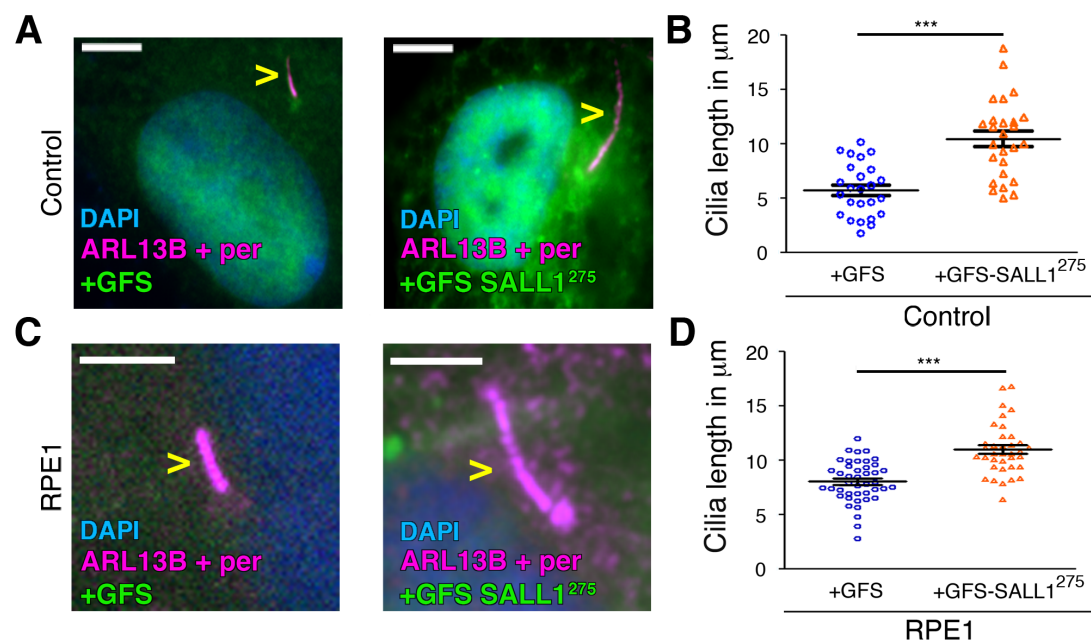


**Figure R 6. Cells overexpressing truncated SALL1 show aberrant cilia length.** (**A,C**) Micrographs of HFF control (**A**) and RPE1 cells (**C**) infected with lentivirus expressing *GFS* alone (GFS, left panels) or *GFS-SALL1*$^{c.826C>T}$ (GFS-SALL1$^{275}$, right panels). Cilia were visualized by ARL13B and basal body by pericentrin (per, purple) and nuclei by DAPI (blue). Yellow arrowheads point at the cilia (**B,D**) Graphical representation of cilia length in control (**B**) and RPE1 cells (**D**) corresponding to (**A**) and (**C**) infected with GFS (blue circles, control n=25; RPE1 n=43 cilia) or GFS-SALL1$^{275}$ (orange triangles: control n=26; RPE1 n=36 cilia). Graphs represent Mean and SEM of three independent experiments. P-values were calculated using two-tailed unpaired Student´s t-test. Scale bars, 5 µm..

### 4.1.4 TBS-derived cells exhibit aberrant Sonic Hedgehog signalling

It is well established that Shh signal transduction is dependent on the presence of functional primary cilia in mammals (Huangfu et al., 2003; Yin et al., 2009). Therefore, we examined whether Shh signalling is compromised in TBS[332] cells. Cells were starved for 24 hours and incubated in the presence or absence of purmorphamine (a Smoothened agonist) for 24 or 48 hours to activate the Shh pathway. mRNA expression of two Shh target genes (*GLI1* and *PTCH1*) was quantified by qRT-PCR (**Figure R 7A and Figure R 7B**). We found that, after induction by purmorphamine for 24 or 48 hours, the fold-activation *GLI1* and *PTCH1* expression levels in TBS cells was higher than in control HFF cells.

GLI3 is the transcription factor that is primarily responsible for repression of Shh target genes, and *Gli3* mutants exhibit polydactyly because they lack the GLI3 repressor (Hill et al., 2009; Litingtung et al., 2002). The proteolytic processing event that produces GLI3 repressor depends on primary cilia (Huangfu et al., 2003). To further study the role of SALL1 truncations in Shh signalling, we analysed GLI3 processing by Western blot analysis using total lysates extracted from control HFF *vs* TBS[332] fibroblasts (**Figure R 7C**). We found that the increase of GLI3-A:GLI3-R ratio upon purmorphamine treatment is significantly higher in TBS[332] cells compared to control fibroblasts (**Figure R 7C and Figure R 7D**). We also examined the effects of truncated SALL1 on Shh signalling using Shh-LIGHT2 cells (Taipale et al., 2000). These are NIH3T3 mouse embryonic fibroblasts that carry an incorporated Shh reporter (firefly luciferase under control of *Gli3*-responsive promoter). We observed aberrations in Shh signalling in Shh-LIGHT2 cells stably expressing *GFS-SALL1*[c.826C>T] (SALL1[275]) *vs* controls (**Figure R 7E**). Like TBS-derived cells, Shh-LIGHT2 cells overexpressing SALL1[275] show oversensitivity to Shh induction compared to control cells (2.3 fold-induction in control cells *vs* 3.9 fold-induction in cells expressing SALL1[275]). Defects in *PTCH1* and *GLI1* gene expression (endogenous, or via reporter assay) and impaired GLI3 processing confirm that truncated SALL1 proteins found in TBS might cause not only defects in ciliogenesis, but also in Shh signalling.
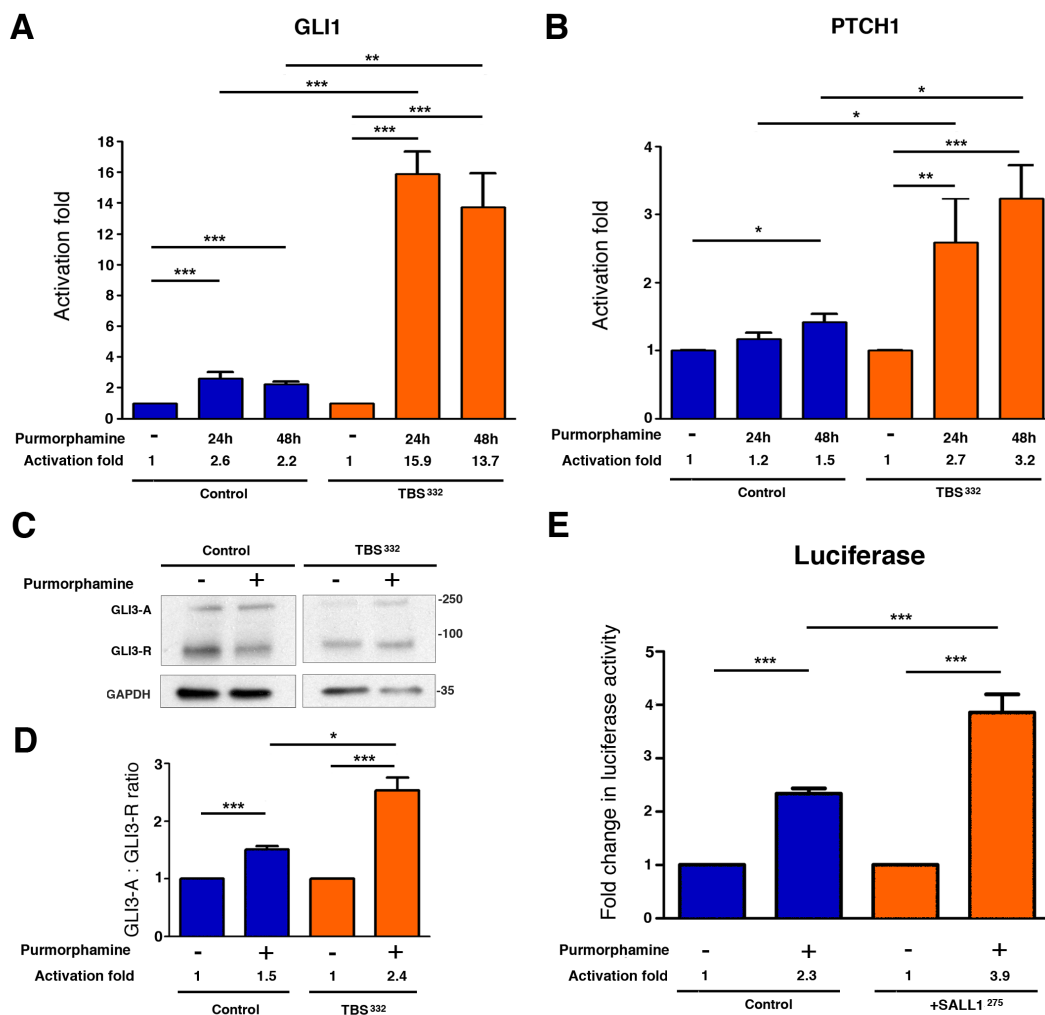
**Figure R 7. TBS[332] fibroblasts show aberrant SHH signaling. (A,B)** Graphical representation of the fold change in the expression of *GLI1* (**A**) and *PTCH1* (**B**) obtained by qPCR from control HFF (n=4; blue bars) or TBS[332] (n=4; orange bars) treated (+) or not (-) with purmorphamine for the indicated times. Numerical quantification of fold activation is indicated below the graphs. (**C**) Western blot analysis of lysates from control ESCTRL#2 and TBS[332]. Samples were probed against GLI3 that detects both GLI3 activating form (GLI3-A) and GLI3 repressive form (GLI3-R) and GAPDH was used as loading control. Molecular weight markers (kDa) are shown to the right. (**D**) Graphical representation of fold activation obtained in (**C**) by calculating the GLI3-A:GLI3-R ratio in control and TBS[332] fibroblasts. Data from at least 3 independent experiments is shown, using ESCTRL#2 (control; n=3; blue bars) and TBS[332] (n=5; orange bars). (**E**) Graphical representation of fold change in luciferase activation when Shh-LIGHT2 control cells (n=8; blue bars) or cells expressing the mutated form *GFS-SALL1$^{c.826C>T}$* (*GFS-SALL1[275]*; n=8; orange bars) are treated (+) or not (-) with purmorphamine. All graphs represent the Mean and SEM. P-values were calculated with the two-tailed unpaired Student´s t-test.

### 4.1.5 New TBS-derived cell line exhibits cilia alterations

To further verify the ciliogenesis defects previously observed in TBS cells, we analysed SALL1 levels and ciliogenesis in fibroblasts derived from an additional individual referred to as TBS[275] (**Figure R 8A**). Of note, this is the same truncation that is used in our exogenous expression constructs (i.e. SALL1[c.826C>T] or SALL1[275]). Individual TBS[275] displayed the characteristic triad of TBS symphtoms (imperforate anus, thumb and ear malformations), in addition to kidney, heart and hearing problems. When analysing TBS[275] cells, we observed a decrease in SALL1[FL] compared to control ESCTRL#2 cells and the presence of a new band of about 42 kDa, consistent with a truncated SALL1 protein (**Figure R 8B**). Interestingly, localization of SALL1[FL] was also altered in human TBS[275] cells (**Figure R 8C and Figure R 8D**). To check whether the presence of the truncated protein in primary human cells is sufficient to produce the localization change of SALL1[FL], ESCTRL#2 or TBS[275] cells were transiently transfected with SALL1[FL]-YFP. SALL1[FL]-YFP localization was limited to the nuclei in control fibroblasts (**Figure R 8E**) while its localization was diffuse in the nucleus and cytoplasm in TBS[275] cells (**Figure R 8F**). Furthermore, when compared to control HFF or ESCRTL#2, TBS[275] cells displayed longer and more abundant cilia in confluent starved conditions, similar to what was observed in TBS[332] cells (**Figure R 9A-C**). Thus, truncated SALL1 is detected in TBS[275] cells and leads to altered SALL1[FL] localization, likely through its recruitment to the cytoplasm. As a result, the truncated SALL1, SALL1[FL], or both could potentially interact and interfere with other proteins.

### 4.1.6 TBS-mimicking cell line exhibits aberrant ciliogenesis

Fibroblasts derived from two different TBS individuals displayed altered frequency of ciliogenesis and longer cilia with respect to control cells. To confirm these results, we attempted to generate a TBS-like mutation in HEK 293FT to assess the cilia phenotype. In addition, in this way we could confirm that the observed differences in ciliogenesis were not dependent on the genetic background of the cells, since the TBS-like model cell line could be compared with the parental cells.
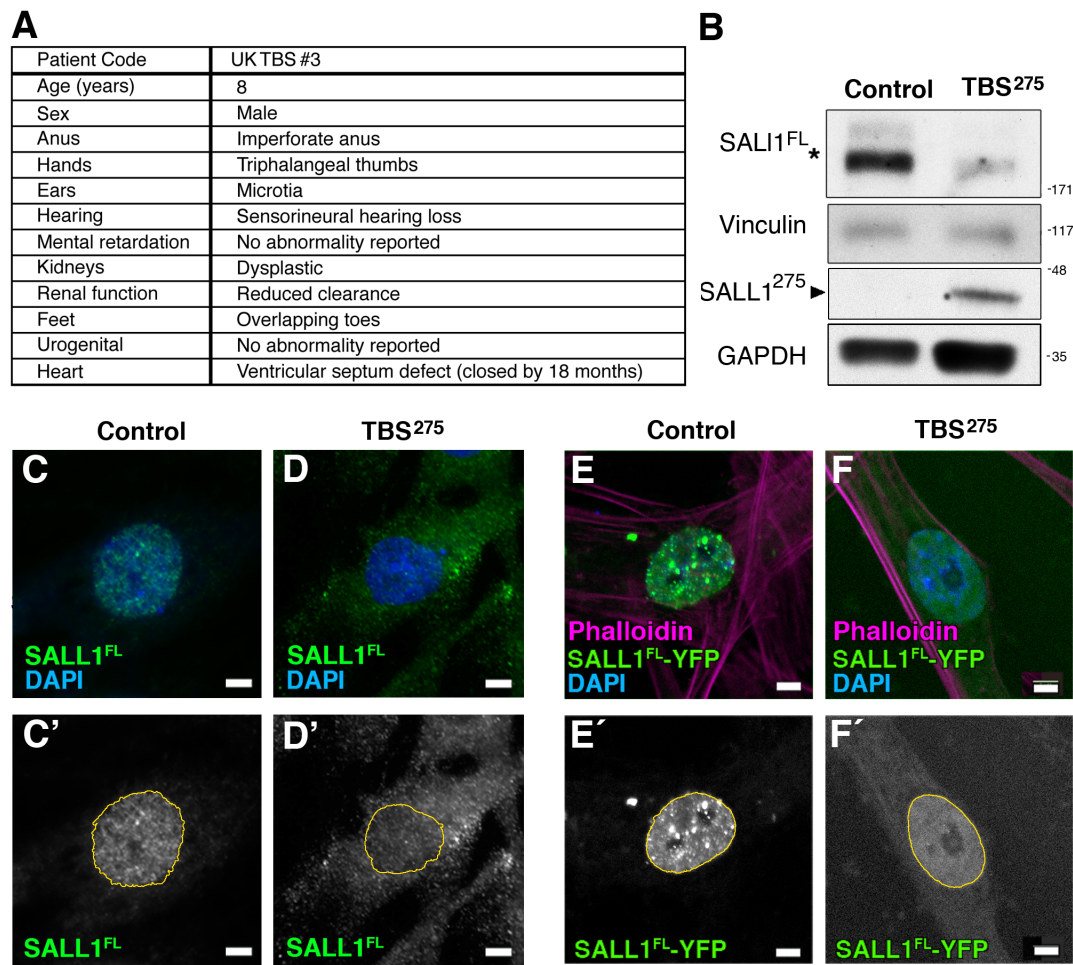
**Figure R 8. SALL1 characterization in fibroblasts derived from an additional TBS individual.** (**A**) Clinical findings of the individual TBS[275]. (**B**) Western blot analysis of lysates from control ESCTRL#2 and TBS[275]. Samples were run in duplicate on the same gel and probed against SALL1[FL] (asterisk, R&D antibody) or against SALL1[275] (black arrowhead, N-terminal specific antibody) (Kiefer, McDill, Yang, & Rauchman, 2002). TBS[275] cells encoded a truncated protein of about 48 kDa that positively reacts against SALL1 antibody. Vinculin and GAPDH were used as loading controls. Molecular weight markers (kDa) are shown to the right. (**C,D**) Confocal micrographs showing in green endogenous SALL1[FL] localization in control ESCTRL#2 (**C**) or TBS[275] fibroblasts (**D**) detected by FL specific antibody (R&D). Scale bar, 5 μm. (**E,F**) Confocal micrographs showing in green SALL1[FL]-YFP localization in control ESCTRL#2 and TBS[275] fibroblasts. Actin was labeled by phalloidin (purple), DAPI was used to counterstain the nuclei (blue) and black and white images show the single green channel (**C´, D´, E´and F´**). Yellow circles idicate the nuclei. Scale bar, 5 μm.
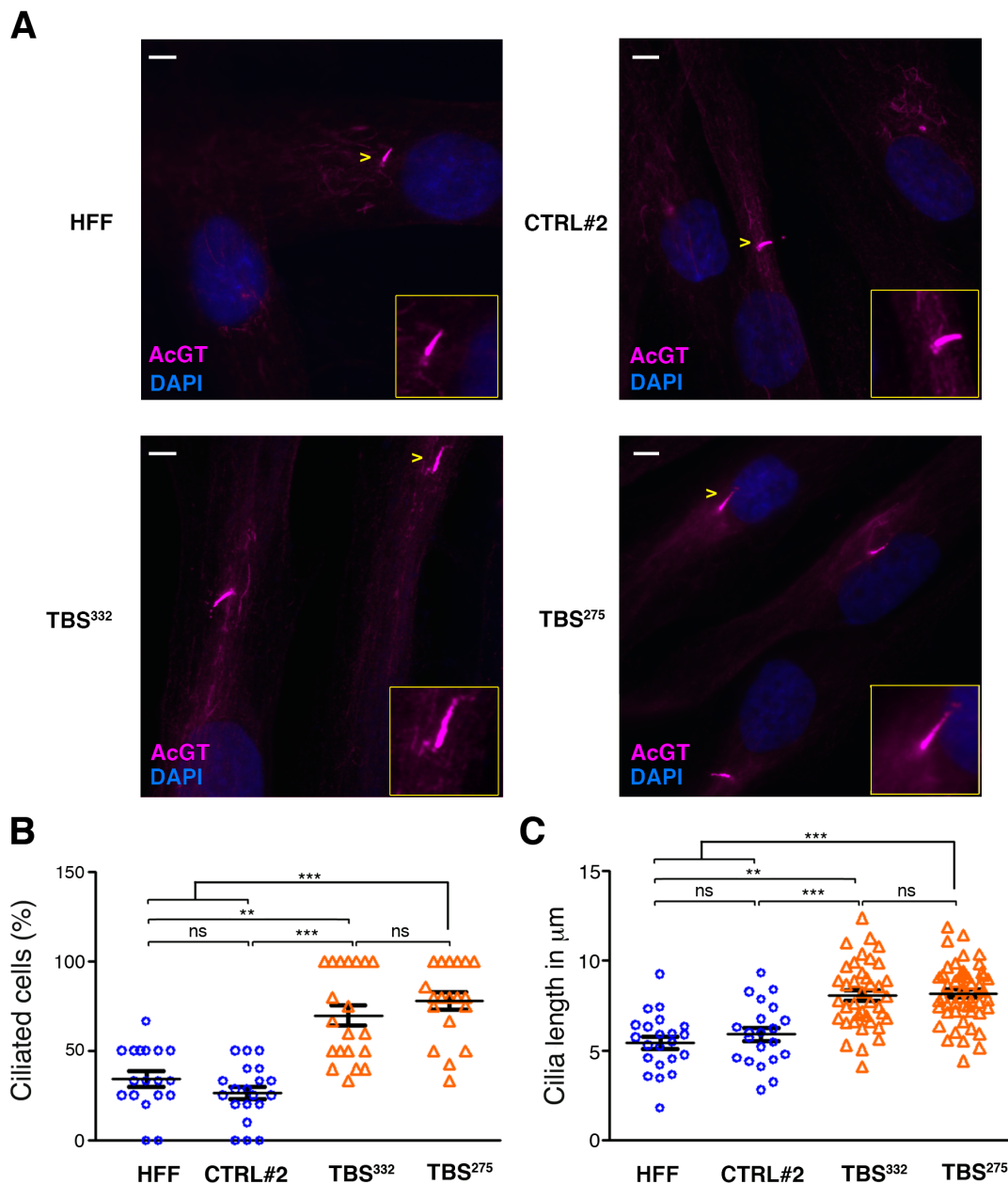
**Figure R 9. TBS$^{275}$ fibroblasts exhibit cilia anomalies.** (**A**) Immunofluorescence micrographs showing cilia marked with acetylated alpha tubulin and basal body marked with gamma tubulin (AcGT, purple) and nuclei counterstained with DAPI (blue) in control HFF or ESCTRL#2 (upper panels) *vs* TBS$^{332}$ or TBS$^{275}$ (lower panels). Pictures were taken using an Axioimager D1 fluorescence microscope, Zeiss with a 63x objective. Scale bar, 5 μm. AcTub: acetylated alpha tubulin; G-Tub: gamma tubulin. (**B**) Graphical representation of cilia frequency of micrographs shown in (**A**). HFF (n=18) and ESCTRL#2 (n=20), blue dots; TBS$^{332}$ (n=20) and TBS$^{275}$ (n=19), orange triangles. (**C**) Graphical representation of cilia length measurements of micrographs shown in (**A**). HFF (n=22) and ESCTRL#2 (n=21), blue dots; TBS$^{332}$ (n=39) and TBS$^{275}$ (n=51), orange triangles. Three independent experiments were pooled together. The graphs represent the Mean and SEM. P-values were calculated using One way ANOVA and Dunn's Multiple Comparison post-hoc test.

We used CRISPR-Cas9 method to target the *SALL1* locus in the "hotspot" region, to approximate the mutation seen in TBS[275] and TBS[332] fibroblasts. We isolated and characterized a clone that is heterozygous for *SALL1* mutation (293[335]), with a sequence-verified single base insertion that leads to a frameshift and a truncated protein. Using extracts from this clone and WT parental cells, we confirmed the protein truncation by Western blot (**Figure R 10A**).

In the 293[335] cells, we observed a dramatic decrease in SALL1[FL] protein compared to unmodified cells (293[WT]) and the presence of a new band of about 48 kDa that shows reactivity with SALL1 antibody. Interestingly, localization of SALL1[FL] changed in 293[335] cells. Whereas SALL1[FL] is nuclear in 293[WT] cells, it is diffusely localized throughout the nucleus and the cytoplasm in 293[335] cells (**Figure R 10B**). Upon starvation and in confluent conditions, cilia were significantly more abundant in 293[335] cells (average 26%) than in 293[WT] cells (average 7%) (**Figure R 10B and Figure R 10C**). Furthermore, 293[335] cells displayed longer cilia (average 7.0 μm) compared to 293[WT] (average 5.1 μm) (**Figure R 10B and Figure R 10D**). These results confirmed that the TBS-mimicking cell line that we generated reproduced the ciliary phenotype found in human TBS fibroblasts

### 4.1.7 Cells derived from Sall1[ΔZn2-10] mouse embryos exhibit aberrant ciliogenesis

Our analysis in TBS-derived fibroblasts and in human cell lines, either genome-edited or exogenously expressing a mutated form of *SALL1*, show coincident phenotypes in the length and frequency of primary cilia. To further confirm these results, we also examined cells from a TBS animal model previously characterized. *Sall1-ΔZn[2-10]* mice mimic a hotspot mutation shown to cause TBS, and they produce a truncated protein lacking all the zinc finger motifs, except for the N-terminal $C_2HC$ finger (Kiefer et al., 2003). We cultured MEFs from tissues derived from E13 *Sall1-ΔZn[2-10]* mice and analysed cilia formation in those MEFs. After confirming the genotype by PCR (**Figure R 11A**), we analysed ciliogenesis in WT (*Sall1^{+/+}*) and heterozygous MEFs (*Sall1[+/Δ]*). In agreement with our previous results, *Sall1[+/Δ]* MEFs displayed more abundant (pooled average 59%) and longer cilia (pooled average 1
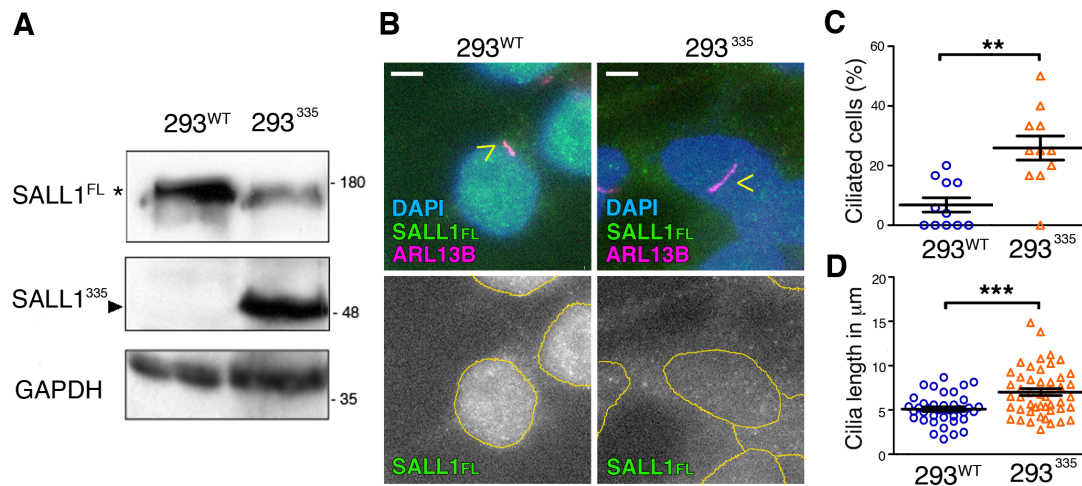
**Figure R 10. Truncated SALL1 leads to TBS-like cilia phenotype in genetically modified cells. (A)** Western blot analysis of lysates from wild-type HEK 293FT cells (293$^{WT}$) or CRISPR/Cas9-modified cells (293$^{335}$) to mimic a TBS mutation in *SALL1* gene (*SALL1*$^{c.1003dup}$). A truncated protein of about 48 kDa was identified in 293$^{335}$ cells by SALL1 antibody (SALL1$^{p.Ser335Lysfs*20}$; black arrowhead). Asterisk indicates SALL1$^{FL}$. GAPDH was used as a loading control. Molecular weight markers (kDa) are to the right. **(B)** Immunofluorescence micrographs showing the subcellular distribution of SALL1$^{FL}$ in 293$^{WT}$ or 293$^{335}$ cells using a specific antibody (green). In purple, ARL13B marks the primary cilium (yellow arrowheads) and in blue, DAPI the nuclei. Yellow circles delimitate the nuclei and black and white images show the single green channel. Scale bar, 5 μm. **(C,D)** Graphical representation of cilia frequency **(C)** and cilia length measurements **(D)** of micrographs shown in **(B)**. Cilia frequency, n=11 micrographs; cilia length, n=38 cilia in 293$^{WT}$ cells (blue dots) and n=48 cilia in 293$^{335}$ cells (orange trinagles). Three independent experiments were pooled together. The graphs represent the Mean and SEM. P-values were calculated using two-tailed unpaired Student's t-test.

μm) than *Sall1*$^{+/+}$ (average 14% and 0,7 μm, respectively), both in starved conditions (**Figures R 11B-D**). These results confirmed that MEFs derived from a mouse TBS model reproduced the ciliary phenotype found in human TBS fibroblasts.
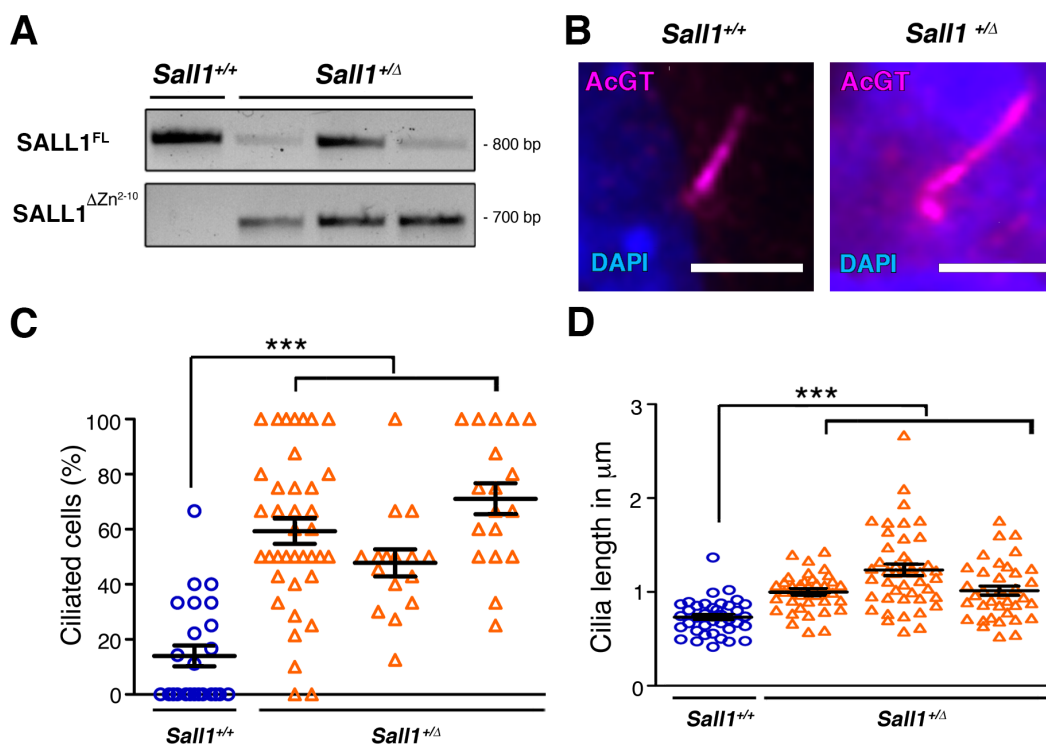
**Figure R 11. Cells derived from *Sall1*<sup></sup>*^{+/Δ}* mouse embryos exhibit cilia defects. (A)** PCR genotyping of MEFs derived from wild-type homozygous (*Sall1^{+/+}*) or *Sall1^{ΔZn2-10}* heterozygous embryos (*Sall1^{+/Δ}*). **(B)** Micrographs of *Sall1^{+/+}* and *Sall1^{+/Δ}* MEFs analysed during cilia assembly. Cilia were visualized by acetylated alpha-tubulin and gamma-tubulin (AcGT, purple) and nuclei were counterstained with DAPI (blue). **(C,D)** Graphical representation of cilia frequency **(C)** and cilia length **(D)** measured in *Sall1^{+/+}* (n= 38 cilia and 24 micrographs, for cilia length and frequency, respectively; blue circles) and *Sall1^{+/Δ}* MEFs in (B) (n=37-45 cilia and n=16-38 micrographs for cilia length and frequency, respectively; orange triangles). Scale bar, 1 μm. P-values were calculated using One way ANOVA and Dunn's Multiple Comparison post-hoc test.

## 4.2 Objective 2: Identification of the cellular and molecular mechanisms mediating the cilia defects observed in TBS.

### 4.2.1 Proximity proteomics of SALL1 identifies interactions with cilia regulators

The BioID method (Roux et al., 2012) relies on a mutant BirA enzyme (BirA*) that has a relaxed specificity and is able to biotinylate any free lysine ε-amino group present in proteins within a radius between 10 and 20 nm (Kim et al., 2014; Van Itallie et al., 2013). When fused to SALL1$^{275}$ or SALL1$^{FL}$, BirA* can biotinylate proximal proteins that either interact directly with them or are closely associated in protein complexes (**see Materials and Methods, Figure M1**).

*Myc-BirA\*-SALL1$^{c.826C>T}$* (BirA*-SALL1$^{275}$) or *Myc-BirA\*-SALL1$^{FL}$* (BirA*-SALL1$^{FL}$) plasmids were transfected in HEK 293FT cells. Staining of transfected cells to visualize biotinylated proteins revealed that, as expected, BirA*-SALL1$^{275}$ localized diffusely throughout the nucleus and cytoplasm, whereas BirA*-SALL1$^{FL}$ localized primarily in the nucleus, enriched in subnuclear domains (**Figure R 12A and Figure R 12B**). Total lysates from BirA*-SALL1$^{275}$ or BirA*-*SALL1$^{FL}$*-transiently transfected cells were subjected to NeutrAvidin pulldown and isolated proteins were analysed by liquid chromatography tandem mass spectrometry (LC-MS/MS). In addition to almost all known interactors of SALL1, such as NuRD complex components (HDAC1, HDAC2, RbAp46, MTA1, MTA2, MBD3, CHD4 and CHD3) (Xue et al., 1998) candidates with exclusive or enriched proximity to SALL1$^{275}$ *vs* SALL1$^{FL}$ were identified. A total of 1032 or 665 proteins were found in at least two out of three experiments done with BirA*-SALL1$^{275}$ or BirA*-SALL1$^{FL}$, respectively (**Figure R 12C**).

Out of those proteins, 744 in the SALL1$^{275}$ and 123 in the SALL1$^{FL}$ subproteome were significantly enriched at least 2-fold change with respect to the other subproteome in at least 2 out of 3 experiments based on label-free protein quantitation (**Figure R 13A and Appendix I**). With the purpose of obtaining a functional overview of the main pathways associated to SALL1$^{275}$, a comparative Gene Ontology (GO) analysis was performed, comparing Cellular Component, Molecular Function and Biological Process fields (**Figure R 13B-D**). In the Cellular
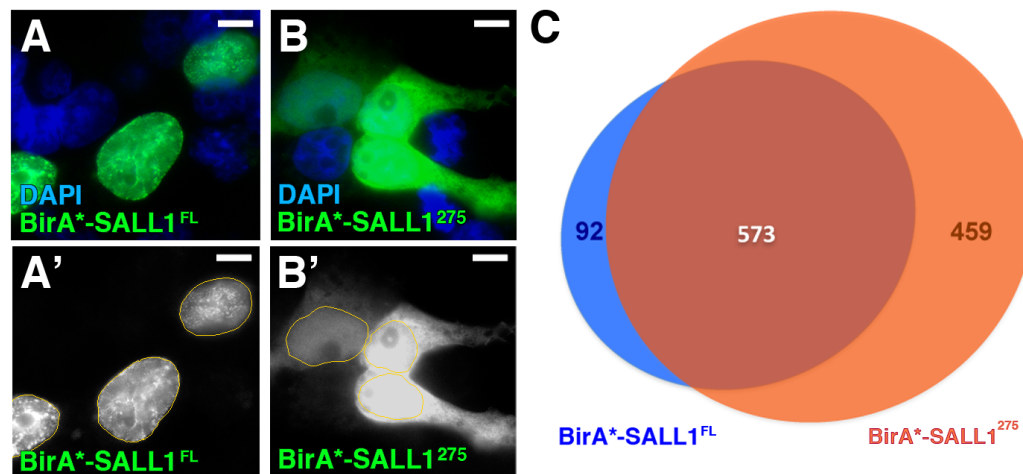
**Figure R 12. Differential interactors for truncated SALL1 and SALL1$^{FL}$.** (**A,B**) Confocal micrographs showing transient expression of transfected *BirA\*-SALL1$^{FL}$* (**A**) or *BirA\*-SALL1$^{c.826C>T}$* (BirA\*-SALL1$^{275}$) (**B**) detected by fluorescence streptavidin in green. Nuclei are marked by DAPI in blue. Single green channels are shown in black an white (**A´,B´**). Scale bar, 5 μm. (**C**) Venn diagram showing the distribution of the identified candidates by MS analysis. 665 and 1032 proteins were found in the close proximity of SALL1$^{FL}$ and SALL1$^{p.Arg275*}$ (SALL1$^{275}$), respectively, in at least 2 independent experiments.

Component domain, a shift towards "cytoplasm", "actin cytoskeleton" and "microtubule cytoskeleton" was observed in the SALL1$^{275}$ proteome **(Figure R 13B)**. Intriguingly, the "centrosome" GO term is found exclusively in the SALL1$^{275}$ proteome (**Appendix 1**). With respect to Molecular Function, SALL1$^{275}$ showed enrichment in cytoplasmic proteins ("actin binding", "microtubule binding" and "ATPase" or "helicase activity" terms; **(Figure R 13C)**. In the category of Biological Process, SALL1$^{275}$ subproteome shows enrichment in the categories "cell cycle", "cytoskeleton organization" and "cellular response to stress" **(Figure R 13D).**

Interestingly, among genes included in the centrosome category term we found CCP110 and CEP97, two proteins that function together to block ciliogenesis (Spektor et al., 2007). The role described for these proteins in cilia formation is compatible with the phenotype observed in TBS fibroblasts, therefore we selected them for further study.
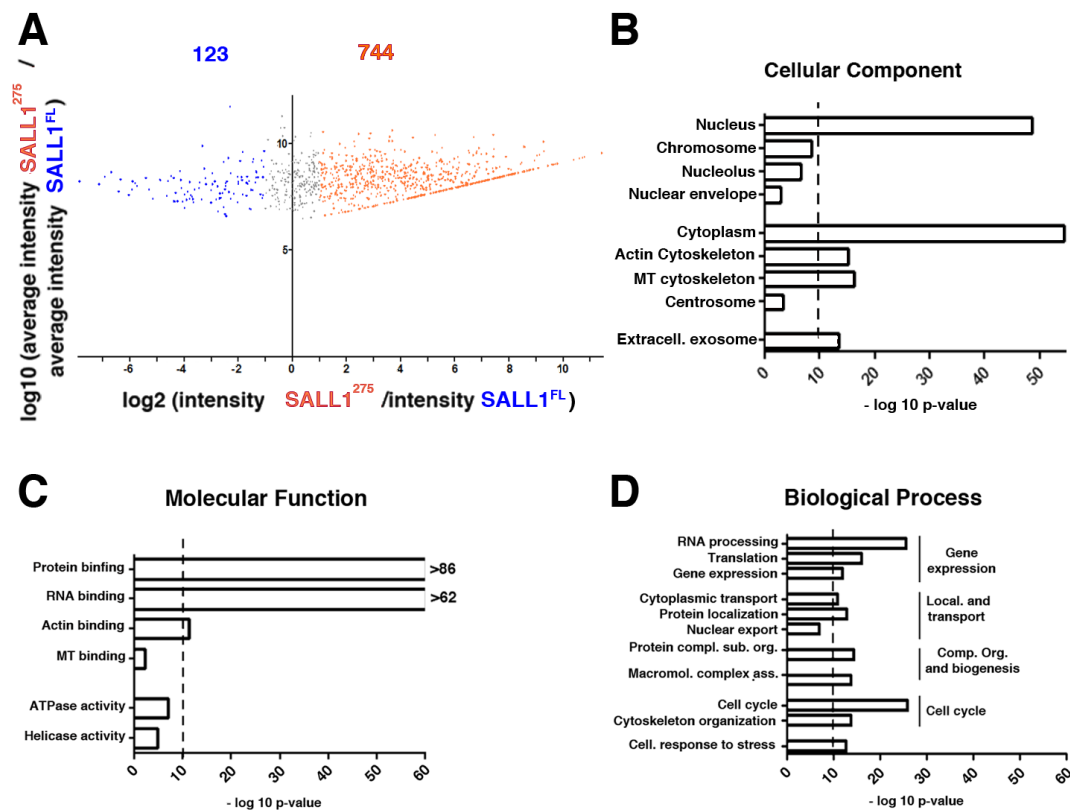
**Figure R 13. GO term analysis of the truncated SALL1 *vs* the SALL1[FL] subproteomes. (A)** Volcano plot representing the distribution of the candidates identified by proximity proteomics in at least two out of three independent experiments. Proteins with 2 or more than 2-fold change in intensity with respect to the wild type proteome ($log_2 \geq 1$) were considered as SALL1[275]-associated candidates (orange dots). Proteins with less than 2 fold change in intensity with respect to the wild-type protein ($log_2 \leq 1$) were considered as SALL1[FL] associated candidates (blue dots). **(B-D)** Graphical representation of the -$log_{10}$ of the P-value for each of the represented Cellular Component (**B**), Molecular Function (**C**) or Biological Process (**D**) GO terms in the BirA*-SALL1[p.Arg275*]proteome (SALL1[275]). MT: microtubules; Extracell.: Extracellular; Cell. response to stress: cellular response to stress; Comp. org. and biogenesis: component organization and biogenesis; Local. and transport: localization and transport; Macromol. complex as.: macromolecular complex assembly; Protein compl. sub. org.: protein complex subunit organization.

### 4.2.2 CCP110 and CEP97 interact with truncated SALL1

We confirmed CCP110 and CEP97 among the most enriched proteins in the subproteome biotinylated by BirA* when fused to SALL1$^{275}$ by independent BioID experiments analysed by Western blot using specific antibodies **(Figure R 14A and Figure R 14B).**
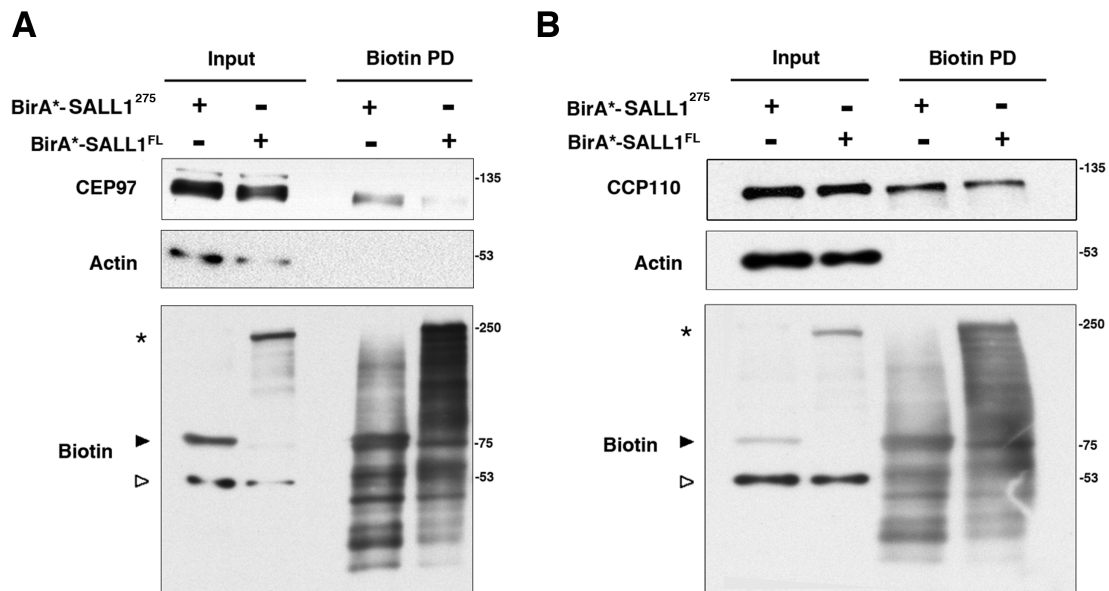


**Figure R 14. CCP110 and CEP97 are in close proximity to truncated SALL1. (A,B)** Western blot analysis of BioID, biotin pulldowns (PD) of HEK 293FT cells expressinng Myc-tagged BirA*-SALL1$^{FL}$ or BirA*-SALL1$^{p.Arg275*}$ (BirA*-SALL1$^{275}$). Specific antibodies against the endogenous proteins CEP97 (**A**) or CCP110 (**B**) were used. Actin was used as loading control. Biotin antibody detected the most biotinylated proteins in the inputs and pulldowns, which are the self-biotinylated forms of BirA*-SALL1$^{FL}$ (asterisks) and BirA*-SALL1$^{275}$ (black arrowhead), as well as other interactors in the pulldowns. White arrowheads indicate actin signal from previous probing. Blots shown are representative of three independent experiments. Molecular weight markers (kDa) are shown to the right.

Most cases of TBS exhibit a monoallelic truncation of SALL1, with likely presence of both truncated and FL forms of SALL1. These proteins can homo- and heterodimerize, leading to aberrant complexes. To characterize the interaction of CCP110 and CEP97 with SALL1, we performed pulldowns with tagged SALL1$^{FL}$-YFP, with SALL1$^{275}$-YFP, or with a combination of both in HEK 293FT cells. Our results showed that both endogenous CCP110 and CEP97 were able to bind to both SALL1$^{FL}$

and SALL1[275], with preferential binding to the truncated SALL1[275] protein, confirming our MS results **(Figure R 15A,** lanes 6 and 7). The binding to SALL1[275] persisted in presence of overexpressed *SALL1[FL]* (**Figure R 15A**, lane 8), indicating that the heterodimerization of the truncated and FL forms does not inhibit the interaction with CCP110 and CEP97. Note that SALL1[275]-YFP can interact with SALL1[FL]-HA (HA panel, lane 8), as it was previously suggested in mice (Sato et al., 2004). We further demonstrated the specificity of the interaction between SALL1 and CCP110 and CEP97 by performing the reciprocal experiment (**Figure R 15B and Figure R 15C**). Our results showed that SALL1[275] was able to immunoprecipitate with both CCP110 and CEP97 using specific antibodies against the last two proteins. These results support the notion that the truncated form of SALL1, either by itself or in complex with the FL form, can bind and perhaps sequester or inhibit the important cilia regulatory factors CCP110 and CEP97, leading to cilia defects.

### 4.2.3 CCP110 and CEP97 dynamics are altered in TBS fibroblasts

One key event in ciliogenesis is the depletion of CCP110 and its partner CEP97 from the distal end of the MC, promoting the ciliary activating program in somatic cells (Goetz et al., 2012; Kleylein-Sohn et al., 2007; Prosser and Morrison, 2015; Spektor et al., 2007; Tsang et al., 2008). Our data suggest that CCP110 interacts with SALL1[275], as well as with the complex between SALL1[275] and SALL1[FL], and that TBS fibroblasts display higher cilia formation rates compared to control cells. Based on these results, we hypothesized that CCP110 and CEP97 might suffer premature displacements from the MC in TBS. In order to check this hypothesis, we analysed their centrosomal localization in primary TBS[332] fibroblasts by immunofluorescence. CCP110 was present at the MC in a higher proportion of control cells (74%) than TBS[332] (36%) (**Figure R 16A and Figure R 16B**). Furthermore, CEP97 was present at the MC in 78% of the control cells while in 33% of the TBS[332] cells (**Figure R 16C and Figure R 16D**)**.**
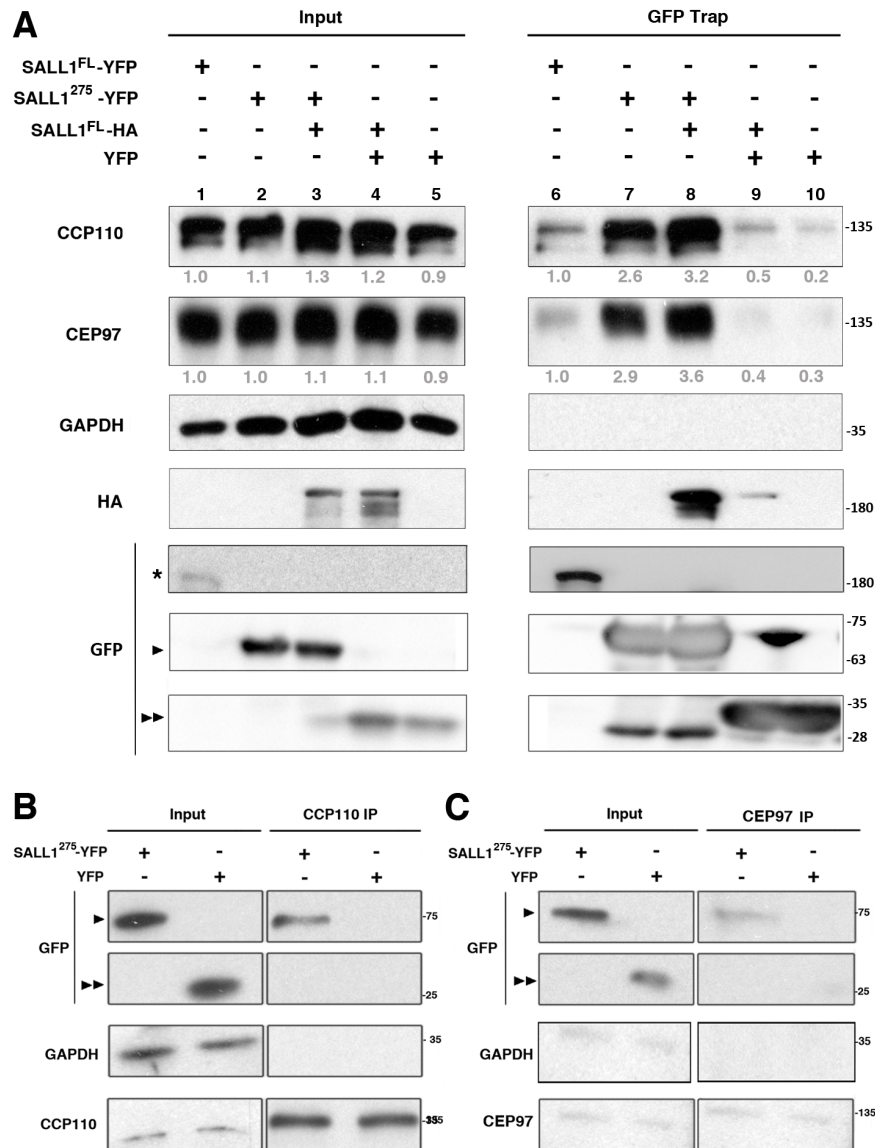
**Figure R 15. CCP110 and CEP97 interact with truncated SALL1.** (**A**) Western blot of inputs or GFP-Trap pulldowns (GFP trap) performed in HEK 293FT cells transfected with *SALL1^FL^-YFP* (lanes 1 and 6), *SALL1^c.826C>T^-YFP* (SALL1^275^-YFP; lanes 2 and 7), *SALL1^275^-YFP* together with *SALL1^FL^-2xHA* (SALL1^FL^-HA; lanes 3 and 8), *SALL1^FL^-HA* together with *YFP* alone (lanes 4 and 9) or *YFP* alone (lanes 5 and 10). Endogenous CCP110 and CEP97 were detected with specific antibodies. GAPDH was used as loading control. Numbers under CCP110 and CEP97 panels result from dividing band intensities of each lane by lane 1 for the inputs or by lane 6 for the pulldowns. (**B,C**) Western blot of inputs and CCP110 (**B**) or CEP97 (**C**) immunoprecipitations (IP) performed in HEK 293FT cells transfected with SALL1^275^-YFP or YFP alone. Endogenous CCP110 and CEP97 in the IP interacted with conjugating G sepharose beads linked to specific antibodies. GAPDH was used as loading control. Molecular weight markers (kDa) are shown to the right. One asterisk indicates SALL1^FL^-YFP, one black arrowhead SALL1^275^-YFP and two black arrowheads YFP alone.
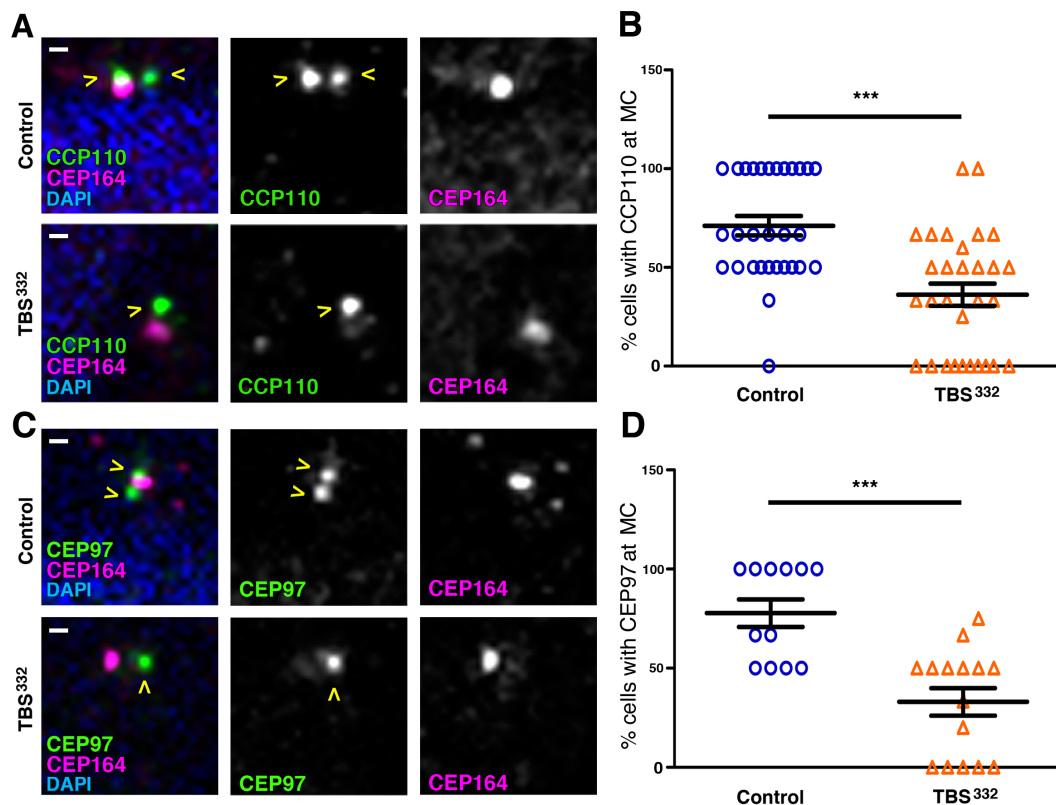
**Figure R 16. TBS<sup>332</sup> cells show changes in the localization of CCP110 and CEP97.** (**A,C**) Immunofluorescence micrographs of cycling human-derived fibroblasts stained with antibodies against endogenous CCP110 (**A**) or CEP97 (**C**) (green, yellow arrowheads), CEP164 to label the mother centriole (MC, purple) and counterstained with DAPI to label the nuclei (blue). Black and white images show the single green and purple channels. Note the different distribution of CCP110 and CEP97 to the MC in TBS<sup>332</sup> compared to control HFF fibroblasts. (**B,D**) Graphical representation of the percentage of cells showing the presence of CCP110 or CEP97 at the MC per micrograph corresponding to the experiments in (**A**) and (**C**), respectively; n=30 micrographs. Three independent experiments were pooled together. Pictures were taken using an Axioimager D1 fluorescence microscope, Zeiss, with a 63x objective. Scale bar, 1 µm. P-values were calculated with the two-tailed unpaired Student´s t-test.

Notably, 10% of the TBS cells displayed multiple foci or more diffuse labeling of CCP110 around the centrioles, suggesting an alteration of CCP110 dynamics (**Figure R 17**). Therefore, the disruption in the localization of CCP110 and CEP97 by the truncated SALL1 or by the presence of the aberrant complex between SALL1<sup>FL</sup> and SALL1 truncations, are potential mechanisms by which CCP110/CEP97 might be depleted from the MC, leading to a higher frequency of ciliogenesis in TBS cells.
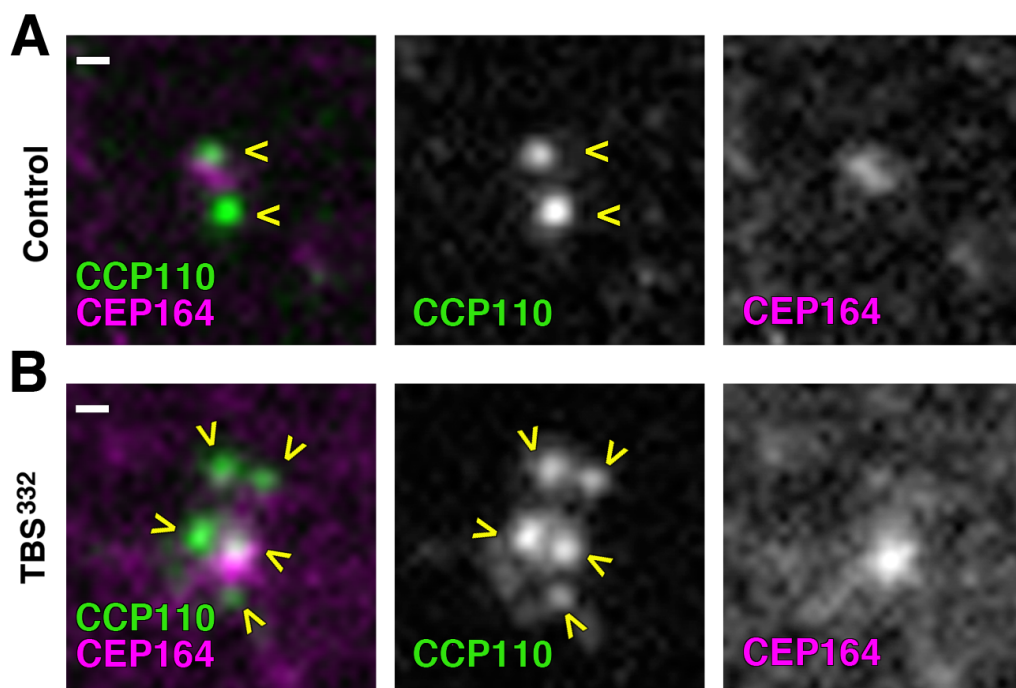
**Figure R 17. CCP110 localizes aberrantly in multiple foci in TBS[332] cells.** Representative fluorescence micrograph of a control (**A**) and a TBS[332] centrosome (**B**) showing CCP110 (green, yellow arrowheads) in a cloudy pattern around the mother centriole marked by CEP164 (purple). 10% of the TBS[332] cells show multiple centrioles. Black and white images show the single green and purple channels. Pictures were taken using a Zeiss Axioimager D1, 63x

In addition, we tried to confirm these aberrations in CCP110 dynamics in TBS model cell lines that displayed ciliogenesis defects: the TBS-mimicking cell line that we had generated (293[335] cells) and in heterozygous MEFs derived from $Sall1\text{-}\Delta Zn^{2\text{-}10}$ mice embryos ($Sall1^{+/\Delta}$ cells). CCP110 foci were absent or reduced at the MC in 89% of the 293[335] cells (**Figure R 18A and Figure R 18B**) and in around 67% of the $Sall1^{+/\Delta}$ MEFs in non starved conditions (**Figure R 18C and Figure R 18D**). Taken together, our results indicate that the presence of truncated SALL1 is sufficient to promote changes in cilia length and CCP110 localization when compared to a control of the same genetic background. Moreover, we show here that both the TBS-mimicking cell line that we generated and MEFs derived from a mouse TBS model reproduced the ciliary phenotype found in human TBS fibroblasts.
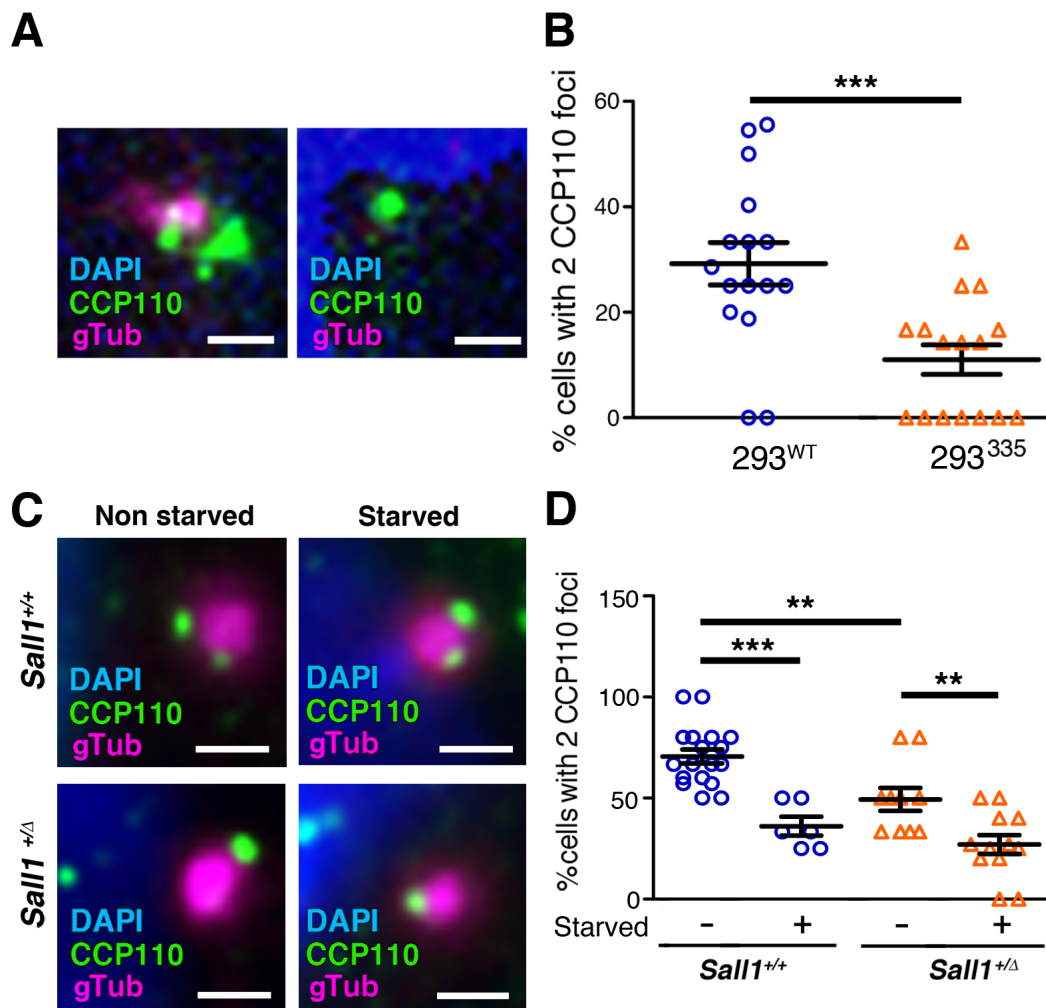
**Figure R 18. CCP110 and CEP97 dynamics are altered in a TBS model cell line and *Sall1*[+/Δ] mouse embryonic cells.** (**A**) Immunofluorescence micrographs of HEK 293FT cells (293[WT]) or CRISPR/Cas9-modified cells (293[335]) to mimic a TBS mutation in *SALL1* gene (*SALL1*[c.1003dup]) showing CCP110 foci (green), centrosomes (gTub, purple) and DAPI (blue). Scale bar, 1 µm. Pictures were taken using an Axioimager D1 fluorescence microscope, Zeiss with a 63x objective. (**B**) Graphical representation of the percentage of cells showing CCP110 in two foci per micrograph in 293[WT] or 293[335] cells, corresponding to the experiment in (**A**). (**C**) Immunofluorescence micrographs of *Sall1*^{+/+} and *Sall1*[+/Δ] MEFs showing CCP110 foci (green), in the centrosomes labelled with gamma tubulin (purple) and nuclei (DAPI, blue). Scale bar, 0.5 µm. Cells that underwent 48 hours of starvation were compared to non-starved cells. Pictures were taken using a Deltavision fluorescence microscope, GE Healthcare Life Sciences, with a 60x objective. (**D**) Graphical representation of the percentage of cells showing CCP110 in two foci in *Sall1*^{+/+} and *Sall1*[+/Δ] MEFs in (**C**) (n>10). The graphs represent the Mean and SEM. P-values were calculated using One way ANOVA and Dunn's Multiple Comparison post-hoc test. gTub: gamma tubulin.

97

### 4.2.4 SALL1 interacts with LUZP1

As previously described, we found that truncated forms of SALL1 present in TBS individuals aberrantly interact with cytoplasmic proteins. Interestingly, in addition to CCP110 and CEP97, we found LUZP1 among the 20 most enriched proteins in the SALL1$^{275}$ subproteome (**Appendix I**). We confirmed this finding by independent BioID experiments analysed by Western blot using a LUZP1 specific antibody. *Myc-BirA\*-SALL1$^{c.826C>T}$* (BirA\*-SALL1$^{275}$) or *Myc-BirA\*-SALL1$^{FL}$* (BirA\*-SALL1$^{FL}$) plasmids were transfected in HEK 293FT cells and lysates were subjected to NeutrAvidin pulldown. We exclusively found LUZP1 in the pulldown of BirA\*-SALL1$^{275}$ (**Figure R 19**), suggesting that LUZP1 is in close proximity and a potential interactor of SALL1$^{275}$.
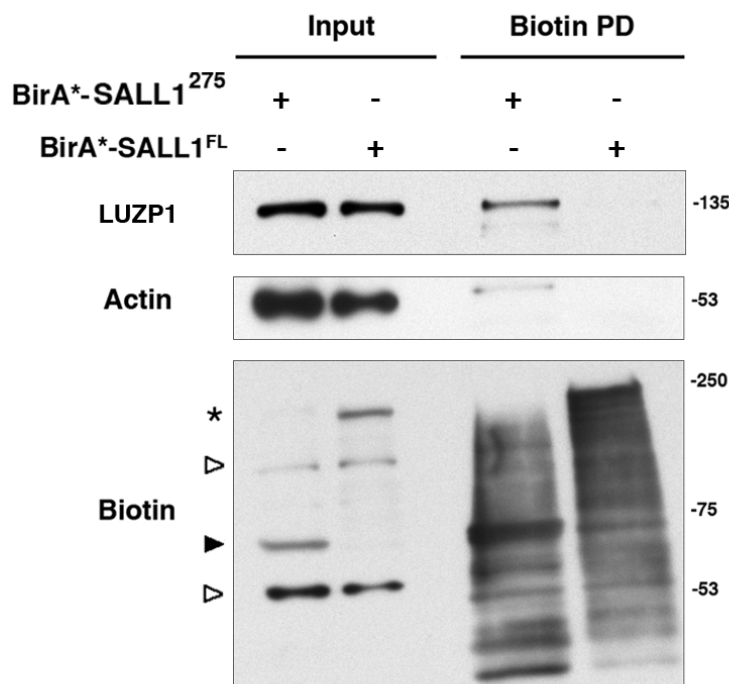


**Figure R 19. LUZP1 is in close proximity to truncated SALL1.** Western blot analysis of BioID, biotin pulldown (PD) of HEK 293FT cells transfected with Myc-tagged *BirA\*-SALL1$^{p.Arg275*}$* (BirA\*-SALL1$^{275}$) or BirA\*-SALL1$^{FL}$. A specific antibody against the endogenous LUZP1 protein was used. Biotin antibody detected the most strongly biotinylated proteins in the inputs and pulldowns, which are the self-biotinylated form of BirA\*-SALL1$^{FL}$ (asterisk) or BirA\*-SALL1$^{275}$ (black arrowhead), as well as other interactors in the pulldowns. White arrowheads indicate LUZP1 and actin signal from previous probing of the same membrane. Molecular weight markers (kDa) are shown to the right.

To further characterize the interaction of LUZP1 with SALL1, we performed pulldowns with tagged SALL1$^{275}$-YFP in HEK 293FT cells. Our results showed that endogenous LUZP1 was able to bind to SALL1$^{275}$, confirming our proximity proteomics data (**Figure R 20**, lane 6). The binding to SALL1$^{275}$ persisted in presence of overexpressed *SALL1$^{FL}$* (**Figure R 20**, lane 9), indicating that the possible heterodimerization of the truncated and FL forms does not inhibit the interaction with LUZP1. LUZP1 also binds SALL1$^{FL}$ when overexpressed alone, although to a lesser extent (**Figure R 20**, lane 7). These results support the notion that the truncated form of SALL1 expressed in TBS individuals, either by itself or in complex with the FL form, can bind to LUZP1.
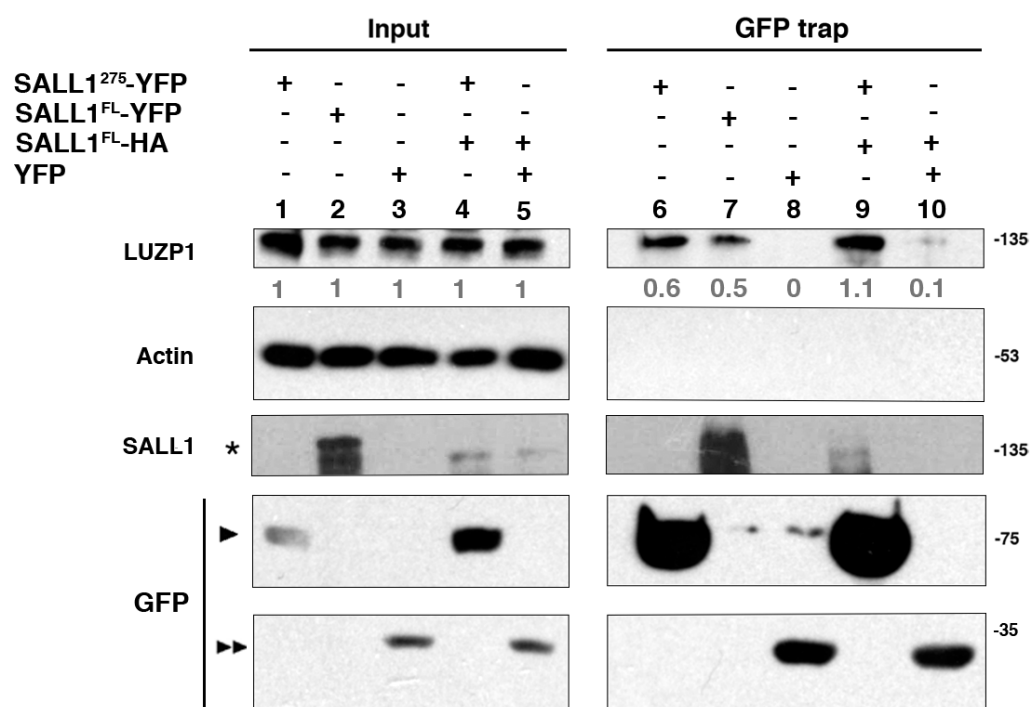


**Figure R 20. LUZP1 interacts with truncated SALL1.** Western blot of inputs or GFP-Trap pulldowns performed in HEK 293FT cells transfected with *SALL1$^{c.826C>T}$-YFP* (SALL1$^{275}$-YFP; lanes 1 and 6), *SALL1$^{FL}$-YFP* (lanes 2 and 7), *YFP* alone (lanes 3 and 8), *SALL1$^{275}$-YFP* together with *SALL1$^{FL}$-2xHA* (SALL1$^{FL}$-HA; lanes 4 and 9) or *SALL1$^{FL}$-HA* together with *YFP* alone (lanes 5 and 10). Endogenous LUZP1 was detected with a specific antibody. Numbers under LUZP1 panel result from dividing band intensities of each pulldown by their respective input levels. One asterisk indicates SALL1$^{FL}$-YFP, one black arrowhead SALL1$^{275}$-YFP and two black arrowheads YFP alone. Molecular weight markers (kDa) are shown to the right. Actin was used as loading control. Blots shown are representative of three independent experiments.

## 4.2.5 LUZP1 localizes to centrosome and is altered in TBS fibroblasts

In order to further study the role that LUZP1 might have in TBS, we checked its subcellular localization in fibroblasts derived from two TBS individuals (TBS[332] and TBS[275]; see Materials and Methods) (Furniss et al., 2007) as well as control fibroblasts (ESCTRL2). Our results showed that, in non starved conditions, LUZP1 was present in 4 foci per centrosome in 91% of the control cells (**Figure R 21A and Figure R 21D**), detected by gamma tubulin) whereas only three foci were present in at least 50% of the TBS cells (**Figure R 21A-D**, 3 foci per centrosome). Upon starvation, one of the LUZP1 foci disappeared from the MC in 100% of both the control and TBS cells (**Figure R 21B-D**, 3 foci per centrosome). These findings suggest that LUZP1 removal from the centrosome might be necessary for ciliogenesis and that this phenomenon is somehow altered in TBS cells. Based on its localization at the centrosome and the defects in ciliogenesis previously observed in TBS cells, we hypothesized that LUZP1 might have a role in cilia formation. To prove this hypothesis, we used Shh-LIGHT2 cells (Taipale et al., 2000). Using CRISPR/Cas9 gene editing directed to exon 1 of murine *Luzp1*, we generated Shh-LIGHT2 mouse fibroblasts null for *Luzp1* (Luzp1^{-/-} cells) and Luzp1^{-/-} cells rescued by the expression of human *LUZP1-YFP* (+LUZP1 cells). First, we characterized LUZP1 expression in WT, Luzp1^{-/-} and +LUZP1 cells by immunofluorescence and Western blot, confirming the lack of LUZP1 signal in Luzp1^{-/-} cells (**Figure R 22A and Figure R 22B, respectively**). In agreement with what was observed in TBS cells, LUZP1 localized in four foci, two per centriole, in both WT and +LUZP1 cells (**Figure R 22C**). As expected, LUZP1 was absent from the centrosome in Luzp1^{-/-} cells.

As observed in human cells, we found by immunofluorescence in WT cells that LUZP1 was also depleted in one of the centrioles upon starvation (**Figure R 23A and Figure R 23B**, green channel).
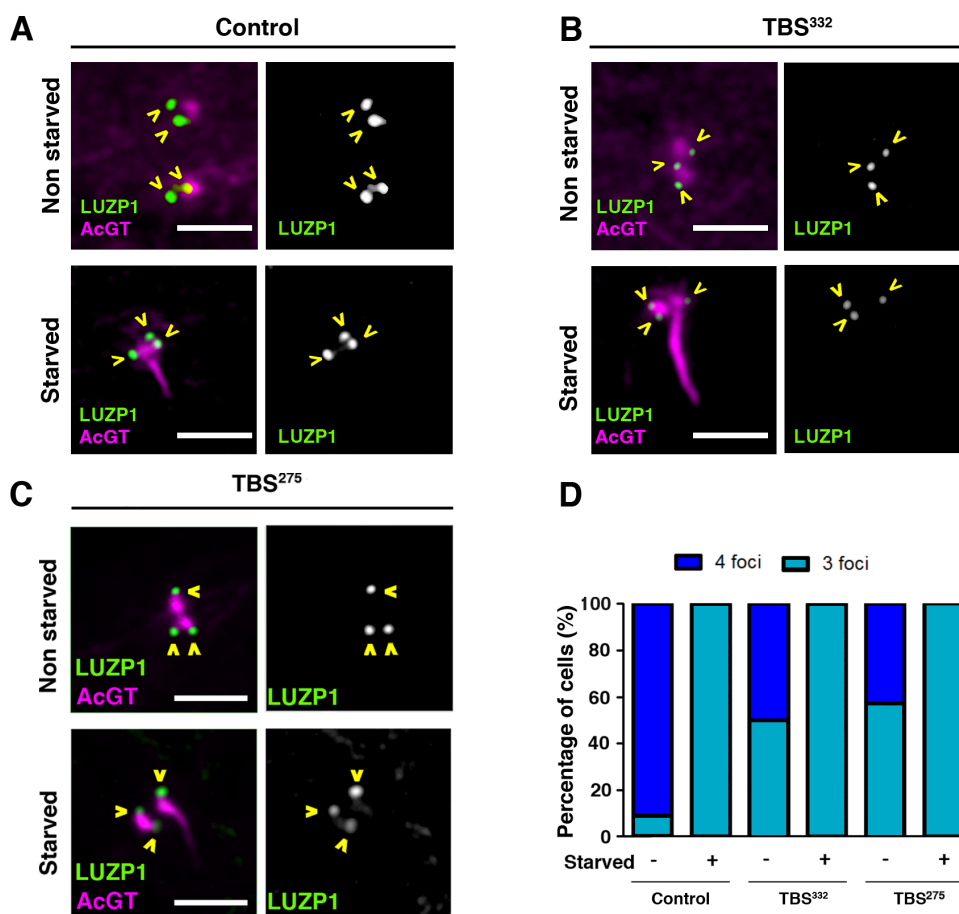
**Figure R 21. TBS cells show changes in LUZP1 localization at the centrosome.** (**A,B,C**) Immunofluorescence micrographs of non starved and starved human-derived control ESCTRL#2 (**A**), TBS[332] fibroblasts (**B**) and TBS[275] fibroblasts (**C**) stained with antibodies against endogenous LUZP1 (green, yellow arrowheads) and acetylated alpha and gamma tubulin to label the cilia and centrosomes, respectively (AcGT, purple). Black and white images show the single green channel. Note the lack of one LUZP1 foci in TBS[332] and TBS[275] compared to control ESCTRL2 fibroblasts in non starved conditions. Scale bars, 5 µm. (**D**) Graphical representation of the percentage of cells showing the presence of LUZP1 at the centrosome in 3 or 4 foci per micrograph, corresponding to the experiments in (**A**), (**B**) and (**C**); n=30 micrographs. Three independent experiments were pooled together. Scale bar, 5 µm. Images were taken with a Zeiss Axioimager D1, 63x objective.
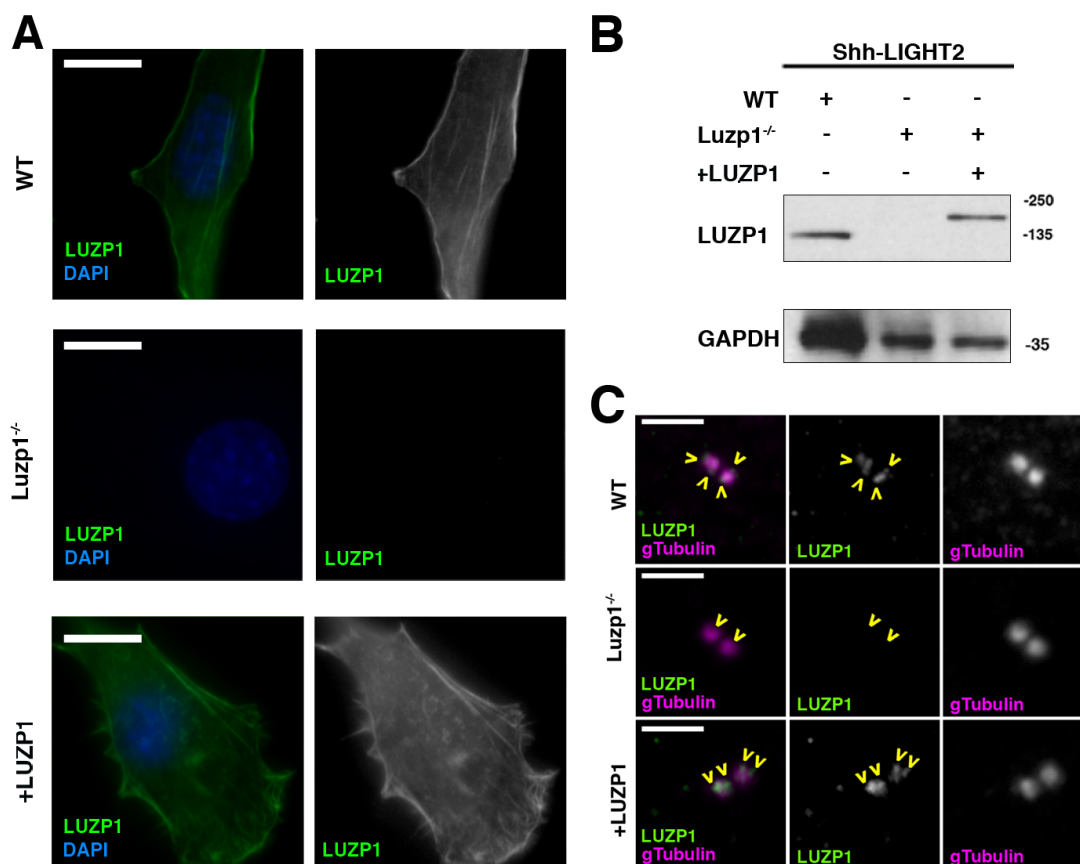
**Figure R 22. LUZP1 is missing from the centrosome in Shh-LIGHT2 cells lacking *Luzp1*.** (**A**) LUZP1 antibody validation**.** Immunofluorescence micrographs of Shh-LIGHT2 cells (WT), Luzp1 depleted Shh-LIGHT2 cells (Luzp1$^{-/-}$) and Luzp1 cells rescued with LUZP1 (+LUZP1 cells) stained with a specific antibody against endogenous LUZP1 (Sigma, green) and counterstained with DAPI (blue). Single green channel is shown in black and white. Note the lack of LUZP1 in Luzp1$^{-/-}$ cells. Scale bar, 10 µm. (**B**) Western blot analysis of total lysates of WT, Luzp1$^{-/-}$ cells and +LUZP1 cells. Anti-LUZP1 antibody from Sigma specifically recognizes LUZP1 and GAPDH was used as loading control. (**C**) Immunofluorescence micrographs of WT, Luzp1$^{-/-}$ and +LUZP1 cells stained with antibodies against endogenous LUZP1 (green) and gamma tubulin (purple). Single green and purple channels are shown in black and white. Note the lack of LUZP1 in Luzp1$^{-/-}$ cells. Scale bar, 2.5 µm. gTub: gamma tubulin.
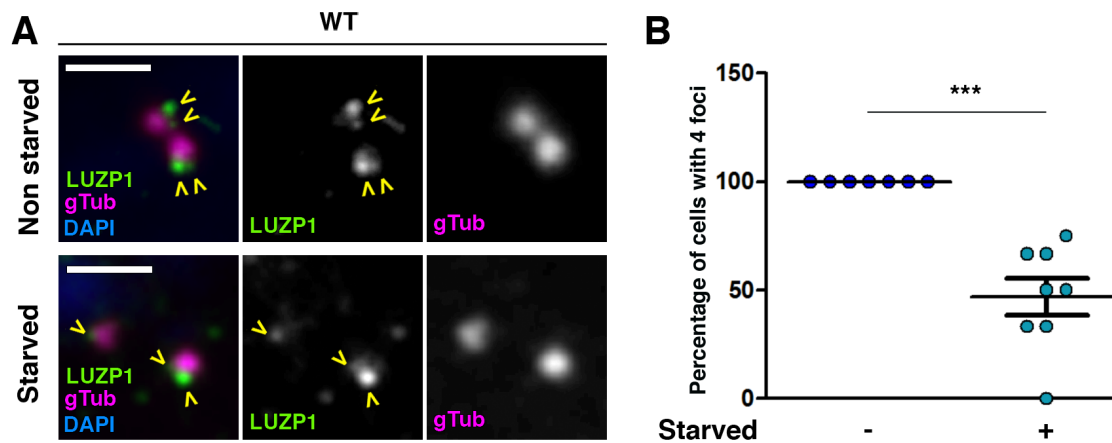
**Figure R 23. LUZP1 is depleted from the centrosome in Shh-LIGHT2 cells upon starvation.** (**A**) Immunofluorescence micrographs of non starved and starved Shh-LIGHT2 cells (WT) stained with antibodies against endogenous LUZP1 (green), gamma tubulin (gTub, purple) and counterstained with DAPI (blue). Black and white images show the single green and purple channels. Scale bar, 5 μm. (**B**) Graphical representation of the percentage of non starved *vs* starved Shh-LIGHT2 control cells (WT) with 4 LUZP1 foci in (**A**). n>7 micrographs. Graphs represent Mean and SEM of three independent experiments. Pictures were taken using a Leica SP2 confocal microscope, with a 63x objective. P-value was calculated using two-tailed unpaired Student´s t-test.

## 4.2.6 LUZP1 localizes to actin and the midbody and is altered in TBS fibroblasts

In addition to localize to the centrosome, we also detected LUZP1 in the actin fibers (**Figure R 24A**). Interestingly, LUZP1 levels were reduced in TBS cells and this reduction was accompanied by decreased actin filaments compared with control, as shown by phalloidin staining (**Figures 24A-C**). Moreover, LUZP1 was also detected in the midbody (**Figure R 24D**). The midbody is an organelle formed at the intercellular bridge in the last phase of citokinesis that recruits crucial proteins for the abscission between the dividing cells (D'Avino and Capalbo, 2016).
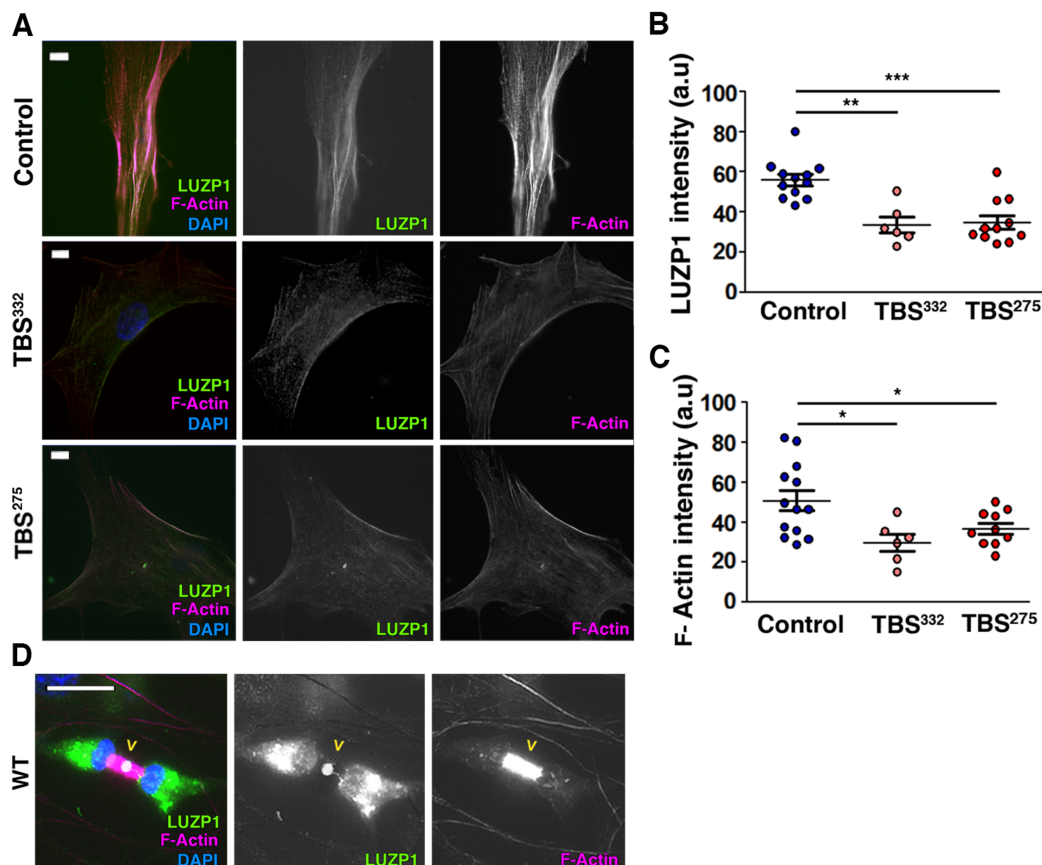
**Figure R 24. A reduction in LUZP1 is accompanied by a decrease in F-actin in TBS cells.** (**A**) Immunofluorescence micrographs of human-derived control ESCTRL#2, TBS[332] and TBS[275] fibroblasts stained with an antibody against endogenous LUZP1 (green), phalloidin to label F-actin (purple), and counterstained with DAPI to label the nuclei (blue). Note the reduction in LUZP1 and F-actin levels in TBS[332] and TBS[275] compared to control fibroblasts. Scale bar, 10 μm. (**B,C**) Graphical representation of the LUZP1 (**B**) and F-actin (**C**) mean intensity, corresponding to the experiments shown in (**A**); n≥6 micrographs. (**D**) Immunofluorescence micrographs of two dividing Shh-LIGHT2 cells stained with antibodies against endogenous LUZP1 (green), F-Actin (purple) to label microtubules and DAPI to label the nuclei (blue). Note the presence of LUZP1 in the midbody (yellow arrowhead). Scale bar, 30 μm. Black and white images show the single green and purple channels. Three independent experiments were pooled together. P-values were calculated using One way ANOVA and Dunn's Multiple Comparison post-hoc test.

TBS cells also showed reduced sensitiveness to a F-actin depolymerizing drug, CytB. When induced with CytB, control cells lost shape and detached more dramatically than TBS cells (**Figure R 25**).
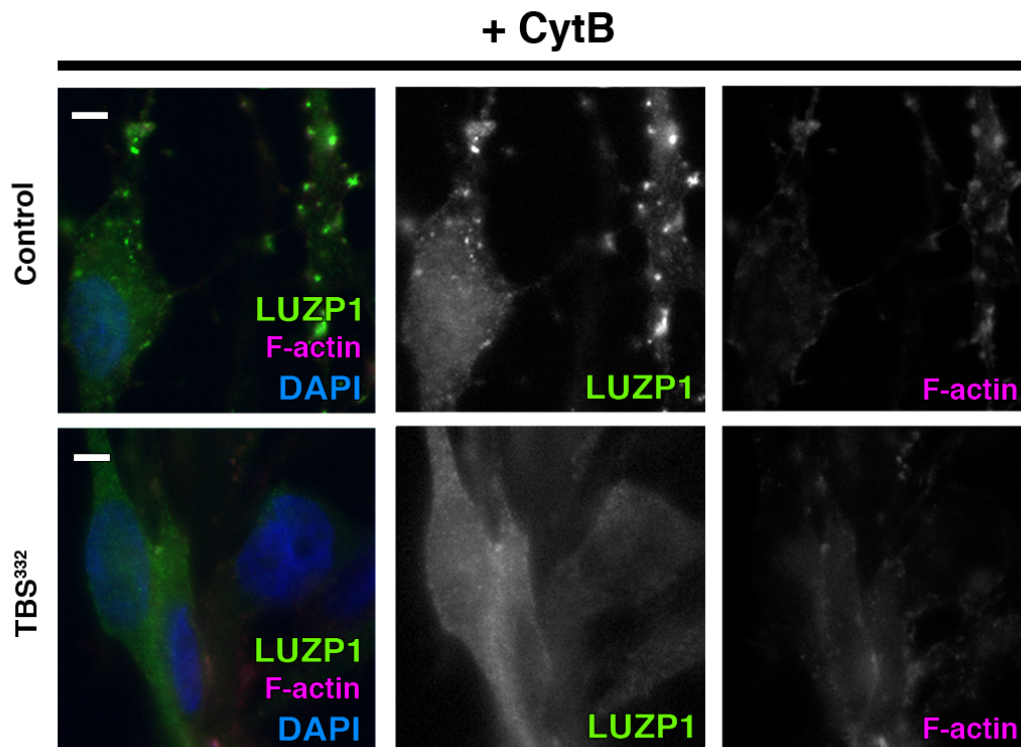
**Figure R 25. TBS cells are more sensitive to Cytochalasin B treatment.** Immunofluorescence micrographs of control and TBS[332] cells treated with cytochalasin B (CytB) and stained with LUZP1 (green), phalloidin to label F-actin (purple) and DAPI to counterstain the nuclei (blue). Note that TBS[332] are less sensitive to CytB treatment than control.

LUZP1 exhibited accumulation in clumps in control cells upon CytB treatment while it did not show significant changes in TBS cells (compare **Figure R 25** with **Figure R 24A**). These results indicate that actin cytoskeleton might be altered in TBS cells, which is in agreemnet with the higher ciliation rates they exhibit.

We also observed a reduction in F-actin (labeled by phalloidin) in the Luzp1^{-/-} cells compared to WT, which was recovered in +LUZP1 cells (**Figure R 26**). Furthermore, LUZP1 levels and filamentous actin were diminished in WT fibroblasts upon starvation (**Figure R 27A and Figure R 27B**). These results suggest that LUZP1 might be a F-actin stabilizing protein and that starvation triggers both LUZP1 and F-
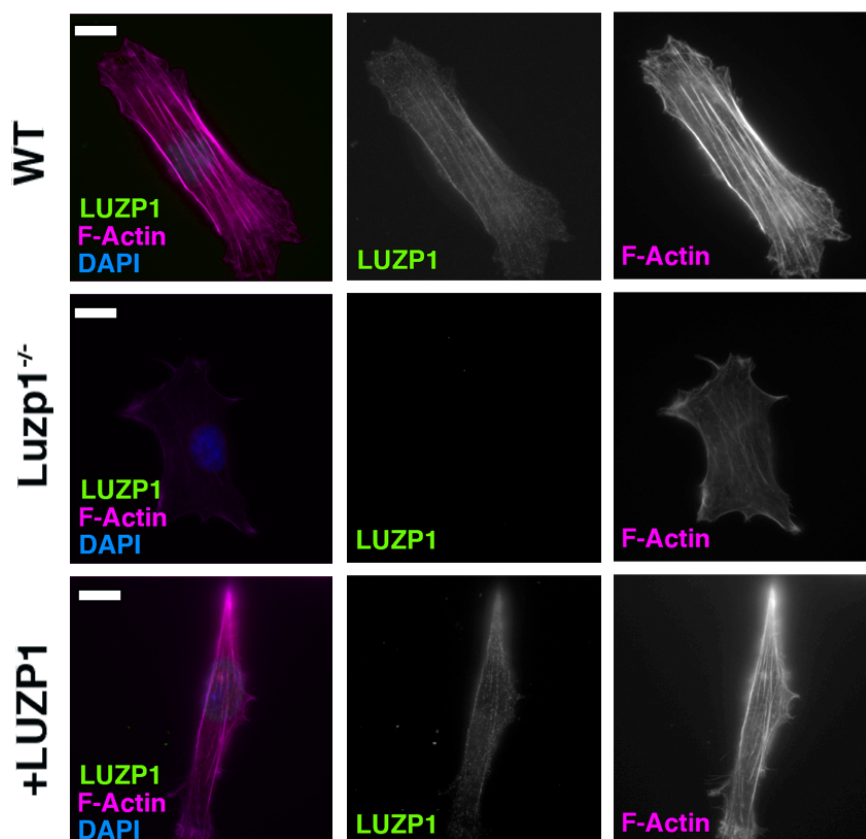
**Figure R 26. The lack of *Luzp1* is accompanied by a decrease in F-actin in Shh-LIGHT2 cells.** (A) Immunofluorescence micrographs of Shh-LIGHT2 cells (WT), Luzp1 depleted Shh-LIGHT2 cells (Luzp1$^{-/-}$) and Luzp1$^{-/-}$ cells rescued with *Luzp1-YFP* (+LUZP1). Cells were stained with an antibody against endogenous LUZP1 (green), phalloidin to detect F-actin (purple), and counterstained with DAPI (blue). Single green and purple channels are shown in black and white. Note the lack of LUZP1 and reduction of F-actin in Luzp1$^{-/-}$ cells. Scale bar, 10 μm.

actin reduction. Consistent with the observed reduction of F-actin, Luzp1$^{-/-}$ cells showed reduced sensitivity to CytB, as previously noted in TBS cells (**Figure R 28**).

Although LUZP1 levels were reduced in TBS cells by immunofluorescence, no transcriptional changes were detected in *LUZP1* expression between control and TBS samples by RT-qPCR (**Figure R 29A**). However, we confirmed a reduction in LUZP1 total levels in TBS cells compared to control cells by western blot (0.8 *vs* 1 folds, lane 1 *vs* 4, respectively; **Figure R 29B**). These results suggest that truncated SALL1 might
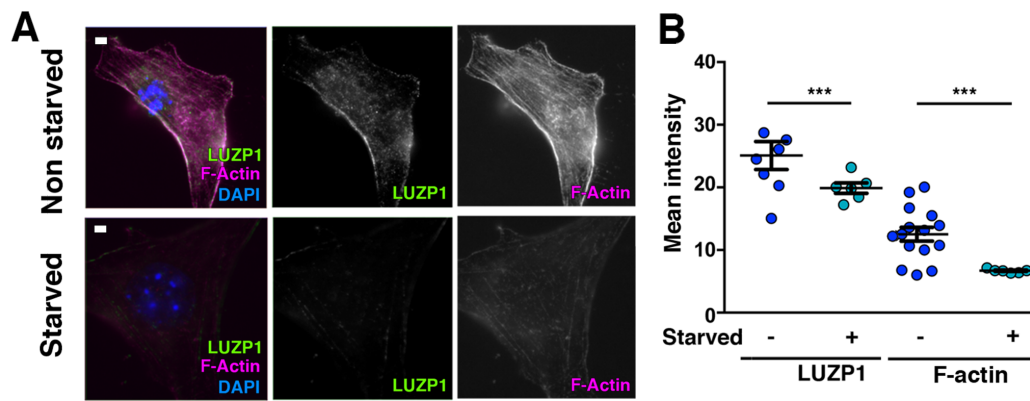
**Figure R 27. A reduction in LUZP1 is linked to a decrease in F-actin in cells upon starvation.** (**A**) Immunofluorescence micrographs of non starved and starved Shh-LIGHT2 WT cells stained with antibodies against endogenous LUZP1 (green), phalloidin to detect F-actin (purple) and counterstained with DAPI (blue). Single green and purple channels are shown in black and white. Scale bar, 5 μm. (**B**) Graphical representation of the LUZP1 or phalloidin mean intensity as shown in (**A**). Pictures were taken using a confocal microscope, Leica SP2, with a 63x objective. Graphs represent Mean and SEM of three independent experiments pooled together. P-values were calculated using One way ANOVA and Bonferroni post-hoc test.
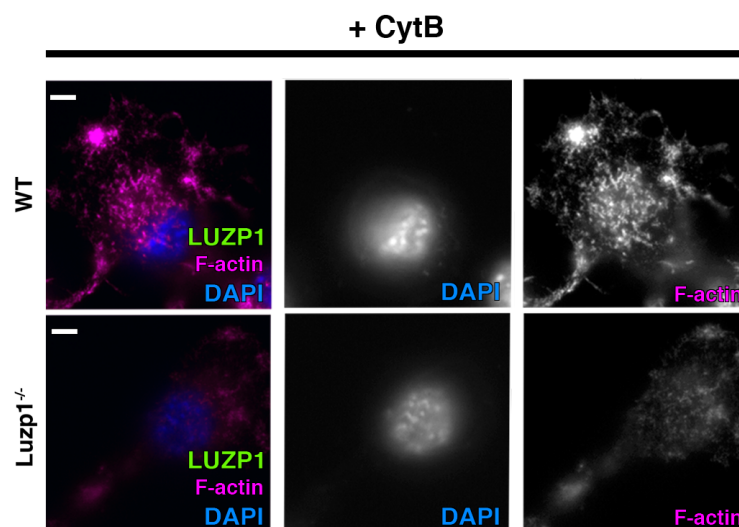


**Figure R 28.** *Luzp1* **depleted cells are more sensitive to Cytochalasin B treatment.** Immunofluorescence micrographs of Shh-LIGHT2 cells (WT) and Shh-LIGHT2 cells lacking *Luzp1* (Luzp1^{-/-}) treated with cytochalasin B (CytB) and stained with phalloidin to label F-actin (purple) and with DAPI to label the nuclei (blue). Note that Luzp1^{-/-} cells are less sensitive to CytB treatment than WT cells.
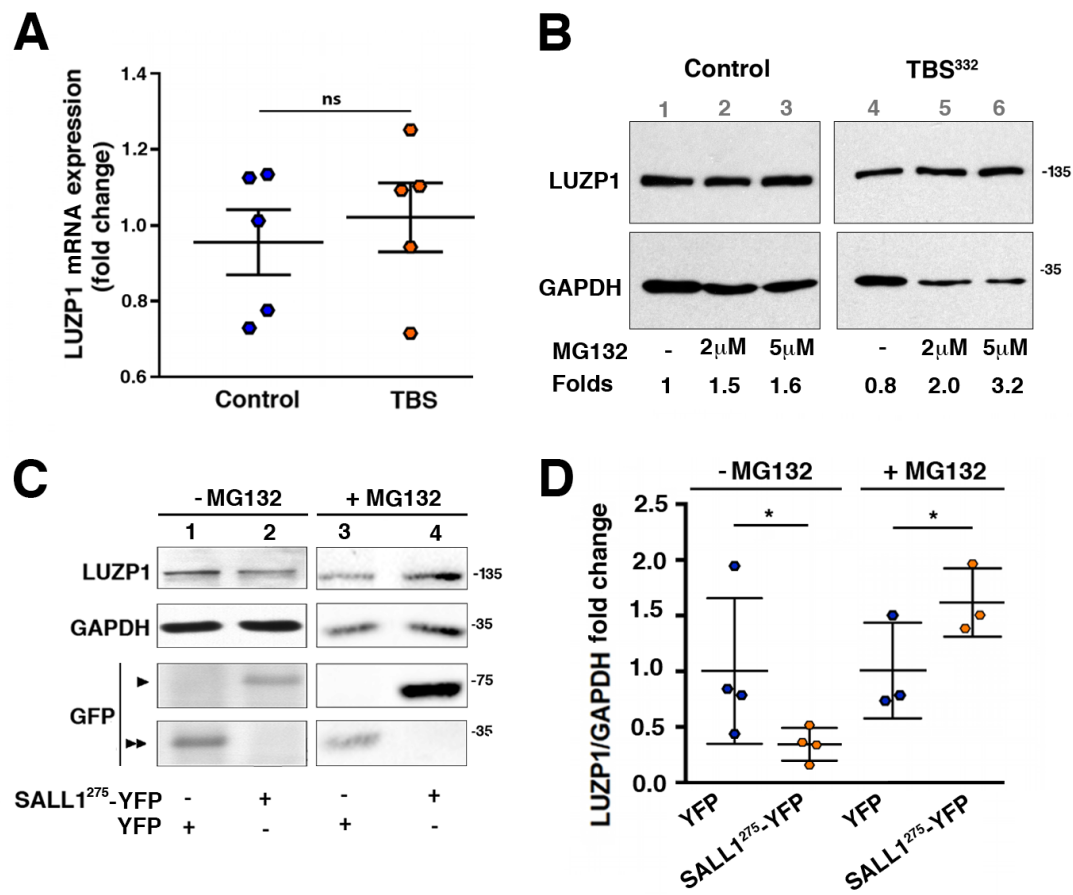
**Figure R 29. Truncated SALL1 leads to LUZP1 destabilization and degradation.** (**A**) Quantification of *LUZP1* expression by qPCR in ESCTRL2 (control) *vs* TBS$^{332}$ and TBS$^{275}$ cells pooled together (TBS). Graphs represent Mean and SEM from 5 independent experiments. P-value was calculated using the Mann Whitney test; ns: no significant. (**B**) Representative Western blot of ESCTRL2 (Control) and TBS$^{332}$ total cell lysates treated or not with MG132 (2 or 5 µM). A specific antibody against LUZP1 detected endogenous LUZP1 and GAPDH was used as loading control. Numbers on top of LUZP1 panel represent the number lanes. Numbers under LUZP1 panel result from dividing band intensities of each lane by control without MG132 treatment (lane 1). Note the more prominent increase of LUZP1 levels in TBS$^{332}$ cells upon MG132 treatment (lanes 2 and 3 *vs* lanes 5 and 6). (**C**) Representative western blot of total lysates of HEK 293FT cells transfected with *SALL1$^{c.826C>T}$-YFP* (SALL1$^{275}$-YFP; lanes 1 and 3) or YFP alone (lanes 2 and 4) treated (+) or not (-) with the proteasome inhibitor MG132. Note an increase in LUZP1 in the presence of MG132 (+MG132) when *SALL1$^{275}$-YFP* was transfected. Specific antibodies against LUZP1, GFP and GAPDH were used. Molecular weight markers (kDa) are shown to the right. **(D)** Graphical representation of the fold changes of LUZP1/GAPDH ratios obtained in (C) for HEK 293FT cells transfected with *SALL1$^{c.826C>T}$-YFP* (SALL1$^{275}$-YFP; orange dots) or YFP alone (blue dots) treated (+) or not (-) with the proteasome inhibitor MG132. Data from at least three independent experiments pooled together are shown. P-values

modulate LUZP1 stability. In order to understand these changes, we analysed LUZP1 levels after treatment with MG132, a known inhibitor of the proteasome, both in control and TBS cells. LUZP1 levels were increased to a higher extent in TBS compared to control cells (**Figure R 29B,** +MG132). Moreover, we confirmed the reduction of LUZP1 levels in HEK 293FT cells overexpressing truncated SALL1 (*SALL1^{275}-YFP*) compared to the control cells overexpressing *YFP* alone (**Figure R 29C and Figure R 29D**). An increase in LUZP1 accumulation upon MG132 treatment was also observed in HEK 293FT cells overexpressing *SALL1^{275}-YFP* compared to their controls overexpressing *YFP*. These results suggest that truncated SALL1 leads to LUZP1 instability and degradation.

### 4.2.7 LUZP1 interacts with actin and centrosome-associated proteins

LUZP1 localization in human cells suggested a relation of this protein with actin and centrosome-related proteins. First, the association between LUZP1 and actin-related proteins was supported by the binding of LUZP1-YFP to beta actin and filamin A, FLNA (**Figure R 30A**). The link between LUZP1 and actin was further demonstrated by treating HEK 293FT cells with CytB. LUZP1 levels were increased in HEK 293FT cells treated with CytB as shown by Western blot (**Figure R 30B and Figure R 30C**). This result might indicate that, when actin depolymerization is induced, LUZP1 becomes more soluble to the extraction buffer.

Next, we found that the two major ciliogenesis suppressors, CCP110 and CEP97, interact with LUZP1-YFP, either in WT HEK 293FT cells or in 293^{335} *SALL1* mutant cells (**Figure R 31A**, lanes 5 and 7, respectively). As shown before in both, TBS cells and HEK 293FT cells overexpressing SALL1^{275} (**Figure R 29B** and **Figure R 29C**), LUZP1 input levels were reduced in total extracts of 293^{335} compared with WT cells (**Figure R 31A**, Input, lane 1 *vs* lane 3), leading to less CCP110 and CEP97 interacting with LUZP1 in those cells in the pulldowns.

Furthermore, we found LUZP1 interacting with the centrosomal proteins
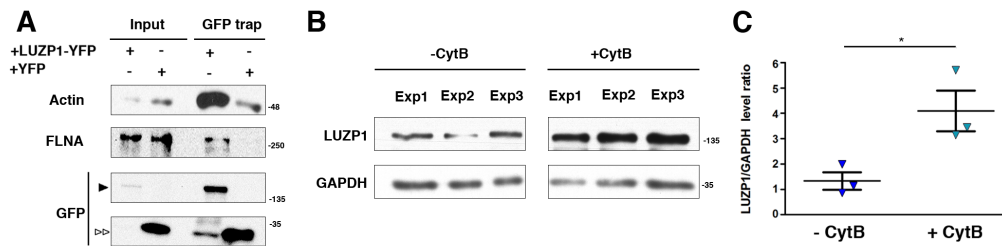
**Figure R 30. LUZP1 interacts with actin-related proteins.** (**A**) Western blot of inputs or GFP-Trap pulldowns performed in HEK 293FT cells transfected with *LUZP1-YFP* (LUZP1-YFP) or *YFP* alone (YFP). Specific antibodies against the endogenous actin and filamin A (FLNA) proteins were used. GFP antibody detected LUZP1-YFP (black arrowhead) and YFP alone (two white arrowheads). (**B**) Western blot of total cell lysates from 3 independent experiments in HEK 293FT treated or not with Cytochalasin B (CytB). Note the increase in LUZP1 levels upon actin polymerization blockage with CytB. Endogenous LUZP1 was detected by a specific antibody against LUZP1 and GAPDH was used as loading control. (**C**) Graphical representation of LUZP1 *vs* GAPDH band intensities in (**B**). Graphs represent Mean and SEM of three independent experiments. P-value was calculated using two tailed unpaired Student´s t-test.

CCP110 and CEP97 by immunoprecipitating endogenous LUZP1 and CEP97, respectively (**Figure R 31B and Figure R 31C**). These results confirm that, in agreement with the localization of the protein to the actin cytoskeleton and the centrosome, LUZP1 interacts with components of both cellular structures and further support the notion that the presence of truncated SALL1 leads to a reduction in the total levels of LUZP1.

### 4.2.8 LUZP1 plays a role in primary cilia formation

In view of LUZP1 localization to the centrosome and its interaction with the centrosome-related proteins CCP110 and CEP97, we hypothesized that LUZP1 might have a role in cilia formation. To analyse this posibility, WT, Luzp1$^{-/-}$ and +LUZP1 cells were plated at equal densities and promoted either to ciliate for 48h by serum withdrawal (−FBS), or to reabsorb their cilia by serum replenishment for 4h (+FBS). We quantified ciliation rates and primary cilia length at all mentioned timepoints.
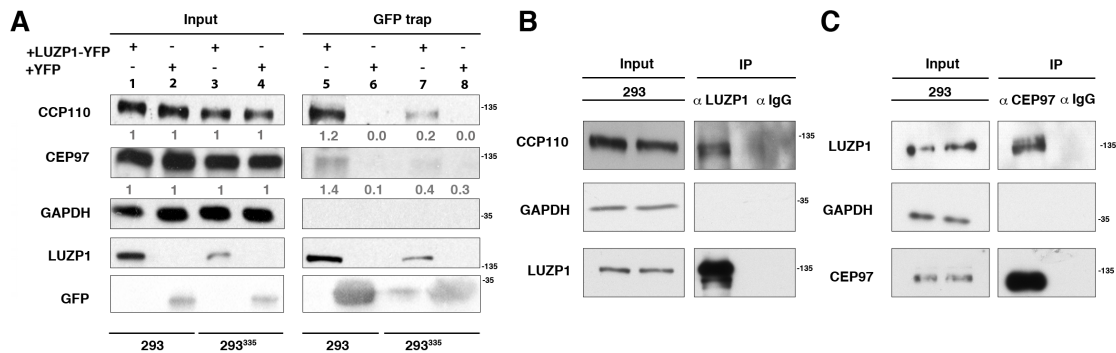
**Figure R 31. LUZP1 interacts with centrosome-related proteins.** (**A**) Western blot of inputs (lines 1 to 4) and GFP-Trap pulldowns (lines 5 to 8) performed in WT HEK 293FT cells (293) or in 293[335] *SALL1* mutant cells transfected with *LUZP1-YFP* (lanes 1,3,5 and 7) or *YFP* alone (lanes 2,4, 6 and 8). Endogenous CEP97 and CCP110 were detected with specific antibodies. Numbers under CCP110 and CEP97 panels result from dividing band intensities of each pulldown by their respective input levels. GAPDH was used as loading control. (**B,C**) Western blot of representative immunoprecipitation (IP) assays using LUZP1 and CEP97 specific antibodies to pull down CCP110

Luzp1^{-/-} fibroblasts displayed higher ciliation rate (60%) than WT (10.5%) and +LUZP1 (22.2%) when the cells were not subjected to starvation (**Figure R 32A and Figure R 32B**). However, Luzp1^{-/-} cells were not significantly more ciliated than WT or +LUZP1 fibroblasts upon 48 hours of starvation (**Figure R 32B**). In addition, primary cilia in Luzp1^{-/-} cells were significantly longer than in non-starved WT cycling cells; under 48 hours of starvation, the differences among WT, Luzp1^{-/-} and +LUZP1 were not significant. In the case of cilia length, Luzp1^{-/-} and +LUZP1 cells behaved similarly (no starvation: average 3.0 μm in Luzp1^{-/-} cells and 2.9 μm in +LUZP1 cells; 48h starvation: average 4.1 μm in Luzp1^{-/-} cells and 4.8 μm in +LUZP1 cells; 4h upon disassembly induction: 3 μm in Luzp1^{-/-} cells and 2.9 μm in +LUZP1 cells) (**Figure R 32A and Figure R 32C**). These results confirm that Luzp1^{-/-} cells display longer and more abundant primary cilia compared to WT cells in cycling conditions and indicate that LUZP1 might affect primary cilia dynamics. This phenotype, partially rescued by

the expression of LUZP1, is reminiscent of the phenotype described in TBS cells.

To check whether the overexpression of *LUZP1* is sufficient to rescue the higher ciliation rates and repress ciliogenesis in primary human TBS cells, TBS[275] cells
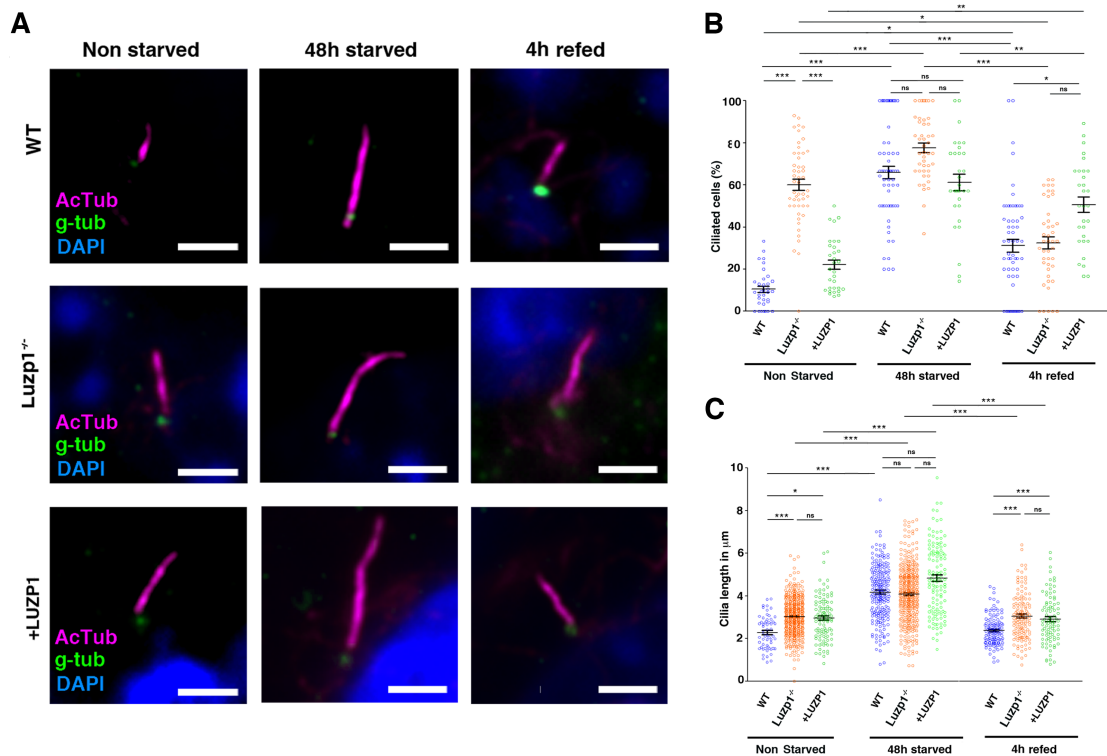
**Figure R 32. *Luzp1*<sup>-/-</sup> cells show aberrant cilia frequency and length.** (**A**) Micrographs of Shh-LIGHT2 cells (WT), Shh-LIGHT2 cells lacking *Luzp1* (Luzp1<sup>-/-</sup>) and Luzp1<sup>-/-</sup> cells rescued with human *LUZP1-YFP* (+LUZP1) analysed in cycling conditions (non starved), or during cilia assembly (48h starved) and disassembly (4h refed). Cilia were visualized by acetylated alpha tubulin (AcTub, purple), basal body by gamma tubulin (g-tub, green) and nuclei by DAPI (blue). Scale bar, 2.5 μm. (**B,C**) Graphical representation of percentage of ciliated cells (**B**) and cilia length (**C**) measured in WT (blue circles, n>34 cilia), Luzp1<sup>-/-</sup> (orange circles, n>44 cilia) or +LUZP1 cells (green circles, n>30 cilia) from three independent experiments. Cells that underwent 48 hours of starvation were compared to non-starved cells. After starvation, cells were supplied with serum for 4 hours (n=21-30 micrographs for all the cases). Pictures were taken using an Axioimager D1 fluorescence microscope, Zeiss with a 63x objective. Graphs represent Mean and SEM of three independent experiments. P-values were calculated using One way ANOVA and Bonferroni post-hoc test or two tailed unpaired Student´s t-test.

were ransiently transfected with *YFP* (**Figure 33A**) or *LUZP1-YFP* (**Figure 33B**). None of the TBS<sup>275</sup> cells transfected with *LUZP1-YFP* were ciliated (yellow arrowhead) (**Figure 33C**) whereas the surrounding non transfected cells displayed cilia (white arrowheads). In contrast, most non-transfected surrounding cells, as well as TBS<sup>275</sup> cells overexpressing *YFP* were ciliated. Thus, these results confirm that LUZP1 might be a potential primary cilium repressor and suggest that the TBS phenotype might be partially caused by the reduction in LUZP1 levels.
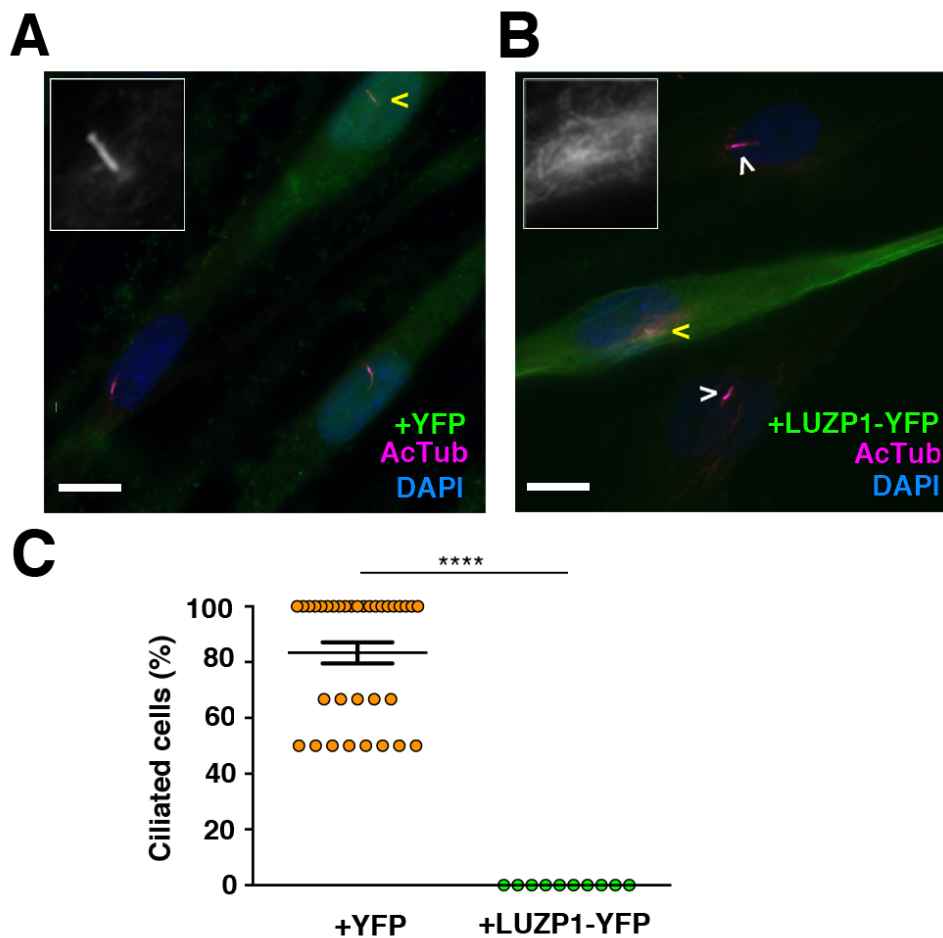
**Figure R 33.** *Luzp1* **expression is sufficient to repress ciliogenesis in TBS cells.** (**A,B**) Representative micrographs of ciliated TBS[275] cells showing in green *YFP* (**A**) or *LUZP1-YFP* (**B**). Cilia were visualized by acetylated alpha tubulin (AcTub, purple), and nuclei by DAPI (blue). Note the lack of cilia in cells overexpressing LUZP1-YFP. Yellow arrowheads point at a magnified region shown in black and white in the upper left panel. White arrowheads point at the cilia of the LUZP1-YFP non transfected cells. Scale bar, 10 µm. Pictures were taken using an Axioimager D1 Zeiss fluorescence microscope, with a 63x objective. (**C**) Graph represents the percentage of ciliated cells in cells overexpressing *YFP* (orange dots, n=34) or *LUZP1-YFP* (green dots, n=10). Mean and SEM of three independent experiments are shown. P-values were calculated using the two tailed unpaired Student´s t-test.

## 4.2.9 Luzp1$^{-/-}$ cells exhibit aberrant Sonic Hedgehog signalling

In view of the previously observed ciliogenesis defects, we examined whether Shh signalling is compromised in Luzp1$^{-/-}$ cells. Cells were starved for 24 hours and incubated in the presence or absence of purmorphamine for 6 or 24 hours to activate the Shh pathway. mRNA expression of two Shh target genes (*Gli1* and *Ptch1*) was quantified by qRT-PCR (**Figure R 34A and Figure R 34B**). We found that the basal *Gli1* and *Ptch1* expression levels in Luzp1$^{-/-}$ cells were higher than in WT cells (*Gli1* 1.5 fold and *Ptch1* 2.3 fold increase in Luzp1$^{-/-}$ *vs* WT cells without purmorphamine). Upon induction by purmorphamine for 24 hours, WT cells increased significantly the expression of both targets, while Luzp1$^{-/-}$ cells did not, indicating the incapacity of Luzp1$^{-/-}$ to respond to Shh signalling induction. To further study the role of LUZP1 in Shh signalling, we analysed GLI3 processing by Western blot using total lysates extracted from WT *vs* Luzp1$^{-/-}$ cells. Without purmorphamine induction, we found a significantly higher ratio of GLI3 activating form *vs* GLI3 repressive form (GLI3-A:GLI3-R) in Luzp1$^{-/-}$ cells compared to WT (2.9 fold increase in Luzp1$^{-/-}$ cells *vs* 1 foldWT) (**Figure R 34C**). After induction, the values were similar for Luzp1$^{-/-}$ and WT cells. We also examined the effects of lacking *Luzp1* on Shh signalling by measuring the activity of a Shh luciferase reporter activity (**Figure R 34D**). Prior to purmorphamine treatment, Luzp1$^{-/-}$ cells showed higher Shh activity compared to control or +LUZP1 cells, as observed in TBS-derived cells. (1.6 fold-activity in Luzp1$^{-/-}$ *vs* 0.5 fold-activity in +LUZP1 cells or 1 fold-activity in WT cells). However, the induction capacity of Luzp1$^{-/-}$ cells upon purmorphamine treatment is reduced compared to WT or +LUZP1 cells. Altogether, the observed defects in *Ptch1* and *Gli1* gene expression, reduced GLI3 processing and Shh reporter missregulation confirm a role for LUZP1 in Shh signalling.

## 4.2.10 LUZP1 regulates cell proliferation

In the course of our centrosome studies in Luzp1$^{-/-}$ cells, immunofluorescence microscopy revealed a striking phenotype: *Luzp1* depletion resulted in the presence of more than four centrioles in Luzp1$^{-/-}$ cells (**Figure R 35A and Figure R 35B**). This
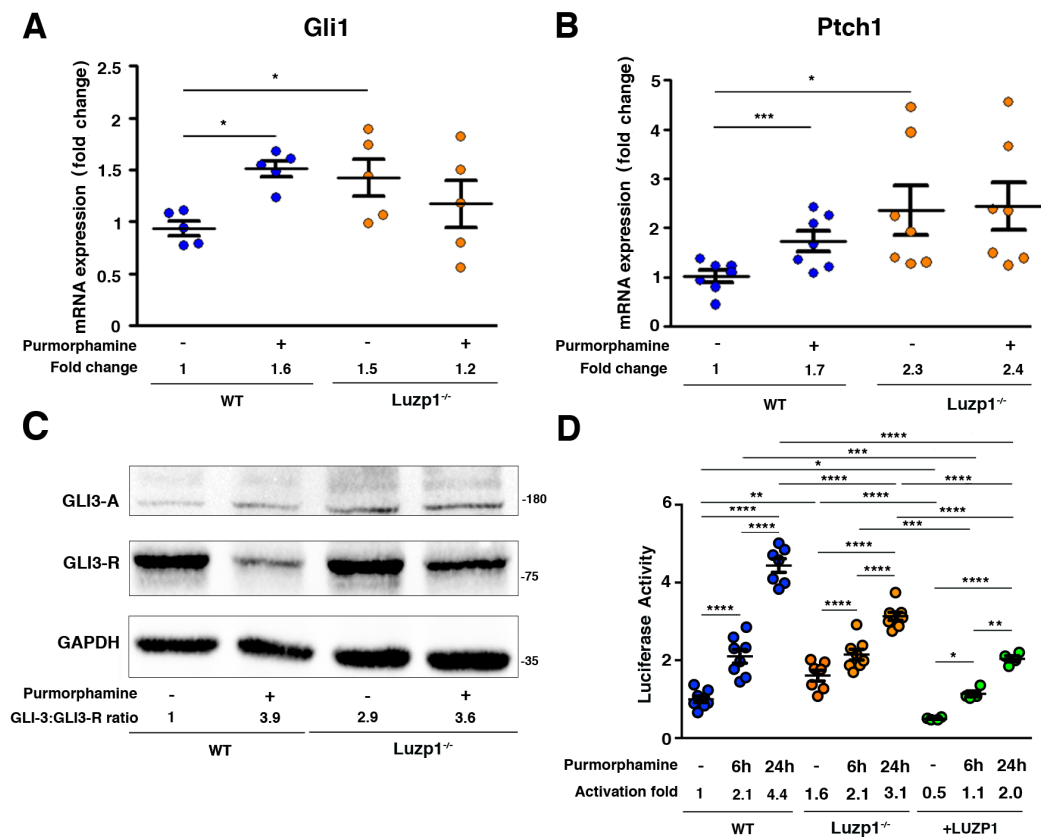
**Figure R 34. Luzp1$^{-/-}$ cells display aberrant Shh signaling. (A,B)** Graphical representation of the fold change in the expression of *Gli1* (n=5) (**A**) and *Ptch1* (n=7) (**B**) obtained by qPCR from Shh-LIGHT2 cells (WT; blue dots) or Shh-LIGHT2 cells lacking *Luzp1* (Luzp1$^{-/-}$; orange dots), treated (+) or not (-) with purmorphamine for 24 hours. (**C**) Western blot analysis of lysates from WT and Luzp1$^{-/-}$ cells. Samples were probed with an anti-GLI3 antibody that detects both GLI3 activating form (GLI3-A) and GLI3 repressive form (GLI3-R), and GAPDH was used as loading control. The ratio of activating:repressing forms of GLI3 (A:R ratio) was calculated using image analysis to quantitate the intensity of the bands, and is indicated at the bottom. The value of the WT, non-induced sample was taken as 1. Molecular weight markers (kDa) are shown to the right. (**D**) Graphical representation of fold change activation of a Shh luciferase reporter when WT cells (n>7; blue dots), Luzp1$^{-/-}$ cells (n>7; orange dots) or +LUZP1 cells (n=4; green dots) were treated or not (-) with purmorphamine for 6 or 24 hours. All graphs represent the Mean and SEM. P-values were calculated using two tailed unpaired Student´s t-test or One way ANOVA and Bonferroni post-hoc test.

phenotype was rescued in +LUZP1 cells, suggesting that lacking *Luzp1* might affect centrosome amplification. The presence of multiple centrioles was further verified in 293$^{LUZP1\ KO}$ cells (**Figure R 35C**).
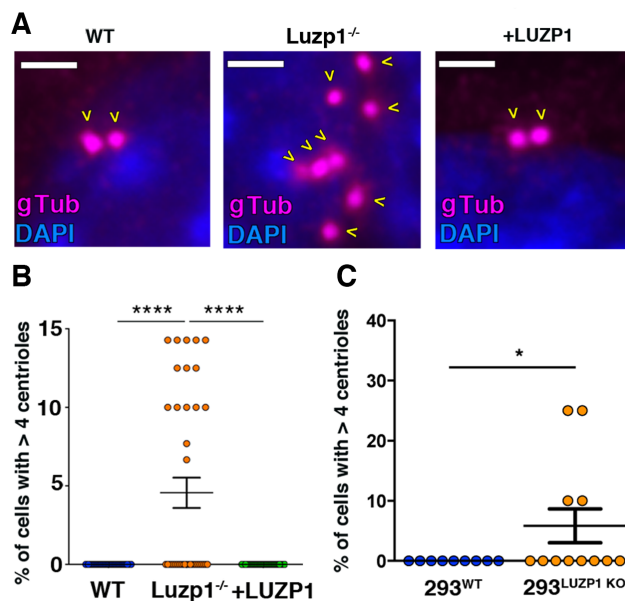
**Figure R 35.** *Luzp1*$^{-/-}$ **cells display multiple centrioles.** (**A**) Micrographs showing centrioles in wild-type Shh-LIGHT2 cells (WT), Shh-LIGHT2 cells lacking *Luzp1* (Luzp1$^{-/-}$) and Luzp1$^{-/-}$ cells rescued with *Luzp1-YFP* (+LUZP1) analysed during cycling conditions. Centrioles were visualized using a gamma tubulin antibody (gTub, purple, yellow arrowheads) and nuclei were counterstained using DAPI (blue). Scale bar, 5 μm. (**B**) Graphical representation of the percentage of cells that exhibit more than 4 centrioles in (**A**). WT, n=37, blue dots; Luzp1$^{-/-}$, n=38, orange dots; +LUZP1, n=35, green dots. P-values were calculated using Kruskall Wallis and Dunn's multiple comparisons tests.

Aberrant centriole numbers could result from defects in the control of the cell cycle, failure in cytokinesis or, alternatively, cell fusion. FACS analysis detected more apoptotic cells among the Luzp1$^{-/-}$ cell population by co-staining cells with DRAQ7 and Annexin V (**Figure R 36A and Figure R 36B**) but it did not reveal significant changes in cell cycle (**Figure R 36C**). In addition, nuclear size was significantly increased in Luzp1$^{-/-}$ cells and it was rescued in +LUZP1 cells (**Figure R 37A**), suggesting that the presence of multiple centrioles might not be a consequence of cell-cycle deregulation in Luzp1$^{-/-}$ cells, but it might be derived from defects in cytokinesis. In line with this, Luzp1$^{-/-}$ cells exhibited a significant delay in proliferation at day 3 and 6 after seeding, compared to WT cells (**Figure R 37B**). +LUZP1 cells partially rescued proliferation impairment (**Figure R 37B**, green line).

### 4.2.11 LUZP1 affects actin polymerization

Based on the actin fibers reduction observed in Luzp1$^{-/-}$ cells and that the loss
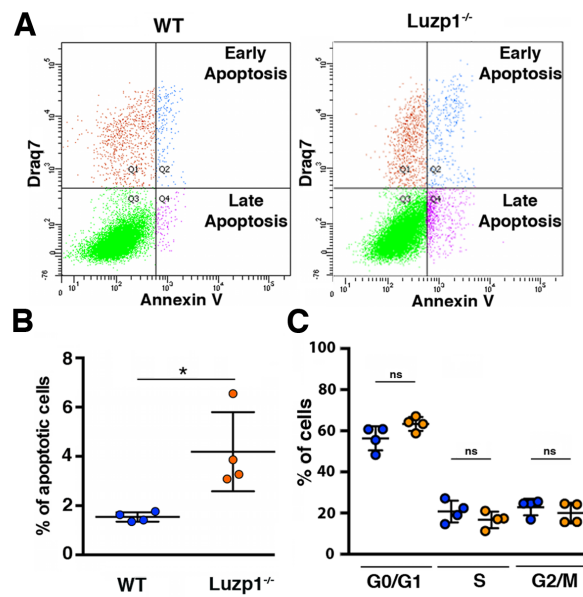
**Figure R 36. Increased apoptosis in *Luzp1*<sup>-/-</sup> cells.** (**A**) Graphical representation of the percentage of Shh-LIGHT2 WT cells (blue dots) and Shh-LIGHT2 cells Luzp1<sup>-/-</sup> cells (orange dots) in G0/G1, S or G2/M phases. P-values were calculated using Two way ANOVA. (**B**) Representative profiles of FACS analysis of apoptosis in WT and Luzp1<sup>-/-</sup> cells. Q2 and Q4 point at early and late apoptosis cells (blue and purple dots, respectively). (**C**) Graphical representation of the results of flow cytometry (FACS) analysis to determine the percentage of apoptotic cells in WT and Luzp1<sup>-/-</sup> cells in (**B**) (n=4). P-value was calculated using Mann Whitney test.
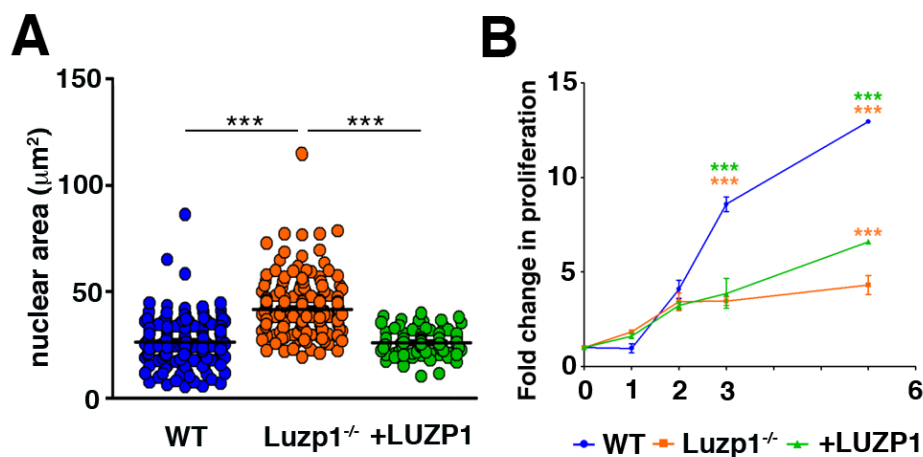


**Figure R 37. Luzp1<sup>-/-</sup> cells exhibit cell division defects.** (**A**) Graphical representation of nuclear area of Shh-LIGHT2 WT (n=178; blue dots), Luzp1<sup>-/-</sup> (n=185; orange dots) and +LUZP1 cells (n=90; green dots). P-values were calculated using Kruskall Wallis and Dunn's multiple comparisons tests. (**B**) Graphical representation of fold change in cell proliferation of WT (n=5; blue line), Luzp1<sup>-/-</sup> (n=5; orange line) and +LUZP1 cells (n=5; green line). The graphs represent the Mean and SEM. P-values were calculated using Two way ANOVA and Sidak's multiple comparisons test.

117

of ARP3 has been previously shown to increase axoneme length in htRPE cells (Kim et al., 2010), we aimed to characterize their actin polymerization state by assessing ARP3 and cofilin levels in those cells by Western blot. The decrease in ARP3 levels (**Figure R 38A and Figure R 38B**) was accompanied by an increase in phosphorylated cofilin in Luzp1$^{-/-}$ cells (**Figure R 38C and Figure R 38D**). Of note, we also analysed Rac1 activation by phosphorylation (pRAC1 *vs* RAC1), but we did not find significant differences between Luzp1$^{-/-}$ and WT cells (**Figure R 38E and Figure R 38F**).

### 4.2.12 LUZP1 interferes with cell migration

Based on the neural tube closure defects that *Luzp1* KO mice display, together with the relevance of actin cytoskeleton dynamics for proper cell migration in the neural tube closure process (Cabrera et al., 2004; Copp et al., 2003; Wallingford, 2005), we analysed cell migration rates in Luzp1$^{-/-}$ cells using a wound-healing assay. This assay typically measures migration of cells by measuring the closure of a standard scratch in time. We found that Luzp1$^{-/-}$ cells had significantly faster migratory capacity compared to WT cells (**Figure R 39A and Figure R 39B**). This phenotype was rescued in +LUZP1 cells. To migrate, a cell must coordinate a number of different inputs into appropriate cellular responses. The cell must polarize and extend lamellipodial and/or filopodial protrusions. Vinculin and phalloidin staining revealed a different migration pattern, where Luzp1$^{-/-}$ cells form more lamellipodia and more focal adhesions than WT in the front of migrating cells (**Figure R 39C**). Filopodia and filopodia-like protrusions are prominent features of migrating cells *in vitro* (Jacquemet et al., 2013; Paul et al., 2015; Petrie and Yamada, 2012). In concordance with their increased migration capacity, Luzp1$^{-/-}$ cells displayed more filopodia than WT cells (**Figure R 39D**).

In a migrating cell, the activities of the different Rho GTPases and/or their effector pathways must be coordinated in a temporal and spatial manner to control cytoskeletal dynamics. In fact, the contractile force is generated by the actomyosin contractility through myosin light chain 2 (MLCII) phosphorylation by ROCK. To deepen in the understanding of the migratory phenotype shown in Luzp1$^{-/-}$ cells, MLCII phosphorylation was assessed on those cells. However, our antibody did not
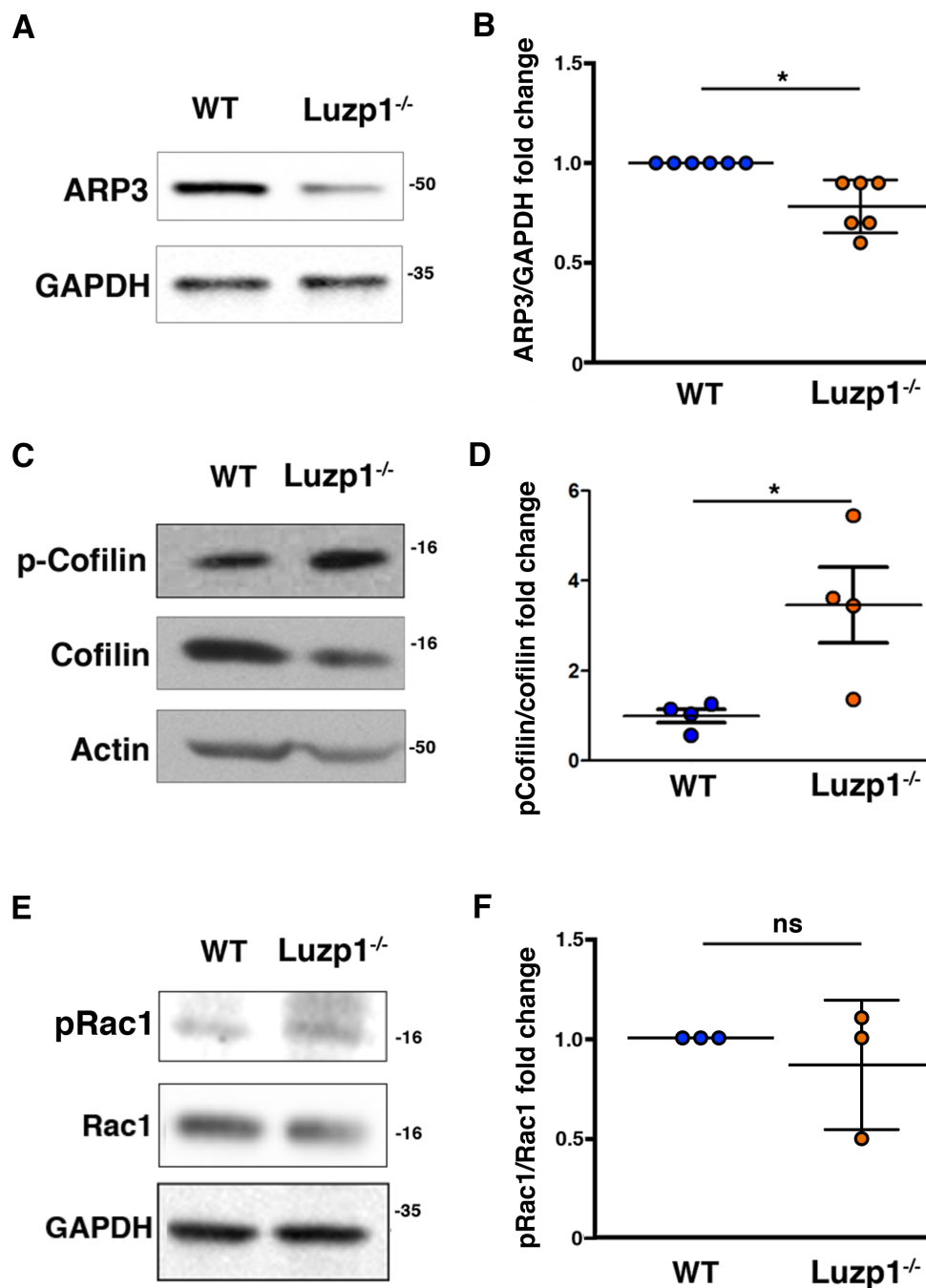
**Figure R 38. Defects in F-actin formation in Luzp1^{-/-} cells. (A,C,E)** Representative western blot of total lysates of Shh-LIGHT2 WT and Luzp1^{-/-} cells. Note a reduction in ARP3 (**A**) and an increase in phosphorylated cofilin (p-Cofilin) (**C**) in Luzp1^{-/-} cells. No significant changes were observed in phosphorylated Rac1 (pRac1) (**E**). Specific antibodies against ARP3, cofilin, phospho-cofilin, pRac1, Rac1 actin and GAPDH were used. Molecular weight markers (kDa) are shown to the right. (**B,D,F**) Graphical representation of the fold change of ARP3/GAPDH ratios obtained in (**A**), the p-cofilin/Cofilin ratios obtained in (**C**) and the pRac1/Rac1 ratios obtained in (**E**). Data from at least three independent experiments pooled together are shown. P-values were calculated using two-tailed unpaired Student´s t-test. ns: no significant.
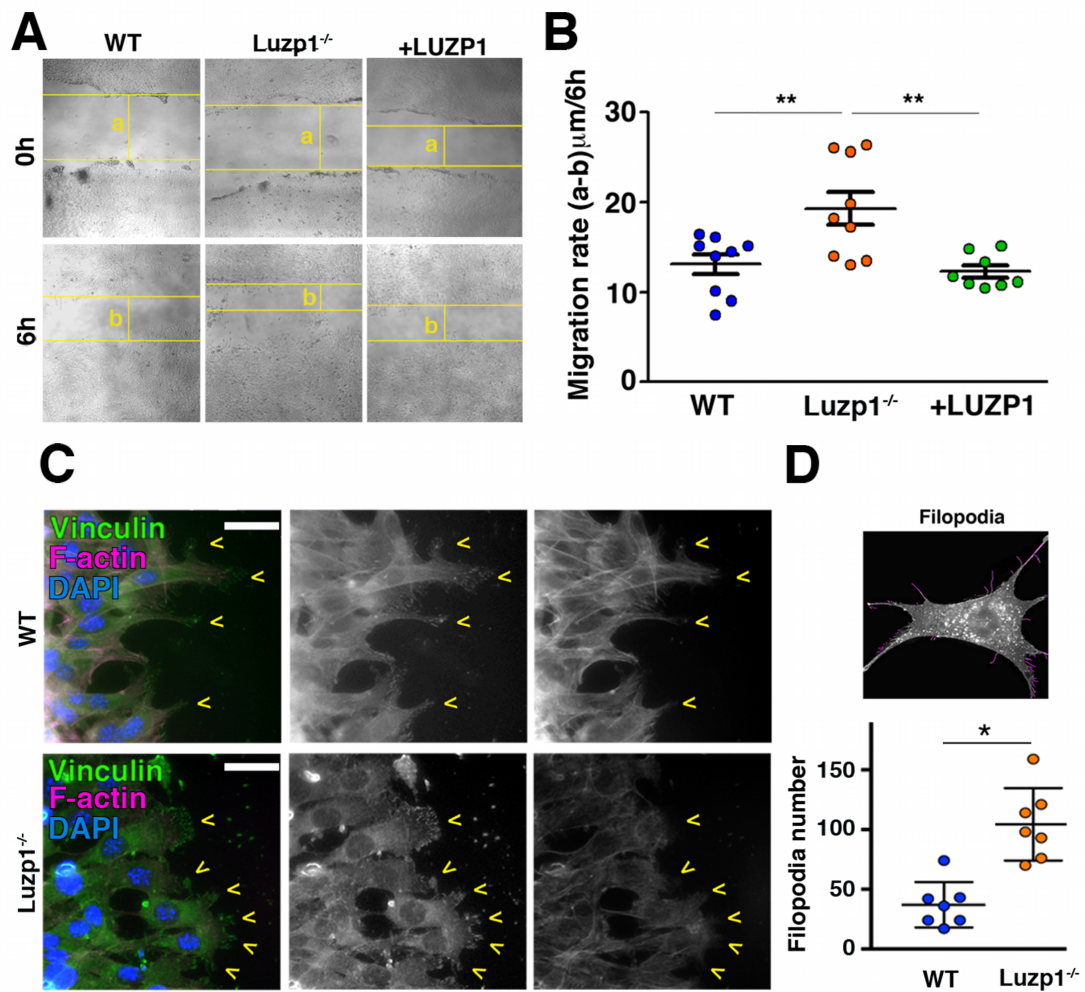
**Figure R 39. *Luzp1$^{-/-}$* cells display cell migration defects.** (**A**) Representative bright-field micrographs of the wound healing assays performed on Shh-LIGHT2 WT, Luzp1$^{-/-}$ and Luzp1$^{-/-}$ cells rescued with *Luzp1-YFP* (+LUZP1). The horizontal yellow lines represent the wound boundary; "a" and "b" are the distances between wound boundaries just after wound was made (0h) and 6 hours later (6h), respectively. (**B**) Quantification of wound healing in (**A**) calculated by subtracting distance "b" to distance "a" and dividing the result by 6 hours (n>8). Data were analysed by One way ANOVA and Bonferroni post-hoc test. (**C**) Micrographs of WT and Luzp1$^{-/-}$ cells during wound-healing assay. Focal adhesions were detected by vinculin antibody (green), F-actin by phalloidin (purple) and nuclei by DAPI (blue). Yellow arrowheads point at lamellipodia. Black and white images show the single green and purple channels. Scale bar, 10 μm. (**D**) Upper panel: example of filopodia detection by Filoquant plugin for ImageJ (in purple) from an original picture (in black and

detect neither the total nor the phosphorylated form of the protein (data not shown). Although further research is needed, the previously observed increase in cofilin phosphorylation might indicate an enhancement in cell contractibility in Luzp1$^{-/-}$ cells (Mseka and Cramer, 2011; Wiggan et al., 2012).

Taken together, this data reveal a mechanism through which LUZP1 may coordinate actin cytoskeleton mechanics in cell migration via actin dynamics.

# Chapter 5: Discussion

## 5.1 The role of SALL1 in primary cilia formation and function

Townes-Brocks Syndrome (TBS) is a rare disease characterized by a spectrum of malformations in digits, ears, heart and kidneys. The phenotypes observed in TBS individuals fall within the spectrum of those observed in ciliopathies. This led us to speculate that defective regulation of cilia function and/or formation might be contributing factors in the TBS-related limb, ear, heart, anus and kidney phenotypes. Our work provides mechanistic connection between truncated SALL1 and aberrations in primary cilia, offering insights into the regulation of cilia formation and function with respect to TBS etiology. In addition to its function as a transcription factor in the nucleus, SALL1 mutations, especially those found in the hotspot (**Figure I 2**) that generate mislocalized truncated proteins (Botzenhart et al., 2007), may lead to aberrant cilia function. Four lines of evidence support our conclusions. First, SALL1[FL] localized to primary cilia in several cell types; Second, while control fibroblasts display primary cilia at a normal length and rates, TBS cells display significantly longer and more abundant cilia; Third, signalling through primary cilia is functionally defective in TBS[332] and in Shh-LIGHT2 cells that exogenously express the mutated form SALL1[332]; Forth, proteins necessary for primary cilia formation and function show aberrant dynamics in TBS[332]-derived fibroblasts, in the 293[335] TBS model cell line, and in *Sall1*[+/Δ] MEFs.

### 5.1.1 Aberrant interactions of truncated SALL1

The presence of truncated SALL1 in the cytoplasm and its capacity to form inappropriate protein interactions may underlie TBS malformations. This hypothesis relies on the presence of the truncated form, which we were able to detect in TBS-derived dermal fibroblasts and in a genome-edited kidney-derived model cell line (293[335]). In all these cases, the observed sizes of FL SALL1 and its truncated forms are higher than their expected molecular weight as shown by Western blot. This has been previously observed (Kiefer et al., 2008) and might be consistent with differential SALL1 binding to SDS detergent or with the presence of excessive proline residues that might cause structural rigidity to the primary sequence, thereby

decreasing the electrophoretic mobility. Alternatively, posttranslational modifications may also account for variations in the expected molecular weight.

By examining dermal fibroblasts, which display primary cilia and are competent for Shh signalling, we show that truncated SALL1 has multiple effects on cilia formation and function. This might be the result of the dominant-negative binding and displacement of cilia-related factors by the truncated forms of SALL1, alone or in complex with SALL1$^{FL}$. Notwithstanding, some aspects of the disease might result from the sequestration of SALL1$^{FL}$ to the cytoplasm, which might interfere with the transcriptional role of SALL1 in the nucleus and alter cilia formation and function through aberrant regulation of downstream genes. Furthermore, other SALL proteins (SALL2, SALL3, SALL4) may also heterodimerize with truncated SALL1 (Kiefer et al., 2003) and thus contribute to the TBS etiology. Furthermore, mouse studies that combine mutations in multiple *Sall* genes report phenotypes including digit and limb malformations, Shh signalling aberrations, and neural tube defects, suggestive of cilia malfunction (Bohm et al., 2008; Kawakami et al., 2009). Interestingly, it has been reported that heterozygous deletions of *SALL1* (i.e., haploinsufficiency) lead to a milder form of TBS than that associated with truncated variants in the hot spot region (Borozdin et al., 2006). This might indicate that there is a certain dosage effect contributing to TBS phenotype. How a reduction or loss of SALL1$^{FL}$ contributes to TBS etiology and cilia formation is highly relevant and remains a subject for future research.

## 5.1.2 Novel SALL1 localization along the ciliary shaft

Extensive studies on SALL1 uncovered its role as a transcriptional regulator at the nuclei (Kiefer et al., 2002; Netzer et al., 2006; Netzer et al., 2001; Nishinakamura et al., 2001; Sweetman et al., 2003). However, the presence of SALL1$^{FL}$ at the cilia, and its displacement to the cytoplasm by the truncated form, may also be a contributing factor in TBS malformations. The partial removal of SALL1$^{FL}$ from the cilia might interfere with its potential function at this organelle. Further investigation would be needed to unveil the mechanism by which a transcription factor like SALL1, described to localize mainly to the nuclei, is also found at the ciliary shaft. The

observations that a nuclear transport system is involved in ciliary targeting, that many nucleoporins (Nups) are localized at ciliary base and that the ciliary base contains a barrier comparable to that of nuclear pores, led to hypothesize that the ciliary base may contain a nuclear pore-like structure (Kee et al., 2012; Obado and Rout, 2012; Takao and Verhey, 2016). Nevertheless, other studies, including super-resolution imaging, revealed that the ciliary diffusion barrier is mechanistically and structurally distinct from those of the nuclear pore complex (Breslow et al., 2013; Del Viso et al., 2016; Lin et al., 2013; Obado and Rout, 2016). Therefore, it is possible that Nups form a different type of diffusion barrier at ciliary base, which could explain why canonical nuclear localization signals (NLS) do not function as a ciliary targeting signal. It is also possible that the cilia may contain additional diffusion mechanisms that need to be overcome to enter the ciliary shaft. For instance, it has been reported that other transcription factors such as GLI proteins contain a ciliary localization sequence (Santos and Reiter, 2014). This sequence may bind a factor or factors that help GLI proteins in crossing the diffusion barrier at the ciliary base in a passive or active way. Like in the case of GLI2, it is possible that a cytoplasmic microtubule network might be required for ciliary targeting of nuclear proteins such as SALL1 (Kim et al., 2009).

Also, future studies will be necessary to examine levels and localization of other SALL proteins in ciliated cells and tissues. Cells or tissues derived from *Sall* knock-out mice *vs* WT mice would be interesting models to asses the localization of SALL proteins at the cilia. *SALL1* transcriptional regulation by the Shh signalling pathway adds further complexity (Kawakami et al., 2009; Koster et al., 1997) and raises the possibility of feedback control, a common theme in Shh pathway regulation (e.g. *PTCH1, GLI1*).

### 5.1.3 Primary cilia aberrations in TBS-derived cells

In this work, we provided evidences that truncated SALL1 results in aberrant cilia formation and function. Furthermore, primary cilia of TBS fibroblasts took longer to be reabsorbed than those of control cells once serum was added to starved cells. The presence of longer cilia in TBS-derived fibroblasts is consistent with other

studies in which ciliary length is coincident to phenotypes shown by TBS individuals. For instance, cells derived from a *Kif7* mutant mice exhibited polydactyly displayed elongated cilia (He et al., 2014; Liem et al., 2009; Tunovic et al., 2015). Although not observed in all individuals, TBS can lead to polycystic kidneys. Consistently, kidney epithelial cells derived from a mouse model of nephronophthisis that develops polycystic kidney disease exhibit abnormally longer cilia (Smith et al., 2006; Sohara et al., 2008). Notably, a recent study concluded that the reduction of ciliary length using R-roscovitine or S-CR8 drugs, attenuated cystic disease progression in these mice (Husson et al., 2016), suggesting that cilia-altering therapies may be beneficial to TBS individuals.

### 5.1.4 Shh signalling aberrations and TBS

Since we found that TBS-derived cells had longer and more abundant primary cilia than control cells, it was not unexpected to observe defects in Shh signalling, due to its dependence on intact cilia. The characteristic triad of TBS symptoms includes digit malformations, misshapen outer ears and hearing problems, and gastrointestinal anomalies, phenotypes that might be consistent with Shh signaling missregulation. TBS[332]-derived cells were hypersensitive to Shh pathway stimulation. Increased Shh activity or expansion of the domain of expression of *Shh* in the developing limb bud can cause pre-axial polydactyly in mice, chick and humans, a phenotype commonly seen in TBS individuals (Lettice et al., 2003; Masuya et al., 1995; Yang et al., 1997). In addition, Shh signalling defects may underlie the pathogenesis of human anorectal malformations in TBS individuals. For instance, it has been shown that *Gli2*^{-/-} mice exhibit imperforate anus, whereas *Gli3*^{-/-} mice display less severe anal stenosis (Mo et al., 2001), both of which are observed in TBS. In humans, some individuals with Pallister-Hall syndrome (PHS [MIM: 165240]), which is caused by mutations in *GLI3* (GLI-Kruppel family member 3 [MIM:165240]), also exhibit anorectal malformations, such as imperforate anus (Kang et al., 1997). On the other hand, ear defects in TBS individuals include dysplastic ears, congenital sensorineural and/or conductive hearing loss. Developmental pathways governing human outer ear morphology are largely unexplored, but Shh signalling might be a

contributing factor to TBS hearing problems since it has been demonstrated that Shh influences proper development of the cochlea and sensory epithelium in mice, and for auditory function in humans (Driver et al., 2008).

## 5.2 Cilia and actin-related proteins as mediators of TBS

### 5.2.1 CCP110 and CEP97, candidate mediators of TBS etiology

Our BioID experiments showed an enrichment of ciliary/centrosomal proteins among the potential interactors of truncated SALL1[275], which may underlie the observed ciliary defects. Approximately 6% of the verified ciliary genes (and 18% of the potential ones) previously identified by the SYSCILIA Consortium (van Dam et al., 2013) were found as SALL1[275]-specific proximal interactors in at least 2 experiments. In addition, 6.5% of the SALL1[275]-specific list was present among the 384 centrosome-localized proteins identified by the Human Protein Atlas project based on subcellular localization (Uhlen et al., 2015). Among the cilia-related candidates we selected CCP110 and CEP97, two of the hits from our list, which are important negative regulators of ciliogenesis (Goetz and Anderson, 2010; Kohlmaier et al., 2009; Schmidt et al., 2009; Spektor et al., 2007). The removal of CCP110 and CEP97 is a key early event in ciliogenesis: depletion of CCP110 and CEP97 leads to the premature formation of aberrant cilia while their overexpression blocks ciliogenesis. Consistently with the observed higher frequency of primary cilia in TBS-derived cells, our experiments show that CCP110 and CEP97 are more often depleted from MCs in TBS[332] cells compared to controls. While some studies demonstrated that removal of CCP110 was sufficient to induce ectopic cilia formation (Spektor et al., 2007; Tsang et al., 2008), others reported that its depletion promoted abnormal elongation of non-docked centriolar microtubules (Franz et al., 2013; Schmidt et al., 2009). A recent publication suggested a dual and context-dependent role of CCP110 in cilia formation relying on the proteins interacting with CCP110 in a determined subcellular environment (Yang et al., 2016). Importantly, consistent with altered levels of CCP110 at the MC in TBS[332] cells, *Ccp110* KO mice exhibited a spectrum of developmental phenotypes including preaxial polydactyly,

heart malformations and cleft palate among others. Understanding the exact contribution of CCP110 and its protein interaction network in the context of TBS, which may function in a tissue- or organ-dependent manner, would be of high relevance.

## 5.2.2 LUZP1, another potential mediator of TBS etiology that localizes to the cilia and actin cytoskeleton

Applying the BioID method, we also found LUZP1 as a truncated SALL1 interactor. It was previously described that LUZP1 localized in the nuclei, which is in line with the presence of three nuclear localization signals in its sequence. Immunohistochemistry using an antibody against the N-terminal part of LUZP1 showed the expression of LUZP1 mainly in the mouse brain (Lee et al., 2001; Sun et al., 1996). However, although we also detected LUZP1 in the nuclei of mouse and human cells (see **Figure R 25**), we observed by immunofluorescence using a LUZP1-specific antibody a prominent localization of LUZP1 to the actin cytoskeleton and centrosomes, both in human and mouse cells. This localization correlates with the one described in the Human Protein Atlas website, where a different antibody was used, and is consistent with our finding that LUZP1 interacts with actin and centrosome-related proteins (**Figure R30 and Figure R 31**). Furthermore, an independent study using the BioID assay identified LUZP1 as an interactor of centriole-related proteins such as PCM1 (Gupta et al., 2015). Discrepancies in LUZP1 localization might be due to the use of different techniques, as immunohistochemistry (Lee et al., 2001; Sun et al., 1996) *vs* immunofluorescence (this study) and/or the use of different antibodies, directed against the N-terminal part of the protein (Lee et al., 2001; Sun et al., 1996) or against its C-terminal part (Sigma, this study). Further investigation will be necessary to examine the localization and role of LUZP1 in the nucleus.

## 5.2.3 LUZP1 is altered in TBS-derived cells

Here we found that truncated SALL1 interacts with LUZP1, stimulating its

degradation. The exact mechanism by which the aberrant complex with truncated SALL1 stimulates LUZP1 depletion, both at the centrosome and actin cytoskeleton, requires further investigation. Importantly, we detected an increase in LUZP1 levels upon proteasome inhibitor MG132 treatment in control cells (**Figure R 29**), suggesting that LUZP1 degradation is proteasome-mediated. We could hypothesize that LUZP1 interaction with truncated SALL1 leads to LUZP1 posttranslational modifications, such as ubiquitylation, and its subsequent degradation.

Based on its localization, we hypothesized that LUZP1 has a function on cilia and cytoskeletal organization. Both Luzp1$^{-/-}$ and TBS cells showed a reduction in F-actin accompanied by an increase in ciliation. Whether cilia dependent signalling influences the actin cytoskeleton or vice versa remains to be elucidated. In this line, it has been recently reported that the axoneme length control can influence primary cilia–mediated Shh signalling, independently of cilia frequency (Drummond et al., 2018). What mediates the increase in Shh signalling in longer axonemes is unknown. Based on these results, we suggest that the reduction in actin fibres might contribute to the higher cilia abundance, longer cilia and increased Shh signalling observed in TBS cells. Together with the impairment of ciliogenesis in TBS[275] cells transiently transfected with *LUZP1-YF*P, these results suggest a role for LUZP1 as a cilia repressor factor and a stabilizer of actin cytoskeleton.

### 5.2.4 LUZP1 as an integrator of actin and primary-cilium dynamics

As mentioned in the introduction, actin dynamics coordinate several processes that are crucial for ciliogenesis (**Figure I 13**). Placing the MC to the appropriate area at the cell cortex, basal body docking and the elongation of the axoneme are all actin-dependent processes. Interfering with actin dynamics through CytB has been demonstrated to promote ciliogenesis (Cao et al., 2012). The exact implication of LUZP1 as an integrator of actin and primary cilia dynamics needs to be more extensively examined.

## A. The role of LUZP1 in neural tube closure and cardiac defects

Several studies have implicated cilia in the etiology of neural tube closure defects (Wallingford, 2005). These studies emphasize the tight links between cell fate and cytoskeletal organization. Shh signalling, a pathway involved in neural tube closure that relies on the presence of functional cilia, is aberrant in TBS patient-derived fibroblasts. Interestingly, ectopic Shh expression was observed in the neuroepithelium of the NTD *Luzp1* KO mouse hindbrain (Hsu et al., 2008). In concordance with these results, we also showed aberrant Shh signalling accompanied by longer cilia in Luzp1$^{-/-}$ cells. Our results, together with others, indicate that LUZP1 is therefore pivotal to the maintenance of a gradient expression of Shh such that cranial neural tube closure may be achieved. Hsu *et. al.* noted that the NTD in *Luzp1 KO* embryos with exencephaly may be caused by failure in bending at the dorsolateral hinge point and that the dorsolateral neural folds was convex instead of the concave morphology observed in WT embryos (Hsu et al., 2008). It has been reported that changes in apical actin architecture are required to convert cells from columnar to wedge-shaped, subsequently forcing neural folds during the proper formation of the neural tube (Sadler et al., 1982). Thus, it is tempting to hypothesize that there might be defects in actin distribution at the neural tube folding in *Luzp1* KO mice

In addition to NTDs, loss-of-function mouse models of *Luzp1* phenocopy other features of human ciliopathies commonly found in TBS patients, such as cardiac malformations (Kohlhase, 1993). Congenital heart disease is present in 50% of the TBS patients with the common p.Arg275[*] allele (Kohlhase et al., 2003) and 12%-25% of patients with other SALL1 pathogenic variants (Botzenhart et al., 2007; Botzenhart et al., 2005; Surka et al., 2001). Cardiac defects include atrial or ventricular septal defect, which is also present in loss-of-function mouse models of *Luzp1.* Whether the differential interaction of the diverse SALL1 pathogenic variants with LUZP1 is responsible for the differences in prevalence of cardiac defects remains unknown. Interestingly, it has been reported that *Sall1* expression is very prominent in the developing brain (Buck et al., 2001) and that compound *Sall1/Sall4* mutant mice show NTD and cardiac problems (Bohm et al., 2008). All together, these evidences could suggest a cross talk between *Sall1* and *Luzp1* during brain and heart

development.

## B. LUZP1 has a role in cell division

We observed that Luzp1$^{-/-}$ cells exhibited multiple centrioles, larger nuclei, decreased cell proliferation and increased apoptosis, which might be indicating cell division failure due to reduced actin cytoskeleton. In concordance with these results, elevated apoptosis was also observed in the neuroepithelium of the NTD *Luzp1* KO mouse hindbrain (Hsu et al., 2008).

Moreover we found that LUZP1 localizes not only to centrioles and actin cytoskeleton, but also to the midbody in dividing cells (**Figure R 24D**). The midbody, an organelle formed at the intercellular bridge in the last phase of citokinesis, recruits crucial proteins for the abscission between the dividing cells (D'Avino and Capalbo, 2016). One hypothesis about the role of the postmitotic midbody remnant in the extracellular milieu is that it might be crucial for cell fate (Chen et al., 2013; Dionne et al., 2015). In fact, Rubio-Bernabé *et. al.* recently reported that the midbody promotes ciliogenesis in polarized epithelial cells (Bernabe-Rubio et al., 2016). Understanding the role of LUZP1 in the midbody would be of major interest.

## C. LUZP1 affects actin polymerization and cell migration

Two main actin binding complexes/proteins control the polymerization and depolymerization of the actin fibers in cells: the Arp2/3 complex and cofilin. It is known that Arp2/3 and cofilin work synergistically in such a way that the newly polymerized filaments from cofilin-generated barbed ends are ATP-rich filaments that promote the nucleation and branching activity of the Arp2/3 complex (DesMarais et al., 2004). In this regard, we observed a reduction in ARP3 and in non-phosphorylated (or active cofilin) in Luzp1$^{-/-}$ cells compared to WT cells, suggesting that actin polymerization might be diminished (**Figure R 38**). The reduction in actin polymerization might lead to a negative feedback over SSH1. As a result, phosphorylated (or inactive) cofilin levels would increase followed by actin turnover suppression and repression of *de novo* actin filament growth in Luzp1$^{-/-}$ cells (**Figure D1**).
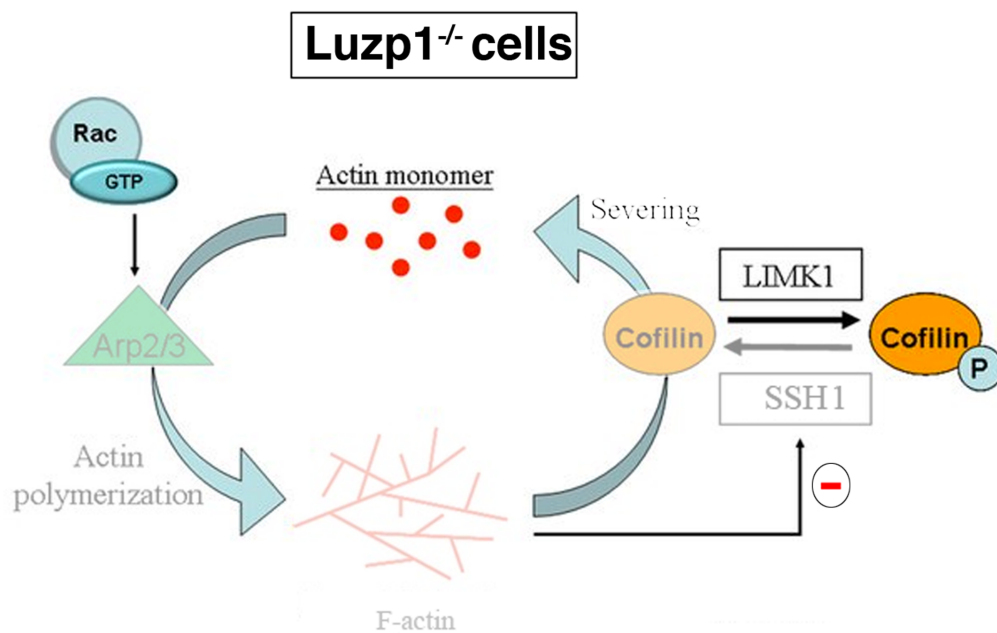
**Figure D 1. F-actin formation dynamics in Luzp1$^{-/-}$ cells.** In the absence of LUZP1, Arp2/3 levels are reduced, leading to diminished F-actin polymerization. The reduction of polymerized F-actin decreases the phosphatase activity of SSH (Slingshot homologue 1), which leads to net phosphorylation and deactivation of cofilin. Therefore, the actin-severing function of cofilin impedes the flexibility of remodeled actin and the regeneration of free monomeric actin for further polymerization. Compare with the WT scenario in **Figure I 12** in the Introduction section.

Although stress fibres contribute to cell shape and adhesion, their exact role in cell migration has been less conclusively demonstrated. Stress fibres are absent from several highly motile cells, such as leukocytes (Valerius et al., 1981) and Dictyostelium discoideum amoeba (Rubino et al., 1984). These observations, together with the lack of stress fibres in cells implanted in a three-dimensional environment led to suggest that they are not essential for cell migration (Burridge et al., 1988). Indeed, stress fibres might, under certain conditions, inhibit rather than drive cell motility. (Badley et al., 1980; Cramer et al., 1997; Herman et al., 1981). In fact, it has been reported that an increase in actin fibres is linked to lower motility (Kemp and Brieher, 2018). These findings match our observations that Luzp1$^{-/-}$ cells that contain less stress fibres were more motile than WT cells (**Figure R 39**).

Importantly, cells use many proteins to regulate actin assembly and cell migration. Actin-related proteins act synergistically to maintain a pool of unpolymerized actin monomers, nucleate, elongate and cap actin filaments, promote dissociation of Pi from ADP-Pi-subunits, sever actin filaments, and crosslink filaments into higher order structures. Despite our promising preliminary results, further analysis of other proteins implied in the regulation of actin dynamics such as profilins or Rho GTPases would be necessary to draw robust conclusions about the function of LUZP1 in the integration of this complex actin network.

## 5.3 Concluding remarks

The results obtained thoroughout this thesis work confirm our initial hypothesis and demonstrate that TBS is a ciliopathy-like disease, with symptoms caused by truncated SALL1 interfering with the normal function of cilia/centrosomal-related proteins such as CPP110, CEP97 and LUZP1. Our findings also indicate that LUZP1 is a novel actin and centrosome-related protein that might facilitate actin polymerization and repress ciliogenesis. Cells adapt to new environments, like serum starvation, through coordinated changes in gene expression, cytoskeletal rearrangements, and cilia signalling. This integrated response requires signal transduction relays that communicate the cytoplasmic actin polymerization status with cilia and nucleus. Here, we propose that LUZP1 might act as a nexus in this complex intracellular network, and that truncated SALL1 disrupts this network in TBS patients.

The ciliopathies are an increasingly recognized class of human genetic disorders, and our work provides a framework for understanding TBS and the contributing role that primary cilia might play in the pathology of the disease. This does not rule out a disruption in the nuclear role of SALL1, or dominant interactions with other SALL family proteins. Different alleles may exhibit different strengths, depending on interactors, and genetic, environmental, or stochastic modifiers might influence the phenotypic spectrum in TBS individuals (Botzenhart et al., 2007; Kiefer

et al., 2003). Defining to which degree primary cilia and other factors are implicated in the etiology of TBS may drive future therapeutic approaches.

**Final model**
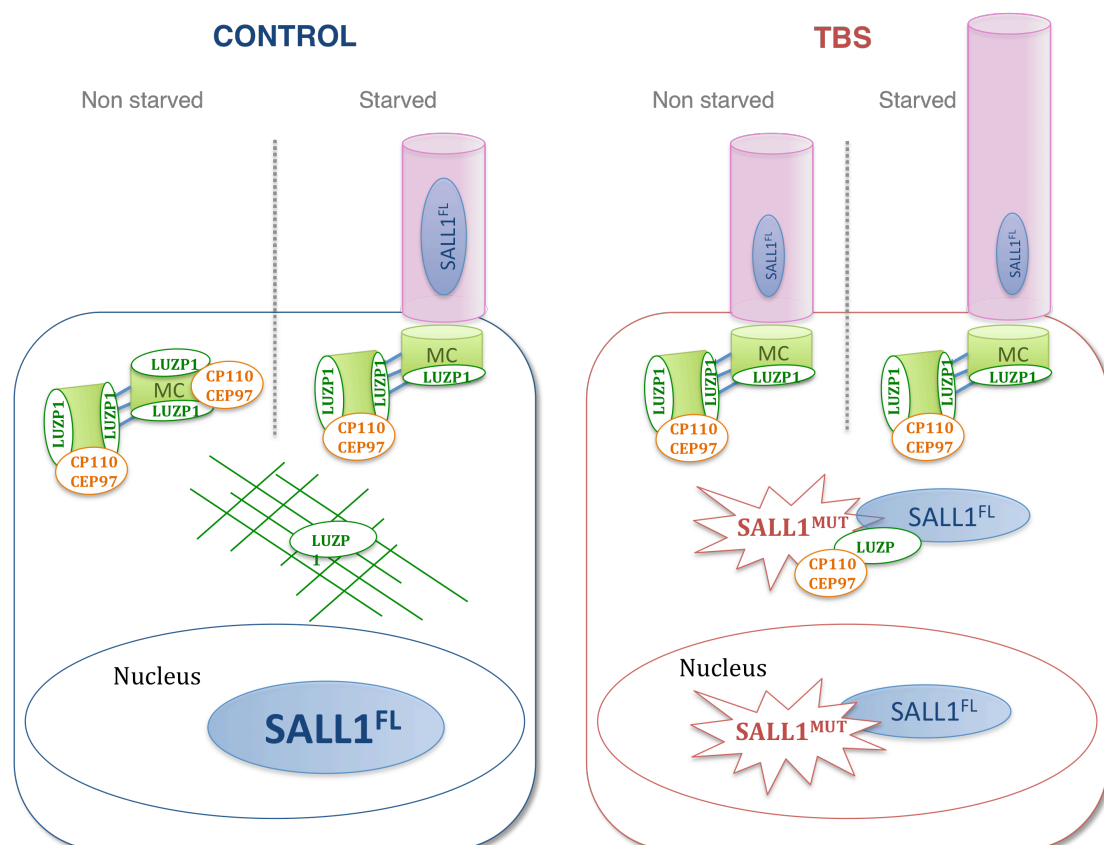


**Figure D 2. Final model. The presence of truncated SALL1 underlies cilia and actin malformations in TBS through the sequestration of key regulatory factors CCP110, CEP97 and LUZP1**. In control cells (left), SALL1$^{FL}$ is mainly nuclear and CCP110/CEP97 complex and LUZP1 localize to the mother (MC) and daughter centrioles inhibiting cilia formation. LUZP1 localizes also to F-actin. Upon starvation, the CCP110/CEP97 complex and one LUZP1 foci are depleted from the MC, which will allow the formation of the primary cilia. By contrast, in TBS cells (right) a truncated form of SALL1 (SALL1$^{MUT}$), together with sequestered SALL1$^{FL}$, localizes to the cytoplasm, where it interacts with LUZP1 and the CCP110/CEP97 complex, leading to their degradation. As a result, the frequency of cilia formation increases, and cilia are longer than in control cells. Problems in cilia formation are accompanied by SHH signaling alterations in TBS cells.

# Chapter 6: Conclusions

**Chapter 6: Conclusions**

The results obtained along this thesis lead to the following conclusions:

1. **SALL1$^{FL}$** is a nuclear and a **ciliary protein** and truncated SALL1 disrupts its localization to the cytoplasm in a dominant-negative manner.

2. **TBS patients-derived fibroblasts display longer and more abundant cilia** than control fibroblasts and **we reproduced those cilia defects** in the following **TBS model cell lines**, eventhough they express different pathogenic variants:

   a. Fibroblasts from a new TBS patient with the pathogenic SALL1c.826C>T variant.

   b. A HEK 293FT TBS-mimicking cell line generated by CRISPR/Cas9 technology.

   c. *Sall1$^{\Delta Zn2-10}$* mouse embryonic fibroblasts.

3. **TBS patients-derived fibroblasts** present **Shh signalling aberrations**.

4. **Truncated SALL1 interacts with** the centrosome negative regulators **CCP110 and CEP97 and with LUZP1** and they are **prematurely depleted** from the mother centriole in TBS cells.

5. **LUZP1 localizes to the centrosome** and **interacts with** the centrosomal **CCP110 and CEP97** negative regulators.

6. **LUZP1 is a cilia negative regulator** implicated in **Shh signalling**.

7. **LUZP1 is an actin-stabilizing** protein reduced in TBS cells.

8. Truncated SALL1 leads to **proteasome-mediated LUZP1 degradation**.

9. The **lack of LUZP1** leads to **cell proliferation and cell migration defects**, presumably, through the regulation of actin dynamics, although further confirmation is needed.

# Chapter 7: Bibliography

## Chapter 7: Bibliography

Amann, K.J., and T.D. Pollard. 2001. The Arp2/3 complex nucleates actin filament branches from the sides of pre-existing filaments. *Nature cell biology*. 3:306-310.

Anderson, R.G. 1972. The three-dimensional structure of the basal body from the rhesus monkey oviduct. *The Journal of cell biology*. 54:246-265.

Andrianantoandro, E., and T.D. Pollard. 2006. Mechanism of actin filament turnover by severing and nucleation at different concentrations of ADF/cofilin. *Molecular cell*. 24:13-23.

Antoniades, I., P. Stylianou, and P.A. Skourides. 2014. Making the connection: ciliary adhesion complexes anchor basal bodies to the actin cytoskeleton. *Developmental cell*. 28:70-80.

Badley, R.A., J.R. Couchman, and D.A. Rees. 1980. Comparison of the cell cytoskeleton in migratory and stationary chick fibroblasts. *Journal of muscle research and cell motility*. 1:5-14.

Barrio, R., and J.F. de Celis. 2004. Regulation of spalt expression in the Drosophila wing blade in response to the Decapentaplegic signaling pathway. *Proceedings of the National Academy of Sciences of the United States of America*. 101:6021-6026.

Behal, R.H., and D.G. Cole. 2013. Analysis of interactions between intraflagellar transport proteins. *Methods in enzymology*. 524:171-194.

Bernabe-Rubio, M., G. Andres, J. Casares-Arias, J. Fernandez-Barrera, L. Rangel, N. Reglero-Real, D.C. Gershlick, J.J. Fernandez, J. Millan, I. Correas, D.G. Miguez, and M.A. Alonso. 2016. Novel role for the midbody in primary ciliogenesis by polarized epithelial cells. *The Journal of cell biology*. 214:259-273.

Bettencourt-Dias, M., and Z. Carvalho-Santos. 2008. Double life of centrioles: CP110 in the spotlight. *Trends in cell biology*. 18:8-11.

Bettencourt-Dias, M., F. Hildebrandt, D. Pellman, G. Woods, and S.A. Godinho. 2011. Centrosomes and cilia in human disease. *Trends in genetics : TIG*. 27:307-315.

Blanchoin, L., and T.D. Pollard. 1999. Mechanism of interaction of Acanthamoeba actophorin (ADF/Cofilin) with actin filaments. *The Journal of biological chemistry*. 274:15538-15546.

Blanchoin, L., T.D. Pollard, and S.E. Hitchcock-DeGregori. 2001. Inhibition of the Arp2/3 complex-nucleated actin polymerization and branch formation by tropomyosin. *Current biology : CB*. 11:1300-1304.

Bloodgood, R.A. 2010. Sensory reception is an attribute of both primary cilia and motile cilia. *Journal of cell science*. 123:505-509.

Bohm, J., A. Buck, W. Borozdin, A.U. Mannan, U. Matysiak-Scholze, I. Adham, W. Schulz-Schaeffer, T. Floss, W. Wurst, J. Kohlhase, and F. Barrionuevo. 2008. Sall1, sall2, and sall4 are required for neural tube closure in mice. *Am J Pathol*. 173:1455-1463.

Boldt, K., J. van Reeuwijk, Q. Lu, K. Koutroumpas, T.M. Nguyen, Y. Texier, S.E. van Beersum, N. Horn, J.R. Willer, D.A. Mans, G. Dougherty, I.J. Lamers, K.L. Coene, H.H. Arts, M.J. Betts, T. Beyer, E. Bolat, C.J. Gloeckner, K. Haidari, L. Hetterschijt, D. Iaconis, D. Jenkins, F. Klose, B. Knapp, B. Latour, S.J.

Letteboer, C.L. Marcelis, D. Mitic, M. Morleo, M.M. Oud, M. Riemersma, S. Rix, P.A. Terhal, G. Toedt, T.J. van Dam, E. de Vrieze, Y. Wissinger, K.M. Wu, G. Apic, P.L. Beales, O.E. Blacque, T.J. Gibson, M.A. Huynen, N. Katsanis, H. Kremer, H. Omran, E. van Wijk, U. Wolfrum, F. Kepes, E.E. Davis, B. Franco, R.H. Giles, M. Ueffing, R.B. Russell, and R. Roepman. 2016. An organelle-specific protein landscape identifies novel diseases and molecular mechanisms. *Nature communications*. 7:11491.

Borozdin, W., K. Steinmann, B. Albrecht, A. Bottani, K. Devriendt, M. Leipoldt, and J. Kohlhase. 2006. Detection of heterozygous SALL1 deletions by quantitative real time PCR proves the contribution of a SALL1 dosage effect in the pathogenesis of Townes-Brocks syndrome. *Human mutation*. 27:211-212.

Botzenhart, E.M., G. Bartalini, E. Blair, A.F. Brady, F. Elmslie, K.L. Chong, K. Christy, W. Torres-Martinez, C. Danesino, M.A. Deardorff, J.P. Fryns, S. Marlin, S. Garcia-Minaur, Y. Hellenbroich, B.N. Hay, M. Penttinen, V. Shashi, P. Terhal, L. Van Maldergem, M.L. Whiteford, E. Zackai, and J. Kohlhase. 2007. Townes-Brocks syndrome: twenty novel SALL1 mutations in sporadic and familial cases and refinement of the SALL1 hot spot region. *Human mutation*. 28:204-205.

Botzenhart, E.M., A. Green, H. Ilyina, R. Konig, R.B. Lowry, I.F. Lo, M. Shohat, L. Burke, J. McGaughran, R. Chafai, G. Pierquin, R.C. Michaelis, M.L. Whiteford, K.O. Simola, B. Rosler, and J. Kohlhase. 2005. SALL1 mutation analysis in Townes-Brocks syndrome: twelve novel mutations and expansion of the phenotype. *Human mutation*. 26:282.

Bozal-Basterra, L., I. Martin-Ruiz, L. Pirone, Y. Liang, J.O. Sigurethsson, M. Gonzalez-Santamarta, I. Giordano, E. Gabicagogeascoa, A. de Luca, J.A. Rodriguez, A.O.M. Wilkie, J. Kohlhase, D. Eastwood, C. Yale, J.V. Olsen, M. Rauchman, K.V. Anderson, J.D. Sutherland, and R. Barrio. 2018. Truncated SALL1 Impedes Primary Cilia Function in Townes-Brocks Syndrome. *American journal of human genetics*. 102:249-265.

Bravo-Cordero, J.J., M.A. Magalhaes, R.J. Eddy, L. Hodgson, and J. Condeelis. 2013. Functions of cofilin in cell locomotion and invasion. *Nature reviews. Molecular cell biology*. 14:405-415.

Breslow, D.K., E.F. Koslover, F. Seydel, A.J. Spakowitz, and M.V. Nachury. 2013. An in vitro assay for entry into cilia reveals unique properties of the soluble diffusion barrier. *The Journal of cell biology*. 203:129-147.

Buck, A., A. Kispert, and J. Kohlhase. 2001. Embryonic expression of the murine homologue of SALL1, the gene mutated in Townes--Brocks syndrome. *Mechanisms of development*. 104:143-146.

Burridge, K., K. Fath, T. Kelly, G. Nuckolls, and C. Turner. 1988. Focal adhesions: transmembrane junctions between the extracellular matrix and the cytoskeleton. *Annual review of cell biology*. 4:487-525.

Cabrera, R.M., D.S. Hill, A.J. Etheredge, and R.H. Finnell. 2004. Investigations into the etiology of neural tube defects. *Birth defects research. Part C, Embryo today : reviews*. 72:330-344.

Campbell, K. 2003. Dorsal-ventral patterning in the mammalian telencephalon. *Current opinion in neurobiology*. 13:50-56.

Campellone, K.G., and M.D. Welch. 2010. A nucleator arms race: cellular control of actin assembly. *Nature reviews. Molecular cell biology*. 11:237-251.

Cantera, R., K. Luer, T.E. Rusten, R. Barrio, F.C. Kafatos, and G.M. Technau. 2002. Mutations in spalt cause a severe but reversible neurodegenerative phenotype in the embryonic central nervous system of Drosophila melanogaster. *Development*. 129:5577-5586.

Cao, J., J. Crest, B. Fasulo, and W. Sullivan. 2010. Cortical actin dynamics facilitate early-stage centrosome separation. *Current biology : CB*. 20:770-776.

Cao, J., Y. Shen, L. Zhu, Y. Xu, Y. Zhou, Z. Wu, Y. Li, X. Yan, and X. Zhu. 2012. miR-129-3p controls cilia assembly by regulating CP110 and actin dynamics. *Nature cell biology*. 14:697-706.

Chen, C.T., A.W. Ettinger, W.B. Huttner, and S.J. Doxsey. 2013. Resurrecting remnants: the lives of post-mitotic midbodies. *Trends in cell biology*. 23:118-128.

Chiang, C., Y. Litingtung, M.P. Harris, B.K. Simandl, Y. Li, P.A. Beachy, and J.F. Fallon. 2001. Manifestation of the limb prepattern: limb development in the absence of sonic hedgehog function. *Developmental biology*. 236:421-435.

Chiang, C., Y. Litingtung, E. Lee, K.E. Young, J.L. Corden, H. Westphal, and P.A. Beachy. 1996. Cyclopia and defective axial patterning in mice lacking Sonic hedgehog gene function. *Nature*. 383:407-413.

Chiu, T.T., N. Patel, A.E. Shaw, J.R. Bamburg, and A. Klip. 2010. Arp2/3- and cofilin-coordinated actin dynamics is required for insulin-mediated GLUT4 translocation to the surface of muscle cells. *Molecular biology of the cell*. 21:3529-3539.

Colas, J.F., and G.C. Schoenwolf. 2001. Towards a cellular and molecular understanding of neurulation. *Developmental dynamics : an official publication of the American Association of Anatomists*. 221:117-145.

Copp, A.J. 2005. Neurulation in the cranial region--normal and abnormal. *Journal of anatomy*. 207:623-635.

Copp, A.J., N.D. Greene, and J.N. Murdoch. 2003. The genetic basis of mammalian neurulation. *Nature reviews. Genetics*. 4:784-793.

Corbit, K.C., P. Aanstad, V. Singla, A.R. Norman, D.Y. Stainier, and J.F. Reiter. 2005. Vertebrate Smoothened functions at the primary cilium. *Nature*. 437:1018-1021.

Cramer, L.P., M. Siebert, and T.J. Mitchison. 1997. Identification of novel graded polarity actin filament bundles in locomoting heart fibroblasts: implications for the generation of motile force. *The Journal of cell biology*. 136:1287-1305.

D'Avino, P.P., and L. Capalbo. 2016. Regulation of midbody formation and function by mitotic kinases. *Seminars in cell & developmental biology*. 53:57-63.

de Celis, J.F., and R. Barrio. 2000. Function of the spalt/spalt-related gene complex in positioning the veins in the Drosophila wing. *Mechanisms of development*. 91:31-41.

de Celis, J.F., and R. Barrio. 2009. Regulation and function of Spalt proteins during animal development. *The International journal of developmental biology*. 53:1385-1398.

Del Viso, F., F. Huang, J. Myers, M. Chalfant, Y. Zhang, N. Reza, J. Bewersdorf, C.P. Lusk, and M.K. Khokha. 2016. Congenital Heart Disease Genetics Uncovers Context-Dependent Organization and Function of Nucleoporins at Cilia. *Developmental cell*. 38:478-492.

DesMarais, V., F. Macaluso, J. Condeelis, and M. Bailly. 2004. Synergistic interaction between the Arp2/3 complex and cofilin drives stimulated lamellipod extension. *Journal of cell science*. 117:3499-3510.

Ding, Q., S. Fukami, X. Meng, Y. Nishizaki, X. Zhang, H. Sasaki, A. Dlugosz, M. Nakafuku, and C. Hui. 1999. Mouse suppressor of fused is a negative regulator of sonic hedgehog signaling and alters the subcellular distribution of Gli1. *Current biology : CB*. 9:1119-1122.

Dingemans, K.P. 1969. The relation between cilia and mitoses in the mouse adenohypophysis. *The Journal of cell biology*. 43:361-367.

Dionne, L.K., X.J. Wang, and R. Prekeris. 2015. Midbody: from cellular junk to regulator of cell polarity and cell fate. *Current opinion in cell biology*. 35:51-58.

Driver, E.C., S.P. Pryor, P. Hill, J. Turner, U. Ruther, L.G. Biesecker, A.J. Griffith, and M.W. Kelley. 2008. Hedgehog signaling regulates sensory cell formation and auditory function in mice and humans. *The Journal of neuroscience : the official journal of the Society for Neuroscience*. 28:7350-7358.

Drummond, M.L., M. Li, E. Tarapore, T.T.L. Nguyen, B.J. Barouni, S. Cruz, K.C. Tan, A.E. Oro, and S.X. Atwood. 2018. Actin polymerization controls cilia-mediated signaling. *The Journal of cell biology*. 217:3255-3266.

Edwards, D.C., L.C. Sanders, G.M. Bokoch, and G.N. Gill. 1999. Activation of LIM-kinase by Pak1 couples Rac/Cdc42 GTPase signalling to actin cytoskeletal dynamics. *Nature cell biology*. 1:253-259.

Elam, W.A., H. Kang, and E.M. De la Cruz. 2013a. Biophysics of actin filament severing by cofilin. *FEBS letters*. 587:1215-1219.

Elam, W.A., H. Kang, and E.M. De La Cruz. 2013b. Competitive displacement of cofilin can promote actin filament severing. *Biochemical and biophysical research communications*. 438:728-731.

Etienne-Manneville, S., and A. Hall. 2002. Rho GTPases in cell biology. *Nature*. 420:629-635.

Euteneuer, U., and M. Schliwa. 1985. Evidence for an involvement of actin in the positioning and motility of centrosomes. *The Journal of cell biology*. 101:96-103.

Fonte, V.G., R.L. Searls, and S.R. Hilfer. 1971. The relationship of cilia with cell division and differentiation. *The Journal of cell biology*. 49:226-229.

Ford, M.J., P.L. Yeyati, G.R. Mali, M.A. Keighren, S.H. Waddell, H.K. Mjoseng, A.T. Douglas, E.A. Hall, A. Sakaue-Sawano, A. Miyawaki, R.R. Meehan, L. Boulter, I.J. Jackson, P. Mill, and R.L. Mort. 2018. A Cell/Cilia Cycle Biosensor for Single-Cell Kinetics Reveals Persistence of Cilia after G1/S Transition Is a General Property in Cells and Mice. *Developmental cell*. 47:509-523 e505.

Francis, S.S., J. Sfakianos, B. Lo, and I. Mellman. 2011. A hierarchy of signals regulates entry of membrane proteins into the ciliary membrane domain in epithelial cells. *The Journal of cell biology*. 193:219-233.

Franz, A., H. Roque, S. Saurya, J. Dobbelaere, and J.W. Raff. 2013. CP110 exhibits novel regulatory activities during centriole assembly in Drosophila. *The Journal of cell biology*. 203:785-799.

Fuccillo, M., A.L. Joyner, and G. Fishell. 2006. Morphogen to mitogen: the multiple roles of hedgehog signalling in vertebrate neural development. *Nature reviews. Neuroscience*. 7:772-783.

Furniss, D., P. Critchley, H. Giele, and A.O. Wilkie. 2007. Nonsense-mediated decay and the molecular pathogenesis of mutations in SALL1 and GLI3. *American journal of medical genetics. Part A*. 143A:3150-3160.

Gerdes, J.M., E.E. Davis, and N. Katsanis. 2009. The vertebrate primary cilium in development, homeostasis, and disease. *Cell*. 137:32-45.

Gilula, N.B., and P. Satir. 1972. The ciliary necklace. A ciliary membrane specialization. *The Journal of cell biology*. 53:494-509.

Goetz, S.C., and K.V. Anderson. 2010. The primary cilium: a signalling centre during vertebrate development. *Nature reviews. Genetics*. 11:331-344.

Goetz, S.C., K.F. Liem, Jr., and K.V. Anderson. 2012. The spinocerebellar ataxia-associated gene Tau tubulin kinase 2 controls the initiation of ciliogenesis. *Cell*. 151:847-858.

Gonzalez, M., I. Martin-Ruiz, S. Jimenez, L. Pirone, R. Barrio, and J.D. Sutherland. 2011. Generation of stable *Drosophila* cell lines using multicistronic vectors. *Scientific reports*. 1:75.

Green, J.A., and K. Mykytyn. 2010. Neuronal ciliary signaling in homeostasis and disease. *Cellular and molecular life sciences : CMLS*. 67:3287-3297.

Gupta, G.D., E. Coyaud, J. Goncalves, B.A. Mojarad, Y. Liu, Q. Wu, L. Gheiratmand, D. Comartin, J.M. Tkach, S.W. Cheung, M. Bashkurov, M. Hasegan, J.D. Knight, Z.Y. Lin, M. Schueler, F. Hildebrandt, J. Moffat, A.C. Gingras, B. Raught, and L. Pelletier. 2015. A Dynamic Protein Interaction Landscape of the Human Centrosome-Cilium Interface. *Cell*. 163:1484-1499.

Harfe, B.D., P.J. Scherz, S. Nissim, H. Tian, A.P. McMahon, and C.J. Tabin. 2004. Evidence for an expansion-based temporal Shh gradient in specifying vertebrate digit identities. *Cell*. 118:517-528.

Haycraft, C.J., B. Banizs, Y. Aydin-Son, Q. Zhang, E.J. Michaud, and B.K. Yoder. 2005. Gli2 and Gli3 localize to cilia and require the intraflagellar transport protein polaris for processing and function. *PLoS Genet*. 1:e53.

Haycraft, C.J., Q. Zhang, B. Song, W.S. Jackson, P.J. Detloff, R. Serra, and B.K. Yoder. 2007. Intraflagellar transport is essential for endochondral bone formation. *Development*. 134:307-316.

He, M., R. Subramanian, F. Bangs, T. Omelchenko, K.F. Liem, Jr., T.M. Kapoor, and K.V. Anderson. 2014. The kinesin-4 protein Kif7 regulates mammalian Hedgehog signalling by organizing the cilium tip compartment. *Nature cell biology*. 16:663-672.

Heng, Y.W., and C.G. Koh. 2010. Actin cytoskeleton dynamics and the cell division cycle. *The international journal of biochemistry & cell biology*. 42:1622-1633.

Herman, I.M., N.J. Crisona, and T.D. Pollard. 1981. Relation between cell activity and the distribution of cytoplasmic actin and myosin. *The Journal of cell biology*. 90:84-91.

Hernandez-Hernandez, V., P. Pravincumar, A. Diaz-Font, H. May-Simera, D. Jenkins, M. Knight, and P.L. Beales. 2013. Bardet-Biedl syndrome proteins control the cilia length through regulation of actin polymerization. *Human molecular genetics*. 22:3858-3868.

Hildebrand, J.D., and P. Soriano. 1999. Shroom, a PDZ domain-containing actin-binding protein, is required for neural tube morphogenesis in mice. *Cell*. 99:485-497.

Hildebrandt, F., T. Benzing, and N. Katsanis. 2011. Ciliopathies. *The New England journal of medicine*. 364:1533-1543.

Hill, P., K. Gotz, and U. Ruther. 2009. A SHH-independent regulation of Gli3 is a significant determinant of anteroposterior patterning of the limb bud. *Developmental biology*. 328:506-516.

Hsu, C.Y., N.C. Chang, M.W. Lee, K.H. Lee, D.S. Sun, C. Lai, and A.C. Chang. 2008. LUZP deficiency affects neural tube closure during brain development. *Biochemical and biophysical research communications*. 376:466-471.

Huangfu, D., and K.V. Anderson. 2006. Signaling from Smo to Ci/Gli: conservation and divergence of Hedgehog pathways from Drosophila to vertebrates. *Development*. 133:3-14.

Huangfu, D., A. Liu, A.S. Rakeman, N.S. Murcia, L. Niswander, and K.V. Anderson. 2003. Hedgehog signalling in the mouse requires intraflagellar transport proteins. *Nature*. 426:83-87.

Husson, H., S. Moreno, L.A. Smith, M.M. Smith, R.J. Russo, R. Pitstick, M. Sergeev, S.R. Ledbetter, N.O. Bukanov, M. Lane, K. Zhang, K. Billot, G. Carlson, J. Shah, L. Meijer, D.R. Beier, and O. Ibraghimov-Beskrovnaya. 2016. Reduction of ciliary length through pharmacologic or genetic inhibition of CDK5 attenuates polycystic kidney disease in a model of nephronophthisis. *Human molecular genetics*. 25:2245-2255.

Hynes, M., D.M. Stone, M. Dowd, S. Pitts-Meek, A. Goddard, A. Gurney, and A. Rosenthal. 1997. Control of cell pattern in the neural tube by the zinc finger transcription factor and oncogene Gli-1. *Neuron*. 19:15-26.

Jacquemet, G., D.M. Green, R.E. Bridgewater, A. von Kriegsheim, M.J. Humphries, J.C. Norman, and P.T. Caswell. 2013. RCP-driven alpha5beta1 recycling suppresses Rac and promotes RhoA activity via the RacGAP1-IQGAP1 complex. *The Journal of cell biology*. 202:917-935.

Jacquemet, G., I. Paatero, A.F. Carisey, A. Padzik, J.S. Orange, H. Hamidi, and J. Ivaska. 2017. FiloQuant reveals increased filopodia density during breast cancer progression. *The Journal of cell biology*. 216:3387-3403.

Kang, G.M., Y.M. Han, H.W. Ko, J. Kim, B.C. Oh, I. Kwon, and M.S. Kim. 2015. Leptin Elongates Hypothalamic Neuronal Cilia via Transcriptional Regulation and Actin Destabilization. *The Journal of biological chemistry*. 290:18146-18155.

Kang, S., J.M. Graham, Jr., A.H. Olney, and L.G. Biesecker. 1997. GLI3 frameshift mutations cause autosomal dominant Pallister-Hall syndrome. *Nature genetics*. 15:266-268.

Kawakami, Y., Y. Uchiyama, C. Rodriguez Esteban, T. Inenaga, N. Koyano-Nakagawa, H. Kawakami, M. Marti, M. Kmita, P. Monaghan-Nichols, R. Nishinakamura, and J.C. Izpisua Belmonte. 2009. Sall genes regulate region-specific morphogenesis in the mouse limb by modulating Hox activities. *Development*. 136:585-594.

Kee, H.L., J.F. Dishinger, T.L. Blasius, C.J. Liu, B. Margolis, and K.J. Verhey. 2012. A size-exclusion permeability barrier and nucleoporins characterize a ciliary

pore complex that regulates transport into cilia. *Nature cell biology*. 14:431-437.

Kemp, J.P., Jr., and W.M. Brieher. 2018. The actin filament bundling protein alpha-actinin-4 actually suppresses actin stress fibers by permitting actin turnover. *The Journal of biological chemistry*. 293:14520-14533.

Kiefer, S.M., B.W. McDill, J. Yang, and M. Rauchman. 2002. Murine Sall1 represses transcription by recruiting a histone deacetylase complex. *The Journal of biological chemistry*. 277:14869-14876.

Kiefer, S.M., K.K. Ohlemiller, J. Yang, B.W. McDill, J. Kohlhase, and M. Rauchman. 2003. Expression of a truncated Sall1 transcriptional repressor is responsible for Townes-Brocks syndrome birth defects. *Human molecular genetics*. 12:2221-2227.

Kiefer, S.M., L. Robbins, A. Barina, Z. Zhang, and M. Rauchman. 2008. SALL1 truncated protein expression in Townes-Brocks syndrome leads to ectopic expression of downstream genes. *Human mutation*. 29:1133-1140.

Kim, D.I., K.C. Birendra, W. Zhu, K. Motamedchaboki, V. Doye, and K.J. Roux. 2014. Probing nuclear pore complex architecture with proximity-dependent biotinylation. *Proceedings of the National Academy of Sciences of the United States of America*. 111:E2453-2461.

Kim, J., H. Jo, H. Hong, M.H. Kim, J.M. Kim, J.K. Lee, W.D. Heo, and J. Kim. 2015. Actin remodelling factors control ciliogenesis by regulating YAP/TAZ activity and vesicle trafficking. *Nature communications*. 6:6781.

Kim, J., M. Kato, and P.A. Beachy. 2009. Gli2 trafficking links Hedgehog-dependent activation of Smoothened in the primary cilium to transcriptional activation in the nucleus. *Proceedings of the National Academy of Sciences of the United States of America*. 106:21666-21671.

Kim, J., J.E. Lee, S. Heynen-Genel, E. Suyama, K. Ono, K. Lee, T. Ideker, P. Aza-Blanc, and J.G. Gleeson. 2010. Functional genomic screen for modulators of ciliogenesis and cilium length. *Nature*. 464:1048-1051.

Kleylein-Sohn, J., J. Westendorf, M. Le Clech, R. Habedanck, Y.D. Stierhof, and E.A. Nigg. 2007. Plk4-induced centriole biogenesis in human cells. *Developmental cell*. 13:190-202.

Kobayashi, T., W.Y. Tsang, J. Li, W. Lane, and B.D. Dynlacht. 2011. Centriolar kinesin Kif24 interacts with CP110 to remodel microtubules and regulate ciliogenesis. *Cell*. 145:914-925.

Kohlhase, J. 1993. Townes-Brocks Syndrome. *In* GeneReviews((R)). M.P. Adam, H.H. Ardinger, R.A. Pagon, S.E. Wallace, L.J.H. Bean, K. Stephens, and A. Amemiya, editors, Seattle (WA).

Kohlhase, J., M. Liebers, J. Backe, A. Baumann-Muller, M. Bembea, A. Destree, M. Gattas, S. Grussner, T. Muller, G. Mortier, C. Skrypnyk, S. Yano, J. Wirbelauer, and R.C. Michaelis. 2003. High incidence of the R276X SALL1 mutation in sporadic but not familial Townes-Brocks syndrome and report of the first familial case. *J Med Genet*. 40:e127.

Kohlhase, J., A. Wischermann, H. Reichenbach, U. Froster, and W. Engel. 1998. Mutations in the SALL1 putative transcription factor gene cause Townes-Brocks syndrome. *Nature genetics*. 18:81-83.

Kohlmaier, G., J. Loncarek, X. Meng, B.F. McEwen, M.M. Mogensen, A. Spektor, B.D. Dynlacht, A. Khodjakov, and P. Gonczy. 2009. Overly long centrioles and defective cell division upon excess of the SAS-4-related protein CPAP. *Current biology : CB*. 19:1012-1018.

Koleske, A.J., A.M. Gifford, M.L. Scott, M. Nee, R.T. Bronson, K.A. Miczek, and D. Baltimore. 1998. Essential roles for the Abl and Arg tyrosine kinases in neurulation. *Neuron*. 21:1259-1272.

Koster, R., R. Stick, F. Loosli, and J. Wittbrodt. 1997. Medaka spalt acts as a target gene of hedgehog signaling. *Development*. 124:3147-3156.

Kuhns, S., K.N. Schmidt, J. Reymann, D.F. Gilbert, A. Neuner, B. Hub, R. Carvalho, P. Wiedemann, H. Zentgraf, H. Erfle, U. Klingmuller, M. Boutros, and G. Pereira. 2013. The microtubule affinity regulating kinase MARK4 promotes axoneme extension during early ciliogenesis. *The Journal of cell biology*. 200:505-522.

Kurnit, D.M., M.W. Steele, L. Pinsky, and A. Dibbins. 1978. Autosomal dominant transmission of a syndrome of anal, ear, renal, and radial congenital malformations. *The Journal of pediatrics*. 93:270-273.

Lauberth, S.M., A.C. Bilyeu, B.A. Firulli, K.L. Kroll, and M. Rauchman. 2007. A phosphomimetic mutation in the Sall1 repression motif disrupts recruitment of the nucleosome remodeling and deacetylase complex and repression of Gbx2. *The Journal of biological chemistry*. 282:34858-34868.

Lee, M.W., A.C. Chang, D.S. Sun, C.Y. Hsu, and N.C. Chang. 2001. Restricted expression of LUZP in neural lineage cells: a study in embryonic stem cells. *Journal of biomedical science*. 8:504-511.

Lettice, L.A., S.J. Heaney, L.A. Purdie, L. Li, P. de Beer, B.A. Oostra, D. Goode, G. Elgar, R.E. Hill, and E. de Graaff. 2003. A long-range Shh enhancer regulates expression in the developing limb and fin and is associated with preaxial polydactyly. *Human molecular genetics*. 12:1725-1735.

Liem, K.F., Jr., M. He, P.J. Ocbina, and K.V. Anderson. 2009. Mouse Kif7/Costal2 is a cilia-associated protein that regulates Sonic hedgehog signaling. *Proceedings of the National Academy of Sciences of the United States of America*. 106:13377-13382.

Lienkamp, S., A. Ganner, and G. Walz. 2012. Inversin, Wnt signaling and primary cilia. *Differentiation; research in biological diversity*. 83:S49-55.

Lin, Y.C., P. Niewiadomski, B. Lin, H. Nakamura, S.C. Phua, J. Jiao, A. Levchenko, T. Inoue, R. Rohatgi, and T. Inoue. 2013. Chemically inducible diffusion trap at cilia reveals molecular sieve-like barrier. *Nature chemical biology*. 9:437-443.

Litingtung, Y., R.D. Dahn, Y. Li, J.F. Fallon, and C. Chiang. 2002. Shh and Gli3 are dispensable for limb skeleton formation but regulate digit number and identity. *Nature*. 418:979-983.

Liu, A., B. Wang, and L.A. Niswander. 2005. Mouse intraflagellar transport proteins regulate both the activator and repressor functions of Gli transcription factors. *Development*. 132:3103-3111.

Machesky, L.M., S.J. Atkinson, C. Ampe, J. Vandekerckhove, and T.D. Pollard. 1994. Purification of a cortical complex containing two unconventional actins from Acanthamoeba by affinity chromatography on profilin-agarose. *The Journal of cell biology*. 127:107-115.

Machesky, L.M., R.D. Mullins, H.N. Higgs, D.A. Kaiser, L. Blanchoin, R.C. May, M.E. Hall, and T.D. Pollard. 1999. Scar, a WASp-related protein, activates nucleation of actin filaments by the Arp2/3 complex. *Proceedings of the National Academy of Sciences of the United States of America*. 96:3739-3744.

Machesky, L.M., E. Reeves, F. Wientjes, F.J. Mattheyse, A. Grogan, N.F. Totty, A.L. Burlingame, J.J. Hsuan, and A.W. Segal. 1997. Mammalian actin-related protein 2/3 complex localizes to regions of lamellipodial protrusion and is composed of evolutionarily conserved proteins. *The Biochemical journal*. 328 ( Pt 1):105-112.

Maekawa, M., T. Ishizaki, S. Boku, N. Watanabe, A. Fujita, A. Iwamatsu, T. Obinata, K. Ohashi, K. Mizuno, and S. Narumiya. 1999. Signaling from Rho to the actin cytoskeleton through protein kinases ROCK and LIM-kinase. *Science*. 285:895-898.

Marchand, J.B., D.A. Kaiser, T.D. Pollard, and H.N. Higgs. 2001. Interaction of WASP/Scar proteins with actin and vertebrate Arp2/3 complex. *Nature cell biology*. 3:76-82.

Masuya, H., T. Sagai, S. Wakana, K. Moriwaki, and T. Shiroishi. 1995. A duplicated zone of polarizing activity in polydactylous mouse mutants. *Genes & development*. 9:1645-1653.

McCloy, R.A., S. Rogers, C.E. Caldon, T. Lorca, A. Castro, and A. Burgess. 2014. Partial inhibition of Cdk1 in G 2 phase overrides the SAC and decouples mitotic events. *Cell Cycle*. 13:1400-1412.

McMahon, A.P., P.W. Ingham, and C.J. Tabin. 2003. Developmental roles and clinical significance of hedgehog signaling. *Current topics in developmental biology*. 53:1-114.

Miller, E.M., R. Hopkin, L. Bao, and S.M. Ware. 2012. Implications for genotype-phenotype predictions in Townes-Brocks syndrome: case report of a novel SALL1 deletion and review of the literature. *American journal of medical genetics. Part A*. 158A:533-540.

Mo, R., J.H. Kim, J. Zhang, C. Chiang, C.C. Hui, and P.C. Kim. 2001. Anorectal malformations caused by defects in sonic hedgehog signaling. *Am J Pathol*. 159:765-774.

Moyer, J.H., M.J. Lee-Tischler, H.Y. Kwon, J.J. Schrick, E.D. Avner, W.E. Sweeney, V.L. Godfrey, N.L. Cacheiro, J.E. Wilkinson, and R.P. Woychik. 1994. Candidate gene associated with a mutation causing recessive polycystic kidney disease in mice. *Science*. 264:1329-1333.

Mseka, T., and L.P. Cramer. 2011. Actin depolymerization-based force retracts the cell rear in polarizing and migrating cells. *Current biology : CB*. 21:2085-2091.

Mullins, R.D., J.A. Heuser, and T.D. Pollard. 1998. The interaction of Arp2/3 complex with actin: nucleation, high affinity pointed end capping, and formation of branching networks of filaments. *Proceedings of the National Academy of Sciences of the United States of America*. 95:6181-6186.

Nagai, T., S. Mukoyama, H. Kagiwada, N. Goshima, and K. Mizuno. 2018. Cullin-3-KCTD10-mediated CEP97 degradation promotes primary cilium formation. *Journal of cell science*.

Nager, A.R., J.S. Goldstein, V. Herranz-Perez, D. Portran, F. Ye, J.M. Garcia-Verdugo, and M.V. Nachury. 2017. An Actin Network Dispatches Ciliary GPCRs into Extracellular Vesicles to Modulate Signaling. *Cell*. 168:252-263 e214.

Netzer, C., S.K. Bohlander, M. Hinzke, Y. Chen, and J. Kohlhase. 2006. Defining the heterochromatin localization and repression domains of SALL1. *Biochimica et biophysica acta*. 1762:386-391.

Netzer, C., L. Rieger, A. Brero, C.D. Zhang, M. Hinzke, J. Kohlhase, and S.K. Bohlander. 2001. SALL1, the gene mutated in Townes-Brocks syndrome, encodes a transcriptional repressor which interacts with TRF1/PIN2 and localizes to pericentromeric heterochromatin. *Human molecular genetics*. 10:3017-3024.

Ngo, K.X., N. Kodera, E. Katayama, T. Ando, and T.Q. Uyeda. 2015. Cofilin-induced unidirectional cooperative conformational changes in actin filaments revealed by high-speed atomic force microscopy. *eLife*. 4.

Nigg, E.A. 2002. Centrosome aberrations: cause or consequence of cancer progression? *Nature reviews. Cancer*. 2:815-825.

Nishinakamura, R., Y. Matsumoto, K. Nakao, K. Nakamura, A. Sato, N.G. Copeland, D.J. Gilbert, N.A. Jenkins, S. Scully, D.L. Lacey, M. Katsuki, M. Asashima, and T. Yokota. 2001. Murine homolog of SALL1 is essential for ureteric bud invasion in kidney development. *Development*. 128:3105-3115.

Nonaka, S., Y. Tanaka, Y. Okada, S. Takeda, A. Harada, Y. Kanai, M. Kido, and N. Hirokawa. 1998. Randomization of left-right asymmetry due to loss of nodal cilia generating leftward flow of extraembryonic fluid in mice lacking KIF3B motor protein. *Cell*. 95:829-837.

Obado, S.O., and M.P. Rout. 2012. Ciliary and nuclear transport: different places, similar routes? *Developmental cell*. 22:693-694.

Obado, S.O., and M.P. Rout. 2016. Cilia and Nuclear Pore Proteins: Pore No More? *Developmental cell*. 38:445-446.

Pan, Y., C.B. Bai, A.L. Joyner, and B. Wang. 2006. Sonic hedgehog signaling regulates Gli2 transcriptional activity by suppressing its processing and degradation. *Molecular and cellular biology*. 26:3365-3377.

Paul, N.R., J.L. Allen, A. Chapman, M. Morlan-Mairal, E. Zindy, G. Jacquemet, L. Fernandez del Ama, N. Ferizovic, D.M. Green, J.D. Howe, E. Ehler, A. Hurlstone, and P.T. Caswell. 2015. alpha5beta1 integrin recycling promotes Arp2/3-independent cancer cell invasion via the formin FHOD3. *The Journal of cell biology*. 210:1013-1031.

Pazour, G.J., S.A. Baker, J.A. Deane, D.G. Cole, B.L. Dickert, J.L. Rosenbaum, G.B. Witman, and J.C. Besharse. 2002. The intraflagellar transport protein, IFT88, is essential for vertebrate photoreceptor assembly and maintenance. *The Journal of cell biology*. 157:103-113.

Pazour, G.J., B.L. Dickert, Y. Vucica, E.S. Seeley, J.L. Rosenbaum, G.B. Witman, and D.G. Cole. 2000. Chlamydomonas IFT88 and its mouse homologue, polycystic kidney disease gene tg737, are required for assembly of cilia and flagella. *The Journal of cell biology*. 151:709-718.

Petrie, R.J., and K.M. Yamada. 2012. At the leading edge of three-dimensional cell migration. *Journal of cell science*. 125:5917-5926.

Phua, S.C., S. Chiba, M. Suzuki, E. Su, E.C. Roberson, G.V. Pusapati, M. Setou, R. Rohatgi, J.F. Reiter, K. Ikegami, and T. Inoue. 2017. Dynamic Remodeling of

Membrane Composition Drives Cell Cycle through Primary Cilia Excision. *Cell*. 168:264-279 e215.

Pigino, G., S. Geimer, S. Lanzavecchia, E. Paccagnini, F. Cantele, D.R. Diener, J.L. Rosenbaum, and P. Lupetti. 2009. Electron-tomographic analysis of intraflagellar transport particle trains in situ. *J Cell Biol*. 187:135-148.

Pitaval, A., Q. Tseng, M. Bornens, and M. Thery. 2010. Cell shape and contractility regulate ciliogenesis in cell cycle-arrested cells. *The Journal of cell biology*. 191:303-312.

Pollard, T.D., and G.G. Borisy. 2003. Cellular motility driven by assembly and disassembly of actin filaments. *Cell*. 112:453-465.

Pollard, T.D., and J.A. Cooper. 2009. Actin, a central player in cell shape and movement. *Science*. 326:1208-1212.

Powell, C.M., and R.C. Michaelis. 1999. Townes-Brocks syndrome. *J Med Genet*. 36:89-93.

Prosser, S.L., and C.G. Morrison. 2015. Centrin2 regulates CP110 removal in primary cilium formation. *The Journal of cell biology*. 208:693-701.

Rankin, K.E., and L. Wordeman. 2010. Long astral microtubules uncouple mitotic spindles from the cytokinetic furrow. *The Journal of cell biology*. 190:35-43.

Reimand, J., T. Arak, P. Adler, L. Kolberg, S. Reisberg, H. Peterson, and J. Vilo. 2016. g:Profiler-a web server for functional interpretation of gene lists (2016 update). *Nucleic acids research*. 44:W83-89.

Reiter, J.F., and M.R. Leroux. 2017. Genes and molecular pathways underpinning ciliopathies. *Nature reviews. Molecular cell biology*. 18:533-547.

Rezabkova, L., S.H. Kraatz, A. Akhmanova, M.O. Steinmetz, and R.A. Kammerer. 2016. Biophysical and Structural Characterization of the Centriolar Protein Cep104 Interaction Network. *The Journal of biological chemistry*. 291:18496-18504.

Ribes, V., and J. Briscoe. 2009. Establishing and interpreting graded Sonic Hedgehog signaling during vertebrate neural tube patterning: the role of negative feedback. *Cold Spring Harbor perspectives in biology*. 1:a002014.

Roessler, E., Y.Z. Du, J.L. Mullor, E. Casas, W.P. Allen, G. Gillessen-Kaesbach, E.R. Roeder, J.E. Ming, A. Ruiz i Altaba, and M. Muenke. 2003. Loss-of-function mutations in the human GLI2 gene are associated with pituitary anomalies and holoprosencephaly-like features. *Proceedings of the National Academy of Sciences of the United States of America*. 100:13424-13429.

Roessler, E., A.N. Ermilov, D.K. Grange, A. Wang, M. Grachtchouk, A.A. Dlugosz, and M. Muenke. 2005. A previously unidentified amino-terminal domain regulates transcriptional activity of wild-type and disease-associated human GLI2. *Human molecular genetics*. 14:2181-2188.

Rohatgi, R., L. Milenkovic, and M.P. Scott. 2007. Patched1 regulates hedgehog signaling at the primary cilium. *Science*. 317:372-376.

Rohatgi, R., and W.J. Snell. 2010. The ciliary membrane. *Current opinion in cell biology*. 22:541-546.

Rottner, K., A. Hall, and J.V. Small. 1999. Interplay between Rac and Rho in the control of substrate contact dynamics. *Current biology : CB*. 9:640-648.

Rouiller, I., X.P. Xu, K.J. Amann, C. Egile, S. Nickell, D. Nicastro, R. Li, T.D. Pollard, N. Volkmann, and D. Hanein. 2008. The structural basis of actin filament branching by the Arp2/3 complex. *The Journal of cell biology*. 180:887-895.

Roux, K.J., D.I. Kim, M. Raida, and B. Burke. 2012. A promiscuous biotin ligase fusion protein identifies proximal and interacting proteins in mammalian cells. *The Journal of cell biology*. 196:801-810.

Rubino, S., M. Fighetti, E. Unger, and P. Cappuccinelli. 1984. Location of actin, myosin, and microtubular structures during directed locomotion of Dictyostelium amebae. *The Journal of cell biology*. 98:382-390.

Rubinson, D.A., C.P. Dillon, A.V. Kwiatkowski, C. Sievers, L. Yang, J. Kopinja, D.L. Rooney, M. Zhang, M.M. Ihrig, M.T. McManus, F.B. Gertler, M.L. Scott, and L. Van Parijs. 2003. A lentivirus-based system to functionally silence genes in primary mammalian cells, stem cells and transgenic mice by RNA interference. *Nat Genet*. 33:401-406.

Sadler, T.W., D. Greenberg, P. Coughlin, and J.L. Lessard. 1982. Actin distribution patterns in the mouse neural tube during neurulation. *Science*. 215:172-174.

Saigusa, T., and P.D. Bell. 2015. Molecular pathways and therapies in autosomal-dominant polycystic kidney disease. *Physiology (Bethesda)*. 30:195-207.

Sanchez, I., and B.D. Dynlacht. 2016. Cilium assembly and disassembly. *Nature cell biology*. 18:711-717.

Santos, N., and J.F. Reiter. 2014. A central region of Gli2 regulates its localization to the primary cilium and transcriptional activity. *Journal of cell science*. 127:1500-1510.

Satir, P., and S.T. Christensen. 2008. Structure and function of mammalian cilia. *Histochemistry and cell biology*. 129:687-693.

Sato, A., S. Kishida, T. Tanaka, A. Kikuchi, T. Kodama, M. Asashima, and R. Nishinakamura. 2004. Sall1, a causative gene for Townes-Brocks syndrome, enhances the canonical Wnt signaling by localizing to heterochromatin. *Biochemical and biophysical research communications*. 319:103-113.

Schmidt, T.I., J. Kleylein-Sohn, J. Westendorf, M. Le Clech, S.B. Lavoie, Y.D. Stierhof, and E.A. Nigg. 2009. Control of centriole length by CPAP and CP110. *Current biology : CB*. 19:1005-1011.

Shah, A.S., Y. Ben-Shahar, T.O. Moninger, J.N. Kline, and M.J. Welsh. 2009. Motile cilia of human airway epithelia are chemosensory. *Science*. 325:1131-1134.

Smith, L.A., N.O. Bukanov, H. Husson, R.J. Russo, T.C. Barry, A.L. Taylor, D.R. Beier, and O. Ibraghimov-Beskrovnaya. 2006. Development of polycystic kidney disease in juvenile cystic kidney mice: insights into pathogenesis, ciliary abnormalities, and common features with human disease. *Journal of the American Society of Nephrology : JASN*. 17:2821-2831.

Sohara, E., Y. Luo, J. Zhang, D.K. Manning, D.R. Beier, and J. Zhou. 2008. Nek8 regulates the expression and localization of polycystin-1 and polycystin-2. *Journal of the American Society of Nephrology : JASN*. 19:469-476.

Song, R., P. Walentek, N. Sponer, A. Klimke, J.S. Lee, G. Dixon, R. Harland, Y. Wan, P. Lishko, M. Lize, M. Kessel, and L. He. 2014. miR-34/449 miRNAs are required for motile ciliogenesis by repressing cp110. *Nature*. 510:115-120.

Sorokin, S. 1962. Centrioles and the formation of rudimentary cilia by fibroblasts and smooth muscle cells. *The Journal of cell biology*. 15:363-377.

Spalluto, C., D.I. Wilson, and T. Hearn. 2013. Evidence for reciliation of RPE1 cells in late G1 phase, and ciliary localisation of cyclin B1. *FEBS Open Bio*. 3:334-340.

Spektor, A., W.Y. Tsang, D. Khoo, and B.D. Dynlacht. 2007. Cep97 and CP110 suppress a cilia assembly program. *Cell*. 130:678-690.

Sun, D.S., A.C. Chang, N.A. Jenkins, D.J. Gilbert, N.G. Copeland, and N.C. Chang. 1996. Identification, molecular characterization, and chromosomal localization of the cDNA encoding a novel leucine zipper motif-containing protein. *Genomics*. 36:54-62.

Surka, W.S., J. Kohlhase, C.E. Neunert, D.S. Schneider, and V.K. Proud. 2001. Unique family with Townes-Brocks syndrome, SALL1 mutation, and cardiac defects. *American journal of medical genetics*. 102:250-257.

Sweetman, D., T. Smith, E.R. Farrell, A. Chantry, and A. Munsterberg. 2003. The conserved glutamine-rich region of chick csal1 and csal3 mediates protein interactions with other spalt family members. Implications for Townes-Brocks syndrome. *The Journal of biological chemistry*. 278:6560-6566.

Taipale, J., J.K. Chen, M.K. Cooper, B. Wang, R.K. Mann, L. Milenkovic, M.P. Scott, and P.A. Beachy. 2000. Effects of oncogenic mutations in Smoothened and Patched can be reversed by cyclopamine. *Nature*. 406:1005-1009.

Takao, D., and K.J. Verhey. 2016. Gated entry into the ciliary compartment. *Cellular and molecular life sciences : CMLS*. 73:119-127.

Tanos, B.E., H.J. Yang, R. Soni, W.J. Wang, F.P. Macaluso, J.M. Asara, and M.F. Tsou. 2013. Centriole distal appendages promote membrane docking, leading to cilia initiation. *Genes & development*. 27:163-168.

Tsang, W.Y., C. Bossard, H. Khanna, J. Peranen, A. Swaroop, V. Malhotra, and B.D. Dynlacht. 2008. CP110 suppresses primary cilia formation through its interaction with CEP290, a protein deficient in human ciliary disease. *Developmental cell*. 15:187-197.

Tsang, W.Y., and B.D. Dynlacht. 2013. CP110 and its network of partners coordinately regulate cilia assembly. *Cilia*. 2:9.

Tunovic, S., K.W. Baranano, J.A. Barkovich, J.B. Strober, L. Jamal, and A.M. Slavotinek. 2015. Novel KIF7 missense substitutions in two patients presenting with multiple malformations and features of acrocallosal syndrome. *American journal of medical genetics. Part A*. 167A:2767-2776.

Tuson, M., M. He, and K.V. Anderson. 2011. Protein kinase A acts at the basal body of the primary cilium to prevent Gli2 activation and ventralization of the mouse neural tube. *Development*. 138:4921-4930.

Uhlen, M., L. Fagerberg, B.M. Hallstrom, C. Lindskog, P. Oksvold, A. Mardinoglu, A. Sivertsson, C. Kampf, E. Sjostedt, A. Asplund, I. Olsson, K. Edlund, E. Lundberg, S. Navani, C.A. Szigyarto, J. Odeberg, D. Djureinovic, J.O. Takanen, S. Hober, T. Alm, P.H. Edqvist, H. Berling, H. Tegel, J. Mulder, J. Rockberg, P. Nilsson, J.M. Schwenk, M. Hamsten, K. von Feilitzen, M. Forsberg, L. Persson, F. Johansson, M. Zwahlen, G. von Heijne, J. Nielsen, and F. Ponten. 2015. Proteomics. Tissue-based map of the human proteome. *Science*. 347:1260419.

Valerius, N.H., O. Stendahl, J.H. Hartwig, and T.P. Stossel. 1981. Distribution of actin-binding protein and myosin in polymorphonuclear leukocytes during locomotion and phagocytosis. *Cell*. 24:195-202.

van Dam, T.J., G. Wheway, G.G. Slaats, M.A. Huynen, and R.H. Giles. 2013. The SYSCILIA gold standard (SCGSv1) of known ciliary components and its applications within a systems biology consortium. *Cilia*. 2:7.

Van Itallie, C.M., A. Aponte, A.J. Tietgens, M. Gucek, K. Fredriksson, and J.M. Anderson. 2013. The N and C termini of ZO-1 are surrounded by distinct proteins and functional protein networks. *The Journal of biological chemistry*. 288:13775-13788.

Wallingford, J.B. 2005. Neural tube closure and neural tube defects: studies in animal models reveal known knowns and known unknowns. *American journal of medical genetics. Part C, Seminars in medical genetics*. 135C:59-68.

Wang, B., J.F. Fallon, and P.A. Beachy. 2000a. Hedgehog-regulated processing of Gli3 produces an anterior/posterior repressor gradient in the developing vertebrate limb. *Cell*. 100:423-434.

Wang, H., Z.A. Wang, and R.R. He. 2000b. [Adenosine inhibits spontaneous and glutamate induced discharges of hippocampal CA1 neurons]. *Sheng li xue bao : [Acta physiologica Sinica]*. 52:281-286.

Weaver, A.M., A.V. Karginov, A.W. Kinley, S.A. Weed, Y. Li, J.T. Parsons, and J.A. Cooper. 2001. Cortactin promotes and stabilizes Arp2/3-induced actin filament network formation. *Current biology : CB*. 11:370-374.

Weinberg, J., and D.G. Drubin. 2012. Clathrin-mediated endocytosis in budding yeast. *Trends in cell biology*. 22:1-13.

Wheatley, D.N. 1995. Primary cilia in normal and pathological tissues. *Pathobiology : journal of immunopathology, molecular and cellular biology*. 63:222-238.

Wiederschain, D., S. Wee, L. Chen, A. Loo, G. Yang, A. Huang, Y. Chen, G. Caponigro, Y.M. Yao, C. Lengauer, W.R. Sellers, and J.D. Benson. 2009. Single-vector inducible lentiviral RNAi system for oncology target validation. *Cell Cycle*. 8:498-504.

Wiggan, O., A.E. Shaw, J.G. DeLuca, and J.R. Bamburg. 2012. ADF/cofilin regulates actomyosin assembly through competitive inhibition of myosin II binding to F-actin. *Developmental cell*. 22:530-543.

Wong, S.Y., and J.F. Reiter. 2008. The primary cilium at the crossroads of mammalian hedgehog signaling. *Current topics in developmental biology*. 85:225-260.

Woolner, S., L.L. O'Brien, C. Wiese, and W.M. Bement. 2008. Myosin-10 and actin filaments are essential for mitotic spindle function. *The Journal of cell biology*. 182:77-88.

Xu, W., H. Baribault, and E.D. Adamson. 1998. Vinculin knockout results in heart and brain defects during embryonic development. *Development*. 125:327-337.

Xue, Y., J. Wong, G.T. Moreno, M.K. Young, J. Cote, and W. Wang. 1998. NURD, a novel complex with both ATP-dependent chromatin-remodeling and histone deacetylase activities. *Molecular cell*. 2:851-861.

Yang, F., Y. Yao, Y. Jiang, L. Lu, Y. Ma, and W. Dai. 2016. Sumoylation is important for stability, subcellular localization, and transcriptional activity of SALL4, an essential stem cell transcription factor. *The Journal of biological chemistry*. 291:428.

Yang, Y., G. Drossopoulou, P.T. Chuang, D. Duprez, E. Marti, D. Bumcrot, N. Vargesson, J. Clarke, L. Niswander, A. McMahon, and C. Tickle. 1997. Relationship between dose, distance and time in Sonic Hedgehog-mediated

regulation of anteroposterior polarity in the chick limb. *Development*. 124:4393-4404.

Yin, Y., F. Bangs, I.R. Paton, A. Prescott, J. James, M.G. Davey, P. Whitley, G. Genikhovich, U. Technau, D.W. Burt, and C. Tickle. 2009. The Talpid3 gene (KIAA0586) encodes a centrosomal protein that is essential for primary cilia formation. *Development*. 136:655-664.

Zaveri, H.P., T.F. Beck, A. Hernandez-Garcia, K.E. Shelly, T. Montgomery, A. van Haeringen, B.M. Anderlid, C. Patel, H. Goel, G. Houge, B.E. Morrow, S.W. Cheung, S.R. Lalani, and D.A. Scott. 2014. Identification of critical regions and candidate genes for cardiovascular malformations and cardiomyopathy associated with deletions of chromosome 1p36. *PloS one*. 9:e85600.

# Appendices

## Appendices

**Appendix I**. List of proteins identified by BioID significantly enriched at least 2-fold in the SALL1[275] subproteome with respect to the SALL1[FL] subproteome in 2 out of 3 experiments based on label-free protein quantitation. Hits are sorted by increasing average ratio.

| Protein names | Gene names | Intensity SALL1[275]1 | Intensity SALL1[275]2 | Intensity SALL1[275]3 | Intensity SALL1[FL]1 | Intensity SALL1[FL]2 | Intensity SALL1[FL]3 | [275]1/[FL]1 | [275]2/[FL]2 | [275]3/[FL]3 | average ratio |
|---|---|---|---|---|---|---|---|---|---|---|---|
| Kinesin-1 heavy chain | KIF5B | 11709000000 | 606220000 | 511450000 | 849090 | 7218600 | 12139000 | 13790.1 | 84.0 | 42.1 | **4638.7** |
| Band 4.1-like protein 2 | EPB41L2 | 9153200000 | 820650000 | 607080000 | 849090 | 1656200 | 1318000 | 10780.0 | 495.5 | 460.6 | **3912.0** |
| La-related protein 1 | LARP1 | 7294500000 | 780580000 | 731460000 | 849090 | 13451000 | 1318000 | 8591.0 | 58.0 | 555.0 | **3068.0** |
| Ataxin-2-like protein | ATXN2L | 5667700000 | 587370000 | 551100000 | 849090 | 1656200 | 1318000 | 6675.0 | 354.6 | 418.1 | **2482.6** |
| LIM domain and actin-binding protein 1 | LIMA1 | 5427600000 | 409460000 | 151410000 | 849090 | 1656200 | 1318000 | 6392.3 | 247.2 | 114.9 | **2251.5** |
| C-Jun-amino-terminal kinase-interacting protein 4 | SPAG9 | 4649500000 | 309140000 | 213600000 | 849090 | 1656200 | 1318000 | 5475.9 | 186.7 | 162.1 | **1941.5** |
| Transforming acidic coiled-coil-containing protein 2 | TACC2 | 1210600000 | 97675 | 5250100000 | 849090 | 1656200 | 1318000 | 1425.8 | 0.1 | 3983.4 | **1803.1** |
| Afadin | AFDN | 5893400000 | 787430000 | 533810000 | 1252800 | 24483000 | 16236000 | 4704.2 | 32.2 | 32.9 | **1589.7** |
| Protein PRRC2C | PRRC2C | 3348400000 | 226490000 | 159440000 | 849090 | 8260200 | 1318000 | 3943.5 | 27.4 | 121.0 | **1364.0** |
| Unconventional myosin-VI | MYO6 | 3306000000 | 49963000 | 55756000 | 849090 | 1656200 | 1318000 | 3893.6 | 30.2 | 42.3 | **1322.0** |
| STE20-like serine/threonine-protein kinase | SLK | 2997300000 | 104840000 | 116620000 | 849090 | 1656200 | 1318000 | 3530.0 | 63.3 | 88.5 | **1227.3** |
| A-kinase anchor protein 12 | AKAP12 | 2996700000 | 31117000 | 29249000 | 849090 | 1656200 | 1318000 | 3529.3 | 18.8 | 22.2 | **1190.1** |
| Condensin complex subunit 2 | NCAPH | 2720900000 | 194050000 | 146540000 | 849090 | 1656200 | 1318000 | 3204.5 | 117.2 | 111.2 | **1144.3** |
| Nuclear pore complex protein Nup153 | NUP153 | 2707900000 | 227690000 | 202280000 | 849090 | 31717000 | 1318000 | 3189.2 | 7.2 | 153.5 | **1116.6** |
| Band 4.1-like protein 3;Band 4.1-like protein 3, N-terminally processed | EPB41L3 | 29726000000 | 3655200000 | 3149500000 | 42213000 | 14779000 | 1318000 | 704.2 | 247.3 | 2389.6 | **1113.7** |
| Kinesin-like protein KIF11 | KIF11 | 2560700000 | 275980000 | 129340000 | 849090 | 1656200 | 1318000 | 3015.8 | 166.6 | 98.1 | **1093.5** |
| Protein 4.1 | EPB41 | 15927000000 | 2467300000 | 2539500000 | 32127000 | 22276000 | 1318000 | 495.8 | 110.8 | 1926.8 | **844.4** |
| Eukaryotic translation initiation factor 4B | EIF4B | 10168000000 | 1908100000 | 1582800000 | 144740000 | 1656200 | 1318000 | 70.3 | 1152.1 | 1200.9 | **807.8** |

| | | | | | | | | | | |
|---|---|---|---|---|---|---|---|---|---|---|
| Leucine zipper protein 1 | LUZP1 | 1966700000 | 98882000 | 13908000 | 849090 | 1656200 | 1318000 | 2316.2 | 59.7 | 10.6 | **795.5** |
| Deubiquitinating protein VCIP135 | VCPIP1 | 1753000000 | 241760000 | 130240000 | 849090 | 37476000 | 30738000 | 2064.6 | 6.5 | 4.2 | **691.8** |
| Zinc finger RNA-binding protein | ZFR | 1740000000 | 15838000 | 77089000 | 849090 | 17753000 | 8659500 | 2049.3 | 0.9 | 8.9 | **686.3** |
| AP2-associated protein kinase 1 | AAK1 | 1582200000 | 159580000 | 81009000 | 849090 | 1656200 | 1318000 | 1863.4 | 96.4 | 61.5 | **673.7** |
| Unconventional myosin-Ib | MYO1B | 1633100000 | 29252000 | 15461000 | 849090 | 1656200 | 1318000 | 1923.4 | 17.7 | 11.7 | **650.9** |
| RalBP1-associated Eps domain-containing protein 1 | REPS1 | 1537400000 | 129480000 | 61728000 | 849090 | 1656200 | 1318000 | 1810.6 | 78.2 | 46.8 | **645.2** |
| Epidermal growth factor receptor substrate 15 | EPS15 | 1504700000 | 92475000 | 70919000 | 849090 | 1656200 | 1318000 | 1772.1 | 55.8 | 53.8 | **627.3** |
| Eukaryotic translation initiation factor 4 gamma 3 | EIF4G3 | 1423700000 | 155810000 | 60176000 | 849090 | 1656200 | 1318000 | 1676.7 | 94.1 | 45.7 | **605.5** |
| Phosphatase and actin regulator 4 | PHACTR4 | 1403600000 | 88402000 | 75011000 | 849090 | 1656200 | 1318000 | 1653.1 | 53.4 | 56.9 | **587.8** |
| Zinc finger protein 1 homolog | ZFP1 | 95968000 | 2567800000 | 1858200 | 849090 | 1656200 | 1318000 | 113.0 | 1550.4 | 1.4 | **555.0** |
| Tight junction protein ZO-1 | TJP1 | 1361000000 | 30492000 | 3835100 | 849090 | 1656200 | 1318000 | 1602.9 | 18.4 | 2.9 | **541.4** |
| GTPase-activating protein and VPS9 domain-containing protein 1 | GAPVD1 | 1297100000 | 102090000 | 44285000 | 849090 | 1656200 | 1318000 | 1527.6 | 61.6 | 33.6 | **541.0** |
| LIM and calponin homology domains-containing protein 1 | LIMCH1 | 1275800000 | 92159000 | 83704000 | 849090 | 1656200 | 1318000 | 1502.5 | 55.6 | 63.5 | **540.6** |
| Cold shock domain-containing protein E1 | CSDE1 | 8278500000 | 1346800000 | 872980000 | 90811000 | 1656200 | 1318000 | 91.2 | 813.2 | 662.4 | **522.2** |
| Protein FAM208A | FAM208A | 1245900000 | 86773000 | 58316000 | 849090 | 18821000 | 8954800 | 1467.3 | 4.6 | 6.5 | **492.8** |
| Zyxin | ZYX | 1006100000 | 247130000 | 188000000 | 849090 | 1656200 | 1318000 | 1184.9 | 149.2 | 142.6 | **492.3** |
| Drebrin | DBN1 | 17878000000 | 1455000000 | 1099100000 | 43988000 | 7125700 | 1318000 | 406.4 | 204.2 | 833.9 | **481.5** |
| E3 ubiquitin-protein ligase CBL | CBL | 1200200000 | 24400000 | 21433000 | 849090 | 1656200 | 1318000 | 1413.5 | 14.7 | 16.3 | **481.5** |
| Double-stranded RNA-specific adenosine deaminase | ADAR | 1219700000 | 36809000 | 52932000 | 849090 | 10280000 | 33782000 | 1436.5 | 3.6 | 1.6 | **480.5** |
| Threonine--tRNA ligase, cytoplasmic | TARS | 1187200000 | 72096000 | 65254000 | 849090 | 6046800 | 18974000 | 1398.2 | 11.9 | 3.4 | **471.2** |
| Glycogen phosphorylase, liver form;Phosphorylase | PYGL | 1160300000 | 169400000 | 103280000 | 849090 | 27796000 | 61182000 | 1366.5 | 6.1 | 1.7 | **458.1** |
| Microtubule-associated protein 1B;MAP1B heavy chain;MAP1 light chain LC1 | MAP1B | 7011300000 | 617510000 | 583360000 | 12591000 | 1656200 | 1318000 | 556.9 | 372.8 | 442.6 | **457.4** |
| Calpastatin | CAST | 1139700000 | 136980000 | 79376000 | 849090 | 7554500 | 7155300 | 1342.3 | 18.1 | 11.1 | **457.2** |
| Ubiquitin carboxyl-terminal hydrolase 15;Ubiquitin | USP15 | 1093700000 | 48094000 | 30163000 | 849090 | 1656200 | 1318000 | 1288.1 | 29.0 | 22.9 | **446.7** |

**carboxyl-terminal hydrolase**

| Protein | Gene | | | | | | | | | | |
|---|---|---|---|---|---|---|---|---|---|---|---|
| CD2-associated protein | CD2AP | 8594800000 | 944890000 | 1500700000 | 107830000 | 8239300 | 1318000 | 79.7 | 114.7 | 1138.6 | **444.3** |
| Cytoplasmic dynein 1 light intermediate chain 2 | DYNC1LI2 | 1084600000 | 28880000 | 37480000 | 849090 | 1656200 | 1318000 | 1277.4 | 17.4 | 28.4 | **441.1** |
| A-kinase anchor protein 1, mitochondrial | AKAP1 | 1064700000 | 57823000 | 40232000 | 849090 | 1656200 | 1318000 | 1253.9 | 34.9 | 30.5 | **439.8** |
| G protein-regulated inducer of neurite outgrowth 1 | GPRIN1 | 1060600000 | 47433000 | 19152000 | 849090 | 1656200 | 1318000 | 1249.1 | 28.6 | 14.5 | **430.8** |
| Zinc finger CCCH domain-containing protein 15 | ZC3H15 | 1075400000 | 15334000 | 11771000 | 849090 | 1656200 | 1318000 | 1266.5 | 9.3 | 8.9 | **428.2** |
| Exocyst complex component 3 | EXOC3 | 1041000000 | 26469000 | 43398000 | 849090 | 1656200 | 1318000 | 1226.0 | 16.0 | 32.9 | **425.0** |
| Eukaryotic translation initiation factor 5B | EIF5B | 1011200000 | 63131000 | 43038000 | 849090 | 1656200 | 1318000 | 1190.9 | 38.1 | 32.7 | **420.6** |
| DNA excision repair protein ERCC-6-like | ERCC6L | 993640000 | 94421000 | 32279000 | 849090 | 1656200 | 1318000 | 1170.2 | 57.0 | 24.5 | **417.2** |
| SH3 and PX domain-containing protein 2B | SH3PXD2B | 1035800000 | 10409000 | 32122000 | 849090 | 1656200 | 1318000 | 1219.9 | 6.3 | 24.4 | **416.9** |
| Striatin | STRN | 1039700000 | 25613000 | 11479000 | 849090 | 1656200 | 1318000 | 1224.5 | 15.5 | 8.7 | **416.2** |
| Cullin-4B | CUL4B | 1054100000 | 7359300 | 1858200 | 849090 | 1656200 | 1318000 | 1241.4 | 4.4 | 1.4 | **415.8** |
| Elongation factor Tu GTP-binding domain-containing protein 1 | EFL1 | 1030400000 | 32579000 | 17521000 | 849090 | 1656200 | 1318000 | 1213.5 | 19.7 | 13.3 | **415.5** |
| Myosin phosphatase Rho-interacting protein | MPRIP | 990790000 | 23770000 | 1858200 | 849090 | 1656200 | 1318000 | 1166.9 | 14.4 | 1.4 | **394.2** |
| Caldesmon | CALD1 | 8226900000 | 983800000 | 603180000 | 64487000 | 1656200 | 1318000 | 127.6 | 594.0 | 457.6 | **393.1** |
| Centrosomal protein of 170 kDa | CEP170 | 3813600000 | 367050000 | 464800000 | 6346300 | 1656200 | 1318000 | 600.9 | 221.6 | 352.7 | **391.7** |
| Neurabin-2 | PPP1R9B | 950640000 | 63141000 | 22882000 | 849090 | 1656200 | 1318000 | 1119.6 | 38.1 | 17.4 | **391.7** |
| Ankyrin-3 | ANK3 | 929250000 | 38146000 | 44672000 | 849090 | 1656200 | 1318000 | 1094.4 | 23.0 | 33.9 | **383.8** |
| cAMP-dependent protein kinase type II-alpha regulatory subunit | PRKAR2A | 947070000 | 30167000 | 1858200 | 849090 | 1656200 | 1318000 | 1115.4 | 18.2 | 1.4 | **378.3** |
| RING finger protein 214 | RNF214 | 952930000 | 9682400 | 8481100 | 849090 | 1656200 | 1318000 | 1122.3 | 5.8 | 6.4 | **378.2** |
| Exosome component 10 | EXOSC10 | 944910000 | 14828000 | 1858200 | 849090 | 1656200 | 24799000 | 1112.9 | 9.0 | 0.1 | **374.0** |
| General vesicular transport factor p115 | USO1 | 926400000 | 19323000 | 22428000 | 849090 | 1656200 | 1318000 | 1091.1 | 11.7 | 17.0 | **373.2** |
| Mitotic checkpoint serine/threonine-protein kinase BUB1 beta | BUB1B | 918920000 | 11493000 | 1858200 | 849090 | 1656200 | 1318000 | 1082.2 | 6.9 | 1.4 | **363.5** |
| Gamma-adducin | ADD3 | 825080000 | 50494000 | 57569000 | 849090 | 1656200 | 1318000 | 971.7 | 30.5 | 43.7 | **348.6** |
| Protein AHNAK2 | AHNAK2 | 873360000 | 4336200 | 2857700 | 849090 | 1656200 | 1318000 | 1028.6 | 2.6 | 2.2 | **344.5** |

| | | | | | | | | | | |
|---|---|---|---|---|---|---|---|---|---|---|
| Mitochondrial antiviral-signalling protein | MAVS | 830810000 | 14886000 | 42974000 | 849090 | 1656200 | 1318000 | 978.5 | 9.0 | 32.6 | **340.0** |
| Ankycorbin | RAI14 | 829670000 | 20625000 | 16988000 | 849090 | 1656200 | 1318000 | 977.1 | 12.5 | 12.9 | **334.2** |
| 26S proteasome non-ATPase regulatory subunit 1 | PSMD1 | 824680000 | 48458000 | 47978000 | 849090 | 26832000 | 16559000 | 971.3 | 1.8 | 2.9 | **325.3** |
| Protein transport protein Sec24B | SEC24B | 750830000 | 65537000 | 67216000 | 849090 | 1656200 | 1318000 | 884.3 | 39.6 | 51.0 | **324.9** |
| Desmoglein-2 | DSG2 | 753000000 | 68337000 | 60386000 | 849090 | 1656200 | 1318000 | 886.8 | 41.3 | 45.8 | **324.6** |
| Dynactin subunit 1 | DCTN1 | 780260000 | 97675 | 65739000 | 849090 | 1656200 | 1318000 | 918.9 | 0.1 | 49.9 | **323.0** |
| Ras-associated and pleckstrin homology domains-containing protein 1 | RAPH1 | 736030000 | 91296000 | 56299000 | 849090 | 1656200 | 1318000 | 866.8 | 55.1 | 42.7 | **321.6** |
| WASH complex subunit WASHC2C | WASHC2C | 787550000 | 17047000 | 13364000 | 849090 | 1656200 | 1318000 | 927.5 | 10.3 | 10.1 | **316.0** |
| Testin | TES | 785720000 | 15736000 | 15746000 | 849090 | 1656200 | 1318000 | 925.4 | 9.5 | 11.9 | **315.6** |
| Protein numb homolog | NUMB | 787920000 | 10453000 | 16356000 | 849090 | 1656200 | 1318000 | 928.0 | 6.3 | 12.4 | **315.6** |
| Regulator of nonsense transcripts 1 | UPF1 | 710550000 | 49332000 | 74290000 | 849090 | 1656200 | 1318000 | 836.8 | 29.8 | 56.4 | **307.7** |
| Pleckstrin homology domain-containing family A member 5 | PLEKHA5 | 755810000 | 10867000 | 22078000 | 849090 | 1656200 | 1318000 | 890.1 | 6.6 | 16.8 | **304.5** |
| WD repeat-containing protein 44 | WDR44 | 743430000 | 37187000 | 10070000 | 849090 | 1656200 | 1318000 | 875.6 | 22.5 | 7.6 | **301.9** |
| Ubiquitin-like modifier-activating enzyme 5 | UBA5 | 752070000 | 6521300 | 6574100 | 849090 | 1656200 | 1318000 | 885.7 | 3.9 | 5.0 | **298.2** |
| ELKS/Rab6-interacting/CAST family member 1 | ERC1 | 735350000 | 30821000 | 10893000 | 849090 | 1656200 | 1318000 | 866.0 | 18.6 | 8.3 | **297.6** |
| Tyrosine-protein phosphatase non-receptor type 23 | PTPN23 | 724570000 | 27092000 | 18386000 | 849090 | 1656200 | 1318000 | 853.3 | 16.4 | 13.9 | **294.6** |
| Receptor-interacting serine/threonine-protein kinase 1 | RIPK1 | 725290000 | 12654000 | 6508700 | 849090 | 1656200 | 1318000 | 854.2 | 7.6 | 4.9 | **288.9** |
| Sorting nexin-6;Sorting nexin-6, N-terminally processed | SNX6 | 698520000 | 35685000 | 22595000 | 849090 | 1656200 | 1318000 | 822.7 | 21.5 | 17.1 | **287.1** |
| Protein NPAT | NPAT | 690500000 | 16046000 | 1858200 | 849090 | 1656200 | 1318000 | 813.2 | 9.7 | 1.4 | **274.8** |
| Trinucleotide repeat-containing gene 6B protein | TNRC6B | 654780000 | 61300000 | 15986000 | 849090 | 1656200 | 1318000 | 771.2 | 37.0 | 12.1 | **273.4** |
| HCLS1-binding protein 3 | HS1BP3 | 684930000 | 4220900 | 1858200 | 849090 | 1656200 | 1318000 | 806.7 | 2.5 | 1.4 | **270.2** |
| Sorting nexin-9 | SNX9 | 625860000 | 97566000 | 9638000 | 849090 | 1656200 | 1318000 | 737.1 | 58.9 | 7.3 | **267.8** |
| CTP synthase 1 | CTPS1 | 16246000000 | 1035000000 | 724150000 | 129860000 | 1656200 | 19315000 | 125.1 | 624.9 | 37.5 | **262.5** |
| Dihydropyrimidinase-related protein 3 | DPYSL3 | 652230000 | 13739000 | 13277000 | 849090 | 1656200 | 1318000 | 768.2 | 8.3 | 10.1 | **262.2** |

| Protein | Gene | | | | | | | | | |
|---|---|---|---|---|---|---|---|---|---|---|
| LIM domain-containing protein 1 | LIMD1 | 642390000 | 23691000 | 18128000 | 849090 | 1656200 | 1318000 | 756.6 | 14.3 | 13.8 | **261.5** |
| Segment polarity protein dishevelled homolog DVL-2 | DVL2 | 600540000 | 28373000 | 73928000 | 849090 | 1656200 | 1318000 | 707.3 | 17.1 | 56.1 | **260.2** |
| HBS1-like protein | HBS1L | 543530000 | 77295000 | 116280000 | 849090 | 1656200 | 1318000 | 640.1 | 46.7 | 88.2 | **258.3** |
| Nesprin-1 | SYNE1 | 322060000 | 266080000 | 280040000 | 849090 | 1656200 | 1318000 | 379.3 | 160.7 | 212.5 | **250.8** |
| Zinc finger FYVE domain-containing protein 16 | ZFYVE16 | 603520000 | 36357000 | 25104000 | 849090 | 1656200 | 1318000 | 710.8 | 22.0 | 19.0 | **250.6** |
| Death-inducer obliterator 1 | DIDO1 | 633200000 | 64369000 | 19633000 | 849090 | 21122000 | 10141000 | 745.7 | 3.0 | 1.9 | **250.2** |
| Glycylpeptide N-tetradecanoyltransferase 1 | NMT1 | 594880000 | 45646000 | 21714000 | 849090 | 1656200 | 1318000 | 700.6 | 27.6 | 16.5 | **248.2** |
| Zinc finger CCCH-type antiviral protein 1 | ZC3HAV1 | 1136800000 | 387180000 | 191260000 | 3293200 | 1656200 | 1318000 | 345.2 | 233.8 | 145.1 | **241.4** |
| Protein unc-45 homolog A | UNC45A | 532250000 | 73153000 | 36881000 | 849090 | 1656200 | 1318000 | 626.8 | 44.2 | 28.0 | **233.0** |
| Nucleosome-remodeling factor subunit BPTF | BPTF | 583790000 | 45527000 | 1858200 | 849090 | 11740000 | 10560000 | 687.5 | 3.9 | 0.2 | **230.5** |
| Serine/threonine-protein kinase 4;Serine/threonine-protein kinase 4 37kDa subunit;Serine/threonine-protein kinase 4 18kDa subunit | STK4 | 574430000 | 17364000 | 1858200 | 849090 | 1656200 | 1318000 | 676.5 | 10.5 | 1.4 | **229.5** |
| Paxillin | PXN | 558120000 | 3196000 | 36674000 | 849090 | 1656200 | 1318000 | 657.3 | 1.9 | 27.8 | **229.0** |
| La-related protein 4 | LARP4 | 570450000 | 5300100 | 7192700 | 849090 | 1656200 | 1318000 | 671.8 | 3.2 | 5.5 | **226.8** |
| Protein phosphatase 1 regulatory subunit 12A | PPP1R12A | 561760000 | 2051000 | 17439000 | 849090 | 1656200 | 1318000 | 661.6 | 1.2 | 13.2 | **225.4** |
| Structural maintenance of chromosomes protein 4;Structural maintenance of chromosomes protein | SMC4 | 557850000 | 11547000 | 15862000 | 849090 | 1656200 | 1318000 | 657.0 | 7.0 | 12.0 | **225.3** |
| Phosphatidylinositol 3,4,5-trisphosphate 5-phosphatase 2 | INPPL1 | 564090000 | 7397400 | 1858200 | 849090 | 1656200 | 1318000 | 664.3 | 4.5 | 1.4 | **223.4** |
| Protein ELYS | AHCTF1 | 1067100000 | 38450000 | 12737000 | 1635200 | 8791500 | 1318000 | 652.6 | 4.4 | 9.7 | **222.2** |
| Vesicle-fusing ATPase | NSF | 540510000 | 10186000 | 30616000 | 849090 | 4119000 | 1318000 | 636.6 | 2.5 | 23.2 | **220.8** |
| Alanine--tRNA ligase, cytoplasmic | AARS | 514370000 | 52521000 | 11048000 | 849090 | 1656200 | 1318000 | 605.8 | 31.7 | 8.4 | **215.3** |
| PERQ amino acid-rich with GYF domain-containing protein 2 | GIGYF2 | 526640000 | 5055200 | 22454000 | 849090 | 1656200 | 1318000 | 620.2 | 3.1 | 17.0 | **213.4** |
| Nuclear fragile X mental retardation-interacting | NUFIP2 | 1717100000 | 408400000 | 258910000 | 8709500 | 1656200 | 1318000 | 197.2 | 246.6 | 196.4 | **213.4** |

**protein 2**

| Protein | Gene | | | | | | | | | | |
|---|---|---|---|---|---|---|---|---|---|---|---|
| Paladin | PALD1 | 522360000 | 15652000 | 16667000 | 849090 | 1656200 | 1318000 | 615.2 | 9.5 | 12.6 | **212.4** |
| Rap guanine nucleotide exchange factor 6 | RAPGEF6 | 525780000 | 4773800 | 10016000 | 849090 | 1656200 | 1318000 | 619.2 | 2.9 | 7.6 | **209.9** |
| 182 kDa tankyrase-1-binding protein | TNKS1BP1 | 513760000 | 15902000 | 8749800 | 849090 | 1656200 | 1318000 | 605.1 | 9.6 | 6.6 | **207.1** |
| C-1-tetrahydrofolate synthase | MTHFD1 | 518050000 | 79397000 | 62110000 | 849090 | 11828000 | 30547000 | 610.1 | 6.7 | 2.0 | **206.3** |
| Ubiquitin carboxyl-terminal hydrolase 28;Ubiquitin carboxyl-terminal hydrolase | USP28 | 515690000 | 67182000 | 63992000 | 849090 | 24960000 | 9814500 | 607.3 | 2.7 | 6.5 | **205.5** |
| Condensin complex subunit 3 | NCAPG | 507900000 | 11286000 | 9409200 | 849090 | 1656200 | 1318000 | 598.2 | 6.8 | 7.1 | **204.0** |
| FH1/FH2 domain-containing protein 1 | FHOD1 | 501890000 | 7720000 | 15127000 | 849090 | 1656200 | 1318000 | 591.1 | 4.7 | 11.5 | **202.4** |
| GRB2-associated-binding protein 1 | GAB1 | 445560000 | 61494000 | 56621000 | 849090 | 1656200 | 1318000 | 524.8 | 37.1 | 43.0 | **201.6** |
| Ubiquitin-associated protein 2 | UBAP2 | 1485000000 | 177560000 | 216530000 | 4460500 | 1656200 | 1318000 | 332.9 | 107.2 | 164.3 | **201.5** |
| Neurofilament medium polypeptide | NEFM | 15150000000 | 388970000 | 263240000 | 41822000 | 1656200 | 46243000 | 362.2 | 234.9 | 5.7 | **200.9** |
| Symplekin | SYMPK | 500600000 | 6936500 | 4919300 | 849090 | 3280900 | 4186300 | 589.6 | 2.1 | 1.2 | **197.6** |
| Apoptotic chromatin condensation inducer in the nucleus | ACIN1 | 1832300000 | 177430000 | 52340000 | 3471000 | 7275400 | 1318000 | 527.9 | 24.4 | 39.7 | **197.3** |
| 40S ribosomal protein S3a | RPS3A | 1203400000 | 392270000 | 428650000 | 41233000 | 1656200 | 1318000 | 29.2 | 236.8 | 325.2 | **197.1** |
| Dihydropyrimidinase-related protein 4 | DPYSL4 | 486220000 | 21668000 | 1858200 | 849090 | 1656200 | 1318000 | 572.6 | 13.1 | 1.4 | **195.7** |
| Septin-9 | SEPT9 | 8154100000 | 744180000 | 516610000 | 60703000 | 12456000 | 1318000 | 134.3 | 59.7 | 392.0 | **195.3** |
| Neuroblast differentiation-associated protein AHNAK | AHNAK | 60113000000 | 8788100000 | 6493600000 | 364080000 | 44535000 | 30197000 | 165.1 | 197.3 | 215.0 | **192.5** |
| Vigilin | HDLBP | 11833000000 | 667440000 | 461040000 | 106410000 | 5735300 | 1318000 | 111.2 | 116.4 | 349.8 | **192.5** |
| Alpha-adducin | ADD1 | 480810000 | 97675 | 11320000 | 849090 | 1656200 | 1318000 | 566.3 | 0.1 | 8.6 | **191.6** |
| PDZ and LIM domain protein 5 | PDLIM5 | 1990200000 | 613310000 | 625450000 | 55318000 | 9674400 | 1318000 | 36.0 | 63.4 | 474.5 | **191.3** |
| Rho GTPase-activating protein 1 | ARHGAP1 | 472990000 | 97675 | 17915000 | 849090 | 1656200 | 1318000 | 557.1 | 0.1 | 13.6 | **190.2** |
| ADP-ribosylation factor-binding protein GGA3 | GGA3 | 416290000 | 57291000 | 50384000 | 849090 | 1656200 | 1318000 | 490.3 | 34.6 | 38.2 | **187.7** |
| Striatin-3 | STRN3 | 453870000 | 16657000 | 17837000 | 849090 | 1656200 | 1318000 | 534.5 | 10.1 | 13.5 | **186.0** |
| Nestin | NES | 3097700000 | 50433000 | 27505000 | 6175500 | 1656200 | 1318000 | 501.6 | 30.5 | 20.9 | **184.3** |
| Coatomer subunit beta | COPB1 | 438910000 | 43294000 | 62120000 | 849090 | 1656200 | 8366100 | 516.9 | 26.1 | 7.4 | **183.5** |

| Protein | Gene | | | | | | | | | |
|---|---|---|---|---|---|---|---|---|---|---|
| Transcriptional repressor CTCF | CTCF | 462050000 | 17991000 | 6382400 | 849090 | 8300200 | 6428700 | 544.2 | 2.2 | 1.0 | **182.4** |
| Hepatocyte growth factor-regulated tyrosine kinase substrate | HGS | 444750000 | 14004000 | 14082000 | 849090 | 1656200 | 1318000 | 523.8 | 8.5 | 10.7 | **181.0** |
| Heat shock 70 kDa protein 4L | HSPA4L | 456820000 | 17179000 | 13755000 | 849090 | 7057400 | 7707800 | 538.0 | 2.4 | 1.8 | **180.7** |
| La-related protein 4B | LARP4B | 450160000 | 10788000 | 1858200 | 849090 | 1656200 | 1318000 | 530.2 | 6.5 | 1.4 | **179.4** |
| Cysteine and histidine-rich domain-containing protein 1 | CHORDC1 | 419460000 | 26272000 | 24740000 | 849090 | 1656200 | 1318000 | 494.0 | 15.9 | 18.8 | **176.2** |
| Calmodulin-regulated spectrin-associated protein 1 | CAMSAP1 | 439080000 | 13577000 | 1858200 | 849090 | 1656200 | 1318000 | 517.1 | 8.2 | 1.4 | **175.6** |
| Staphylococcal nuclease domain-containing protein 1 | SND1 | 427970000 | 19100000 | 6292600 | 849090 | 1656200 | 3514600 | 504.0 | 11.5 | 1.8 | **172.5** |
| Protein CDV3 homolog | CDV3 | 1564300000 | 362870000 | 330140000 | 33743000 | 1656200 | 1318000 | 46.4 | 219.1 | 250.5 | **172.0** |
| Heterogeneous nuclear ribonucleoprotein U-like protein 1 | HNRNPUL1 | 417400000 | 19243000 | 12571000 | 849090 | 1656200 | 1318000 | 491.6 | 11.6 | 9.5 | **170.9** |
| Poly(ADP-ribose) glycohydrolase | PARG | 423640000 | 17720000 | 1858200 | 849090 | 4987000 | 1318000 | 498.9 | 3.6 | 1.4 | **168.0** |
| Zinc finger CCHC domain-containing protein 8 | ZCCHC8 | 417880000 | 10416000 | 1858200 | 849090 | 1656200 | 1318000 | 492.2 | 6.3 | 1.4 | **166.6** |
| 5-3 exoribonuclease 1 | XRN1 | 392150000 | 36250000 | 20277000 | 849090 | 1656200 | 1318000 | 461.8 | 21.9 | 15.4 | **166.4** |
| Charged multivesicular body protein 2b | CHMP2B | 72550000 | 620250000 | 502880000 | 849090 | 19679000 | 1318000 | 85.4 | 31.5 | 381.5 | **166.2** |
| THO complex subunit 2 | THOC2 | 379820000 | 31844000 | 31657000 | 849090 | 1656200 | 1318000 | 447.3 | 19.2 | 24.0 | **163.5** |
| 26S proteasome non-ATPase regulatory subunit 2 | PSMD2 | 406790000 | 25987000 | 14384000 | 849090 | 4639900 | 17716000 | 479.1 | 5.6 | 0.8 | **161.8** |
| Rho GTPase-activating protein 17 | ARHGAP17 | 399920000 | 12922000 | 1858200 | 849090 | 1656200 | 1318000 | 471.0 | 7.8 | 1.4 | **160.1** |
| NEDD4-binding protein 2 | N4BP2 | 392870000 | 13312000 | 10453000 | 849090 | 1656200 | 1318000 | 462.7 | 8.0 | 7.9 | **159.6** |
| Calmin | CLMN | 391950000 | 11800000 | 8928300 | 849090 | 1656200 | 1318000 | 461.6 | 7.1 | 6.8 | **158.5** |
| Ubiquitin carboxyl-terminal hydrolase 10 | USP10 | 1092500000 | 241610000 | 186580000 | 5863900 | 1656200 | 1318000 | 186.3 | 145.9 | 141.6 | **157.9** |
| Synergin gamma | SYNRG | 384570000 | 13977000 | 15275000 | 849090 | 1656200 | 1318000 | 452.9 | 8.4 | 11.6 | **157.6** |
| Clathrin interactor 1 | CLINT1 | 5695800000 | 663680000 | 583720000 | 823730000 | 1656200 | 9066000 | 6.9 | 400.7 | 64.4 | **157.3** |
| Filamin-B | FLNB | 392720000 | 35537000 | 11678000 | 849090 | 11594000 | 2728400 | 462.5 | 3.1 | 4.3 | **156.6** |
| Numb-like protein | NUMBL | 350800000 | 47322000 | 34646000 | 849090 | 1656200 | 1318000 | 413.1 | 28.6 | 26.3 | **156.0** |
| Endophilin-A2 | SH3GL1 | 348120000 | 62809000 | 24148000 | 849090 | 1656200 | 1318000 | 410.0 | 37.9 | 18.3 | **155.4** |

| Protein | Gene | | | | | | | | | | |
|---|---|---|---|---|---|---|---|---|---|---|---|
| Protein diaphanous homolog 2 | DIAPH2 | 379320000 | 17545000 | 1858200 | 849090 | 1656200 | 1318000 | 446.7 | 10.6 | 1.4 | **152.9** |
| Niban-like protein 1 | FAM129B | 380040000 | 14190000 | 1858200 | 849090 | 1656200 | 1318000 | 447.6 | 8.6 | 1.4 | **152.5** |
| Protein CIP2A | CIP2A | 354020000 | 27929000 | 8282300 | 849090 | 1656200 | 1318000 | 416.9 | 16.9 | 6.3 | **146.7** |
| Lethal(2) giant larvae protein homolog 1 | LLGL1 | 358140000 | 4843800 | 15776000 | 849090 | 1656200 | 1318000 | 421.8 | 2.9 | 12.0 | **145.6** |
| Centromere/kinetochore protein zw10 homolog | ZW10 | 359200000 | 10030000 | 8716100 | 849090 | 1656200 | 1318000 | 423.0 | 6.1 | 6.6 | **145.2** |
| Inositol polyphosphate 5-phosphatase OCRL-1 | OCRL | 348830000 | 97675 | 17478000 | 849090 | 1656200 | 1318000 | 410.8 | 0.1 | 13.3 | **141.4** |
| Serine/threonine-protein kinase Nek9 | NEK9 | 339310000 | 7771900 | 25165000 | 849090 | 1656200 | 1318000 | 399.6 | 4.7 | 19.1 | **141.1** |
| Bifunctional glutamate/proline--tRNA ligase;Glutamate--tRNA ligase;Proline--tRNA ligase | EPRS | 337320000 | 31097000 | 1858200 | 849090 | 1656200 | 1318000 | 397.3 | 18.8 | 1.4 | **139.2** |
| Serine/threonine-protein phosphatase 6 regulatory subunit 1 | PPP6R1 | 315890000 | 55343000 | 1858200 | 849090 | 1656200 | 1318000 | 372.0 | 33.4 | 1.4 | **135.6** |
| ATPase WRNIP1 | WRNIP1 | 340810000 | 97675 | 6155200 | 849090 | 1656200 | 1318000 | 401.4 | 0.1 | 4.7 | **135.4** |
| Eukaryotic translation initiation factor 4 gamma 2 | EIF4G2 | 2759600000 | 295640000 | 150110000 | 24637000 | 1656200 | 1318000 | 112.0 | 178.5 | 113.9 | **134.8** |
| SURP and G-patch domain-containing protein 2 | SUGP2 | 335220000 | 8600700 | 1858200 | 849090 | 1656200 | 1318000 | 394.8 | 5.2 | 1.4 | **133.8** |
| Peroxisomal membrane protein PEX14 | PEX14 | 6906600000 | 81993000 | 126450000 | 27029000 | 1656200 | 1318000 | 255.5 | 49.5 | 95.9 | **133.7** |
| Eukaryotic translation initiation factor 2A | EIF2A | 3669500000 | 413560000 | 387080000 | 94050000 | 7121300 | 1318000 | 39.0 | 58.1 | 293.7 | **130.3** |
| Serine/threonine-protein kinase Nek1 | NEK1 | 321260000 | 7032300 | 5158500 | 849090 | 1656200 | 1318000 | 378.4 | 4.2 | 3.9 | **128.8** |
| Focal adhesion kinase 1 | PTK2 | 306010000 | 10325000 | 23689000 | 849090 | 1656200 | 1318000 | 360.4 | 6.2 | 18.0 | **128.2** |
| Palladin | PALLD | 308320000 | 14462000 | 16453000 | 849090 | 1656200 | 1318000 | 363.1 | 8.7 | 12.5 | **128.1** |
| HMG box transcription factor BBX | BBX | 317640000 | 97675 | 9108000 | 849090 | 11272000 | 1318000 | 374.1 | 0.0 | 6.9 | **127.0** |
| Serine/threonine-protein phosphatase PP1-gamma catalytic subunit;Serine/threonine-protein phosphatase | PPP1CC | 309560000 | 11027000 | 18244000 | 849090 | 7819600 | 1318000 | 364.6 | 1.4 | 13.8 | **126.6** |
| Protein transport protein Sec16A | SEC16A | 296590000 | 2017400 | 29221000 | 849090 | 1656200 | 1318000 | 349.3 | 1.2 | 22.2 | **124.2** |
| Shootin-1 | CCAR2 | 1800500000 | 130520000 | 83608000 | 7838500 | 1656200 | 1318000 | 229.7 | 78.8 | 63.4 | **124.0** |
| ATP-binding cassette sub-family F member 1 | ABCF1 | 1376900000 | 38397000 | 12462000 | 4011900 | 1656200 | 2636700 | 343.2 | 23.2 | 4.7 | **123.7** |
| Transforming acidic coiled-coil-containing protein 3 | TACC3 | 1904100000 | 144210000 | 74658000 | 8477100 | 1656200 | 1318000 | 224.6 | 87.1 | 56.6 | **122.8** |
| Golgin subfamily B member 1 | GOLGB1 | 301690000 | 4383600 | 4166200 | 849090 | 1656200 | 1318000 | 355.3 | 2.6 | 3.2 | **120.4** |

| | | | | | | | | | | | |
|---|---|---|---|---|---|---|---|---|---|---|---|
| 116 kDa U5 small nuclear ribonucleoprotein component | EFTUD2 | 293730000 | 12618000 | 32152000 | 849090 | 1656200 | 5963300 | 345.9 | 7.6 | 5.4 | **119.6** |
| Talin-1 | TLN1 | 316100000 | 11225000 | 4572700 | 918180 | 1656200 | 1318000 | 344.3 | 6.8 | 3.5 | **118.2** |
| SLAIN motif-containing protein 2 | SLAIN2 | 292080000 | 8747900 | 1858200 | 849090 | 1656200 | 1318000 | 344.0 | 5.3 | 1.4 | **116.9** |
| Centriolar coiled-coil protein of 110 kDa | CCP110 | 289010000 | 97675 | 11112000 | 849090 | 1656200 | 1318000 | 340.4 | 0.1 | 8.4 | **116.3** |
| Inositol hexakisphosphate kinase 1 | IP6K1 | 288270000 | 97675 | 7917000 | 849090 | 1656200 | 1318000 | 339.5 | 0.1 | 6.0 | **115.2** |
| Lipopolysaccharide-responsive and beige-like anchor protein | LRBA | 276110000 | 14329000 | 9230200 | 849090 | 1656200 | 1318000 | 325.2 | 8.7 | 7.0 | **113.6** |
| Septin-2 | SEPT2 | 961910000 | 59352000 | 107420000 | 4518600 | 1656200 | 1318000 | 212.9 | 35.8 | 81.5 | **110.1** |
| Epidermal growth factor receptor substrate 15-like 1 | EPS15L1 | 3518400000 | 316210000 | 286040000 | 65324000 | 6354600 | 1318000 | 53.9 | 49.8 | 217.0 | **106.9** |
| Round spermatid basic protein 1-like protein | RSBN1L | 261910000 | 6274300 | 6344300 | 849090 | 1656200 | 1318000 | 308.5 | 3.8 | 4.8 | **105.7** |
| ATP-dependent RNA helicase DHX29 | DHX29 | 259110000 | 14752000 | 1858200 | 849090 | 1656200 | 1318029 | 305.2 | 8.9 | 1.4 | **105.2** |
| Protein scribble homolog | SCRIB | 248250000 | 24668000 | 10100000 | 849090 | 1656200 | 1318000 | 292.4 | 14.9 | 7.7 | **105.0** |
| Ran GTPase-activating protein 1 | RANGAP1 | 12032000000 | 1116500000 | 1058600000 | 857520000 | 15940000 | 4656800 | 14.0 | 70.0 | 227.3 | **103.8** |
| Torsin-1A-interacting protein 1 | TOR1AIP1 | 253600000 | 8130500 | 8545700 | 849090 | 1656200 | 1318000 | 298.7 | 4.9 | 6.5 | **103.4** |
| Tubulin alpha-1A chain | TUBA1A | 257680000 | 32185000 | 1858200 | 849090 | 6468900 | 1318000 | 303.5 | 5.0 | 1.4 | **103.3** |
| Tumor suppressor p53-binding protein 1 | TP53BP1 | 2084800000 | 28343000 | 75923000 | 7311400 | 4359200 | 6460400 | 285.1 | 6.5 | 11.8 | **101.1** |
| Protein SMG9 | SMG9 | 253850000 | 97675 | 2953900 | 849090 | 1656200 | 1318000 | 299.0 | 0.1 | 2.2 | **100.4** |
| Probable ATP-dependent RNA helicase YTHDC2 | YTHDC2 | 249970000 | 97675 | 2609000 | 849090 | 1656200 | 1318000 | 294.4 | 0.1 | 2.0 | **98.8** |
| Zinc finger CCCH domain-containing protein 4 | ZC3H4 | 244050000 | 11334000 | 1858200 | 849090 | 1656200 | 1318000 | 287.4 | 6.8 | 1.4 | **98.6** |
| Rab GTPase-activating protein 1-like | RABGAP1L | 220880000 | 23761000 | 23799000 | 849090 | 1656200 | 1318000 | 260.1 | 14.3 | 18.1 | **97.5** |
| Insulin receptor substrate 4 | IRS4 | 239620000 | 97675 | 9859600 | 849090 | 8379600 | 1318000 | 282.2 | 0.0 | 7.5 | **96.6** |
| Unconventional myosin-Ie | MYO1E | 231880000 | 13242000 | 10524000 | 849090 | 1656200 | 1318000 | 273.1 | 8.0 | 8.0 | **96.4** |
| Zinc finger protein 638 | ZNF638 | 380360000 | 97675 | 10033000 | 1388900 | 1656200 | 1318000 | 273.9 | 0.1 | 7.6 | **93.8** |
| 60 kDa SS-A/Ro ribonucleoprotein | TROVE2 | 226550000 | 8064500 | 8325100 | 849090 | 1656200 | 5352300 | 266.8 | 4.9 | 1.6 | **91.1** |
| Huntingtin-interacting protein 1 | HIP1 | 224960000 | 97675 | 4220500 | 849090 | 1656200 | 1318000 | 264.9 | 0.1 | 3.2 | **89.4** |
| Endoribonuclease Dicer | DICER1 | 210110000 | 97675 | 18905000 | 849090 | 1656200 | 1318000 | 247.5 | 0.1 | 14.3 | **87.3** |

| Protein | Gene | | | | | | | | | | |
|---|---|---|---|---|---|---|---|---|---|---|---|
| Protein transport protein Sec24A | SEC24A | 209770000 | 97675 | 15662000 | 849090 | 1656200 | 1318000 | 247.1 | 0.1 | 11.9 | **86.3** |
| Kinesin light chain 1 | KLC1 | 3978000000 | 54935000 | 89433000 | 25323000 | 1656200 | 1318000 | 157.1 | 33.2 | 67.9 | **86.0** |
| Sorting nexin-1 | SNX1 | 1199600000 | 263030000 | 216380000 | 47342000 | 3890600 | 1318000 | 25.3 | 67.6 | 164.2 | **85.7** |
| Rab GTPase-binding effector protein 1 | RABEP1 | 213850000 | 3375300 | 2685900 | 849090 | 1656200 | 1318000 | 251.9 | 2.0 | 2.0 | **85.3** |
| Glomulin | GLMN | 209260000 | 9026600 | 1858200 | 849090 | 1656200 | 1318000 | 246.5 | 5.5 | 1.4 | **84.4** |
| 4F2 cell-surface antigen heavy chain | SLC3A2 | 210230000 | 71995000 | 86757000 | 849090 | 22570000 | 48847000 | 247.6 | 3.2 | 1.8 | **84.2** |
| Elongator complex protein 4 | ELP4 | 148680000 | 58916000 | 55024000 | 849090 | 1656200 | 1318000 | 175.1 | 35.6 | 41.7 | **84.1** |
| Replication factor C subunit 1 | RFC1 | 210140000 | 30900000 | 13855000 | 849090 | 9482400 | 17707000 | 247.5 | 3.3 | 0.8 | **83.8** |
| Synembryn-A | RIC8A | 207200000 | 97675 | 9113100 | 849090 | 1656200 | 1318000 | 244.0 | 0.1 | 6.9 | **83.7** |
| Transport and Golgi organization protein 6 homolog | TANGO6 | 207200000 | 97675 | 6274500 | 849090 | 1656200 | 1318000 | 244.0 | 0.1 | 4.8 | **82.9** |
| Myosin-9 | MYH9 | 9701200000 | 1267500000 | 955390000 | 42470000 | 107510000 | 183670000 | 228.4 | 11.8 | 5.2 | **81.8** |
| HAUS augmin-like complex subunit 6 | HAUS6 | 1845300000 | 201540000 | 130920000 | 76277000 | 1656200 | 1318000 | 24.2 | 121.7 | 99.3 | **81.7** |
| Microtubule-associated protein;Microtubule-associated protein 4 | MAP4 | 47850000000 | 5865200000 | 4782700000 | 299910000 | 130060000 | 129330000 | 159.5 | 45.1 | 37.0 | **80.5** |
| Caspase-3;Caspase-3 subunit p17;Caspase-3 subunit p12 | CASP3 | 167960000 | 97675 | 56992000 | 849090 | 1656200 | 1318000 | 197.8 | 0.1 | 43.2 | **80.4** |
| Cytoskeleton-associated protein 5 | CKAP5 | 4428800000 | 700190000 | 537220000 | 21787000 | 37128000 | 29903000 | 203.3 | 18.9 | 18.0 | **80.0** |
| Coatomer subunit beta | COPB2 | 159000000 | 18051000 | 50657000 | 849090 | 1656200 | 1318000 | 187.3 | 10.9 | 38.4 | **78.9** |
| Cytoskeleton-associated protein 4 | CKAP4 | 191120000 | 13803000 | 20858000 | 849090 | 1656200 | 7379800 | 225.1 | 8.3 | 2.8 | **78.7** |
| Protein Shroom2 | SHROOM2 | 195300000 | 6188800 | 1858200 | 849090 | 1656200 | 1318000 | 230.0 | 3.7 | 1.4 | **78.4** |
| Nuclear pore complex protein Nup93 | NUP93 | 151350000 | 15745000 | 60534000 | 849090 | 1656200 | 1318000 | 178.2 | 9.5 | 45.9 | **77.9** |
| Oxysterol-binding protein-related protein 11 | OSBPL11 | 170070000 | 15390000 | 30268000 | 849090 | 1656200 | 1318000 | 200.3 | 9.3 | 23.0 | **77.5** |
| Src substrate cortactin | CTTN | 57414000000 | 9708300000 | 7164400000 | 1730800000 | 102100000 | 69348000 | 33.2 | 95.1 | 103.3 | **77.2** |
| Calmodulin-regulated spectrin-associated protein 3 | CAMSAP3 | 185200000 | 20392000 | 1858200 | 849090 | 1656200 | 3519800 | 218.1 | 12.3 | 0.5 | **77.0** |
| Biotin--protein ligase;Biotin--[methylmalonyl-CoA-carboxytransferase] ligase;Biotin--[propionyl-CoA-carboxylase [ATP-hydrolyzing]] ligase;Biotin--[methylcrotonoyl-CoA-carboxylase] ligase;Biotin-- | HLCS | 189350000 | 343260000 | 277090000 | 849090 | 113120000 | 80190000 | 223.0 | 3.0 | 3.5 | **76.5** |

**[acetyl-CoA-carboxylase] ligase**

| Protein | Gene | | | | | | | | | | |
|---|---|---|---|---|---|---|---|---|---|---|---|
| Drebrin-like protein | DBNL | 3895900000 | 154560000 | 120190000 | 87578000 | 1656200 | 1318000 | 44.5 | 93.3 | 91.2 | **76.3** |
| Methionine--tRNA ligase, cytoplasmic | MARS | 190310000 | 26404000 | 22580000 | 849090 | 9322000 | 16379000 | 224.1 | 2.8 | 1.4 | **76.1** |
| Secretory carrier-associated membrane protein 1 | SCAMP1 | 182450000 | 7759700 | 14775000 | 849090 | 12840000 | 1318000 | 214.9 | 0.6 | 11.2 | **75.6** |
| Zinc finger protein 687 | ZNF687 | 176750000 | 21856000 | 10924000 | 849090 | 1656200 | 5328000 | 208.2 | 13.2 | 2.1 | **74.5** |
| RNA polymerase II-associated protein 3 | RPAP3 | 3009400000 | 108230000 | 85673000 | 32655000 | 1656200 | 1318000 | 92.2 | 65.3 | 65.0 | **74.2** |
| Eukaryotic translation initiation factor 4 gamma 1 | EIF4G1 | 5930500000 | 546240000 | 522470000 | 31174000 | 37287000 | 31174000 | 190.2 | 14.6 | 16.8 | **73.9** |
| TGF-beta-activated kinase 1 and MAP3K7-binding protein 2 | TAB2 | 172710000 | 15712000 | 10008000 | 849090 | 1656200 | 1318000 | 203.4 | 9.5 | 7.6 | **73.5** |
| Ankyrin repeat domain-containing protein 17 | ANKRD17 | 388000000 | 20248000 | 18662000 | 2007800 | 1656200 | 1318000 | 193.2 | 12.2 | 14.2 | **73.2** |
| Glutamine--tRNA ligase | QARS | 178140000 | 17230000 | 16725000 | 849090 | 3546600 | 5792900 | 209.8 | 4.9 | 2.9 | **72.5** |
| Protein SMG7 | SMG7 | 169850000 | 97675 | 15862000 | 849090 | 1656200 | 1318000 | 200.0 | 0.1 | 12.0 | **70.7** |
| NF-kappa-B inhibitor epsilon | NFKBIE | 157850000 | 22060000 | 16518000 | 849090 | 1656200 | 1318000 | 185.9 | 13.3 | 12.5 | **70.6** |
| Golgi reassembly-stacking protein 2 | GORASP2 | 1777100000 | 97675 | 24509000 | 9411300 | 1656200 | 1318000 | 188.8 | 0.1 | 18.6 | **69.2** |
| Putative RNA polymerase II subunit B1 CTD phosphatase RPAP2 | RPAP2 | 168960000 | 11575000 | 1858200 | 849090 | 1656200 | 1318000 | 199.0 | 7.0 | 1.4 | **69.1** |
| Perilipin-3 | PLIN3 | 4505000000 | 215540000 | 190460000 | 433030000 | 4270500 | 1318000 | 10.4 | 50.5 | 144.5 | **68.5** |
| Serine/threonine-protein phosphatase 6 regulatory subunit 3 | PPP6R3 | 3449700000 | 86433000 | 104610000 | 47322000 | 1656200 | 1318000 | 72.9 | 52.2 | 79.4 | **68.2** |
| Microtubule-associated protein tau | MAPT | 1533800000 | 84562000 | 22048000 | 11385000 | 1656200 | 1318000 | 134.7 | 51.1 | 16.7 | **67.5** |
| DNA polymerase alpha catalytic subunit;DNA polymerase | POLA1 | 166770000 | 97675 | 6206300 | 849090 | 1656200 | 1318000 | 196.4 | 0.1 | 4.7 | **67.1** |
| WW domain-containing oxidoreductase | WWOX | 1822200000 | 120950000 | 162310000 | 503870000 | 1656200 | 1318000 | 3.6 | 73.0 | 123.1 | **66.6** |
| Zinc finger protein 131 | ZNF131 | 162160000 | 11958000 | 1858200 | 849090 | 1656200 | 1318000 | 191.0 | 7.2 | 1.4 | **66.5** |
| TBC1 domain family member 15 | TBC1D15 | 84989000 | 74889000 | 71434000 | 849090 | 1656200 | 1318000 | 100.1 | 45.2 | 54.2 | **66.5** |
| Reticulon-4 | RTN4 | 7898100000 | 276460000 | 209580000 | 46752000 | 14465000 | 20055000 | 168.9 | 19.1 | 10.5 | **66.2** |
| Ataxin-2 | ATXN2 | 159970000 | 97675 | 13024000 | 849090 | 1656200 | 1318000 | 188.4 | 0.1 | 9.9 | **66.1** |
| Stromal membrane-associated protein 1 | SMAP1 | 3427300000 | 173520000 | 70826000 | 88160000 | 1656200 | 1318000 | 38.9 | 104.8 | 53.7 | **65.8** |

| Protein | Gene | | | | | | | | | |
|---|---|---|---|---|---|---|---|---|---|---|
| Protein SON | SON | 2472600000 | 68825000 | 65117000 | 17506000 | 1656200 | 5081300 | 141.2 | 41.6 | 12.8 | **65.2** |
| LIM and SH3 domain protein 1 | LASP1 | 959290000 | 113370000 | 154660000 | 118430000 | 1656200 | 1318000 | 8.1 | 68.5 | 117.3 | **64.6** |
| Interferon-induced protein with tetratricopeptide repeats 5 | IFIT5 | 159390000 | 5687400 | 1858200 | 849090 | 1656200 | 1318000 | 187.7 | 3.4 | 1.4 | **64.2** |
| Tropomodulin-3 | TMOD3 | 675810000 | 18946000 | 17106000 | 4021300 | 1656200 | 1318000 | 168.1 | 11.4 | 13.0 | **64.2** |
| Protein kinase C and casein kinase substrate in neurons protein 2 | PACSIN2 | 816140000 | 47896000 | 11312000 | 5290200 | 1656200 | 1318000 | 154.3 | 28.9 | 8.6 | **63.9** |
| Vacuolar protein sorting-associated protein VTA1 homolog | VTA1 | 145640000 | 97675 | 26227000 | 849090 | 10145000 | 1318000 | 171.5 | 0.0 | 19.9 | **63.8** |
| Zinc finger MYM-type protein 4 | ZMYM4 | 149640000 | 97675 | 18672000 | 849090 | 1656200 | 1318000 | 176.2 | 0.1 | 14.2 | **63.5** |
| Aftiphilin | AFTPH | 155860000 | 7529800 | 1858200 | 849090 | 1656200 | 1318000 | 183.6 | 4.5 | 1.4 | **63.2** |
| Ribosomal protein S6 kinase alpha-3 | RPS6KA3 | 155980000 | 97675 | 6654700 | 849090 | 1656200 | 1318000 | 183.7 | 0.1 | 5.0 | **62.9** |
| Serine/threonine-protein kinase PAK 2;PAK-2p27;PAK-2p34 | PAK2 | 2406200000 | 159830000 | 78853000 | 79925000 | 1656200 | 1318000 | 30.1 | 96.5 | 59.8 | **62.1** |
| GPN-loop GTPase 1 | GPN1 | 1213900000 | 122190000 | 137350000 | 251150000 | 1656200 | 1318000 | 4.8 | 73.8 | 104.2 | **60.9** |
| Autophagy-related protein 2 homolog B | ATG2B | 391930000 | 11767000 | 16610000 | 2420500 | 1656200 | 1318000 | 161.9 | 7.1 | 12.6 | **60.5** |
| Glucose-6-phosphate 1-dehydrogenase | G6PD | 787300000 | 5613700 | 10987000 | 4648800 | 1656200 | 1318000 | 169.4 | 3.4 | 8.3 | **60.4** |
| Utrophin | UTRN | 127880000 | 30801000 | 13144000 | 849090 | 1656200 | 1318000 | 150.6 | 18.6 | 10.0 | **59.7** |
| Septin-7 | SEPT7 | 2201500000 | 189430000 | 162200000 | 54161000 | 1656200 | 7353500 | 40.6 | 114.4 | 22.1 | **59.0** |
| Protein diaphanous homolog 1 | DIAPH1 | 140340000 | 9082200 | 1858200 | 849090 | 1656200 | 1318000 | 165.3 | 5.5 | 1.4 | **57.4** |
| YLP motif-containing protein 1 | YLPM1 | 1410500000 | 228520000 | 138680000 | 12565000 | 6117400 | 6829200 | 112.3 | 37.4 | 20.3 | **56.6** |
| Syntenin-1 | SDCBP | 824970000 | 111980000 | 83718000 | 9249500 | 1656200 | 7887900 | 89.2 | 67.6 | 10.6 | **55.8** |
| Sorting nexin-2 | SNX2 | 360040000 | 88029000 | 73921000 | 6195800 | 1656200 | 1318000 | 58.1 | 53.2 | 56.1 | **55.8** |
| Phosphatidylinositol 5-phosphate 4-kinase type-2 gamma | PIP4K2C | 137290000 | 97675 | 4588500 | 849090 | 1656200 | 1318000 | 161.7 | 0.1 | 3.5 | **55.1** |
| TIP41-like protein | TIPRL | 737070 | 219700000 | 134820000 | 9843400 | 1656200 | 4557500 | 0.1 | 132.7 | 29.6 | **54.1** |
| Interleukin-1 receptor-associated kinase 1 | IRAK1 | 119170000 | 31430000 | 1858200 | 849090 | 1656200 | 1318000 | 140.4 | 19.0 | 1.4 | **53.6** |
| Phenylalanine--tRNA ligase beta subunit | FARSB | 573700000 | 54861000 | 33963000 | 3704000 | 15661000 | 24449000 | 154.9 | 3.5 | 1.4 | **53.3** |

| Protein | Gene | | | | | | | | | | |
|---|---|---|---|---|---|---|---|---|---|---|---|
| Fragile X mental retardation syndrome-related protein 2 | FXR2 | 110000000 | 23382000 | 21000000 | 849090 | 1656200 | 1318000 | 129.6 | 14.1 | 15.9 | **53.2** |
| Ran-binding protein 9 | RANBP9 | 127540000 | 6848800 | 8763000 | 849090 | 3933600 | 1318000 | 150.2 | 1.7 | 6.6 | **52.9** |
| Nibrin | NBN | 1312900000 | 10431000 | 6827500 | 9066600 | 1656200 | 1318000 | 144.8 | 6.3 | 5.2 | **52.1** |
| Serine/threonine-protein phosphatase 2A 56 kDa regulatory subunit delta isoform | PPP2R5D | 118660000 | 12997000 | 10720000 | 849090 | 1656200 | 1318000 | 139.7 | 7.8 | 8.1 | **51.9** |
| 26S proteasome non-ATPase regulatory subunit 3 | PSMD3 | 2973000000 | 149900000 | 106170000 | 47240000 | 12449000 | 1318000 | 62.9 | 12.0 | 80.6 | **51.8** |
| DBIRD complex subunit CCAR2 | CCAR2 | 121740000 | 37870000 | 74342000 | 849090 | 16906000 | 9751700 | 143.4 | 2.2 | 7.6 | **51.1** |
| tRNA (cytosine(34)-C(5))-methyltransferase | NSUN2 | 124510000 | 3906400 | 3781600 | 849090 | 1656200 | 1318000 | 146.6 | 2.4 | 2.9 | **50.6** |
| Ezrin | EZR | 2721200000 | 209720000 | 184160000 | 22307000 | 9171400 | 26876000 | 122.0 | 22.9 | 6.9 | **50.6** |
| Antigen KI-67 | MKI67 | 2054000000 | 54166000 | 56927000 | 14007000 | 15261000 | 38049000 | 146.6 | 3.5 | 1.5 | **50.6** |
| EF-hand domain-containing protein D2 | EFHD2 | 228880000 | 189360000 | 161620000 | 39072000 | 8836900 | 1318000 | 5.9 | 21.4 | 122.6 | **50.0** |
| Gem-associated protein 5 | GEMIN5 | 90337000 | 8817100 | 49751000 | 849090 | 1656200 | 1318000 | 106.4 | 5.3 | 37.7 | **49.8** |
| Protein phosphatase methylesterase 1 | PPME1 | 1375800000 | 128320000 | 86121000 | 223240000 | 1656200 | 1318000 | 6.2 | 77.5 | 65.3 | **49.7** |
| Translational activator GCN1 | GCN1 | 653800000 | 350950000 | 318450000 | 5317900 | 32155000 | 22658000 | 122.9 | 10.9 | 14.1 | **49.3** |
| E3 SUMO-protein ligase RanBP2;Putative peptidyl-prolyl cis-trans isomerase | RANBP2 | 15311000000 | 1659200000 | 1575100000 | 299510000 | 76456000 | 22995000 | 51.1 | 21.7 | 68.5 | **47.1** |
| Biorientation of chromosomes in cell division protein 1-like 1 | BOD1L1 | 1099300000 | 28430000 | 25249000 | 10616000 | 1656200 | 1318000 | 103.6 | 17.2 | 19.2 | **46.6** |
| mRNA-decapping enzyme 1A | DCP1A | 549970000 | 131520000 | 73651000 | 191200000 | 1656200 | 1318000 | 2.9 | 79.4 | 55.9 | **46.1** |
| DNA replication licensing factor MCM6 | MCM6 | 110730000 | 9777000 | 3477200 | 849090 | 1656200 | 19284000 | 130.4 | 5.9 | 0.2 | **45.5** |
| YTH domain family protein 2 | YTHDF2 | 1472600000 | 47546000 | 134470000 | 264090000 | 1656200 | 1318000 | 5.6 | 28.7 | 102.0 | **45.4** |
| Fermitin family homolog 2 | FERMT2 | 737070 | 52429000 | 131130000 | 849090 | 1656200 | 1318000 | 0.9 | 31.7 | 99.5 | **44.0** |
| Aminoacyl tRNA synthase complex-interacting multifunctional protein 2 | AIMP2 | 259530000 | 14340000 | 30319000 | 2180400 | 1656200 | 7373800 | 119.0 | 8.7 | 4.1 | **43.9** |
| Rab11 family-interacting protein 1 | RAB11FIP1 | 108600000 | 97675 | 4397700 | 849090 | 1656200 | 1318000 | 127.9 | 0.1 | 3.3 | **43.8** |
| Bifunctional protein NCOAT;Protein O-GlcNAcase;Histone acetyltransferase | MGEA5 | 102110000 | 8564400 | 7883500 | 849090 | 1656200 | 1852900 | 120.3 | 5.2 | 4.3 | **43.2** |

| Protein | Gene | | | | | | | | | | |
|---|---|---|---|---|---|---|---|---|---|---|---|
| Signal recognition particle 54 kDa protein | SRP54 | 2065900000 | 14939000 | 56392000 | 27215000 | 1656200 | 1318000 | 75.9 | 9.0 | 42.8 | **42.6** |
| Synapse-associated protein 1 | SYAP1 | 989570000 | 6233100 | 33954000 | 10137000 | 1656200 | 1318000 | 97.6 | 3.8 | 25.8 | **42.4** |
| Ran-specific GTPase-activating protein | RANBP1 | 737070 | 199490000 | 95084000 | 16068000 | 1656200 | 17489000 | 0.0 | 120.5 | 5.4 | **42.0** |
| Phosphatidylinositol-binding clathrin assembly protein | PICALM | 927490000 | 97608000 | 28146000 | 20582000 | 1656200 | 1318000 | 45.1 | 58.9 | 21.4 | **41.8** |
| Enhancer of mRNA-decapping protein 4 | EDC4 | 614600000 | 104030000 | 59321000 | 40868000 | 1656200 | 1318000 | 15.0 | 62.8 | 45.0 | **41.0** |
| Coiled-coil domain-containing protein 43 | CCDC43 | 27370000 | 54203000 | 115330000 | 849090 | 20252000 | 1318000 | 32.2 | 2.7 | 87.5 | **40.8** |
| Coatomer subunit gamma-2 | COPG2 | 6728600000 | 2281200000 | 1878700000 | 151870000 | 46221000 | 67302000 | 44.3 | 49.4 | 27.9 | **40.5** |
| Zinc finger CCCH domain-containing protein 7A | ZC3H7A | 96408000 | 7394300 | 4392100 | 849090 | 1656200 | 1318000 | 113.5 | 4.5 | 3.3 | **40.4** |
| Wiskott-Aldrich syndrome protein family member 2 | WASF2 | 95668000 | 97675 | 10089000 | 849090 | 1656200 | 1318000 | 112.7 | 0.1 | 7.7 | **40.1** |
| Tetratricopeptide repeat protein 28 | TTC28 | 99563000 | 97675 | 2974300 | 849090 | 1656200 | 1318000 | 117.3 | 0.1 | 2.3 | **39.9** |
| Serine/threonine-protein phosphatase PP1-beta catalytic subunit;Serine/threonine-protein phosphatase | PPP1CB | 96737000 | 5623700 | 5562300 | 849090 | 4138100 | 1318000 | 113.9 | 1.4 | 4.2 | **39.8** |
| Disks large-associated protein 5 | DLGAP5 | 1673600000 | 159790000 | 191670000 | 18328000 | 12390000 | 13505000 | 91.3 | 12.9 | 14.2 | **39.5** |
| SCY1-like protein 2 | SCYL2 | 1144600000 | 36330000 | 23484000 | 14723000 | 1656200 | 1318000 | 77.7 | 21.9 | 17.8 | **39.2** |
| ADP-ribosylation factor GTPase-activating protein 1 | ARFGAP1 | 982620000 | 85958000 | 48401000 | 35822000 | 1656200 | 1318000 | 27.4 | 51.9 | 36.7 | **38.7** |
| Protein kinase C-binding protein 1 | ZMYND8 | 1560300000 | 177220000 | 121220000 | 18974000 | 15930000 | 5440300 | 82.2 | 11.1 | 22.3 | **38.5** |
| Activator of 90 kDa heat shock protein ATPase homolog 1 | AHSA1 | 2973900000 | 479110000 | 381580000 | 707440000 | 5003100 | 29345000 | 4.2 | 95.8 | 13.0 | **37.7** |
| Treacle protein | TCOF1 | 1674300000 | 18309000 | 69461000 | 28169000 | 23033000 | 1318000 | 59.4 | 0.8 | 52.7 | **37.6** |
| Msx2-interacting protein | SPEN | 1817800000 | 132160000 | 86320000 | 17244000 | 45005000 | 24368000 | 105.4 | 2.9 | 3.5 | **37.3** |
| Putative ribosomal RNA methyltransferase NOP2 | NOP2 | 91927000 | 14436000 | 6677600 | 849090 | 5113400 | 8932700 | 108.3 | 2.8 | 0.7 | **37.3** |
| Pre-mRNA-splicing factor ATP-dependent RNA helicase PRP16 | DHX38 | 91223000 | 3198500 | 2767800 | 849090 | 1656200 | 1318000 | 107.4 | 1.9 | 2.1 | **37.2** |
| Nucleolar RNA helicase 2 | DDX21 | 85120000 | 15974000 | 1858200 | 849090 | 1656200 | 1318000 | 100.2 | 9.6 | 1.4 | **37.1** |
| Centrosomal protein of 97 kDa | CEP97 | 872380000 | 14546000 | 1858200 | 8639100 | 1656200 | 1318000 | 101.0 | 8.8 | 1.4 | **37.1** |
| Telomere-associated protein RIF1 | RIF1 | 1366200000 | 50004000 | 38999000 | 17735000 | 11137000 | 1318000 | 77.0 | 4.5 | 29.6 | **37.0** |

| Protein | Gene | | | | | | | | | | |
|---|---|---|---|---|---|---|---|---|---|---|---|
| Adenylyl cyclase-associated protein 1 | CAP1 | 1040700000 | 25891000 | 41367000 | 12108000 | 1656200 | 5292200 | 86.0 | 15.6 | 7.8 | **36.5** |
| G patch domain-containing protein 1 | GPATCH1 | 88097000 | 5499000 | 1858200 | 849090 | 1656200 | 1318000 | 103.8 | 3.3 | 1.4 | **36.2** |
| 26S proteasome non-ATPase regulatory subunit 4 | PSMD4 | 2008400000 | 146890000 | 104600000 | 86870000 | 25813000 | 1318000 | 23.1 | 5.7 | 79.4 | **36.1** |
| TGF-beta-activated kinase 1 and MAP3K7-binding protein 1 | TAB1 | 754340000 | 19106000 | 19416000 | 9264200 | 1656200 | 1318000 | 81.4 | 11.5 | 14.7 | **35.9** |
| Ubiquitin-associated protein 2-like | UBAP2L | 3539200000 | 390530000 | 256930000 | 53872000 | 26590000 | 9582300 | 65.7 | 14.7 | 26.8 | **35.7** |
| LIM and cysteine-rich domains protein 1 | LMCD1 | 644290000 | 13014000 | 12541000 | 7220700 | 1656200 | 1318000 | 89.2 | 7.9 | 9.5 | **35.5** |
| Probable ATP-dependent RNA helicase DDX46 | DDX46 | 1141800000 | 39356000 | 27711000 | 16845000 | 2229700 | 1318000 | 67.8 | 17.7 | 21.0 | **35.5** |
| Elongation factor 1-delta | EEF1D | 774730000 | 152820000 | 122690000 | 76497000 | 1656200 | 44050000 | 10.1 | 92.3 | 2.8 | **35.1** |
| Ubiquitin carboxyl-terminal hydrolase 14;Ubiquitin carboxyl-terminal hydrolase | USP14 | 2625500000 | 64787000 | 63475000 | 153600000 | 1656200 | 1318000 | 17.1 | 39.1 | 48.2 | **34.8** |
| Oxysterol-binding protein-related protein 6 | OSBPL6 | 81819000 | 5182600 | 5182100 | 849090 | 1656200 | 1318000 | 96.4 | 3.1 | 3.9 | **34.5** |
| Extended synaptotagmin-1 | ESYT1 | 67292000 | 30256000 | 6347500 | 849090 | 1656200 | 1318000 | 79.3 | 18.3 | 4.8 | **34.1** |
| Ankyrin repeat and SAM domain-containing protein 1A | ANKS1A | 1519100000 | 29782000 | 84023000 | 74520000 | 1656200 | 1318000 | 20.4 | 18.0 | 63.8 | **34.0** |
| Moesin | MSN | 82828000 | 5175800 | 1858200 | 849090 | 1656200 | 1318000 | 97.5 | 3.1 | 1.4 | **34.0** |
| Fatty acid synthase;[Acyl-carrier-protein] S-acetyltransferase;[Acyl-carrier-protein] S-malonyltransferase;3-oxoacyl-[acyl-carrier-protein] synthase;3-oxoacyl-[acyl-carrier-protein] reductase;3-hydroxyacyl-[acyl-carrier-protein] dehydratase;Enoyl-[acyl-carrier-protein] reductase;Oleoyl-[acyl-carrier-protein] hydrolase | FASN | 1277700000 | 480180000 | 331410000 | 13447000 | 101400000 | 143840000 | 95.0 | 4.7 | 2.3 | **34.0** |
| Developmentally-regulated GTP-binding protein 2 | DRG2 | 737740000 | 33498000 | 31687000 | 13633000 | 1656200 | 1318000 | 54.1 | 20.2 | 24.0 | **32.8** |
| MAP7 domain-containing protein 1 | MAP7D1 | 76503000 | 10421000 | 1858200 | 849090 | 1656200 | 1318000 | 90.1 | 6.3 | 1.4 | **32.6** |
| Tyrosine--tRNA ligase, cytoplasmic;Tyrosine--tRNA ligase, cytoplasmic, N-terminally processed | YARS | 567400000 | 47682000 | 1858200 | 8459700 | 1656200 | 1318000 | 67.1 | 28.8 | 1.4 | **32.4** |
| Transforming acidic coiled-coil-containing protein 1 | TACC1 | 76192000 | 10036000 | 1858200 | 849090 | 1656200 | 1318000 | 89.7 | 6.1 | 1.4 | **32.4** |

| | | | | | | | | | | |
|---|---|---|---|---|---|---|---|---|---|---|
| Nuclear pore complex protein Nup214 | NUP214 | 4439200000 | 460530000 | 327940000 | 75649000 | 23513000 | 17357000 | 58.7 | 19.6 | 18.9 | **32.4** |
| Charged multivesicular body protein 5 | CHMP5 | 888240000 | 136180000 | 156840000 | 28222000 | 8868300 | 3134000 | 31.5 | 15.4 | 50.0 | **32.3** |
| Myotubularin-related protein 6 | MTMR6 | 469320000 | 26560000 | 62833000 | 14288000 | 1656200 | 1318000 | 32.8 | 16.0 | 47.7 | **32.2** |
| Eukaryotic translation initiation factor 3 subunit G | EIF3G | 2866400000 | 77241000 | 37686000 | 138590000 | 1656200 | 1318000 | 20.7 | 46.6 | 28.6 | **32.0** |
| CREB-regulated transcription coactivator 1 | CRTC1 | 66758000 | 13324000 | 11832000 | 849090 | 1656200 | 1318000 | 78.6 | 8.0 | 9.0 | **31.9** |
| AP-2 complex subunit beta | AP2B1 | 76264000 | 16638000 | 1858200 | 849090 | 7654300 | 1318000 | 89.8 | 2.2 | 1.4 | **31.1** |
| Arf-GAP domain and FG repeat-containing protein 1 | AGFG1 | 1545300000 | 125190000 | 106210000 | 385100000 | 1656200 | 8077200 | 4.0 | 75.6 | 13.1 | **30.9** |
| Ubiquitin carboxyl-terminal hydrolase CYLD | CYLD | 73284000 | 97675 | 8190500 | 849090 | 1656200 | 1318000 | 86.3 | 0.1 | 6.2 | **30.9** |
| Tyrosine-protein phosphatase non-receptor type 11 | PTPN11 | 9611700000 | 552520000 | 346870000 | 1090700000 | 13339000 | 8451500 | 8.8 | 41.4 | 41.0 | **30.4** |
| Protein-methionine sulfoxide oxidase MICAL3 | MICAL3 | 69150000 | 13948000 | 1858200 | 849090 | 1656200 | 1318000 | 81.4 | 8.4 | 1.4 | **30.4** |
| Proliferation-associated protein 2G4 | PA2G4 | 543310000 | 43197000 | 60961000 | 29029000 | 1656200 | 1318000 | 18.7 | 26.1 | 46.3 | **30.4** |
| Microtubule-associated protein 1A;MAP1A heavy chain;MAP1 light chain LC2 | MAP1A | 564070000 | 8962500 | 1858200 | 6922600 | 1656200 | 1318000 | 81.5 | 5.4 | 1.4 | **29.4** |
| Dihydropyrimidinase-related protein 2 | DPYSL2 | 966390000 | 43637000 | 19237000 | 20551000 | 1656200 | 1318000 | 47.0 | 26.3 | 14.6 | **29.3** |
| SUMO-activating enzyme subunit 2 | UBA2 | 552030000 | 25189000 | 29554000 | 11018000 | 1656200 | 1318000 | 50.1 | 15.2 | 22.4 | **29.2** |
| Carboxypeptidase D | CPD | 66286000 | 12037000 | 1858200 | 849090 | 1656200 | 1318000 | 78.1 | 7.3 | 1.4 | **28.9** |
| Obg-like ATPase 1 | OLA1 | 54054000 | 27635000 | 8248300 | 849090 | 1656200 | 1318000 | 63.7 | 16.7 | 6.3 | **28.9** |
| Eukaryotic translation initiation factor 3 subunit C;Eukaryotic translation initiation factor 3 subunit C-like protein | EIF3C | 661780000 | 80199000 | 66732000 | 10090000 | 6784800 | 8054900 | 65.6 | 11.8 | 8.3 | **28.6** |
| Oxysterol-binding protein-related protein 9;Oxysterol-binding protein | OSBPL9 | 61219000 | 97675 | 16841000 | 849090 | 1656200 | 1318000 | 72.1 | 0.1 | 12.8 | **28.3** |
| Ankyrin repeat and FYVE domain-containing protein 1 | ANKFY1 | 61370000 | 9927700 | 8768900 | 849090 | 1656200 | 1318000 | 72.3 | 6.0 | 6.7 | **28.3** |
| E3 ubiquitin-protein ligase RBBP6 | RBBP6 | 410720000 | 11144000 | 42880000 | 9010500 | 1656200 | 1318000 | 45.6 | 6.7 | 32.5 | **28.3** |
| Protein prune homolog | PRUNE1 | 3097200000 | 118360000 | 65410000 | 239700000 | 5394300 | 1318000 | 12.9 | 21.9 | 49.6 | **28.2** |
| Aminoacyl tRNA synthase complex-interacting multifunctional protein 1;Endothelial monocyte- | AIMP1 | 67352000 | 6219400 | 1858200 | 849090 | 1656200 | 1318000 | 79.3 | 3.8 | 1.4 | **28.2** |

activating polypeptide 2

| Protein | Gene | | | | | | | | | | |
|---|---|---|---|---|---|---|---|---|---|---|---|
| Cohesin subunit SA-2 | STAG2 | 66694000 | 6414300 | 1858200 | 849090 | 1656200 | 1318000 | 78.5 | 3.9 | 1.4 | **27.9** |
| Protein PBDC1 | PBDC1 | 297780000 | 97675 | 10135000 | 3914600 | 1656200 | 1318000 | 76.1 | 0.1 | 7.7 | **27.9** |
| AP-3 complex subunit beta-1 | AP3B1 | 60549000 | 97675 | 16239000 | 849090 | 1656200 | 1318000 | 71.3 | 0.1 | 12.3 | **27.9** |
| Ras GTPase-activating protein-binding protein 1 | G3BP1 | 1004100000 | 22822000 | 51145000 | 32793000 | 1656200 | 1318000 | 30.6 | 13.8 | 38.8 | **27.7** |
| Tudor domain-containing protein 3 | TDRD3 | 63832000 | 97675 | 10048000 | 849090 | 1656200 | 1318000 | 75.2 | 0.1 | 7.6 | **27.6** |
| Pachytene checkpoint protein 2 homolog | TRIP13 | 763080000 | 41539000 | 43820000 | 11334000 | 4298400 | 8004700 | 67.3 | 9.7 | 5.5 | **27.5** |
| Centromere protein H | CENPH | 1018200000 | 33830000 | 64087000 | 77853000 | 1656200 | 1318000 | 13.1 | 20.4 | 48.6 | **27.4** |
| Interleukin enhancer-binding factor 3 | ILF3 | 2508600000 | 240570000 | 247260000 | 33306000 | 112380000 | 85583000 | 75.3 | 2.1 | 2.9 | **26.8** |
| Ankyrin repeat and KH domain-containing protein 1 | ANKHD1 | 888050000 | 37717000 | 24352000 | 24128000 | 1656200 | 1318000 | 36.8 | 22.8 | 18.5 | **26.0** |
| WW domain-containing adapter protein with coiled-coil | WAC | 840650000 | 74718000 | 74237000 | 82878000 | 6661100 | 1318000 | 10.1 | 11.2 | 56.3 | **25.9** |
| Serine/threonine-protein kinase WNK1 | WNK1 | 1335000000 | 28270000 | 59841000 | 91474000 | 1656200 | 1318000 | 14.6 | 17.1 | 45.4 | **25.7** |
| Protein DDI1 homolog 2 | DDI2 | 63026000 | 97675 | 5391800 | 849090 | 1656200 | 2237400 | 74.2 | 0.1 | 2.4 | **25.6** |
| Trifunctional purine biosynthetic protein adenosine-3;Phosphoribosylamine--glycine ligase;Phosphoribosylformylglycinamidine cyclo-ligase;Phosphoribosylglycinamide formyltransferase | GART | 53818000 | 14553000 | 5000700 | 849090 | 1656200 | 1318000 | 63.4 | 8.8 | 3.8 | **25.3** |
| Paired amphipathic helix protein Sin3a | SIN3A | 870000000 | 9876000 | 39445000 | 21888000 | 1656200 | 1318000 | 39.7 | 6.0 | 29.9 | **25.2** |
| General transcription factor 3C polypeptide 5 | GTF3C5 | 1282700000 | 49129000 | 54245000 | 267630000 | 1656200 | 1318000 | 4.8 | 29.7 | 41.2 | **25.2** |
| Double-stranded RNA-binding protein Staufen homolog 1 | STAU1 | 3403000000 | 30222000 | 34685000 | 114160000 | 1656200 | 1318000 | 29.8 | 18.2 | 26.3 | **24.8** |
| Centromere protein F | CENPF | 12533000 | 95868000 | 1858200 | 849090 | 1656200 | 1318000 | 14.8 | 57.9 | 1.4 | **24.7** |
| Elongation factor 1-alpha 2 | EEF1A2 | 979900000 | 48216000 | 40444000 | 15381000 | 6378100 | 14792000 | 63.7 | 7.6 | 2.7 | **24.7** |
| 28 kDa heat- and acid-stable phosphoprotein | PDAP1 | 737070 | 59746000 | 49786000 | 33327000 | 1656200 | 1318000 | 0.0 | 36.1 | 37.8 | **24.6** |
| Protein NDRG1 | NDRG1 | 2342000000 | 30991000 | 71192000 | 157170000 | 7823600 | 1318000 | 14.9 | 4.0 | 54.0 | **24.3** |
| Protein LSM14 homolog B | LSM14B | 690740000 | 10934000 | 11593000 | 12049000 | 1656200 | 1318000 | 57.3 | 6.6 | 8.8 | **24.2** |

| | | | | | | | | | | | |
|---|---|---|---|---|---|---|---|---|---|---|---|
| Catenin delta-1 | CTNND1 | 704010000 | 16951000 | 37826000 | 20872000 | 1656200 | 1318000 | 33.7 | 10.2 | 28.7 | **24.2** |
| Protein TALPID3 | KIAA0586 | 4421600 | 109100000 | 1858200 | 849090 | 1656200 | 1318000 | 5.2 | 65.9 | 1.4 | **24.2** |
| Lamin-B receptor | LBR | 42231000 | 27579000 | 39584000 | 849090 | 1656200 | 7684700 | 49.7 | 16.7 | 5.2 | **23.8** |
| Anaphase-promoting complex subunit 4 | ANAPC4 | 552930000 | 29821000 | 16737000 | 13700000 | 1656200 | 1318000 | 40.4 | 18.0 | 12.7 | **23.7** |
| Pre-mRNA-processing-splicing factor 8 | PRPF8 | 52297000 | 30502000 | 13162000 | 849090 | 3399400 | 31087000 | 61.6 | 9.0 | 0.4 | **23.7** |
| IST1 homolog | IST1 | 1343400000 | 13621000 | 1858200 | 21968000 | 1656200 | 1318000 | 61.2 | 8.2 | 1.4 | **23.6** |
| Coiled-coil domain-containing protein 50 | CCDC50 | 600230000 | 53639000 | 1858200 | 17252000 | 1656200 | 1318000 | 34.8 | 32.4 | 1.4 | **22.9** |
| Myosin-14 | MYH14 | 163090000 | 20648000 | 1858200 | 3034600 | 1656200 | 1318000 | 53.7 | 12.5 | 1.4 | **22.5** |
| V-type proton ATPase catalytic subunit A | ATP6V1A | 232110000 | 66438000 | 15087000 | 14574000 | 1656200 | 1318000 | 15.9 | 40.1 | 11.4 | **22.5** |
| Thyroid hormone receptor-associated protein 3 | THRAP3 | 1155200000 | 44480000 | 22646000 | 49428000 | 1656200 | 1318000 | 23.4 | 26.9 | 17.2 | **22.5** |
| BAG family molecular chaperone regulator 3 | BAG3 | 3474000000 | 189680000 | 114320000 | 139430000 | 8312500 | 5876200 | 24.9 | 22.8 | 19.5 | **22.4** |
| ATP-dependent RNA helicase DDX19A;ATP-dependent RNA helicase DDX19B | DDX19A | 617410000 | 11666000 | 1858200 | 10749000 | 1656200 | 1318000 | 57.4 | 7.0 | 1.4 | **22.0** |
| Histone-lysine N-methyltransferase, H3 lysine-36 and H4 lysine-20 specific | NSD1 | 23150000 | 61411000 | 1858200 | 849090 | 1656200 | 1318000 | 27.3 | 37.1 | 1.4 | **21.9** |
| Cyclin-K | CCNK | 3146800000 | 132880000 | 94985000 | 52212000 | 52489000 | 32927000 | 60.3 | 2.5 | 2.9 | **21.9** |
| Eukaryotic translation initiation factor 5 | EIF5 | 45909000000 | 4006300000 | 4070400000 | 2090400000 | 188960000 | 184990000 | 22.0 | 21.2 | 22.0 | **21.7** |
| Syntaxin-5 | STX5 | 593870000 | 8278400 | 10012000 | 11549000 | 1656200 | 1318000 | 51.4 | 5.0 | 7.6 | **21.3** |
| Nuclear pore complex protein Nup98-Nup96;Nuclear pore complex protein Nup98;Nuclear pore complex protein Nup96 | NUP98 | 1001900000 | 20431000 | 58621000 | 140970000 | 1656200 | 1318000 | 7.1 | 12.3 | 44.5 | **21.3** |
| Peptidyl-prolyl cis-trans isomerase D | PPID | 773090000 | 41300000 | 27079000 | 42109000 | 1656200 | 1318000 | 18.4 | 24.9 | 20.5 | **21.3** |
| Ubiquitin carboxyl-terminal hydrolase 8;Ubiquitin carboxyl-terminal hydrolase | USP8 | 50303000 | 97675 | 5470100 | 849090 | 1656200 | 1318000 | 59.2 | 0.1 | 4.2 | **21.2** |
| Ubiquitin-like-conjugating enzyme ATG3 | ATG3 | 558050000 | 38430000 | 22713000 | 25198000 | 1656200 | 1318000 | 22.1 | 23.2 | 17.2 | **20.9** |
| Filamin-C | FLNC | 244000000 | 4904900 | 6843000 | 4488000 | 1656200 | 1318000 | 54.4 | 3.0 | 5.2 | **20.8** |
| PDZ and LIM domain protein 4 | PDLIM4 | 1180600000 | 37392000 | 48533000 | 381190000 | 1656200 | 1318000 | 3.1 | 22.6 | 36.8 | **20.8** |
| Coatomer subunit gamma-1 | COPG1 | 49826000 | 5572700 | 7124800 | 849090 | 2637600 | 10339000 | 58.7 | 2.1 | 0.7 | **20.5** |

| Protein | Gene | | | | | | | | | | |
|---|---|---|---|---|---|---|---|---|---|---|---|
| Tetratricopeptide repeat protein 1 | TTC1 | 462780000 | 28494000 | 21404000 | 16650000 | 1656200 | 1318000 | 27.8 | 17.2 | 16.2 | **20.4** |
| Protein misato homolog 1 | MSTO1 | 869420000 | 18360000 | 18087000 | 24191000 | 1656200 | 1318000 | 35.9 | 11.1 | 13.7 | **20.2** |
| ATP-dependent RNA helicase DDX3X;ATP-dependent RNA helicase DDX3Y | DDX3X | 4333200000 | 507390000 | 531840000 | 476460000 | 12659000 | 47484000 | 9.1 | 40.1 | 11.2 | **20.1** |
| Tryptophan--tRNA ligase, cytoplasmic;T1-TrpRS;T2-TrpRS | WARS | 2466400000 | 100040000 | 45285000 | 174080000 | 9246500 | 1318000 | 14.2 | 10.8 | 34.4 | **19.8** |
| NSFL1 cofactor p47 | NSFL1C | 1529600000 | 42837000 | 35508000 | 277160000 | 1656200 | 1318000 | 5.5 | 25.9 | 26.9 | **19.4** |
| Tetratricopeptide repeat protein 4 | TTC4 | 402440000 | 57573000 | 10440000 | 25906000 | 1656200 | 1318000 | 15.5 | 34.8 | 7.9 | **19.4** |
| COP9 signalosome complex subunit 3 | COPS3 | 84387000 | 26885000 | 26740000 | 1594800 | 9350500 | 12070000 | 52.9 | 2.9 | 2.2 | **19.3** |
| Signal transducing adapter molecule 2 | STAM2 | 189300000 | 7460500 | 9872100 | 4155800 | 1656200 | 1318000 | 45.6 | 4.5 | 7.5 | **19.2** |
| Hsp90 co-chaperone Cdc37;Hsp90 co-chaperone Cdc37, N-terminally processed | CDC37 | 793650000 | 206470000 | 167100000 | 119360000 | 7798700 | 6993100 | 6.6 | 26.5 | 23.9 | **19.0** |
| Histone deacetylase complex subunit SAP130 | SAP130 | 861810000 | 12148000 | 12185000 | 17934000 | 1656200 | 7842900 | 48.1 | 7.3 | 1.6 | **19.0** |
| U4/U6.U5 tri-snRNP-associated protein 1 | SART1 | 1238500000 | 100590000 | 39238000 | 90594000 | 7556300 | 1318000 | 13.7 | 13.3 | 29.8 | **18.9** |
| Pinin | PNN | 3313400000 | 343960000 | 141080000 | 189600000 | 10364000 | 34064000 | 17.5 | 33.2 | 4.1 | **18.3** |
| Eukaryotic peptide chain release factor subunit 1 | ETF1 | 1409900000 | 31170000 | 17442000 | 62087000 | 1656200 | 1318000 | 22.7 | 18.8 | 13.2 | **18.3** |
| Nucleosome assembly protein 1-like 1 | NAP1L1 | 4050800000 | 243250000 | 225730000 | 304720000 | 7388300 | 26515000 | 13.3 | 32.9 | 8.5 | **18.2** |
| Coatomer subunit delta | ARCN1 | 2189800000 | 66627000 | 119470000 | 311480000 | 1656200 | 16259000 | 7.0 | 40.2 | 7.3 | **18.2** |
| Twinfilin-2 | TWF2 | 985920000 | 27146000 | 34826000 | 83790000 | 1656200 | 1318000 | 11.8 | 16.4 | 26.4 | **18.2** |
| Host cell factor 1 | HCFC1 | 43177000 | 20556000 | 23986000 | 849090 | 14898000 | 11992000 | 50.9 | 1.4 | 2.0 | **18.1** |
| Transaldolase | TALDO1 | 494400000 | 66181000 | 42262000 | 56893000 | 1656200 | 7679000 | 8.7 | 40.0 | 5.5 | **18.1** |
| Pleckstrin homology domain-containing family A member 1 | PLEKHA1 | 202220000 | 10145000 | 1858200 | 4342800 | 1656200 | 1318000 | 46.6 | 6.1 | 1.4 | **18.0** |
| Splicing factor 3B subunit 1 | SF3B1 | 9547400000 | 1170400000 | 1073300000 | 217130000 | 226880000 | 216370000 | 44.0 | 5.2 | 5.0 | **18.0** |
| 60S ribosomal protein L5 | RPL5 | 100970000 | 59239000 | 17273000 | 22390000 | 1656200 | 1318000 | 4.5 | 35.8 | 13.1 | **17.8** |
| Pseudouridylate synthase 7 homolog | PUS7 | 416560000 | 54297000 | 21188000 | 94251000 | 1656200 | 1318000 | 4.4 | 32.8 | 16.1 | **17.8** |
| PAS domain-containing serine/threonine-protein kinase | PASK | 40763000 | 5558800 | 1858200 | 849090 | 1656200 | 1318000 | 48.0 | 3.4 | 1.4 | **17.6** |

| Protein | Gene | | | | | | | | | | |
|---|---|---|---|---|---|---|---|---|---|---|---|
| T-complex protein 1 subunit alpha | TCP1 | 383120000 | 201770000 | 130700000 | 8175900 | 47023000 | 83715000 | 46.9 | 4.3 | 1.6 | **17.6** |
| T-complex protein 1 subunit epsilon | CCT5 | 174620000 | 53968000 | 25403000 | 4472500 | 5501100 | 10430000 | 39.0 | 9.8 | 2.4 | **17.1** |
| Uncharacterized protein C1orf198 | C1orf198 | 690220000 | 55586000 | 13130000 | 91012000 | 1656200 | 1318000 | 7.6 | 33.6 | 10.0 | **17.0** |
| Tubulin-specific chaperone cofactor E-like protein | TBCEL | 1169400000 | 18801000 | 26212000 | 59748000 | 1656200 | 1318000 | 19.6 | 11.4 | 19.9 | **16.9** |
| WD repeat and HMG-box DNA-binding protein 1 | WDHD1 | 1655000000 | 148070000 | 119990000 | 40550000 | 41956000 | 21760000 | 40.8 | 3.5 | 5.5 | **16.6** |
| Splicing factor 45 | RBM17 | 2199800000 | 34009000 | 23373000 | 193270000 | 1656200 | 1318000 | 11.4 | 20.5 | 17.7 | **16.6** |
| Splicing factor 3A subunit 1 | SF3A1 | 5669100000 | 250960000 | 84416000 | 160810000 | 20208000 | 52016000 | 35.3 | 12.4 | 1.6 | **16.4** |
| L-aminoadipate-semialdehyde dehydrogenase-phosphopantetheinyl transferase | AASDHPPT | 236960000 | 22364000 | 19687000 | 11563000 | 1656200 | 1318000 | 20.5 | 13.5 | 14.9 | **16.3** |
| Alpha-globin transcription factor CP2 | TFCP2 | 977680000 | 105750000 | 78055000 | 38325000 | 20091000 | 4371000 | 25.5 | 5.3 | 17.9 | **16.2** |
| Importin-9 | IPO9 | 33460000 | 8223400 | 5544700 | 849090 | 1656200 | 1318000 | 39.4 | 5.0 | 4.2 | **16.2** |
| Alpha-centractin | ACTR1A | 737070 | 13813000 | 51423000 | 849090 | 1656200 | 1318000 | 0.9 | 8.3 | 39.0 | **16.1** |
| Nascent polypeptide-associated complex subunit alpha | NACA | 1130700000 | 43016000 | 19644000 | 158390000 | 1656200 | 1318000 | 7.1 | 26.0 | 14.9 | **16.0** |
| U2 snRNP-associated SURP motif-containing protein | U2SURP | 1616600000 | 136560000 | 170570000 | 42807000 | 28741000 | 31343000 | 37.8 | 4.8 | 5.4 | **16.0** |
| Vesicle-associated membrane protein-associated protein B/C | VAPB | 10991000 | 32679000 | 33020000 | 3553600 | 1656200 | 1318000 | 3.1 | 19.7 | 25.1 | **16.0** |
| Protein FAM208B | FAM208B | 230260000 | 97675 | 5870500 | 5383000 | 1656200 | 1318000 | 42.8 | 0.1 | 4.5 | **15.8** |
| Keratin, type I cytoskeletal 18 | KRT18 | 30679000000 | 779470000 | 619490000 | 6465400000 | 25937000 | 49744000 | 4.7 | 30.1 | 12.5 | **15.8** |
| RanBP2-like and GRIP domain-containing protein 3;RanBP2-like and GRIP domain-containing protein 4;RANBP2-like and GRIP domain-containing protein 1;RANBP2-like and GRIP domain-containing protein 2 | RGPD3 | 314610000 | 96007000 | 70622000 | 8877200 | 12120000 | 19336000 | 35.4 | 7.9 | 3.7 | **15.7** |
| Nucleosome assembly protein 1-like 4 | NAP1L4 | 7963500000 | 445910000 | 392680000 | 773690000 | 25024000 | 21038000 | 10.3 | 17.8 | 18.7 | **15.6** |
| Spectrin alpha chain, non-erythrocytic 1 | SPTAN1 | 705150000 | 37183000 | 33711000 | 34088000 | 1656200 | 9286700 | 20.7 | 22.5 | 3.6 | **15.6** |
| Signal transducer and activator of transcription 1-alpha/beta | STAT1 | 4336700000 | 366020000 | 259530000 | 143280000 | 36255000 | 40736000 | 30.3 | 10.1 | 6.4 | **15.6** |

| | | | | | | | | | | |
|---|---|---|---|---|---|---|---|---|---|---|
| **Heterogeneous nuclear ribonucleoprotein R** | HNRNPR | 1148900000 | 221080000 | 167060000 | 31384000 | 43979000 | 35698000 | 36.6 | 5.0 | 4.7 | **15.4** |
| **TOM1-like protein 1** | TOM1L1 | 255280000 | 97675 | 7739000 | 6414200 | 1656200 | 1318000 | 39.8 | 0.1 | 5.9 | **15.2** |
| **Protein kintoun** | DNAAF2 | 366210000 | 17307000 | 23782000 | 21378000 | 1656200 | 1318000 | 17.1 | 10.4 | 18.0 | **15.2** |
| **Protein phosphatase inhibitor 2;Putative protein phosphatase inhibitor 2-like protein 3** | PPP1R2 | 165910000 | 29607000 | 99494000 | 6499700 | 1656200 | 54618000 | 25.5 | 17.9 | 1.8 | **15.1** |
| **CCR4-NOT transcription complex subunit 1** | CNOT1 | 35122000 | 2652000 | 2703900 | 849090 | 1656200 | 1318000 | 41.4 | 1.6 | 2.1 | **15.0** |
| **Upstream-binding protein 1** | UBP1 | 405540000 | 12572000 | 15509000 | 14459000 | 2714700 | 1318000 | 28.0 | 4.6 | 11.8 | **14.8** |
| **Regulation of nuclear pre-mRNA domain-containing protein 2** | RPRD2 | 1019300000 | 127590000 | 71609000 | 30459000 | 25908000 | 12328000 | 33.5 | 4.9 | 5.8 | **14.7** |
| **Exosome complex exonuclease RRP44** | DIS3 | 760270000 | 41994000 | 44406000 | 19189000 | 22758000 | 20505000 | 39.6 | 1.8 | 2.2 | **14.5** |
| **Phosducin-like protein** | PDCL | 907980000 | 43191000 | 15895000 | 174310000 | 1656200 | 1318000 | 5.2 | 26.1 | 12.1 | **14.4** |
| **Plastin-3** | PLS3 | 519160000 | 102070000 | 102650000 | 14426000 | 21790000 | 43668000 | 36.0 | 4.7 | 2.4 | **14.3** |
| **Polyadenylate-binding protein 4** | PABPC4 | 17414000 | 17504000 | 15721000 | 849090 | 1656200 | 1318000 | 20.5 | 10.6 | 11.9 | **14.3** |
| **Bifunctional purine biosynthesis protein PURH;Phosphoribosylaminoimidazolecarboxamide formyltransferase;IMP cyclohydrolase** | ATIC | 264220000 | 11838000 | 11399000 | 7626400 | 2488800 | 3652700 | 34.6 | 4.8 | 3.1 | **14.2** |
| **Serine/threonine-protein kinase BRSK2** | BRSK2 | 30240000 | 8807900 | 1858200 | 849090 | 1656200 | 1318000 | 35.6 | 5.3 | 1.4 | **14.1** |
| **Transcription elongation regulator 1** | TCERG1 | 2786700000 | 622640000 | 365240000 | 78145000 | 137150000 | 196890000 | 35.7 | 4.5 | 1.9 | **14.0** |
| **Asparagine synthetase [glutamine-hydrolyzing]** | ASNS | 849110000 | 21449000 | 18425000 | 56243000 | 1656200 | 1318000 | 15.1 | 13.0 | 14.0 | **14.0** |
| **PIH1 domain-containing protein 1** | PIH1D1 | 2352500000 | 107120000 | 90138000 | 103310000 | 10397000 | 10285000 | 22.8 | 10.3 | 8.8 | **13.9** |
| **Scaffold attachment factor B2** | SAFB2 | 416850000 | 18436000 | 33133000 | 88771000 | 1656200 | 1318000 | 4.7 | 11.1 | 25.1 | **13.7** |
| **Tubulin-specific chaperone E** | TBCE | 612490000 | 8159500 | 27775000 | 42305000 | 1656200 | 1318000 | 14.5 | 4.9 | 21.1 | **13.5** |
| **Anamorsin** | CIAPIN1 | 5092400000 | 305070000 | 355650000 | 845270000 | 17887000 | 20543000 | 6.0 | 17.1 | 17.3 | **13.5** |
| **Eukaryotic translation initiation factor 3 subunit J** | EIF3J | 350990000 | 15326000 | 8343000 | 14270000 | 1656200 | 1318000 | 24.6 | 9.3 | 6.3 | **13.4** |
| **Mitochondrial inner membrane protein** | IMMT | 25368000 | 8478700 | 34930000 | 849090 | 1656200 | 6969400 | 29.9 | 5.1 | 5.0 | **13.3** |
| **E3 ubiquitin-protein ligase XIAP** | XIAP | 1289000000 | 12468000 | 9958200 | 52131000 | 1656200 | 1318000 | 24.7 | 7.5 | 7.6 | **13.3** |
| **Echinoderm microtubule-associated protein-like 4** | EML4 | 16502000 | 16996000 | 13318000 | 849090 | 1656200 | 1318000 | 19.4 | 10.3 | 10.1 | **13.3** |
| **DNA polymerase delta subunit 3** | POLD3 | 441480000 | 27817000 | 40928000 | 62282000 | 16905000 | 1318000 | 7.1 | 1.6 | 31.1 | **13.3** |

| Protein | Gene | | | | | | | | | | |
|---|---|---|---|---|---|---|---|---|---|---|---|
| Calponin-2 | CNN2 | 85498000 | 57392000 | 4528600 | 82212000 | 1656200 | 1318000 | 1.0 | 34.7 | 3.4 | **13.0** |
| ATP-dependent RNA helicase DDX42 | DDX42 | 1803200000 | 109140000 | 72964000 | 57792000 | 19761000 | 36789000 | 31.2 | 5.5 | 2.0 | **12.9** |
| Serpin H1 | SERPINH1 | 107880000 | 18619000 | 11760000 | 4174300 | 1656200 | 8623800 | 25.8 | 11.2 | 1.4 | **12.8** |
| Protein EMSY | EMSY | 1955000000 | 143360000 | 72931000 | 55541000 | 65523000 | 72541000 | 35.2 | 2.2 | 1.0 | **12.8** |
| RNA polymerase-associated protein RTF1 homolog | RTF1 | 371650000 | 7989900 | 40978000 | 180930000 | 1656200 | 1318000 | 2.1 | 4.8 | 31.1 | **12.7** |
| Coronin-1B | CORO1B | 1285000000 | 215460000 | 142830000 | 199240000 | 13328000 | 9362600 | 6.4 | 16.2 | 15.3 | **12.6** |
| Heat shock protein 105 kDa | HSPH1 | 2753000000 | 43369000 | 102460000 | 114840000 | 6410000 | 14579000 | 24.0 | 6.8 | 7.0 | **12.6** |
| Insulin-like growth factor 2 mRNA-binding protein 2 | IGF2BP2 | 578630000 | 16088000 | 1858200 | 21726000 | 1656200 | 1318000 | 26.6 | 9.7 | 1.4 | **12.6** |
| Serine--tRNA ligase, cytoplasmic | SARS | 69922000 | 27885000 | 24813000 | 55340000 | 1656200 | 1318000 | 1.3 | 16.8 | 18.8 | **12.3** |
| PDZ and LIM domain protein 7 | PDLIM7 | 409350000 | 12880000 | 12985000 | 21440000 | 1656200 | 1318000 | 19.1 | 7.8 | 9.9 | **12.2** |
| Heterogeneous nuclear ribonucleoprotein D-like | HNRNPDL | 790620000 | 48463000 | 45581000 | 175580000 | 1656200 | 17688000 | 4.5 | 29.3 | 2.6 | **12.1** |
| Nuclear protein localization protein 4 homolog | NPLOC4 | 386430000 | 31704000 | 21204000 | 361990000 | 1656200 | 1318000 | 1.1 | 19.1 | 16.1 | **12.1** |
| Switch-associated protein 70 | SWAP70 | 15438000 | 15390000 | 33894000 | 14113000 | 1656200 | 1318000 | 1.1 | 9.3 | 25.7 | **12.0** |
| T-complex protein 1 subunit theta | CCT8 | 80377000000 | 18651000000 | 17353000000 | 5650700000 | 1785400000 | 1551100000 | 14.2 | 10.4 | 11.2 | **12.0** |
| RNA-binding protein Raly | RALY | 324210000 | 22885000 | 34494000 | 39679000 | 17383000 | 1318000 | 8.2 | 1.3 | 26.2 | **11.9** |
| Protein Spindly | SPDL1 | 30908000 | 28379000 | 34895000 | 589130000 | 3300400 | 1318000 | 0.1 | 8.6 | 26.5 | **11.7** |
| Filamin-A | FLNA | 30763000000 | 14129000000 | 12686000000 | 2178100000 | 1286100000 | 1281000000 | 14.1 | 11.0 | 9.9 | **11.7** |
| Melanoma-associated antigen D2 | MAGED2 | 1887500000 | 55258000 | 89017000 | 86586000 | 14669000 | 9692000 | 21.8 | 3.8 | 9.2 | **11.6** |
| Lamin-B1 | LMNB1 | 611610000 | 205070000 | 263520000 | 112690000 | 8040800 | 82753000 | 5.4 | 25.5 | 3.2 | **11.4** |
| Dynamin-1-like protein | DNM1L | 22167000 | 97675 | 10392000 | 849090 | 1656200 | 1318000 | 26.1 | 0.1 | 7.9 | **11.4** |
| Eukaryotic translation initiation factor 2 subunit 3;Putative eukaryotic translation initiation factor 2 subunit 3-like protein | EIF2S3 | 737070 | 23804000 | 25800000 | 12500000 | 1656200 | 1318000 | 0.1 | 14.4 | 19.6 | **11.3** |
| Polyadenylate-binding protein-interacting protein 1 | PAIP1 | 290100000 | 97675 | 14527000 | 12672000 | 1656200 | 1318000 | 22.9 | 0.1 | 11.0 | **11.3** |
| Insulin-like growth factor 2 mRNA-binding protein 1 | IGF2BP1 | 3262500000 | 422820000 | 333600000 | 300030000 | 22457000 | 83662000 | 10.9 | 18.8 | 4.0 | **11.2** |
| Bcl-2-associated transcription factor 1 | BCLAF1 | 802370000 | 12044000 | 23668000 | 97658000 | 1656200 | 1318000 | 8.2 | 7.3 | 18.0 | **11.1** |
| BRCA2 and CDKN1A-interacting protein | BCCIP | 653370000 | 21141000 | 24728000 | 23303000 | 14445000 | 6753000 | 28.0 | 1.5 | 3.7 | **11.1** |
| Coatomer subunit alpha;Xenin;Proxenin | COPA | 25961000 | 97675 | 15864000 | 849090 | 9629500 | 7465800 | 30.6 | 0.0 | 2.1 | **10.9** |

| Protein | Gene | | | | | | | | | | |
|---|---|---|---|---|---|---|---|---|---|---|---|
| ADP-ribosylation factor-binding protein GGA1 | GGA1 | 22451000 | 97675 | 8128500 | 849090 | 1656200 | 1318000 | 26.4 | 0.1 | 6.2 | **10.9** |
| 26S proteasome non-ATPase regulatory subunit 12 | PSMD12 | 1471400000 | 1500500 | 19941000 | 89318000 | 1656200 | 1318000 | 16.5 | 0.9 | 15.1 | **10.8** |
| KH domain-containing, RNA-binding, signal transduction-associated protein 1 | KHDRBS1 | 214170000 | 97675 | 29870000 | 23335000 | 10055000 | 1318000 | 9.2 | 0.0 | 22.7 | **10.6** |
| Nuclear migration protein nudC | NUDC | 29029000000 | 4247800000 | 3294800000 | 2255000000 | 407670000 | 404660000 | 12.9 | 10.4 | 8.1 | **10.5** |
| Annexin A5;Annexin | ANXA5 | 10707000 | 70289000 | 125290000 | 849090 | 4335900 | 56928000 | 12.6 | 16.2 | 2.2 | **10.3** |
| Synaptic vesicle membrane protein VAT-1 homolog | VAT1 | 21974000 | 65986000 | 12535000 | 849090 | 18421000 | 9239400 | 25.9 | 3.6 | 1.4 | **10.3** |
| Heat shock 70 kDa protein 4 | HSPA4 | 1178300000 | 151740000 | 117990000 | 52925000 | 20993000 | 92695000 | 22.3 | 7.2 | 1.3 | **10.3** |
| Peroxiredoxin-6 | PRDX6 | 737070 | 45990000 | 43276000 | 172240000 | 1656200 | 14696000 | 0.0 | 27.8 | 2.9 | **10.2** |
| Acyl-coenzyme A thioesterase 1;Acyl-coenzyme A thioesterase 2, mitochondrial | ACOT1 | 35846000 | 32400000 | 10949000 | 12609000 | 1656200 | 1318000 | 2.8 | 19.6 | 8.3 | **10.2** |
| Guanine nucleotide-binding protein G(k) subunit alpha;Guanine nucleotide-binding protein G(s) subunit alpha isoforms short;Guanine nucleotide-binding protein G(i) subunit alpha-2;Guanine nucleotide-binding protein G(i) subunit alpha-1;Guanine nucleotide-binding protein G(o) subunit alpha;Guanine nucleotide-binding protein G(olf) subunit alpha;Guanine nucleotide-binding protein G(t) subunit alpha-2;Guanine nucleotide-binding protein G(t) subunit alpha-3;Guanine nucleotide-binding protein G(t) subunit alpha-1;Guanine nucleotide-binding protein G(s) subunit alpha isoforms XLas | GNAI3 | 18897000 | 97675 | 10948000 | 849090 | 1656200 | 1318000 | 22.3 | 0.1 | 8.3 | **10.2** |
| Eukaryotic translation initiation factor 3 subunit M | EIF3M | 22828000 | 2872600 | 3152300 | 849090 | 2585100 | 1318000 | 26.9 | 1.1 | 2.4 | **10.1** |
| Annexin A6;Annexin | ANXA6 | 737070 | 20339000 | 22325000 | 849090 | 1656200 | 1318000 | 0.9 | 12.3 | 16.9 | **10.0** |
| Probable ATP-dependent RNA helicase DDX41 | DDX41 | 99520000 | 10954000 | 1858200 | 4521500 | 1656200 | 1318000 | 22.0 | 6.6 | 1.4 | **10.0** |
| RuvB-like 2 | RUVBL2 | 1522500000 | 16003000 | 63186000 | 83260000 | 7724500 | 6728700 | 18.3 | 2.1 | 9.4 | **9.9** |

| Protein | Gene | | | | | | | | | | |
|---|---|---|---|---|---|---|---|---|---|---|---|
| Serine hydroxymethyltransferase, mitochondrial;Serine hydroxymethyltransferase | SHMT2 | 737070 | 42823000 | 17669000 | 849090 | 1656200 | 6184700 | 0.9 | 25.9 | 2.9 | **9.9** |
| RNA-binding protein 12 | RBM12 | 659800000 | 97675 | 8816300 | 29193000 | 1656200 | 1318000 | 22.6 | 0.1 | 6.7 | **9.8** |
| Nucleoprotein TPR | TPR | 604920000 | 17984000 | 25528000 | 27745000 | 4439800 | 7364400 | 21.8 | 4.1 | 3.5 | **9.8** |
| Signal recognition particle subunit SRP72 | SRP72 | 375510000 | 12950000 | 18546000 | 51684000 | 1656200 | 1318000 | 7.3 | 7.8 | 14.1 | **9.7** |
| H/ACA ribonucleoprotein complex non-core subunit NAF1 | NAF1 | 84853000 | 4330300 | 1858200 | 3378800 | 1656200 | 1318000 | 25.1 | 2.6 | 1.4 | **9.7** |
| Nuclear-interacting partner of ALK | ZC3HC1 | 394730000 | 8013700 | 5923100 | 19967000 | 1656200 | 1318000 | 19.8 | 4.8 | 4.5 | **9.7** |
| Multifunctional protein ADE2;Phosphoribosylaminoimidazole-succinocarboxamide synthase;Phosphoribosylaminoimidazole carboxylase | PAICS | 2500600000 | 530460000 | 569190000 | 120160000 | 133860000 | 140700000 | 20.8 | 4.0 | 4.0 | **9.6** |
| Heterogeneous nuclear ribonucleoprotein K | HNRNPK | 67156000 | 40946000 | 1858200 | 32962000 | 1656200 | 1318000 | 2.0 | 24.7 | 1.4 | **9.4** |
| Nuclear pore glycoprotein p62 | NUP62 | 1054600000 | 7050500 | 6845100 | 56428000 | 1656200 | 1318000 | 18.7 | 4.3 | 5.2 | **9.4** |
| U5 small nuclear ribonucleoprotein 200 kDa helicase | SNRNP200 | 228300000 | 45452000 | 55599000 | 10045000 | 22458000 | 17514000 | 22.7 | 2.0 | 3.2 | **9.3** |
| Uncharacterized protein CXorf57 | CXorf57 | 55489000 | 5991300 | 9797800 | 2441800 | 1656200 | 6331700 | 22.7 | 3.6 | 1.5 | **9.3** |
| Immunoglobulin-binding protein 1 | IGBP1 | 520250000 | 10802000 | 21557000 | 107000000 | 1656200 | 1318000 | 4.9 | 6.5 | 16.4 | **9.2** |
| Plasminogen activator inhibitor 1 RNA-binding protein | SERBP1 | 12756000000 | 507360000 | 494520000 | 768620000 | 164560000 | 61771000 | 16.6 | 3.1 | 8.0 | **9.2** |
| HIV Tat-specific factor 1 | HTATSF1 | 1847400000 | 200220000 | 114950000 | 154570000 | 54645000 | 9524500 | 12.0 | 3.7 | 12.1 | **9.2** |
| Phosphoribosyl pyrophosphate synthase-associated protein 2 | PRPSAP2 | 15797000 | 14066000 | 1858200 | 849090 | 1656200 | 3296400 | 18.6 | 8.5 | 0.6 | **9.2** |
| Microtubule-associated protein RP/EB family member 2 | MAPRE2 | 3653100000 | 518670000 | 334150000 | 323510000 | 157250000 | 25655000 | 11.3 | 3.3 | 13.0 | **9.2** |
| N6-adenosine-methyltransferase 70 kDa subunit | METTL3 | 95547000 | 31778000 | 31707000 | 123970000 | 11656000 | 1318000 | 0.8 | 2.7 | 24.1 | **9.2** |
| Eukaryotic translation initiation factor 3 subunit D | EIF3D | 266820000 | 15626000 | 17281000 | 54385000 | 1656200 | 1318000 | 4.9 | 9.4 | 13.1 | **9.2** |

| Protein | Gene | | | | | | | | | | |
|---|---|---|---|---|---|---|---|---|---|---|---|
| Vimentin | VIM | 31943000000 | 1760000000 | 2503400000 | 1669700000 | 352010000 | 785990000 | 19.1 | 5.0 | 3.2 | **9.1** |
| Probable ATP-dependent RNA helicase DDX6 | DDX6 | 720930000 | 13592000 | 11137000 | 71173000 | 1656200 | 1318000 | 10.1 | 8.2 | 8.4 | **8.9** |
| Zinc finger CCCH domain-containing protein 11A | ZC3H11A | 9200300000 | 1270700000 | 846170000 | 425730000 | 488970000 | 384760000 | 21.6 | 2.6 | 2.2 | **8.8** |
| Cell division cycle protein 27 homolog | CDC27 | 354010000 | 8353600 | 1858200 | 17850000 | 1656200 | 1318000 | 19.8 | 5.0 | 1.4 | **8.8** |
| Arginine--tRNA ligase, cytoplasmic | RARS | 566770000 | 665920000 | 420120000 | 109410000 | 48439000 | 57312000 | 5.2 | 13.7 | 7.3 | **8.8** |
| Ubiquitin carboxyl-terminal hydrolase 7;Ubiquitin carboxyl-terminal hydrolase | USP7 | 624130000 | 52224000 | 42059000 | 29279000 | 17163000 | 23022000 | 21.3 | 3.0 | 1.8 | **8.7** |
| AP-3 complex subunit delta-1 | AP3D1 | 16632000 | 8013000 | 1858200 | 849090 | 1656200 | 1318000 | 19.6 | 4.8 | 1.4 | **8.6** |
| BRISC and BRCA1-A complex member 1 | BABAM1 | 361950000 | 97675 | 23725000 | 47653000 | 1656200 | 1318000 | 7.6 | 0.1 | 18.0 | **8.6** |
| Serine/threonine-protein phosphatase PP1-alpha catalytic subunit;Serine/threonine-protein phosphatase | PPP1CA | 319360000 | 23963000 | 7370300 | 58539000 | 1656200 | 1318000 | 5.5 | 14.5 | 5.6 | **8.5** |
| DnaJ homolog subfamily C member 13 | DNAJC13 | 18202000 | 4210200 | 1858200 | 849090 | 1656200 | 1318000 | 21.4 | 2.5 | 1.4 | **8.5** |
| Cyclin-dependent kinase 11B;Cyclin-dependent kinase 11A | CDK11B | 2056400000 | 27094000 | 1858200 | 271260000 | 1656200 | 1318000 | 7.6 | 16.4 | 1.4 | **8.4** |
| SWI/SNF-related matrix-associated actin-dependent regulator of chromatin subfamily E member 1 | SMARCE1 | 1701100000 | 7148100 | 13524000 | 124950000 | 4966900 | 1318000 | 13.6 | 1.4 | 10.3 | **8.4** |
| Small acidic protein | SMAP | 74302000 | 54726000 | 70684000 | 8390100 | 17750000 | 5303700 | 8.9 | 3.1 | 13.3 | **8.4** |
| YEATS domain-containing protein 2 | YEATS2 | 1984000000 | 43628000 | 54381000 | 92069000 | 20819000 | 42672000 | 21.5 | 2.1 | 1.3 | **8.3** |
| Charged multivesicular body protein 4b | CHMP4B | 1333500000 | 27192000 | 24819000 | 295610000 | 17266000 | 1318000 | 4.5 | 1.6 | 18.8 | **8.3** |
| COP9 signalosome complex subunit 5 | COPS5 | 436890000 | 9250700 | 7026000 | 31734000 | 1656200 | 1318000 | 13.8 | 5.6 | 5.3 | **8.2** |
| T-complex protein 1 subunit delta | CCT4 | 123270000 | 108080000 | 83327000 | 6982600 | 36375000 | 23473000 | 17.7 | 3.0 | 3.5 | **8.1** |
| PDZ and LIM domain protein 1 | PDLIM1 | 9214900000 | 1995300000 | 2024800000 | 1049000000 | 281580000 | 251560000 | 8.8 | 7.1 | 8.0 | **8.0** |
| 26S protease regulatory subunit 8 | PSMC5 | 450810000 | 23864000 | 1858200 | 56485000 | 1656200 | 1318000 | 8.0 | 14.4 | 1.4 | **7.9** |
| ATP-binding cassette sub-family E member 1 | ABCE1 | 17630000 | 97675 | 3455200 | 849090 | 1656200 | 1318000 | 20.8 | 0.1 | 2.6 | **7.8** |
| ADP-sugar pyrophosphatase | NUDT5 | 130120000 | 388680000 | 458910000 | 10759000 | 77073000 | 78695000 | 12.1 | 5.0 | 5.8 | **7.7** |
| Mitotic checkpoint protein BUB3 | BUB3 | 737070 | 15010000 | 17965000 | 4832800 | 1656200 | 1318000 | 0.2 | 9.1 | 13.6 | **7.6** |
| Plasma membrane calcium-transporting ATPase | ATP2B1 | 13803000 | 8528600 | 1858200 | 849090 | 1656200 | 1318000 | 16.3 | 5.1 | 1.4 | **7.6** |

1;Plasma membrane calcium-transporting ATPase 4

| Protein | Gene | | | | | | | | | | |
|---|---|---|---|---|---|---|---|---|---|---|---|
| Calmodulin-regulated spectrin-associated protein 2 | CAMSAP2 | 15689000 | 4551100 | 1858200 | 849090 | 1656200 | 1318000 | 18.5 | 2.7 | 1.4 | **7.5** |
| PC4 and SFRS1-interacting protein | PSIP1 | 228830000 | 21238000 | 16533000 | 28576000 | 11093000 | 1318000 | 8.0 | 1.9 | 12.5 | **7.5** |
| Serine/arginine-rich splicing factor 11 | SRSF11 | 11834000 | 10380000 | 8100300 | 849090 | 1656200 | 3665400 | 13.9 | 6.3 | 2.2 | **7.5** |
| Pericentriolar material 1 protein | PCM1 | 214190000 | 97675 | 12544000 | 16970000 | 1656200 | 1318000 | 12.6 | 0.1 | 9.5 | **7.4** |
| Bromodomain-containing protein 4 | BRD4 | 622630000 | 38129000 | 28978000 | 32731000 | 44728000 | 12883000 | 19.0 | 0.9 | 2.2 | **7.4** |
| WD repeat domain phosphoinositide-interacting protein 2 | WIPI2 | 737070 | 26925000 | 6309000 | 849090 | 1656200 | 1318000 | 0.9 | 16.3 | 4.8 | **7.3** |
| Exportin-5 | XPO5 | 11058000 | 12171000 | 1858200 | 849090 | 1656200 | 1318000 | 13.0 | 7.3 | 1.4 | **7.3** |
| Peptidyl-prolyl cis-trans isomerase FKBP4;Peptidyl-prolyl cis-trans isomerase FKBP4, N-terminally processed | FKBP4 | 1282700000 | 57244000 | 48197000 | 70232000 | 42543000 | 23108000 | 18.3 | 1.3 | 2.1 | **7.2** |
| Calponin-3 | CNN3 | 10088000000 | 1711900000 | 1647700000 | 1355900000 | 289410000 | 201180000 | 7.4 | 5.9 | 8.2 | **7.2** |
| BRCA1-associated protein | BRAP | 151410000 | 5875300 | 5165500 | 10964000 | 1656200 | 1318000 | 13.8 | 3.5 | 3.9 | **7.1** |
| Tubulin alpha-4A chain | TUBA4A | 254900000 | 32025000 | 32944000 | 29812000 | 6178100 | 4370700 | 8.6 | 5.2 | 7.5 | **7.1** |
| Cyclin-dependent kinase 2 | CDK2 | 410940000 | 49592000 | 18685000 | 129080000 | 13079000 | 1318000 | 3.2 | 3.8 | 14.2 | **7.1** |
| Double-strand break repair protein MRE11 | MRE11 | 3072900000 | 395960000 | 422060000 | 257830000 | 114920000 | 73574000 | 11.9 | 3.4 | 5.7 | **7.0** |
| Insulin-like growth factor 2 mRNA-binding protein 3 | IGF2BP3 | 256350000 | 27358000 | 24890000 | 36188000 | 3110400 | 4886700 | 7.1 | 8.8 | 5.1 | **7.0** |
| Pogo transposable element with ZNF domain | POGZ | 326430000 | 10526000 | 1858200 | 22702000 | 1656200 | 20183000 | 14.4 | 6.4 | 0.1 | **6.9** |
| DNA primase large subunit | PRIM2 | 1298700000 | 8382500 | 5557800 | 113210000 | 1656200 | 1318000 | 11.5 | 5.1 | 4.2 | **6.9** |
| Signal transducing adapter molecule 1 | STAM | 951870000 | 10578000 | 1858200 | 73840000 | 1656200 | 1318000 | 12.9 | 6.4 | 1.4 | **6.9** |
| Guanine nucleotide-binding protein-like 3 | GNL3 | 70538000 | 15645000 | 1858200 | 7182300 | 1656200 | 1318000 | 9.8 | 9.4 | 1.4 | **6.9** |
| AP-1 complex subunit beta-1 | AP1B1 | 364770000 | 97675 | 22529000 | 20899000 | 1656200 | 7708900 | 17.5 | 0.1 | 2.9 | **6.8** |
| Dihydrolipoyllysine-residue succinyltransferase component of 2-oxoglutarate dehydrogenase complex, mitochondrial | DLST | 12297000 | 97675 | 23491000 | 4859000 | 1656200 | 1318000 | 2.5 | 0.1 | 17.8 | **6.8** |
| Stromal membrane-associated protein 2 | SMAP2 | 261070000 | 97675 | 11658000 | 22802000 | 1656200 | 1318000 | 11.4 | 0.1 | 8.8 | **6.8** |
| Kanadaptin | SLC4A1AP | 1894600000 | 39209000 | 43341000 | 116480000 | 21097000 | 20885000 | 16.3 | 1.9 | 2.1 | **6.7** |

| | | | | | | | | | | |
|---|---|---|---|---|---|---|---|---|---|---|
| Poly(U)-binding-splicing factor PUF60 | PUF60 | 702670000 | 54195000 | 68643000 | 72824000 | 21045000 | 8662600 | 9.6 | 2.6 | 7.9 | **6.7** |
| Stress-induced-phosphoprotein 1 | STIP1 | 565300000 | 21488000 | 18737000 | 34921000 | 7862400 | 18200000 | 16.2 | 2.7 | 1.0 | **6.7** |
| 60S acidic ribosomal protein P0;60S acidic ribosomal protein P0-like | RPLP0 | 833170000 | 108950000 | 107500000 | 120230000 | 9774300 | 63097000 | 6.9 | 11.1 | 1.7 | **6.6** |
| Mitogen-activated protein kinase 9;Mitogen-activated protein kinase 10 | MAPK9 | 1059800000 | 11203000 | 7446200 | 153090000 | 1656200 | 1318000 | 6.9 | 6.8 | 5.6 | **6.4** |
| GTP-binding nuclear protein Ran | RAN | 737070 | 24833000 | 159760000 | 66123000 | 1656200 | 36997000 | 0.0 | 15.0 | 4.3 | **6.4** |
| Negative elongation factor E | NELFE | 572420000 | 63927000 | 44036000 | 190310000 | 14236000 | 3777700 | 3.0 | 4.5 | 11.7 | **6.4** |
| Biliverdin reductase A | BLVRA | 90766000 | 97675 | 8316200 | 7127300 | 1656200 | 1318000 | 12.7 | 0.1 | 6.3 | **6.4** |
| ATP-citrate synthase | ACLY | 33664000 | 25888000 | 13216000 | 2185400 | 8423100 | 24617000 | 15.4 | 3.1 | 0.5 | **6.3** |
| DnaJ homolog subfamily C member 7 | DNAJC7 | 554050000 | 5750900 | 5658900 | 49445000 | 1656200 | 1318000 | 11.2 | 3.5 | 4.3 | **6.3** |
| Nuclear pore complex protein Nup133 | NUP133 | 433160000 | 7258700 | 25972000 | 28151000 | 7151700 | 10379000 | 15.4 | 1.0 | 2.5 | **6.3** |
| Serine-threonine kinase receptor-associated protein | STRAP | 4081000000 | 290580000 | 252030000 | 575100000 | 42139000 | 58045000 | 7.1 | 6.9 | 4.3 | **6.1** |
| Transcription intermediary factor 1-beta | TRIM28 | 7039700000 | 283990000 | 252600000 | 502510000 | 160820000 | 104260000 | 14.0 | 1.8 | 2.4 | **6.1** |
| 5-3 exoribonuclease 2 | XRN2 | 6816400 | 97675 | 13292000 | 849090 | 4812300 | 1318000 | 8.0 | 0.0 | 10.1 | **6.0** |
| Puromycin-sensitive aminopeptidase | NPEPPS | 12264000 | 15226000 | 1858200 | 849090 | 4393600 | 29959000 | 14.4 | 3.5 | 0.1 | **6.0** |
| Hydroxyacyl-coenzyme A dehydrogenase, mitochondrial | HADH | 10565000 | 97675 | 7176600 | 849090 | 2881800 | 1318000 | 12.4 | 0.0 | 5.4 | **6.0** |
| FACT complex subunit SPT16 | SUPT16H | 108400000 | 44250000 | 42304000 | 7312800 | 18709000 | 58329000 | 14.8 | 2.4 | 0.7 | **6.0** |
| Lamina-associated polypeptide 2, isoforms beta/gamma;Thymopoietin;Thymopentin | TMPO | 2473600000 | 306500000 | 309280000 | 276460000 | 78723000 | 63670000 | 8.9 | 3.9 | 4.9 | **5.9** |
| Splicing factor 3B subunit 2 | SF3B2 | 6279400000 | 311360000 | 304440000 | 800680000 | 55736000 | 71799000 | 7.8 | 5.6 | 4.2 | **5.9** |
| Serine/threonine-protein phosphatase 6 regulatory subunit 2 | PPP6R2 | 801560000 | 10739000 | 12980000 | 601760000 | 1656200 | 1318000 | 1.3 | 6.5 | 9.8 | **5.9** |
| Importin-5 | IPO5 | 8655600 | 33030000 | 12202000 | 849090 | 5048400 | 14921000 | 10.2 | 6.5 | 0.8 | **5.9** |
| Nuclear pore complex protein Nup50 | NUP50 | 2089900000 | 201710000 | 267160000 | 327790000 | 29571000 | 62779000 | 6.4 | 6.8 | 4.3 | **5.8** |
| RNA-binding protein 26 | RBM26 | 7138300000 | 627450000 | 552090000 | 495810000 | 319300000 | 521650000 | 14.4 | 2.0 | 1.1 | **5.8** |
| Tubulin alpha-1B chain | TUBA1B | 63537000000 | 7299700000 | 7483000000 | 6918900000 | 1574800000 | 2099700000 | 9.2 | 4.6 | 3.6 | **5.8** |

| Protein | Gene | | | | | | | | | | |
|---|---|---:|---:|---:|---:|---:|---:|---:|---:|---:|---:|
| Kinesin-like protein KIF1A | KIF1A | 12726000 | 97675 | 3025400 | 849090 | 1656200 | 1318000 | 15.0 | 0.1 | 2.3 | **5.8** |
| Zinc finger protein 318 | ZNF318 | 1264200000 | 100030000 | 100280000 | 113050000 | 33174000 | 45476000 | 11.2 | 3.0 | 2.2 | **5.5** |
| Hepatoma-derived growth factor | HDGF | 225550000 | 97675 | 18747000 | 111760000 | 1656200 | 1318000 | 2.0 | 0.1 | 14.2 | **5.4** |
| Mediator of DNA damage checkpoint protein 1 | MDC1 | 4023200000 | 793840000 | 800170000 | 572430000 | 177830000 | 167640000 | 7.0 | 4.5 | 4.8 | **5.4** |
| Heterogeneous nuclear ribonucleoprotein Q | SYNCRIP | 406210000 | 37195000 | 79118000 | 38262000 | 11871000 | 33489000 | 10.6 | 3.1 | 2.4 | **5.4** |
| Vinculin | VCL | 193790000 | 14547000 | 14297000 | 30524000 | 1656200 | 14983000 | 6.3 | 8.8 | 1.0 | **5.4** |
| Ribonucleoside-diphosphate reductase subunit M2 | RRM2 | 24306000 | 2513600 | 4113200 | 2123500 | 1656200 | 1318000 | 11.4 | 1.5 | 3.1 | **5.4** |
| 40S ribosomal protein SA | RPSA | 404720000 | 55699000 | 45894000 | 265320000 | 4669200 | 18293000 | 1.5 | 11.9 | 2.5 | **5.3** |
| Parafibromin | CDC73 | 846440000 | 13897000 | 14347000 | 154480000 | 1656200 | 7080400 | 5.5 | 8.4 | 2.0 | **5.3** |
| RuvB-like 1 | RUVBL1 | 37936000000 | 3625300000 | 3320600000 | 4259400000 | 991680000 | 1008200000 | 8.9 | 3.7 | 3.3 | **5.3** |
| T-complex protein 1 subunit beta | CCT2 | 449950000 | 83207000 | 57682000 | 39732000 | 23897000 | 55687000 | 11.3 | 3.5 | 1.0 | **5.3** |
| Protein disulfide-isomerase A3 | PDIA3 | 909490000 | 178720000 | 203930000 | 87149000 | 64985000 | 77485000 | 10.4 | 2.8 | 2.6 | **5.3** |
| Pyruvate kinase PKM | PKM | 3281700000 | 741200000 | 805970000 | 327590000 | 198830000 | 404710000 | 10.0 | 3.7 | 2.0 | **5.2** |
| Peptidylprolyl isomerase domain and WD repeat-containing protein 1 | PPWD1 | 107150000 | 5152800 | 1858200 | 9761600 | 1656200 | 1318000 | 11.0 | 3.1 | 1.4 | **5.2** |
| 26S proteasome non-ATPase regulatory subunit 6 | PSMD6 | 28397000 | 19171000 | 22851000 | 15565000 | 1656200 | 11068000 | 1.8 | 11.6 | 2.1 | **5.2** |
| Serine/threonine-protein phosphatase 5;Serine/threonine-protein phosphatase | PPP5C | 737070 | 6873700 | 13662000 | 849090 | 1656200 | 1318000 | 0.9 | 4.2 | 10.4 | **5.1** |
| Serine/threonine-protein phosphatase 4 regulatory subunit 3A | SMEK1 | 3716100000 | 337840000 | 221430000 | 379760000 | 115260000 | 84728000 | 9.8 | 2.9 | 2.6 | **5.1** |
| Elongation factor 1-alpha 1;Putative elongation factor 1-alpha-like 3 | EEF1A1 | 48440000000 | 11085000000 | 12165000000 | 7991500000 | 2365900000 | 2663000000 | 6.1 | 4.7 | 4.6 | **5.1** |
| PDZ and LIM domain protein 3 | PDLIM3 | 4955400000 | 630370000 | 499760000 | 1092700000 | 138000000 | 80819000 | 4.5 | 4.6 | 6.2 | **5.1** |
| Actin-binding protein anillin | ANLN | 3043400000 | 223340000 | 122340000 | 285890000 | 97685000 | 52771000 | 10.6 | 2.3 | 2.3 | **5.1** |
| Calcyclin-binding protein | CACYBP | 737070 | 211760000 | 223470000 | 849090 | 25008000 | 37979000 | 0.9 | 8.5 | 5.9 | **5.1** |
| F-actin-capping protein subunit alpha-1 | CAPZA1 | 267540000 | 97675 | 10393000 | 37713000 | 1656200 | 1318000 | 7.1 | 0.1 | 7.9 | **5.0** |
| Inorganic pyrophosphatase | PPA1 | 35746000 | 14613000 | 13050000 | 7515500 | 1656200 | 9393800 | 4.8 | 8.8 | 1.4 | **5.0** |
| SWI/SNF-related matrix-associated actin-dependent | SMARCA5 | 1774600000 | 274280000 | 171260000 | 220400000 | 61707000 | 71049000 | 8.1 | 4.4 | 2.4 | **5.0** |

**regulator of chromatin subfamily A member 5**

| Protein | Gene | | | | | | | | | | |
|---|---|---|---|---|---|---|---|---|---|---|---|
| Cell division cycle 5-like protein | CDC5L | 946380000 | 41466000 | 69487000 | 79599000 | 70746000 | 29676000 | 11.9 | 0.6 | 2.3 | **4.9** |
| Chloride intracellular channel protein 1 | CLIC1 | 39728000 | 75712000 | 182390000 | 7597000 | 13555000 | 46077000 | 5.2 | 5.6 | 4.0 | **4.9** |
| UBX domain-containing protein 7 | UBXN7 | 779490000 | 9964400 | 6386900 | 93255000 | 6673700 | 1318000 | 8.4 | 1.5 | 4.8 | **4.9** |
| CWF19-like protein 1 | CWF19L1 | 521940000 | 97675 | 12959000 | 112710000 | 1656200 | 1318000 | 4.6 | 0.1 | 9.8 | **4.8** |
| TAR DNA-binding protein 43 | TARDBP | 1613500000 | 157900000 | 166180000 | 379630000 | 28386000 | 35821000 | 4.3 | 5.6 | 4.6 | **4.8** |
| Glutaredoxin-3 | GLRX3 | 208480000 | 3337500 | 1858200 | 19058000 | 1656200 | 1318000 | 10.9 | 2.0 | 1.4 | **4.8** |
| Craniofacial development protein 1 | CFDP1 | 621250000 | 92733000 | 151670000 | 315010000 | 118020000 | 13294000 | 2.0 | 0.8 | 11.4 | **4.7** |
| Acyl-CoA synthetase family member 4 | AASDH | 8323900 | 4595800 | 1858200 | 849090 | 1656200 | 1318000 | 9.8 | 2.8 | 1.4 | **4.7** |
| Serine/threonine-protein kinase 38 | STK38 | 2379700000 | 140870000 | 132200000 | 488160000 | 25985000 | 36631000 | 4.9 | 5.4 | 3.6 | **4.6** |
| Splicing factor, arginine/serine-rich 15 | SCAF4 | 199850000 | 9462000 | 5479500 | 50139000 | 1656200 | 1318000 | 4.0 | 5.7 | 4.2 | **4.6** |
| UV excision repair protein RAD23 homolog B | RAD23B | 229560000 | 4110000 | 4074200 | 27715000 | 1656200 | 1318000 | 8.3 | 2.5 | 3.1 | **4.6** |
| Coiled-coil domain-containing protein 174 | CCDC174 | 762270000 | 34433000 | 13281000 | 351700000 | 22588000 | 1318000 | 2.2 | 1.5 | 10.1 | **4.6** |
| Histone-lysine N-methyltransferase 2A;MLL cleavage product N320;MLL cleavage product C180 | KMT2A | 300650000 | 3083300 | 2829500 | 31037000 | 1656200 | 1318000 | 9.7 | 1.9 | 2.1 | **4.6** |
| Transcription initiation factor TFIID subunit 6 | TAF6 | 662420000 | 97675 | 24568000 | 73230000 | 12348000 | 5304900 | 9.0 | 0.0 | 4.6 | **4.6** |
| Unconventional prefoldin RPB5 interactor 1 | URI1 | 7307700 | 97675 | 6566100 | 849090 | 1656200 | 1318000 | 8.6 | 0.1 | 5.0 | **4.5** |
| Histone acetyltransferase type B catalytic subunit | HAT1 | 258560000 | 136060000 | 127470000 | 132500000 | 20631000 | 25195000 | 2.0 | 6.6 | 5.1 | **4.5** |
| T-complex protein 1 subunit eta | CCT7 | 326740000 | 45271000 | 58213000 | 32333000 | 18901000 | 80081000 | 10.1 | 2.4 | 0.7 | **4.4** |
| Peroxisomal multifunctional enzyme type 2;(3R)-hydroxyacyl-CoA dehydrogenase;Enoyl-CoA hydratase 2 | HSD17B4 | 4064800 | 4597700 | 7381600 | 849090 | 1656200 | 1318000 | 4.8 | 2.8 | 5.6 | **4.4** |
| Signal transducer and activator of transcription 3 | STAT3 | 2012500000 | 8267500 | 21593000 | 351210000 | 1656200 | 8968700 | 5.7 | 5.0 | 2.4 | **4.4** |
| Isocitrate dehydrogenase [NADP] cytoplasmic | IDH1 | 447740000 | 5117800 | 1858200 | 53587000 | 1656200 | 1318000 | 8.4 | 3.1 | 1.4 | **4.3** |
| Nuclear autoantigenic sperm protein | NASP | 13326000000 | 2874300000 | 1958300000 | 1856700000 | 858670000 | 921890000 | 7.2 | 3.3 | 2.1 | **4.2** |
| Hsc70-interacting protein;Putative protein FAM10A4;Putative protein FAM10A5 | ST13 | 163450000 | 55213000 | 60192000 | 43361000 | 8675000 | 27236000 | 3.8 | 6.4 | 2.2 | **4.1** |
| Heterogeneous nuclear ribonucleoprotein L | HNRNPL | 3414400000 | 304880000 | 450080000 | 554340000 | 128080000 | 120830000 | 6.2 | 2.4 | 3.7 | **4.1** |

| | | | | | | | | | | | |
|---|---|---|---|---|---|---|---|---|---|---|---|
| Nuclear receptor-binding factor 2 | NRBF2 | 200950000 | 14512000 | 1858200 | 99163000 | 1656200 | 1318000 | 2.0 | 8.8 | 1.4 | **4.1** |
| 5-nucleotidase domain-containing protein 1 | NT5DC1 | 668960000 | 17677000 | 17274000 | 104430000 | 7031100 | 5318300 | 6.4 | 2.5 | 3.2 | **4.1** |
| Poly(rC)-binding protein 2 | PCBP2 | 3207700000 | 524140000 | 611120000 | 537630000 | 186870000 | 187450000 | 6.0 | 2.8 | 3.3 | **4.0** |
| Heterogeneous nuclear ribonucleoprotein A3 | HNRNPA3 | 1942300000 | 156260000 | 54348000 | 875460000 | 61316000 | 7571000 | 2.2 | 2.5 | 7.2 | **4.0** |
| Uncharacterized protein GPALPP1 | GPALPP1 | 177440000 | 12167000 | 1858200 | 56093000 | 1656200 | 1318000 | 3.2 | 7.3 | 1.4 | **4.0** |
| Apoptosis-inducing factor 1, mitochondrial | AIFM1 | 737070 | 11338000 | 5454100 | 849090 | 1656200 | 1318000 | 0.9 | 6.8 | 4.1 | **4.0** |
| Heterogeneous nuclear ribonucleoprotein U | HNRNPU | 4377900000 | 883700000 | 1071900000 | 579190000 | 326640000 | 678100000 | 7.6 | 2.7 | 1.6 | **3.9** |
| Aspartate aminotransferase, mitochondrial;Aspartate aminotransferase | GOT2 | 33220000 | 65700000 | 70385000 | 4032800 | 32202000 | 66086000 | 8.2 | 2.0 | 1.1 | **3.8** |
| Ubiquitin-conjugating enzyme E2 O | UBE2O | 5568900 | 4063200 | 3064300 | 849090 | 1656200 | 1318000 | 6.6 | 2.5 | 2.3 | **3.8** |
| Calnexin | CANX | 161860000 | 33103000 | 19750000 | 28381000 | 9135400 | 9950700 | 5.7 | 3.6 | 2.0 | **3.8** |
| Vacuolar protein sorting-associated protein 72 homolog | VPS72 | 359360000 | 97675 | 4799600 | 48076000 | 1656200 | 1318000 | 7.5 | 0.1 | 3.6 | **3.7** |
| Eukaryotic translation initiation factor 3 subunit A | EIF3A | 87568000 | 48206000 | 7928400 | 19196000 | 9088600 | 8297300 | 4.6 | 5.3 | 1.0 | **3.6** |
| Protein phosphatase 1G | PPM1G | 609960000 | 83701000 | 17607000 | 91140000 | 25695000 | 24530000 | 6.7 | 3.3 | 0.7 | **3.6** |
| Rac GTPase-activating protein 1 | RACGAP1 | 206410000 | 9350700 | 1858200 | 57858000 | 1656200 | 1318000 | 3.6 | 5.6 | 1.4 | **3.5** |
| Spliceosome RNA helicase DDX39B | DDX39B | 1674500000 | 233360000 | 226930000 | 284420000 | 100380000 | 97988000 | 5.9 | 2.3 | 2.3 | **3.5** |
| DNA fragmentation factor subunit alpha | DFFA | 548620000 | 18431000 | 12164000 | 77391000 | 8049500 | 11718000 | 7.1 | 2.3 | 1.0 | **3.5** |
| Protein KNL1 | KNL1 | 627270000 | 22840000 | 7775800 | 300850000 | 9639200 | 1318000 | 2.1 | 2.4 | 5.9 | **3.5** |
| Acidic leucine-rich nuclear phosphoprotein 32 family member E | ANP32E | 1101300000 | 48194000 | 22526000 | 167190000 | 16160000 | 37086000 | 6.6 | 3.0 | 0.6 | **3.4** |
| Far upstream element-binding protein 2 | KHSRP | 1135100000 | 223090000 | 148110000 | 172100000 | 92329000 | 140620000 | 6.6 | 2.4 | 1.1 | **3.4** |
| Nuclear receptor coactivator 6 | NCOA6 | 256060000 | 3317700 | 2672200 | 35751000 | 3867600 | 1318000 | 7.2 | 0.9 | 2.0 | **3.3** |
| Voltage-dependent anion-selective channel protein 1 | VDAC1 | 127590000 | 30376000 | 89437000 | 21087000 | 35575000 | 29215000 | 6.1 | 0.9 | 3.1 | **3.3** |
| Poly(rC)-binding protein 1 | PCBP1 | 2682300000 | 1306900000 | 1118300000 | 1299000000 | 294750000 | 324170000 | 2.1 | 4.4 | 3.4 | **3.3** |
| Suppressor of G2 allele of SKP1 homolog | SUGT1 | 2575600000 | 133870000 | 938050000 | 456810000 | 202350000 | 258130000 | 5.6 | 0.7 | 3.6 | **3.3** |
| Polyadenylate-binding protein 1 | PABPC1 | 373250000 | 260660000 | 162780000 | 621220000 | 40030000 | 58143000 | 0.6 | 6.5 | 2.8 | **3.3** |

| Protein | Gene | | | | | | | | | | |
|---|---|---|---|---|---|---|---|---|---|---|---|
| Interleukin enhancer-binding factor 2 | ILF2 | 42930000 | 117190000 | 119860000 | 7644900 | 38896000 | 101990000 | 5.6 | 3.0 | 1.2 | **3.3** |
| Peptidyl-prolyl cis-trans isomerase-like 4 | PPIL4 | 1902600000 | 68365000 | 27155000 | 542950000 | 13624000 | 21994000 | 3.5 | 5.0 | 1.2 | **3.3** |
| Lysine-specific demethylase 3B | KDM3B | 313880000 | 3290800 | 3886100 | 42361000 | 1656200 | 12067000 | 7.4 | 2.0 | 0.3 | **3.2** |
| Aconitate hydratase, mitochondrial | ACO2 | 120180000 | 10871000 | 31541000 | 117800000 | 1656200 | 14962000 | 1.0 | 6.6 | 2.1 | **3.2** |
| Kinesin-like protein KIF23 | KIF23 | 516280000 | 3520600 | 7535900 | 162230000 | 5214400 | 1318000 | 3.2 | 0.7 | 5.7 | **3.2** |
| Synaptojanin-1 | SYNJ1 | 5220400 | 3309000 | 1858200 | 849090 | 1656200 | 1318000 | 6.1 | 2.0 | 1.4 | **3.2** |
| ATP-dependent RNA helicase DDX39A | DDX39A | 56909000 | 97675 | 7009400 | 13996000 | 1656200 | 1318000 | 4.1 | 0.1 | 5.3 | **3.1** |
| Importin-7 | IPO7 | 654360000 | 70481000 | 75835000 | 113230000 | 34774000 | 47794000 | 5.8 | 2.0 | 1.6 | **3.1** |
| Cyclin-dependent kinase 7 | CDK7 | 362260000 | 97675 | 6392600 | 80988000 | 1656200 | 1318000 | 4.5 | 0.1 | 4.9 | **3.1** |
| Ran-binding protein 3 | RANBP3 | 1331600000 | 215990000 | 166220000 | 867360000 | 48098000 | 49839000 | 1.5 | 4.5 | 3.3 | **3.1** |
| Heat shock protein HSP 90-beta | HSP90AB1 | 3949100000 | 1779200000 | 1835400000 | 701690000 | 801400000 | 1236900000 | 5.6 | 2.2 | 1.5 | **3.1** |
| Transferrin receptor protein 1;Transferrin receptor protein 1, serum form | TFRC | 6100200 | 97675 | 2642500 | 849090 | 1656200 | 1318000 | 7.2 | 0.1 | 2.0 | **3.1** |
| Four and a half LIM domains protein 1 | FHL1 | 878150000 | 47935000 | 193020000 | 178020000 | 51777000 | 59480000 | 4.9 | 0.9 | 3.2 | **3.0** |
| Ubiquitin fusion degradation protein 1 homolog | UFD1 | 85487000 | 3788700 | 1858200 | 16022000 | 1656200 | 1318000 | 5.3 | 2.3 | 1.4 | **3.0** |
| Eukaryotic initiation factor 4A-I | EIF4A1 | 882820000 | 233030000 | 196920000 | 393110000 | 42716000 | 147890000 | 2.2 | 5.5 | 1.3 | **3.0** |
| Heterogeneous nuclear ribonucleoprotein A0 | HNRNPA0 | 1252000000 | 45047000 | 54031000 | 293250000 | 16069000 | 28628000 | 4.3 | 2.8 | 1.9 | **3.0** |
| Putative pre-mRNA-splicing factor ATP-dependent RNA helicase DHX16 | DHX16 | 54510000 | 5459200 | 1858200 | 13013000 | 1656200 | 1318000 | 4.2 | 3.3 | 1.4 | **3.0** |
| Heterogeneous nuclear ribonucleoprotein M | HNRNPM | 3326200000 | 778080000 | 769530000 | 1223600000 | 209600000 | 316460000 | 2.7 | 3.7 | 2.4 | **3.0** |
| Polypyrimidine tract-binding protein 1 | PTBP1 | 1274500000 | 257560000 | 318940000 | 277680000 | 85405000 | 260190000 | 4.6 | 3.0 | 1.2 | **2.9** |
| Crk-like protein | CRKL | 444250000 | 83862000 | 69140000 | 499580000 | 16131000 | 25309000 | 0.9 | 5.2 | 2.7 | **2.9** |
| Importin subunit alpha-1 | KPNA2 | 91339000 | 9761200 | 38985000 | 16309000 | 11512000 | 16927000 | 5.6 | 0.8 | 2.3 | **2.9** |
| Malate dehydrogenase, mitochondrial;Malate dehydrogenase | MDH2 | 111910000 | 60938000 | 45095000 | 26813000 | 16404000 | 59730000 | 4.2 | 3.7 | 0.8 | **2.9** |
| Poly(A) polymerase alpha | PAPOLA | 4864600000 | 1096000000 | 820530000 | 1183700000 | 431520000 | 423270000 | 4.1 | 2.5 | 1.9 | **2.9** |
| Amyloid beta A4 precursor protein-binding family B member 1 | APBB1 | 318420000 | 2300000 | 5810100 | 115360000 | 1656200 | 1318000 | 2.8 | 1.4 | 4.4 | **2.9** |

| Protein | Gene | | | | | | | | | | |
|---|---|---|---|---|---|---|---|---|---|---|---|
| Spindle and kinetochore-associated protein 3 | SKA3 | 877150000 | 97675 | 7620600 | 325680000 | 1656200 | 1318000 | 2.7 | 0.1 | 5.8 | **2.8** |
| Putative pre-mRNA-splicing factor ATP-dependent RNA helicase DHX15 | DHX15 | 1796300000 | 240610000 | 174580000 | 399750000 | 95657000 | 114700000 | 4.5 | 2.5 | 1.5 | **2.8** |
| Heat shock protein HSP 90-alpha | HSP90AA1 | 575620000 | 948010000 | 887220000 | 105200000 | 461700000 | 882630000 | 5.5 | 2.1 | 1.0 | **2.8** |
| Replication factor C subunit 4 | RFC4 | 1510200000 | 42723000 | 59284000 | 392810000 | 16748000 | 29027000 | 3.8 | 2.6 | 2.0 | **2.8** |
| Centrosomal protein of 44 kDa | CEP44 | 475010000 | 97675 | 7868100 | 210440000 | 1656200 | 1318000 | 2.3 | 0.1 | 6.0 | **2.8** |
| DnaJ homolog subfamily B member 1 | DNAJB1 | 2125900000 | 186940000 | 253970000 | 1089800000 | 67526000 | 71930000 | 2.0 | 2.8 | 3.5 | **2.7** |
| TATA-binding protein-associated factor 2N | TAF15 | 1462400000 | 131080000 | 109890000 | 471520000 | 56487000 | 39558000 | 3.1 | 2.3 | 2.8 | **2.7** |
| Heterogeneous nuclear ribonucleoproteins A2/B1 | HNRNPA2B1 | 13959000000 | 510820000 | 721470000 | 3204300000 | 233110000 | 445060000 | 4.4 | 2.2 | 1.6 | **2.7** |
| Nucleolin | NCL | 17877000000 | 2052800000 | 2415800000 | 4401900000 | 950860000 | 1265900000 | 4.1 | 2.2 | 1.9 | **2.7** |
| Integrin-linked kinase-associated serine/threonine phosphatase 2C | ILKAP | 1420000000 | 208710000 | 131170000 | 392070000 | 62715000 | 112460000 | 3.6 | 3.3 | 1.2 | **2.7** |
| Prohibitin | PHB | 737070 | 153970000 | 137940000 | 849090 | 37317000 | 44790000 | 0.9 | 4.1 | 3.1 | **2.7** |
| Phosphoglycerate mutase 1 | PGAM1 | 219900000 | 355750000 | 386780000 | 75726000 | 106820000 | 216210000 | 2.9 | 3.3 | 1.8 | **2.7** |
| SAP domain-containing ribonucleoprotein | SARNP | 115620000 | 30214000 | 1858200 | 32349000 | 7207300 | 7769900 | 3.6 | 4.2 | 0.2 | **2.7** |
| Protein-L-isoaspartate(D-aspartate) O-methyltransferase;Protein-L-isoaspartate O-methyltransferase | PCMT1 | 737070 | 60144000 | 45718000 | 849090 | 14350000 | 15758000 | 0.9 | 4.2 | 2.9 | **2.7** |
| Alpha-enolase | ENO1 | 3712600000 | 1911300000 | 1704200000 | 859650000 | 846010000 | 1582200000 | 4.3 | 2.3 | 1.1 | **2.6** |
| Proliferating cell nuclear antigen | PCNA | 737070 | 31574000 | 39825000 | 3990300 | 6164800 | 17370000 | 0.2 | 5.1 | 2.3 | **2.5** |
| UPF0552 protein ARPIN | ARPIN | 737070 | 164080000 | 98048000 | 5111400 | 32644000 | 42456000 | 0.1 | 5.0 | 2.3 | **2.5** |
| Apoptosis inhibitor 5 | API5 | 1932900000 | 81480000 | 1858200 | 376330000 | 36361000 | 19778000 | 5.1 | 2.2 | 0.1 | **2.5** |
| DNA-(apurinic or apyrimidinic site) lyase;DNA-(apurinic or apyrimidinic site) lyase, mitochondrial | APEX1 | 29472000 | 6274400 | 1858200 | 13897000 | 1656200 | 1318000 | 2.1 | 3.8 | 1.4 | **2.4** |
| Voltage-dependent anion-selective channel protein 2 | VDAC2 | 36815000 | 86195000 | 90425000 | 14714000 | 41183000 | 34023000 | 2.5 | 2.1 | 2.7 | **2.4** |
| Sex comb on midleg-like protein 2 | SCML2 | 3257500000 | 512170000 | 503640000 | 982510000 | 306960000 | 247450000 | 3.3 | 1.7 | 2.0 | **2.3** |
| Phosphorylated adapter RNA export protein | PHAX | 1230900000 | 88764000 | 79471000 | 357590000 | 38179000 | 70847000 | 3.4 | 2.3 | 1.1 | **2.3** |

| Protein | Gene | | | | | | | | | | |
|---|---|---|---|---|---|---|---|---|---|---|---|
| Splicing factor 1 | SF1 | 2102300000 | 265620000 | 54193000 | 947100000 | 62591000 | 131690000 | 2.2 | 4.2 | 0.4 | **2.3** |
| L-lactate dehydrogenase B chain;L-lactate dehydrogenase | LDHB | 1291600000 | 2992400000 | 2790900000 | 415830000 | 1208800000 | 2193100000 | 3.1 | 2.5 | 1.3 | **2.3** |
| Heat shock 70 kDa protein 6 | HSPA6 | 1519700000 | 944580000 | 679090000 | 1315600000 | 261950000 | 326020000 | 1.2 | 3.6 | 2.1 | **2.3** |
| PEST proteolytic signal-containing nuclear protein | PCNP | 737070 | 608610000 | 822020000 | 849090 | 175920000 | 344300000 | 0.9 | 3.5 | 2.4 | **2.2** |
| DnaJ homolog subfamily C member 9 | DNAJC9 | 193430000 | 13183000 | 1858200 | 71652000 | 5079400 | 1318000 | 2.7 | 2.6 | 1.4 | **2.2** |
| Exosome complex component RRP45 | EXOSC9 | 117880000 | 28188000 | 10368000 | 45485000 | 9455700 | 10121000 | 2.6 | 3.0 | 1.0 | **2.2** |
| Protein disulfide-isomerase A6 | PDIA6 | 147340000 | 4692600 | 25110000 | 54703000 | 1656200 | 25368000 | 2.7 | 2.8 | 1.0 | **2.2** |
| Pleiotropic regulator 1 | PLRG1 | 1379200000 | 79756000 | 27984000 | 532620000 | 23350000 | 56411000 | 2.6 | 3.4 | 0.5 | **2.2** |
| Heat shock 70 kDa protein 1A/1B | HSPA1A | 37658000000 | 17242000000 | 16337000000 | 15976000000 | 7794300000 | 8560900000 | 2.4 | 2.2 | 1.9 | **2.2** |
| Heterogeneous nuclear ribonucleoprotein A1;Heterogeneous nuclear ribonucleoprotein A1-like 2 | HNRNPA1 | 7078000000 | 1810200000 | 1307200000 | 2536900000 | 700470000 | 1207300000 | 2.8 | 2.6 | 1.1 | **2.2** |
| Proteasome activator complex subunit 3 | PSME3 | 80572000 | 97675 | 13901000 | 18806000 | 6080100 | 6643000 | 4.3 | 0.0 | 2.1 | **2.1** |
| Heterogeneous nuclear ribonucleoprotein A/B | HNRNPAB | 906620000 | 19445000 | 71816000 | 257840000 | 26796000 | 33588000 | 3.5 | 0.7 | 2.1 | **2.1** |
| WD repeat-containing protein 70 | WDR70 | 956670000 | 105050000 | 151310000 | 535140000 | 46197000 | 65355000 | 1.8 | 2.3 | 2.3 | **2.1** |
| Serine/threonine-protein kinase greatwall | MASTL | 1068400000 | 94675000 | 68752000 | 507020000 | 39963000 | 36854000 | 2.1 | 2.4 | 1.9 | **2.1** |
| Heterogeneous nuclear ribonucleoprotein F;Heterogeneous nuclear ribonucleoprotein F, N-terminally processed | HNRNPF | 160400000 | 68369000 | 26049000 | 67676000 | 19418000 | 89031000 | 2.4 | 3.5 | 0.3 | **2.1** |
| Elongation factor 2 | EEF2 | 1169300000 | 366150000 | 451450000 | 487510000 | 232210000 | 205110000 | 2.4 | 1.6 | 2.2 | **2.1** |
| Creatine kinase B-type | CKB | 259330000 | 235490000 | 296630000 | 102510000 | 120060000 | 177240000 | 2.5 | 2.0 | 1.7 | **2.1** |
| 60 kDa heat shock protein, mitochondrial | HSPD1 | 394820000 | 861210000 | 820570000 | 149000000 | 334110000 | 927740000 | 2.6 | 2.6 | 0.9 | **2.0** |
| Tuftelin-interacting protein 11 | TFIP11 | 2010400000 | 106690000 | 121680000 | 907960000 | 67471000 | 54050000 | 2.2 | 1.6 | 2.3 | **2.0** |
| G patch domain and KOW motifs-containing protein | GPKOW | 2586200000 | 72476000 | 25434000 | 790270000 | 33721000 | 46293000 | 3.3 | 2.1 | 0.5 | **2.0** |
| Eukaryotic initiation factor 4A-III;Eukaryotic initiation factor 4A-III, N-terminally processed | EIF4A3 | 156480000 | 17418000 | 32051000 | 134820000 | 8400300 | 12649000 | 1.2 | 2.1 | 2.5 | **1.9** |
| T-complex protein 1 subunit gamma | CCT3 | 423980000 | 39449000 | 71316000 | 429880000 | 18575000 | 27193000 | 1.0 | 2.1 | 2.6 | **1.9** |

| | | | | | | | | | | |
|---|---|---|---|---|---|---|---|---|---|---|
| Replication protein A 70 kDa DNA-binding subunit;Replication protein A 70 kDa DNA-binding subunit, N-terminally processed | RPA1 | 2265200000 | 217710000 | 193870000 | 1103300000 | 135900000 | 94456000 | 2.1 | 1.6 | 2.1 | **1.9** |
| Rho GDP-dissociation inhibitor 1 | ARHGDIA | 737070 | 26664000 | 35883000 | 849090 | 11302000 | 15741000 | 0.9 | 2.4 | 2.3 | **1.8** |
| ADP/ATP translocase 2;ADP/ATP translocase 2, N-terminally processed | SLC25A5 | 737070 | 66944000 | 109080000 | 849090 | 30783000 | 48797000 | 0.9 | 2.2 | 2.2 | **1.8** |
| Zinc finger protein 207 | ZNF207 | 1400900000 | 80703000 | 18731000 | 548010000 | 34113000 | 65307000 | 2.6 | 2.4 | 0.3 | **1.7** |
| DnaJ homolog subfamily C member 8 | DNAJC8 | 792050000 | 72191000 | 21944000 | 333860000 | 35469000 | 31185000 | 2.4 | 2.0 | 0.7 | **1.7** |
| Sideroflexin-1 | SFXN1 | 737070 | 18845000 | 39019000 | 849090 | 9084600 | 18597000 | 0.9 | 2.1 | 2.1 | **1.7** |

# Contributed publications

**Contributed Publications**

**Bozal-Basterra, L.,** Gonzalez-Santamarta, M., Bermejo-Arteagabeitia, A., Martín, N., Carracedo, A., Barrio, R. and Sutherland, J.D. (2018) Changes in LUZP1, a regulator of primary cilia and the actin cytoskeleton, contribute to Townes-Brocks Syndrome (submitted).

**ABSTRACT**

Townes-Brocks Syndrome (TBS) is a rare disease characterized by a spectrum of malformations in digits, ears, heart and kidneys, symptoms that are also found in many human ciliopathies. TBS patient-derived fibroblasts display longer and more frequent cilia compared to controls. TBS is caused by mutations in SALL1 gene, which often lead to expression of a truncated protein that interferes with the normal function of the cell. Here, we show that truncated SALL1 interacts with the leucine-zipper containing protein LUZP1, leading to its degradation, placing LUZP1 as a mediator of TBS symptoms. We demonstrate that LUZP1 localizes to the centrosome, actin cytoskeleton, and midbody. CRISPR/Cas9-mediated loss of LUZP1 in mouse fibroblasts changes actin dynamics and cell migration, while facilitating ciliogenesis and altering Sonic Hedgehog signaling. Given its localization to both actin stress fibers and the centrosome, LUZP1 might be a key factor for integrating cytoskeletal changes to cilia formation and function. Disruption of LUZP1 function may be a contributing factor to TBS, opening a possibility for pharmacological intervention by cytoskeletal modulators.

**ABSTRACT**

Townes-Brocks syndrome (TBS) is characterized by a spectrum of malformations in the digits, ears, and kidneys. These anomalies overlap those seen in a growing number of ciliopathies, which are genetic syndromes linked to defects in the formation or function of the primary cilia. TBS is caused by mutations in the gene encoding the transcriptional repressor SALL1 and is associated with the presence of a truncated protein that localizes to the cytoplasm. Here, we provide evidence that SALL1 mutations might cause TBS by means beyond its transcriptional capacity. By using proximity proteomics, we show that truncated SALL1 interacts with factors related to cilia function, including the negative regulators of ciliogenesis CCP110 and CEP97. This most likely contributes to more frequent cilia formation in TBS-derived fibroblasts, as well as in a CRISPR/Cas9-generated model cell line and in TBS-modeled mouse embryonic fibroblasts, than in wild-type controls. Furthermore, TBS-like cells show changes in cilia length and disassembly rates in combination with aberrant SHH signalling transduction. These findings support the hypothesis that aberrations in primary cilia and SHH signalling are contributing factors in TBS phenotypes, representing a paradigm shift in understanding TBS etiology. These results open possibilities for the treatment of TBS.

Torrano, V., Valcarcel-Jimenez, … **Bozal-Basterra, L**., *et al.* (2016). The metabolic co-regulator PGC1α suppresses prostate cancer metastasis. Nature Cell Biology (18), 645-656.

**ABSTRACT**

Cellular transformation and cancer progression is accompanied by changes in the metabolic landscape. Master co-regulators of metabolism orchestrate the modulation of multiple metabolic pathways through transcriptional programs, and hence constitute a probabilistically parsimonious mechanism for general metabolic rewiring. Here we show that the transcriptional co-activator peroxisome proliferator-activated receptor gamma co-activator 1α (PGC1α) suppresses prostate cancer progression and metastasis. A metabolic co-regulator data mining analysis unveiled that PGC1α is downregulated in prostate cancer and associated with disease progression. Using genetically engineered mouse models and xenografts, we demonstrated that PGC1α opposes prostate cancer progression and metastasis. Mechanistically, the use of integrative metabolomics and transcriptomics revealed that PGC1α activates an oestrogen-related receptor alpha (ERRα)-dependent transcriptional program to elicit a catabolic state and metastasis suppression. Importantly, a signature based on the PGC1α-ERRα pathway exhibited prognostic potential in prostate cancer, thus uncovering the relevance of monitoring and manipulating this pathway for prostate cancer stratification and treatment.

Schaafsma, W., **Bozal-Basterra, L.**, Jacobs, S., Brouwer, N., Meerlo, P., Schaafsma, A., Bodekke, E.W.G.M., Eggen, B. J. L. (2017). Maternal inflammation induces immune activation of fetal microglia and leads to disrupted microglia immune responses, behavior, and learning performance in adulthood. Neurobiology of disease (106), 291-300.

**ABSTRACT**

Maternal inflammation during pregnancy can have detrimental effects on embryonic development that persist during adulthood. However, the underlying mechanisms and insights in the responsible cell types are still largely unknown. Here we report the effect of maternal inflammation on fetal microglia, the innate immune cells of the central nervous system (CNS). In mice, a challenge with LPS during late gestation stages (days 15-16-17) induced a pro-inflammatory response in fetal microglia. Adult whole brain microglia of mice that were exposed to LPS during embryonic development displayed a persistent reduction in pro-inflammatory activation in response to a re-challenge with LPS. In contrast, hippocampal microglia of these mice displayed an increased inflammatory response to an LPS re-challenge. In addition, a reduced expression of brain-derived neurotrophic factor (BDNF) was observed in hippocampal microglia of LPS-offspring. Microglia-derived BDNF has been shown to be important for learning and memory processes. In line with these observations, behavioral- and learning tasks with mice that were exposed to maternal inflammation revealed reduced home cage activity, reduced anxiety and reduced learning performance in a T-maze. These data show that exposure to maternal inflammation during late gestation results in long term changes in microglia responsiveness during adulthood, which is different in nature in hippocampus compared to total brain microglia.

**Resumen versión extendida**

Introducción

El síndrome de Townes-Brocks (TBS, MIM: 107480) se caracteriza por, al menos, dos de estos fenotipos principales: ano imperforado, orejas displásicas y malformaciones del pulgar (pulgares trifalángicos, polidactilia preaxial e hipoplasia del pulgar). TBS también suele asociarse con otros síntomas menos frecuentes como la deficiencia auditiva neurosensorial y/o conductiva, malformaciones del pie, insuficiencia renal (incluyendo los riñones poliquísticos), junto con malformaciones genitourinarias y cardiopatía congenita. Aunque más atípicos, también se puede observar disfuncionalidad intelectual, retrasos en el crecimiento, paladar hendido y defectos oculares.

TBS está causado por mutaciones en el gen que codifica el represor transcripcional SALL1 que, mayoritariamente, dan lugar a una proteína truncada que se localiza en el citoplasma. Existen cuatro genes *SALL* en mamíferos, *SALL1-4*. Estudios anteriores han demostrado que ratones con mutaciones dobles/triples en *Sall1/Sall2/Sall4* exhiben defectos en el tubo neural y hendidura palatina.

TBS está considerada como una enfermedad genética rara. La investigación llevada a cabo hasta ahora se ha centrado en la función de SALL1 en el núcleo y en la perturbación de dicha función nuclear en la regulación transcripcional como posible causas de TBS. Hemos observado que los síntomas de TBS se incluyen dentro del espectro observado en una clase emergente de enfermedades denominadas "ciliopatías". Éstas son en su mayoría síndromes genéticos raros causados por la disfunción del cilio primario. Los cilios son estructuras basadas en microtúbulos que se originan a raíz de dos estructuras con forma de barril, los centríolos. Durante el desarrollo, la generación e interpretación de gradientes morfogénicos tales como Wnt, TGFbeta o Hedgehog (Hh) son esenciales para la correcta formación del organismo. Entre todas estas funciones, la vía de Sonic hedgehog (Shh) juega un papel importante en la formación de dígitos durante el desarrollo de las extremidades. Se ha demostrado que la señalización por Shh requiere la presencia del cilio primario en vertebrados.

Las características comunes entre las ciliopatías y TBS podrían sugerir causas

moleculares similares. Por lo tanto, nos planteamos la hipótesis de que defectos en la formación y/o función de los cilios primarios podrían contribuir al desarrollo de TBS e iniciamos el estudio de la formación y función de los cilios primarios en TBS. Para ello nos marcamos los objetivos detallados a continuación.

## Objetivos

**1. Analizar el papel de SALL1 en la formación y función de los cilios.**

Obtuvimos células derivadas de pacientes con TBS y generamos líneas celulares modelo de TBS para analizar el efecto de proteínas SALL1 truncadas en la ciliogénesis y la función de los cilios.

**2. Identificar los mecanismos celulares y moleculares que median los defectos de los cilios observados en TBS.**

Con el fin de identificar mediadores de los defectos relacionadas con los cilios detectados en TBS, utilizamos el método de proteómica de proximidad, BioID, para identificar interactores de la proteína SALL1 truncada. Los candidatos seleccionados se estudiaron en relación con los cilios y/o centrosomas en el contexto de TBS.

## Materiales y Métodos

El trabajo aquí presentado se llevó a cabo en células en cultivo, tanto de líneas celulares como de células derivadas de tejidos primarios de ratón y humano. Además, generaron líneas celulares modelo mediante el uso de la tecnología CRISPR/Cas9. Por otro lado, se emplearon técnicas de biología molecular tales como la extracción de RNA, qRT-PCR, western blot, BioID e immunoprecipitaciones. También se llevaron a cabo ensayos de actividad reportera, de espectrometría de masas así como análisis con microscopía de inmunofluorescencia, con citometría de flujo y análisis de proliferación y migración.

## Resultados

**Objetivo 1. Analizar el papel de SALL1 en la formación y función de los cilios.**

1.1 La proteína SALL1 truncada expresada en los pacientes de TBS altera la localización subcelular de *full-length* SALL1.

En este trabajo hemos caracterizado la localización nuclear y ciliar de *full-*

*length* SALL1 (SALL1^FL) tanto en células humanas como de ratón por inmunofluorescencia. Sin embargo, observamos que en células derivadas de pacientes de TBS, SALL1^FL se localizaba difusamente entre el núcleo y el citoplasma, siendo su expresión más reducida en el cilio comparado con células control. Para comprobar que dicho cambio en la localización de SALL1^FL estaba mediado por la proteína truncada, sobrexpresamos la proteína SALL1 truncada junto con SALL1^FL en células U2OS. Corroboramos que, cuando ambas formas se expresaban en combinación, SALL1^FL colocalizaba con la proteína truncada, demostrando que esta última secuestra a SALL1^FL del núcleo y la arrastra al citoplasma.

## 1.2 Los fibroblastos de paciente de Townes-Brocks (TBS) muestran defectos en el cilio primario en comparación con células de donante control.

Mediante la reducción de nutrientes durante 24 ó 48h para inducir la ciliogénesis, se llevó a cabo la visualización del cilio primario mediante inmunofluorescencia con marcadores del cuerpo basal y del axonema ciliar. Se observó que los fibroblastos del paciente de TBS muestran una mayor frecuencia de ciliación así como cilios primarios de mayor longitud en comparación con el individuo control. Estas diferencias son significativas en todas las series temporales de inducción de la ciliogénesis.

Dado que la vía de señalización de Shh depende de la presencia del cilio primario funcional, analizamos cómo responden a la activación por Shh las células procedentes del paciente de TBS y de dos individuos control. Observamos que la activación basal de la vía Shh era significativamente menor en células TBS que en las control. Sin embargo, las células TBS mostraban hipersensibilidad ante la activación de la vía y, como consecuencia, una alteración en la funcionalidad del cilio primario.

## 1.3 Los modelos celulares de TBS reproducen los defectos en la ciliogénesis observados en las células derivadas de TBS.

Para confirmar los defectos en la ciliogénesis que presentaban las células derivadas de pacientes de TBS, se caracterizaró y analizó la ciliogénisis en los siguientes modelos celulares de TBS:

- Células humanas RPEI sobrexpresando *SALL1* mutada.

- Células derivadas del modelo de ratón TBS (*Sall1*$^{+/\Delta}$).

- HEK 293FT modificadas con la tecnología CRISPR/Cas9 para generar una mutación en la región de SALL1 generalmente presente en la mayor parte de los pacientes de TBS (293[335]).

En todos los casos, los citados modelos celulares presentaron cilios más largos y un mayor índice de ciliación en comparación con las células control, confirmando los resultados previamente observados en células derivadas de paciente de TBS.

**Objetivo 2. Identificar los mecanismos celulares y moleculares que median los defectos de los cilios observados en TBS.**

2.1 Análsis de los reguladores negativos de ciliogénesis CCP110 y CEP97 en el centriolo madre de fibroblastos derivados de TBS y fibroblastos control.

Mediante el método BioID, identificamos dos proteínas centrosomales encargadas de bloquear la ciliogénesis, CEP97 y CCP110, que se encontraron mayoritaria o exclusivamente asociadas a SALL1 truncado. Dado que se sabe que la degradación de CCP110 y CEP97 en el centriolo madre (CM) que da lugar al cilio es determinate para la iniciación de la ciliogénesis, analizamos la expresión de ambas proteínas exclusivamente a nivel del CM. Los resultados mostraron que CCP110 ni CEP97 no se localizan en CM de las células de TBS en un porcentaje mayor que las células control incluso antes de inducir la ciliogénesis y, por tanto, el proceso de ciliogénesis se encuentra desinhibido. Estos resultados concuerdan con experimentos previos en los que observamos una formación prematura de cilios primarios en células de paciente de TBS en comparación con células control. La desaparición prematura de CCP110 del CM se confirmó también en células *Sall1*$^{+/\Delta}$ y en 293[335] comparadas con sus controles.

2.2 Caracterización de LUZP1 en células TBS.

Mediante el método BioID, identificamos también a LUZP1 como una proteína asociada exclusivamente a SALL1 truncado. La función molecular de LUZP1 se desconocía hasta este trabajo. Observamos que LUZP1 se localiza en el

centrosoma, en el citoesqueleto de actina y en el cuerpo medio o *midbody*. Descubrimos que la degradación de LUZP1 en el CM es determinate para la iniciación de la ciliogénesis y analizamos su expresión en células de pacientes TBS y control. Nuestros resultados mostraron que en las células TBS LUZP1 no se localiza en el CM en un porcentaje mayor que las células control incluso antes de inducir la ciliogénesis y, por tanto, el proceso de ciliogénesis está desinhibido. Dada la reducción tanto de los niveles totales de LUZP1 como de fibras de actina, estos resultados concuerdan con experimentos previos en los que observamos una formación prematura de cilios primarios en células de paciente de TBS en comparación con células control.

## 2.3 Interacción de la proteína LUZP1 con proteínas centrosomales y asociadas al citoesqueleto de actina

Para corroborar la localización observada en células de pacientes de TBS, se observó mediante un análisis de Pull Down usando la resina GFPtrap la interacción directa de LUZP1 con las proteínas centrosomales CCP110 y CEP97 y proteínas relacionadas con el citoesqueleto celular FLNA y beta actina.

## 2.4 Análisis del cilio primario y la vía de señalización Shh en fibroblastos derivados de embriones de ratón en ausencia de LUZP1.

Para estudiar la función molecular de *Luzp1*, modificamos fibroblastos embrionarios de ratón para obtener células *knock out* (Luzp1$^{-/-}$). Tras genotipar dichos fibroblastos, comparamos tanto la longitud del cilio como la frecuencia de ciliación con células de ratones control (Luzp1$^{+/+}$). En consistencia con los datos obtenidos en células humanas TBS en las que los niveles de LUZP1 se encontraban reducidos, los fibroblastos de ratones Luzp1$^{-/-}$ presentaron cilios más largos y un mayor índice de ciliación en comparación con las células control. Estos defectos en la ciliogénesis fueron rescatados mediante la sobrexpresión de *LUZP1* humano en las células Luzp1$^{-/-}$ (+LUZP1). Además, se observaron defectos en la señalización de la vía Shh en las células mutantes.

## 2.5 Análisis de la proliferación, migración e invasión celular en ausencia de LUZP1.

Durante la cuantificación de los cilios, se observó que las células Luzp1$^{-/-}$ presentan un porcentaje significativamente mayor de centriolos múltiples y unos núcleos significativamente más grandes respecto a las control. Estos defectos pueden ser indicativos de fallos en la proliferación o división celular. Mediante cristal violeta, se observó una menor proliferación de las células Luzp1$^{-/-}$ en comparación con las células Luzp1$^{+/+}$. Curiosamente, las células Luzp1$^{-/-}$ mostraron una mayor capacidad de migración e invasión celular que las células Luzp1$^{+/+}$. Estos defectos en la migración e invasión celular fueron rescatados mediante la sobrexpresión de *LUZP1* en las células Luzp1$^{-/-}$. Por último, nuestros resultados preliminares mostraron que los mediadores de la polimerización de la actina Arp2/3 y cofilina están alterados en células Luzp1$^{-/-}$.

## Conclusiones

Los resultados de esta tesis permiten concluir que el síndrome de Townes-Brocks es una enfermedad similar a las ciliopatías, cuya etiología está mediada por la interfencia de SALL1 truncado con la red citoesqueleto de actina-cilia a través de su interacción con las proteínas CCP110, CEP97 y LUZP1.

Los resultados de esta tesis permiten concluir:


1. SALL1$^{FL}$ es una proteína nuclear y ciliar, y la proteína SALL1 truncada provoca su localización en el citoplasma de manera dominante-negativa.


2. Los fibroblastos derivados de pacientes con TBS muestran cilios más largos y más abundantes que los fibroblastos control y estos defectos en la ciliogénesis se han reproducido en las siguientes líneas celulares modelo de TBS, aunque expresen diferentes variantes patógenas:
a. Fibroblastos de un nuevo paciente de TBS con la variante patológica SALL1c.826C> T.
b. Una línea celular modelo de TBS generada en células HEK 293FT por la tecnología CRISPR/Cas9.
c. Fibroblastos embrionarios del modelo de TBS en ratón Sall1-ΔZn2-10.

3. Los fibroblastos derivados de pacientes con TBS presentan defectos en señalización de Shh.

4. La proteína SALL1 truncada interactúa con los reguladores negativos del cilio primario CCP110 y CEP97, y con LUZP1, provocando su desaparición prematura del centríolo madre en las células TBS.

5. LUZP1 se localiza en el centrosoma e interactúa con CCP110 y CEP97.

6. LUZP1 es un regulador negativo de la ciliogénesis implicado en la señalización de Shh.

7. LUZP1 es una proteína estabilizadora de actina reducida en células TBS.

8. La presencia de la proteína SALL1 truncada conduce a la degradación de LUZP1 mediada por proteasoma.

9. La falta de LUZP1 da lugar a defectos en la proliferación y migración celular, presumiblemente, a través de la regulación del citoesqueleto de actina.

**Personal Resumé (CV): Laura Bozal Basterra**

Avda. del Ferrocarril, 4, 5B        48013 Bilbao (Vizcaya)
+34 629979926 [lbozal@cicbiogune.es](mailto:lbozal@cicbiogune.es)

### Education
01/2015 - 12/2018. **Molecular Biology and Biomedicine Ph.D**. CIC bioGUNE, Technology Park of Bizkaia, Spain.
09/2017 – 07/2018 **Teaching Training M.S.** Universidad Isabel I, Burgos, Spain.
09/2013 – 06/2014 **Molecular Biology and Biomedicine M.S.** University of Basque Country (UPV- EHU).
09/2011 – 06/2012 **Erasmus Exchange Programme.** University of Groningen (RUG), The Netherlands.
09/2006 – 07/2012 **Bachelor of Biochemistry, BS.** University of Navarre, Spain.
09/2006 – 07/2012. **Bachelor of Biology, BS.** University of Navarre, Spain.

### Research experience
01/2015-12/2018. **Molecular Biology and Biomedicine Ph.D**. CIC bioGUNE, Technology Park of Bizkaia, Spain. Supervisor: Dr. Rosa Barrio.
04/2017 – 07/2017. **International Ph.D. Programme Internship.** Memorial Sloan Kettering Cancer Center, MSKCC. Supervisor: Dr. Kathryn Anderson.
01/2013 – 12/2014. **Training contract.** CIC bioGUNE, Technology Park of Bizkaia,Spain. Supervisor: Dr. Rosa Barrio.
09/2011 – 07/2012 **Neurophysiology Research Project.** University Medical Center of Groningen, The Netherlands. Supervisor: Dr. Erik Bodekke.
09/2009 – 06/2011 **Cancer research Project.** Centro de investigación Médica Aplicada (CIMA), Pamplona, Spain. Supervisor: Dr. Jackeline Agorreta

### Grants and awards
10/2018. **Outstanding Poster Presentation Award**. Cilia 2018 EMBO workshop. Copenhague, Denmark.
04/2017-07/2017. **Travel Grant: 3 month International PhD Programme Internship in Memorial Sloan Kettering Cancer Research Center, New York, USA**. Boehringer Ingelheim Fonds. Cantidad: 8680 €.
01/2015-11/2018. **4-year PhD Programme Grant** by Basque Government**,** Spain. Cantidad: 65.300 €.
09/2011-07/2012. **Erasmus Exchange Programme Grant** by The European Commission.
06/2006. **Secondary School Graduation with honors** by Gonzalo de Berceo Highschool**,** Rioja, Spain.

### Publications
**Bozal-Basterra, L.,** Gonzalez-Santamarta, M., Martín, N., Carracedo, A., Barrio, R. and Sutherland, J.D*.* (2018) **LUZP1 underlies primary cilia and actin cytoskeleton defects in Townes-Brocks Syndrome.** The Journal of Cell Biology (submitted).

**Bozal-Basterra, L.,** Martín-Ruíz I., Pirone, L., Liang, Y., Sigurðsson, JO., Gonzalez-Santamarta, M., Giordano, I., Gabicagogeascoa, E., de Luca, A., Rodríguez, JA., Wilkie, AOM., Kohlhase, J., Eastwood, D., Yale, C., Olsen, JV., Rauchman, M., Anderson, KV., Sutherland, JD., Barrio, R. (2018). **Primary cilium defects are contributing factors in Townes-Brocks Syndrome.** American Journal of Human Genetics, 102 (2), 249-265.

Torrano, V., Valcarcel-Jimenez, … **Bozal-Basterra, L.,** *et al.* (2016). **The metabolic co-regulator PGC1α suppresses prostate cancer metastasis**. Nature Cell Biology (18), 645-656.

Schaafsma, W., **Bozal-Basterra, L.,** Jacobs, S., Brouwer, N., Meerlo, P., Schaafsma, A., Bodekke, E.W.G.M., Eggen, B. J. L. (2017). **Maternal inflammation induces immune activation of fetal microglia and leads to disrupted microglia immune responses, behavior, and learning performance in adulthood.** Neurobiology of disease (106), 291-300.

**Leadership experience**
**1. Supervised Master Thesis:**
(2016) E. Gabikagogeascoa
(2017) M. González,
**2. Supervised Bachelor of Science Thesis from:**
(2018) A. Cenigaonandia.
**3. Supervised tecnician trainee from:**
(2015) A. Fernández,
**4. Supervised Erasmus internship from:**
(2016) K.A. Haly
(2016) A. de Luca.

**Contributions to Congresses**
2/5-10-2016. **Cilia 2018, EMBO workshop**, Copenhagen, Denmark.
24-27/10/2017. **1st Joint Meeting SEDB, SEG, SEBC**, Gijón. Poster presentation.
4/7-10-2016. **Cilia 2016, EMBO**, Amsterdam, The Netherlands. Poster presentation.
10-2013. **8th International Conference on Neural Tube Defects**, Austin, USA. Poster presentation.
03-2012. **Behavioural and Cognitive Neurosciences (BCN)**, Groningen, The Netherlands. Poster presentation

**Other interests**
9/2012-Currently. **Professional winemaker**, La Rioja, Spain.
1/2006-Currently. **Secretary of the Valjoven Young Association** to promote cultural activities in rural areas.